THE UNIVERSITY OF SYDNEY

The Holocene geomorphic history of the lower Murray River and Murray Estuary

Author:

Anna Martine

HELFENSDORFER

Supervisors:

A/Prof. Thomas HUBBLE

Dr. Hannah POWER

A thesis submitted in fulfilment of the
requirements for the degree of Doctor of Philosophy

in the

School of Geosciences
Faculty of Science

2019

Statement of originality

This is to certify that to the best of my knowledge, the content of this thesis is my own work. This thesis has not been submitted for any degree or other purposes.

I certify that the intellectual content of this thesis is the product of my own work and that all the assistance received in preparing this thesis and sources have been acknowledged.

Signature: ███████

Name: Anna Martine Helfensdorfer

Date: 31/07/19

Statement of contributions to jointly authored works contained in the thesis

Helfensdorfer, A.M., Power, H.E., Hubble, T.C.T. (2019), Modelling Holocene analogues of coastal plain estuaries reveals the magnitude of sea-level threat, *Scientific Reports* **9**, Article number: 2667.

- HEP - assisted with experimental design and edited drafts of manuscript

- TCTH - assisted with experimental design and edited drafts of manuscript

- AMH - completed all other work

Helfensdorfer, A.M., Power, H.E., Hubble, T.C.T. (2019), Atypical responses of a large catchment river to the Holocene sea-level highstand: The Murray River, Australia, *Scientific Reports*, accepted.

- HEP - assisted with experimental design and edited drafts of manuscript

- TCTH - assisted with experimental design, field work, and edited drafts of manuscript

- AMH - completed all other work

Helfensdorfer, A.M., Hubble, T.C.T., Power, H.E., (2019), Simple 2D simulations sufficiently resolve 3D hydrodynamics for assessments of estuarine palaeo-environmental change: A case study of the Holocene Murray estuary, *In Preperation*.

- HEP - assisted with experimental design and edited drafts of manuscript

- TCTH - assisted with experimental design and edited drafts of manuscript

- AMH - completed all other work

Published works by the author incorporated into the thesis

Helfensdorfer, A.M., Power, H.E., Hubble, T.C.T. (2019), Modelling Holocene analogues of coastal plain estuaries reveals the magnitude of sea-level threat, *Scientific Reports* **9**, Article number: 2667.

- Incorporated into Chapter 2

Acknowledgements

I would like to express my deepest gratitude to my supervisors, A/Prof Tom Hubble and Dr Hannah Power, who sparked my curiosity and guided me on this journey. Their yin-yang supervision not only generated wonderful insights, ideas and thought provoking debate, but also provided some great moments of comedic relief. Their passion and enthusiasm for the project and belief in my ability has made this thesis possible.

I wish to thank David Mitchell and Tom Savage for their technical expertise, on numerous trips down the Murray and in the laboratory, and to Bern Antonio for her assistance. Kendall Mollison for her friendship and laughter, making the countless hours in the lab enjoyable. 'Team Tsunami/Murray' and all the office buddies of 358, but especially Samantha Clarke, Tegan Hall and Tom Job for their support, friendship and coffee and lunch debriefs.

To Richard Afford for enthusiastically allowing access to his property for the collection of cores and CPTs; without this generosity the project would not have been possible. BMT WBM for providing an in-kind TUFLOW FV licence and valuable technical assistance. Chris Cooke for his expertise in setting up a virtual server to run the models.

To my parents, Mary and Walter, and to Elise and Zanna for their continued support and enthusiasm, and to my wonderful friends. Finally, to my partner, Dan, for his expertise in building an amazing core rack, but especially for his love, laughter and ability to keep things in perspective.

Abstract

Palaeo-environmental studies form an important basis for natural resource management and provide an understanding of pre-anthropogenic conditions as well as an indication of a natural system's likely response to change. A palaeo-estuary's response to the Holocene sea-level highstand can provide a useful analogue to predict potential future change due to sea-level rise associated with anthropogenic climate change. Such knowledge is particularly important in the management of intensively modified systems, such as the Murray-Darling Basin. Australia's largest and most important river system has a long and contentious history of intensive water management. Conflicting scientific accounts of the palaeo-environmental history of the Murray estuary diminish our understanding of this system's behaviour and reduces the efficacy of natural resource management in the region. This study presents a well-constrained model of the geomorphic evolution of the lower Murray River and Murray estuary with a specific focus on the response of the system to the Holocene sea-level highstand.

Hydrodynamic modelling of the lower Murray River and Murray estuary was conducted to evaluate the primary drivers of palaeo-environmental change during the Holocene and constrain the plausible response of the Murray estuary to the +2 m higher-than-present sea level of the Holocene sea-level highstand. Sensitivity testing conducted in 2D demonstrates that variation in sea level significantly altered the regional palaeo-environment and dominated the response of the system, with variation in bathymetry, riverine discharge or barrier morphology resulting in minimal change. The elevated sea level of the Holocene highstand generated an extensive estuarine environment with an elongate central basin extending a minimum of 100 river kilometres upstream from the Murray Mouth and into the confines of the Murray Gorge. The gorge-confined lower Murray River acted as a landward extension of the Murray estuary for much of the Holocene, presenting a unique and unusual geomorphic response that does not conform to conventional estuarine facies models for incised systems. The extremely low gradient of this system facilitated this significant marine incursion and generated an extensive backwater environment with very low current velocities.

The utility of applying 2D simulations in lieu of complex and computationally expensive 3D simulations for assessments of palaeo-environmental change has been considered. Two-dimensional simulations are inherently unable to resolve any potential saline stratification within the estuary. Consequently, a comparative analysis of 2D and 3D simulations was

conducted to determine whether 2D models are appropriate for assessments of palaeo-environmental change within the lower Murray River and Murray estuary. The 2D-3D comparison demonstrates that evaluations of 2D psu limits can be applied as a proxy for the maximum ingression of the salt wedge at depth resolved in 3D. Overall, results demonstrate a consistency in both salinity and flow velocity magnitude outputs between 2D and 3D simulations such that 2D results provide a meaningful representation of results resolved in 3D. Crucially, a comparison between estuarine zonation and inferred morphology derived from both 2D and 3D simulations generates directly comparable and similar results. Together these results confirm that 2D simulations of the lower Murray River and Murray estuary can be adopted as efficient and meaningful alternatives to 3D simulations, a finding which could be applied to other preliminary studies which may not have access to high-performance computing facilities.

Best-estimate Holocene highstand and modern pre-modification 3D hydrodynamic models are validated against sedimentologic data acquired at Monteith, 104 river kilometres upstream from the Murray Mouth. This 3D modelling constrains the upstream limit of the Murray estuary's central basin to 140 river kilometres upstream from the river mouth and confirms that conditions within this palaeo-environment promoted and enabled the deposition and preservation of a laminated silt-clay sequence similar to the mid- to late-Holocene sequence that characterises the central basin deposit of Lake Alexandrina.

Analysis of a 30 m sediment core, Monteith-A, reveals an uninterrupted sedimentary succession from lowstand, through transgression, to highstand and demonstrates the response of this large catchment river to fluctuations in sea level during the late-Pleistocene and early-Holocene. The initiation of the Murray estuary presents in core Monteith-A as a shift in deposition to a laminated backwater sequence at 8,518 cal yr BP, that continued to be deposited at least until 5,067 cal yr BP resulting in continuous, conformable deposition of an uninterrupted sequence at a rate of 3.2 m per thousand years. A transect of cone penetrometer soundings demonstrates that the Murray estuary's central basin deposit occupied the entire width of the several kilometre-wide Murray Gorge. The accommodation space provided within the Lower Lakes and Murray Gorge generated an extremely low gradient, backwater environment that captured the river's sediment discharge and essentially prevented the delivery of terrigenous sediment derived from the entire Murray-Darling Basin to the offshore marine environment between 8,518 and 5,067 cal yr BP. The existence of this previously unrecognised natural sediment trap located upstream of the point of discharge to the ocean suggests that mid-Holocene climate reconstructions based on fluctuations of terrigenous sediment in marine cores taken offshore of the Murray's Mouth should be re-evaluated.

Contents

List of Figures

List of Tables

Chapter 1

Introduction

The Murray-Darling Basin (MDB) is Australia's largest river basin reaching the ocean, spanning four states and territories. As the most productive agricultural region in the country it is known as the nation's food bowl. The intensity of water management to support this agricultural industry has produced a long history of over-allocation of water resources, causing water use and management within the MDB to become highly politically contentious. Palaeo-environmental studies form an important basis for natural resource management, with an understanding of pre-anthropogenic, natural conditions and system responses to environmental change particularly important in the management of intensively modified systems such as the MDB (Gell et al., 2009; Mills et al., 2013b). More specifically, understanding responses to change during the Holocene is crucial as environmental change over the past 12,000 years bears some similarities to predicted future changes due to climate change, with higher-than-present sea levels and a warmer, more variable climate (Gell et al., 2009). The Holocene geomorphic history of the Murray River channels and floodplain within the Riverine Plain in NSW and Victoria has been well studied (e.g. Firman, 1966; Stone, 2006); however, given the intensity and importance of management of the lower Murray River's (LMR) floodplain, it is surprising that a detailed analysis of its geomorphology has not been conducted (Clarke et al., 2008).

Numerous studies have sought to constrain the geomorphic history of the Murray estuary, focusing on the development of the Holocene beach barrier system and the palaeo-environmental character of the Lower Lakes, Alexandrina and Albert (e.g. Bourman and Murray-Wallace, 1991; Bourman et al., 2000; Fluin et al., 2007; Harvey, 2006; Luebbers, 1981). Studies of the Lower Lakes are typically based on palaeo-limnology, particularly diatom analyses (e.g. Barnett, 1993; 1994; Fluin, 2002; Von der Borch and Altmann, 1979). The lack of consensus on the palaeo-environmental character of the Lower Lakes during the Holocene (Fluin et al., 2009; Fluin et al., 2007; Gell, 2019), and the associated uncertainty of the extent of the palaeo-Murray estuary, gives impetus for an alternate means of analysis on the Murray estuary's Holocene evolution.

When considering responses of coastal systems to sea level change, a recognised field requiring further study is the integration of models with regional geology and sedimentology (Woodroffe and Murray-Wallace, 2012). Woodroffe and Murray-Wallace (2012) explain that a greater emphasis on this approach is required to better validate model conclusions which will further assist policy-makers plan for change. This study seeks to apply such an approach, employing both hydrodynamic modelling and sedimentary analyses to better understand the Holocene geomorphic history of the LMR and Murray estuary. A key impetus is the recent description of the Holocene sedimentary sequence within the upper-valley fill of the LMR. The presence of a mid-Holocene laminated silt-clay sequence contained within sediment cores taken from the banks of the LMR led Hubble, De Carli and co-workers to hypothesise that a lacustrine-like depositional environment may have existed at this time (De Carli and Hubble, 2014; Hubble and De Carli, 2015; Jaksa et al., 2013). The laminated mud sequence described by De Carli and Hubble (2014) is not typical of sediments of a meandering river, but rather these materials are almost identical to the Holocene laminated, central basin muds of Lake Alexandrina described by Barnett (1993; 1994). Based on these observations, this thesis tests the overarching hypothesis that the palaeo-Murray estuary may have been more extensive than previously thought, and that the mid-Holocene sea-level highstand and late-Holocene recession of sea level to present was the controlling influence on the geomorphic development of the LMR.

Constraining the regional palaeo-environment that prevailed throughout the LMR at the Holocene sea-level highstand is particularly important given that natural resource management policies are guided by our understanding of the natural, pre-anthropogenic state as well as system responses to palaeo-environmental change. The +2 m higher-than-present sea level of the Holocene highstand provides a useful analogue when evaluating the plausible response of the Murray estuary to the expected current and future sea-level rise due to anthropogenic global warming.

1.1   Aims and objectives

This study seeks to investigate the nature and response of the LMR and Murray estuary to the Holocene sea-level highstand through two complementary hydrodynamic modelling studies and a sedimentary facies analysis. Specifically, these two approaches aim to:

- Evaluate the spatial extent of estuarine facies at the Holocene sea-level highstand;

- Characterise the LMR's Holocene stratigraphy;

- Determine the main drivers in the Holocene geomorphic evolution of the Murray estuary; and

- Identify future drivers of environmental change to the LMR and Murray estuary due to climate-change induced sea-level rise.

These aims will be achieved through the following objectives:

- Develop 2D and 3D hydrodynamic models for the LMR and Murray estuary to:

  - Conduct an extensive sensitivity analysis in 2D to constrain the plausible response of the Murray estuary to the +2 m higher-than-present sea level of the Holocene sea-level highstand;

  - Evaluate the suitability and reliability of 2D models in determining palaeo-environmental conditions by contrasting the results of key 2D scenarios with their 3D replicates;

- Conduct a sedimentary and chronological analysis of a 30 m sediment core, Monteith-A, recovered from a site located within a modern-day backswamp of the LMR at Monteith (rkm 104);

- Identify and correlate sedimentary units within core Monteith-A with a cross-valley transect of ten cone penetrometer soundings spanning the entire width of the Murray Gorge at Monteith (rkm 104) to develop a whole-of-valley overview of Holocene stratigraphy;

- Assign facies designation to the distinct sedimentary units identified within core Monteith-A and correlate these facies with fluctuation of sea level during the Holocene;

- Validate, refute or modify the model of the lower Murray Gorge's sedimentary infill proposed by Jaksa et al. (2013).

1.2   Overview of study area

The MDB drains 14% of Australia's landmass and is the nation's most politically, economically, and agriculturally important river system. The origins of the MDB stem back to the late-Paleocene, however it wasn't until the late-Pleistocene that significant erosion enabled by gradual uplift and fluctuating sea level resulted in the formation of the Murray Gorge in South Australia (Stephenson and Brown, 1989). The lower Murray River (LMR) from Overland Corner (rkm 439) to Wellington (rkm 78) is incised into this gorge, a process that has been facilitated by confinement (Figure 1.1). From Overland Corner (rkm 439) to Mannum (rkm 154) the near-vertical limestone cliffs confine the gorge to typically 2-3 km wide, with the LMR characterised by long, straight reaches and tight meander bends fringed by a series of elongated backswamps (Figures 1.1 & 1.2; Mackay and Eastburn, 1990). Downstream of

Mannum (rkm 154) the valley broadens, and the river and its floodplain are set within a 3-6 km bedrock valley with moderately to gently sloping margins (Figures 1.1 & 1.2). The LMR reaches the extent of the Murray Gorge at Wellington and debouches into the Pomanda Embayment before reaching the terminal lakes Alexandrina and Albert. Here, at the terminus of the LMR, is the Murray estuary, a wave-dominated estuary comprising Sir Richard and Younghusband peninsulas, the Coorong lagoon and the Lower Lakes (Figures 1.1 & 1.2).

1.2.1   Water management within the MDB

Water within the MDB is intensively managed with flow regimes subject to extensive modification at national and state levels for irrigation and environmental purposes. Significant flow diversions for irrigation have been a source of political tension since as early as the 1880s when water extraction threatened the navigability of the Murray River (Leblanc et al., 2012). The 1900s saw considerable investment in water storage infrastructure, including the construction of dams and the development of a network of locks and weirs on the Murray River (Leblanc et al., 2012). The LMR downstream of Mannum (rkm 154), known as the Lower Murray Reclaimed Irrigation Area (LMRIA), has been subject to extensive modification including levee construction, land reclamation and laser levelling, for the pursuit of irrigated agricultural activities.

A network of five barrages were constructed within the modern flood-tide delta by 1940 to prevent saline incursion and ensure the viability of the LMR's waters for irrigation and watering stock. The barrages held water levels within the Lower Lakes artificially high at 0.75 m above sea level and converted them to permanent freshwater bodies significantly altering their ecological character (Bourman and Barnett, 1995). Prior to the installation of the barrages, saline ingression during periods of low-flow resulted in repeated occurrences of saline water upstream as far as Mannum (rkm 154), with some accounts of river water being unsuitable for watering stock or irrigation as far upstream as Morgan (Figure 1.1; rkm 322; Bourman and Murray-Wallace, 1991; Davis, 1978; McIntosh, 1949). Installation of the barrages has resulted in an obvious and significant reduction in the tidal prism by over 85% (Harvey, 1996), and has also altered the morphology and development of the flood-tide delta, most notably with the evolution of Bird Island (Bourman and Murray-Wallace, 1991; James et al., 2015).

Currently, only approximately one third of pre-anthropogenic flows reach the Murray estuary and debouch through the Murray Mouth to the ocean (Connor et al., 2009; Pittock and Finlayson, 2011). On 40% of days there is no outflow at the Murray Mouth, a distinct change from the previous one cease-to-flow day in a hundred under natural, pre-modification conditions (Kingsford et al., 2011; Pittock and Finlayson, 2011). The significant reduction
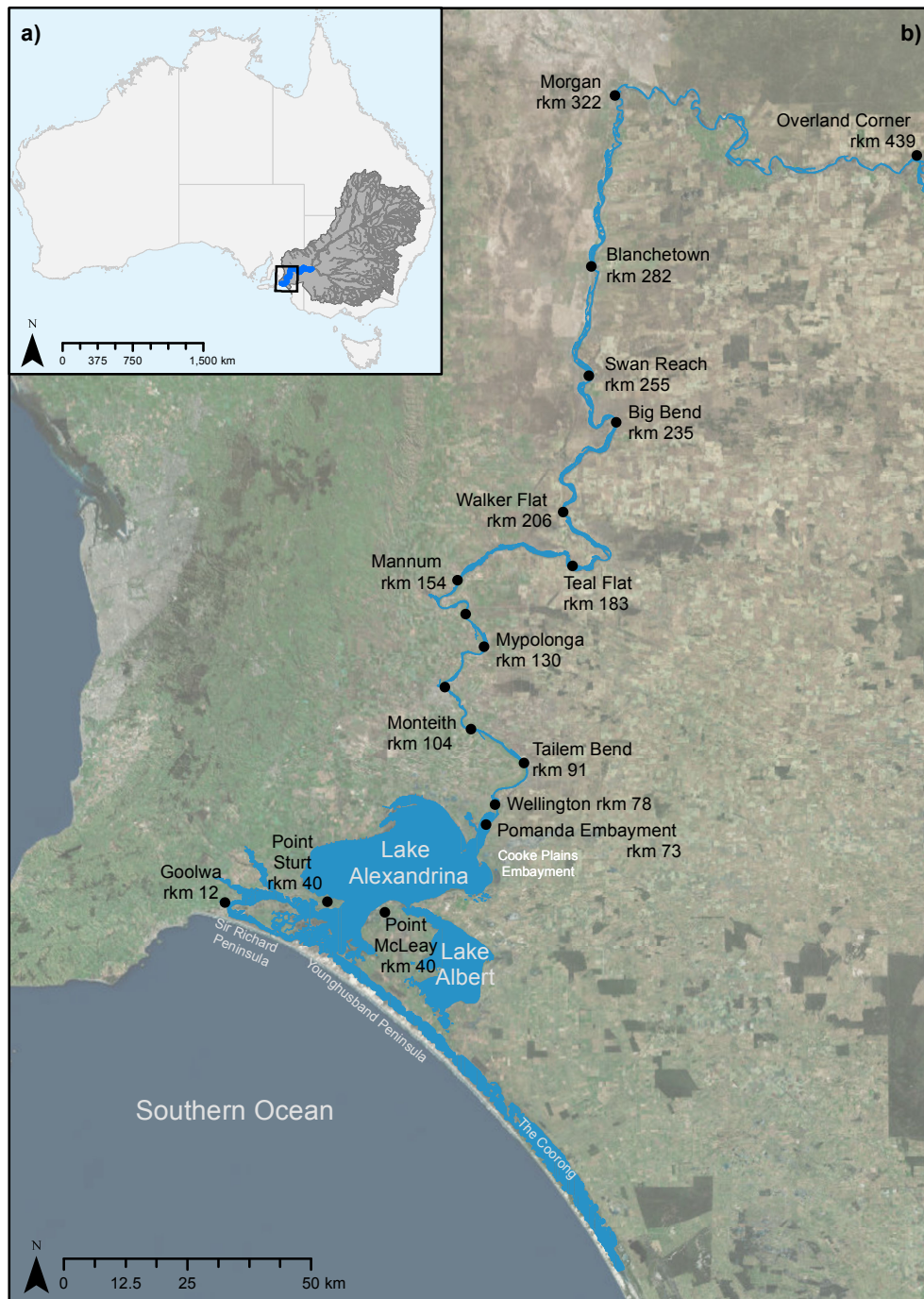
Figure 1.1: Overview map of the study area. (**a**) The Murray-Darling Basin (grey, with major watercourses in dark grey) drains 14% of the Australian continent and cumulates in the lower Murray River and Murray estuary (blue) before debouching into the Southern Ocean. (**b**) The lower Murray River is entrenched in the Murray Gorge from Overland Corner (rkm 439) to Wellington (rkm 78). The Lower Lakes comprise the two terminal lakes Alexandrina and Albert. The modern-day flood-tide delta is situated seaward of Point Sturt and Point McLeay (rkm 40). The Murray Mouth is situated between Sir Richard and Younghusband peninsulas. Satellite imagery source: Esri.
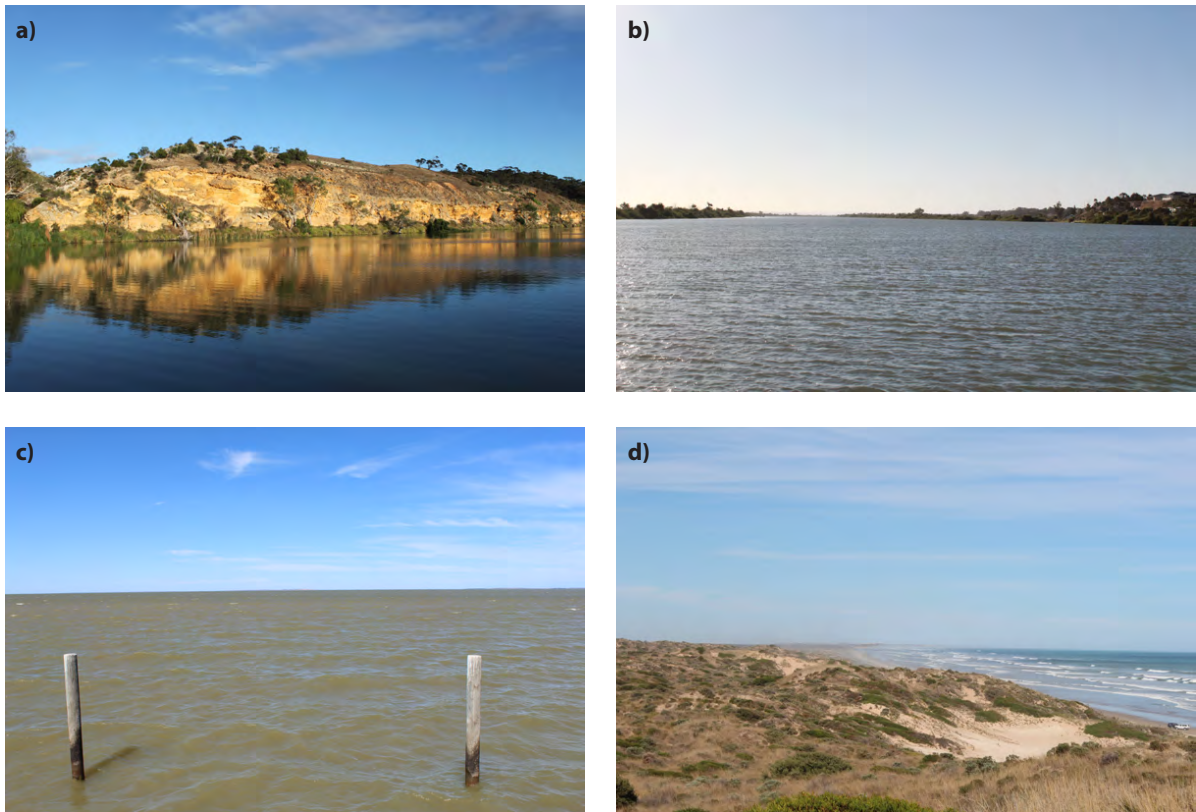
Figure 1.2: Photographs of the study area. (**a**) From Overland Corner (rkm 439) to Mannum (rkm 154) the lower Murray River is confined by steep near-vertical limestone cliffs. (**b**) The Murray Gorge broadens and is characterised by moderately to gently sloping margins downstream to Wellington (rkm 78). (**c**) The lower Murray River debouches into Lake Alexandrina. (**d**) Looking east along Sir Richard Peninsula showing the vegetated barrier complex and offshore wave climate.

in flow and associated flow velocities caused by upstream over-extraction has led some authors to describe the LMR not as a river but rather as resembling a series of interconnected pools (Hotzel and Croome, 1996). This reduction in flow, in conjunction with the reduced tidal prism and flows, now necessitates periodic dredging of the Murray Mouth to prevent its permanent closure (Bourman et al., 2000).

Historically within the MDB, ecological considerations have been subjugated to economic and social considerations when it came to water policy, with decades of mismanagement now cumulating in 'crises' in areas such as the Ramsar listed Lower Lakes and Coorong lagoon (Kingsford et al., 2011; Walker, 2019). Whole-of-basin reforms are required for any attempt to equilibrate to a healthy state (Kingsford et al., 2011; Walker, 2019). Given the immense difficulties of enacting a whole-of-basin reform, management policies to date have instead typically focused on addressing the consequences of water over-allocation, such as acidification, rather than tackling the root cause itself (Kingsford et al., 2011).

The impacts of the recent Millennium Drought (1997-2011) drove natural resource management within the MDB into the spotlight, with failures of the current water resource allocations highlighting the inadequacy of Australia's drought policy in safeguarding communities, industries and ecosystems into the future. The Murray-Darling Basin Authority (MDBA) and The Basin Plan, introduced as key reforms billed to instigate whole-of-basin policy adaptations, instead sparked widespread public debate on the plan's viability and intent, particularly given the uncertainties surrounding future climate change (Kiem, 2013). Crucially, the Basin Plan does not directly account for the impacts of climate change, but rather simply acknowledges it as a significant threat to the MDB (Kirby et al., 2014; Walker, 2019). Despite this, climate change is likely to have a more significant impact on flows within the MDB than any negotiated redistribution in water allocations from irrigation to the environment (Kirby et al., 2014). Despite uncertainty in projected future rainfall trends and variability in extreme climatic events posing a significant challenge for policy-makers, there is undoubtedly a clear need for predicted climate change impacts to the MDB to be integrated into future water policy (Reisinger et al., 2014).

The recent demonstration of the significant vulnerability of Australia's largest, and most politically and economically important river basin to extremes of climate refocused attention to how scientific understanding of palaeo-climates and palaeo-environments within the MDB should shape management into the future. The time series of Australia's temperature, rainfall and river flow records is insufficiently short to capture long term trends and climatic oscillations, and therefore cannot be relied upon to provide a robust or reliable understanding of ecosystem response to future projections of climatic change (Gell et al., 2009; Harle et al., 2007). Therefore in order to accurately model ecosystem responses to future climate change, palaeo-environmental data is required (Mills et al., 2013a).

1.2.2   Climate and sea level

1.2.2.1   Climate drivers

There are three primary drivers which control the modern-day climate of southeastern Australia: the El Nino-Southern Oscillation (ENSO), the Indian Ocean sector of the Southern Annular Mode (IOS-SAM), and the Indian Ocean Dipole (IOD; Figure 1.3; Gouramanis et al., 2013). The MDB extends from summer-dominated monsoon rainfall affecting the Darling sub-catchment in the north of the basin, to winter-dominated rainfall affecting the Murray sub-catchment in the south (Gell et al., 2009; Gingele et al., 2007). The highly episodic nature of flows in the Darling sub-catchment is a consequence of ENSO variability which is the primary driver of the monsoon (Gingele et al., 2007). Flows in the Murray sub-catchment are seasonal, principally driven by melting of the winter snow pack on the Australian Alps, as well as seasonal precipitation (Gingele et al., 2007).
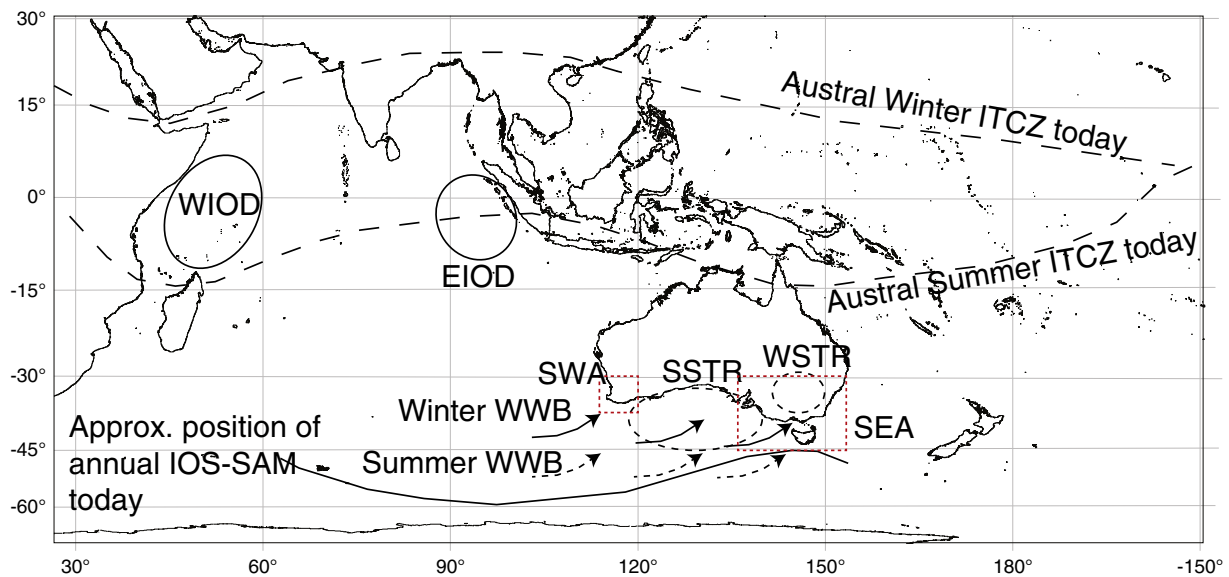
Figure 1.3: Significant climate drivers influencing southern Australia. The Indian Ocean Sector of the Southern Annual Mode (IOS-SAM) lies between 45 - 65 degrees. The mean position of the Indian Ocean Dipole's western and eastern poles are given by WIOD and EIOD respectively. The mean winter and summer positions are differentiated for the Intertropical Convergence Zaitlin (ITCZ), sub-tropical ridge (WSTR and SSTR, respectively) and westerly wind belt (WWB; after Gouramanis et al., 2013).

ENSO's variation in winds and sea surface temperatures are categorised into three phases – El Nino, Neutral and La Nina – and account for approximately 20% of rainfall variability across the MDB (Gallant et al., 2012). The El Nino and La Nina phases produce opposite effects over the MDB with lower than average rainfall during El Nino events and higher than average rainfall during La Nina events, with their extremes producing major drought and flood events respectively (Petherick et al., 2013). ENSO is the primary driver of inter-annual climate variability in the region, however, its cyclicity also operates up to the millennial timescale, although this variability is not as well understood (Petherick et al., 2013).

IOS-SAM produces inter-annual variability in the hydroclimate of the MDB through variations to the location of the Southern Hemisphere mid-latitude storm track (Gallant et al., 2012). This influence, therefore, varies greatly across the MDB based on season and latitude (Gallant et al., 2012). A negative IOS-SAM increases seasonal winter precipitation over southeastern Australia through a strengthening of the Westerly winds which forces a northward migration of weather fronts; while a positive IOS-SAM has the opposite effect (Gouramanis et al., 2013). A further inter-annual driver of hydroclimatic variability is the IOD. The IOD's climatic influence on southeastern Australia is regionally restricted depending on its mode, with positive IOD reducing seasonal precipitation in the western portion of this region, and negative IOD increasing seasonal precipitation in the northern portion (Gouramanis et al., 2013). However, the influence of Indian Ocean sea surface temperature

fluctuations on MDB hydroclimate is considered intermediary only (Gallant et al., 2012).

On the decadal-scale, hydroclimatic oscillations are driven by the Pacific Decadal Oscillation (PDO) in the North Pacific, and the Pacific Basin-wide Interdecadal Pacific Oscillation (IPO; Gallant et al., 2012). The 15-30 year PDO/IPO epochs interact with ENSO to influence rainfall patterns across the entire MDB (Gallant et al., 2012; Kiem et al., 2003; Petherick et al., 2013). Inter-decadal variability in sea surface temperature, oscillating from warm to cool phases, produces lower than average and higher than average rainfall across the MDB respectively (Gallant et al., 2012).

1.2.2.2   Holocene climate of southeastern Australia

The Holocene has been a climatically variable period which, in conjunction with dramatic changes in sea level, has allowed this period to be characterised by significant fluvial and coastal change (Blum and Tornqvist, 2000; Knox, 1993; Mayewski et al., 2004). Within southeastern Australia the early- to mid-Holocene is characterised as more humid, warmer and wetter than present, with associated increases in fluvial discharge (Figure 1.4; Gingele et al., 2007; Kemp et al., 2012; Petherick et al., 2013). Indeed, such is the characterisation of the early- to mid-Holocene as a period of enhanced fluvial discharge across southeastern Australia that the period 10,000 – 4,500 yr BP has been termed the Nambucca Phase (Cohen and Nanson, 2007; Nanson et al., 2003; Petherick et al., 2013). Significant environmental change through these warmer and wetter conditions saw abrupt changes in vegetation during the early-Holocene, altering runoff and fluvial sediment regimes (Petherick et al., 2013).

Records of lake levels across southeastern Australia typically reveal that lakes were at their largest areal extents at approximately 6,000 yr BP, followed by a period of fluctuation then regression, suggesting an increased variability in discharge and a shift to dryer conditions in the late-Holocene (Figure 1.4; Gingele et al., 2007; Gouramanis et al., 2013; Hesse et al., 2004; Marx et al., 2009; Petherick et al., 2013). The drying trend and increased climatic variability of the late-Holocene is attributed to the strengthening of ENSO (Gingele et al., 2007; Kemp et al., 2012). Gouramanis et al. (2013) attribute increasing aridity in the second half of the Holocene to two climate drivers: the IOS-SAM and the Inter-Tropical Convergence Zone (ITCZ), both of which migrated in a southerly direction during this time. The southerly migration of the ITCZ caused a weakening of the Asian summer monsoon and a corresponding strengthening of the Australian monsoon (Gouramanis et al., 2013).

Two marine sediment cores – MD03-2611 and MD03-2607 – are of particular importance for reconstruction of palaeo-climates of the MDB due to their resolution and location (Gell et al., 2009). To date these cores provide the only continuous, high resolution records capable of
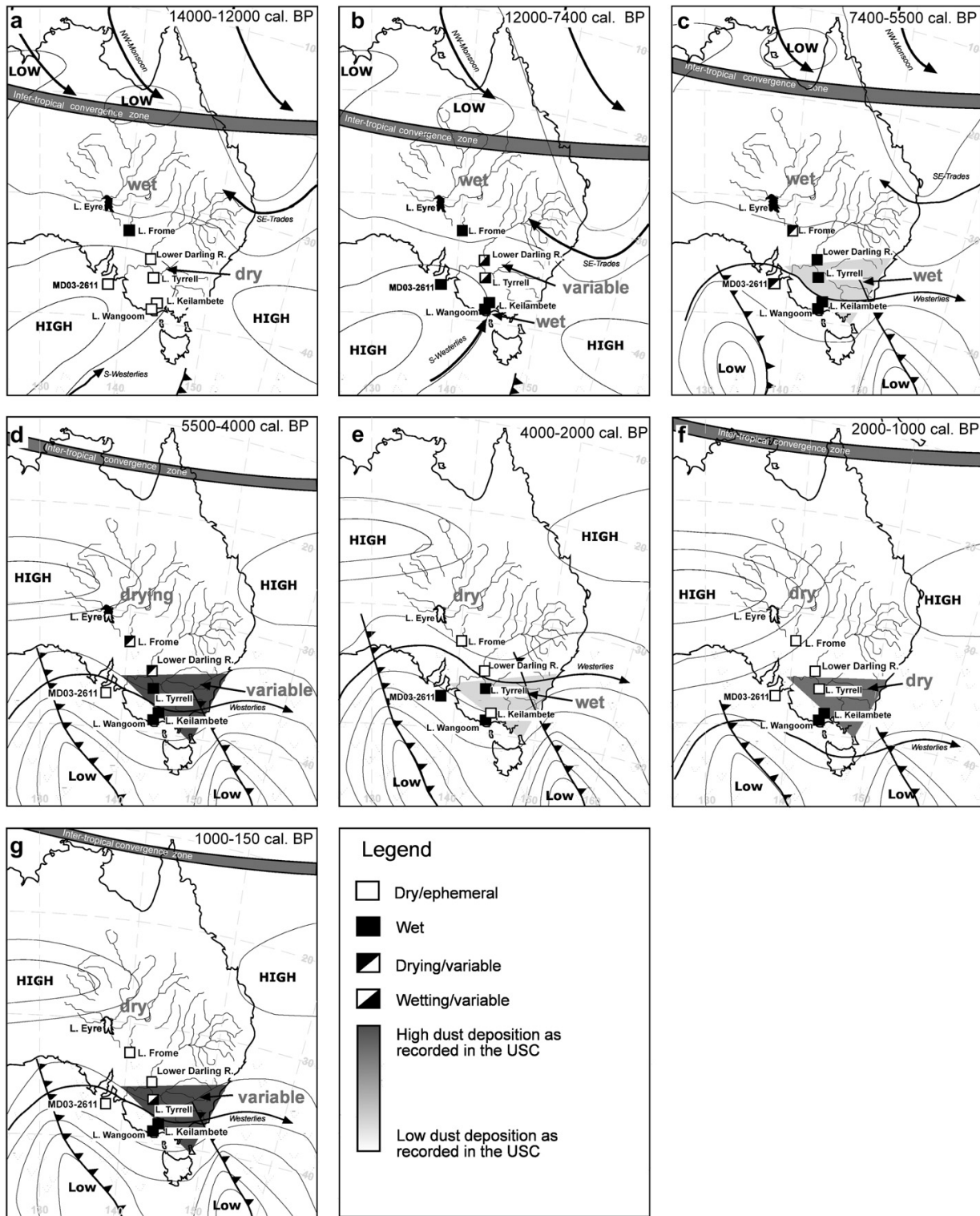
Figure 1.4: Weather within the MDB during the Holocene. Generalised Holocene wind and pressure patterns for the MDB inferred from dust signals within a sediment core collected from the Australian Alps (after Marx et al., 2011).

representing the whole MDB (Gell et al., 2009). Their location within the Murray Canyons directly off the palaeo-Murray Mouth has been suggested to present an ideal location to capture terrigenous sediment from the MDB (Figure 1.5; Gingele et al., 2004). The continuous conformable sedimentation of these hemipelagic marine muds provides a climate record that has been utilised to characterise and understand climate variability of the MDB during the Holocene with implications for natural resource management decisions within the region. This is particularly true for core MD03-2611 which is relied on by this research community to validate the onshore record of hydrological and geomorphological change which is riddled with uncertainty (Gell et al., 2009). The climatic reconstructions of the MDB based on the marine record have also been extrapolated to wider interpretations of climatic trends across southeastern Australia as this Basin spans two distinct climatic zones (Figure 1.6; Gingele et al., 2007).
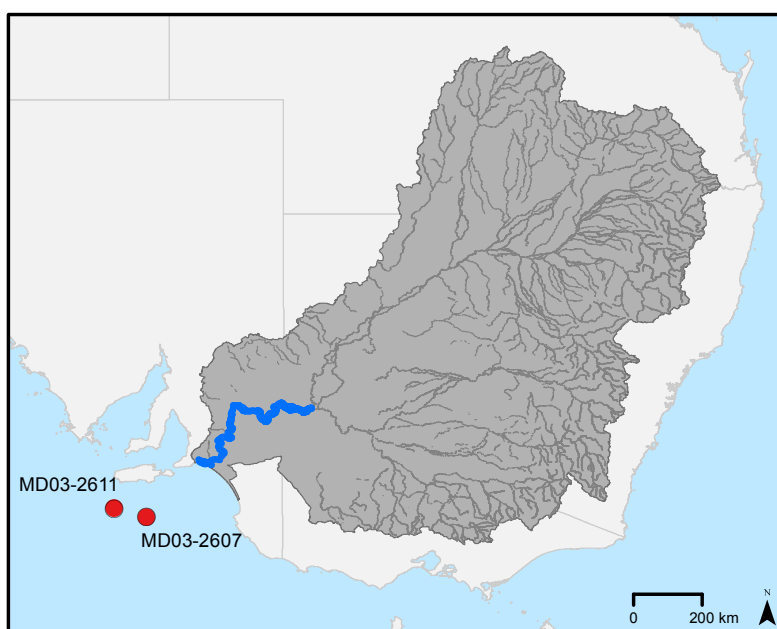
Figure 1.5: Marine cores collected offshore from the Murray Mouth. Marine cores MD03-2611 and MD03-2607 (red) are located within the deep-sea Murray Canyons region on the edge of the Lacepede Shelf directly offshore of the lower Murray River (blue). The Murray-Darling Basin is shown in grey, with its major watercourses in dark grey.

1.2.2.3   Holocene sea level

At the last interglacial optimum, approximately 123 ka, sea level was 2-4 m above present with the last glacial maxima, approximately 20,000 – 18,000 yr BP, resulting in a fall in sea level to a lowstand of -130 m below present in southern Australia (Figure 1.7; Belperio et al., 1995; Hill et al., 2009). The late-Pleistocene and early-Holocene saw a rapid rise in sea level leading to the mid-Holocene sea-level highstand (Figure 1.7; Belperio et al., 1995; Hill et al.,
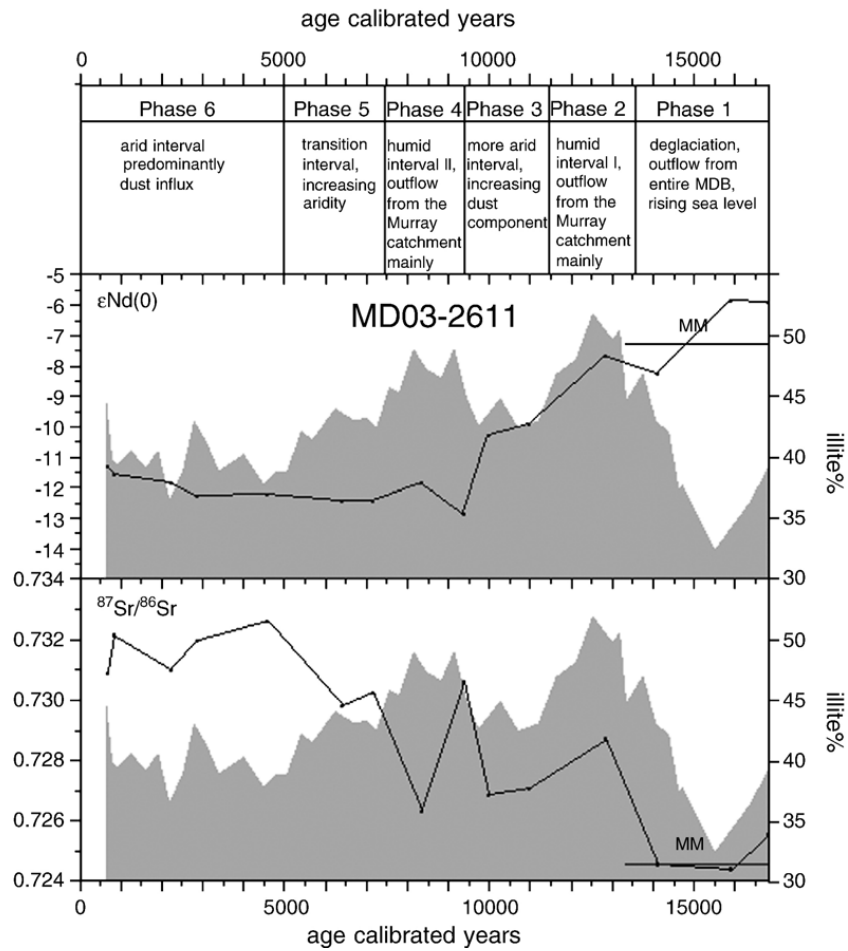
Figure 1.6: MDB Holocene climate signal. Holocene climate signal inferred from analysis of percent illite and the clay:silt ratio of marine core MD03-2611 (after Gingele et al., 2007).

2009). Lewis et al. (2013) and Belperio et al. (2002) place the Holocene sea-level highstand of approximately 2 m above current sea level at between 7,000 – 6,000 yr BP on the southern Australian coast. Analysis of dated shells, middens and diatom assemblages within the Murray estuary indicate that sea level stabilised at the present day level by approximately 3,500 yr BP in this region (Bourman et al., 2000; Cann et al., 2000; Fluin, 2002; Luebbers, 1982).
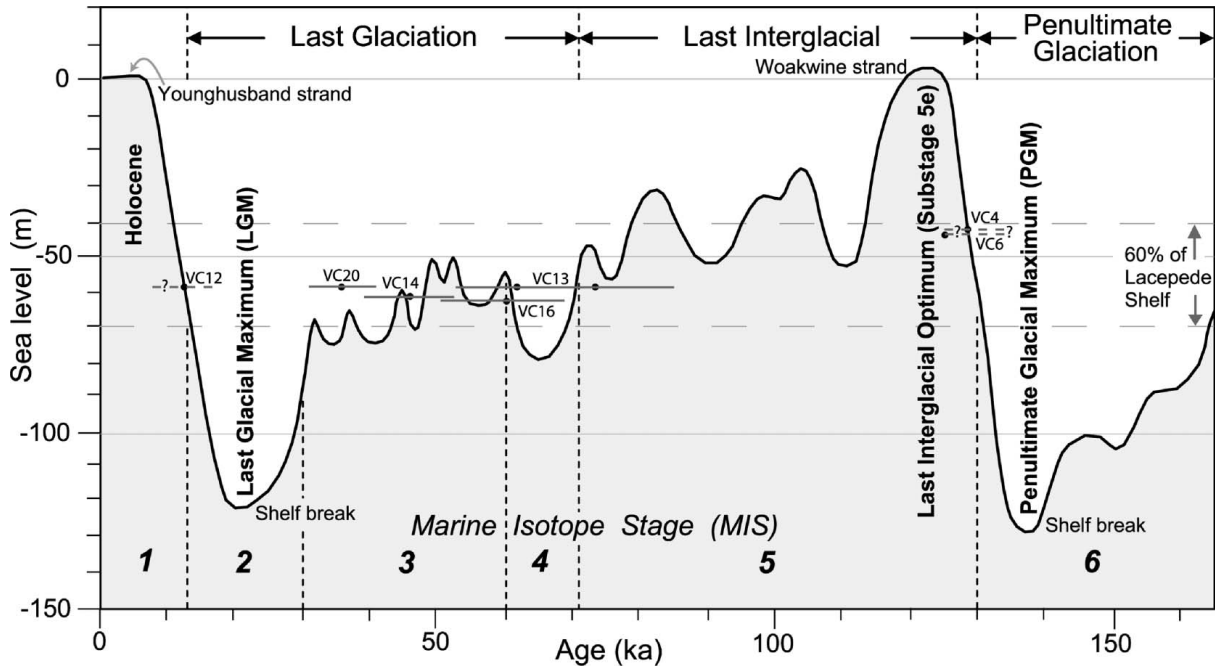
Figure 1.7: Sea level fluctuations during the late-Quaternary. Global sea level curve for the late-Quaternary (the past 165,000 years; after Hill et al., 2009).

1.2.2.4 Future climate change

Median temperatures across Australia have increased between 0.4 – 0.7 °C since 1950, while mean sea level has risen 70 mm (Reisinger et al., 2014). Similarly there has been a higher frequency of extreme climatic events such as drought (Reisinger et al., 2014). Such trends are projected to continue with warmer temperatures and increased intensity and frequency of extreme climatic events considered 'virtually certain' as a consequence of increasing CO_2 concentrations in the atmosphere due to burning of fossil fuels (Reisinger et al., 2014). In 2014, the IPCC projected that given a high emissions scenario, global mean sea level would rise by 0.53 – 0.97 m by 2100, with a 'best case scenario' restricting this rise to 0.28 – 0.6 m (Reisinger et al., 2014). More recently, an assessment by the National Oceanic and Atmospheric Administration (NOAA) suggests that a 2 m rise in global mean sea level by 2100 is now be considered plausible, with an extreme 'worst case scenario' of 2.5 m (Sweet et al., 2017). Rates of sea-level rise across Australia are projected to exceed the global average

by approximately 10% (Reisinger et al., 2014). Due to inertia in polar ice sheets, sea levels are projected to continue to increase for several more centuries regardless of CO_2 emissions reductions and associated global average temperature stabilisation or decline (Reisinger et al., 2014).

The agricultural productivity of the MDB is projected to significantly decline due to global warming and associated climate change with water security posing an increasing political threat to the region (Reisinger et al., 2014). The IPCC identifies water security within the MDB as a 'hotspot of high vulnerability' and an issue of concern for the Australasia region over the coming decades (Reisinger et al., 2014). Given a 1 °C rise in average temperature, inflows within the MDB are predicted to decrease by 15%, irrespective of rainfall; this can be considered a conservative estimate given that a reduction in rainfall is likely (Cai and Cowan, 2008). In actuality, this is highly conservative as emissions targets required to limit warming to 1.5 °C have likely already been exceeded, with the Paris Agreement target of holding warming below 2 °C now considered possible only given radical societal change (Rogelj et al., 2016). Climate models suggest that the median average rainfall over the MDB is likely to decrease by 5-15% over the next 40 years (Cai and Cowan, 2008; Christensen et al., 2007). Extrapolating this out to a 2 °C increase in average temperature, and accounting for the associated increase in evapotranspiration and projected reduction in rainfall, may result in a 55% reduction in inflows within the MDB by 2060 (Cai and Cowan, 2008; Pittock and Finlayson, 2011). Owing to their location at the terminus of this immense catchment, the resulting reduction in flows will have highly significant implications for the LMR and Murray estuary, both with regard to irrigated agricultural productivity and the viability of sensitive ecological communities (Connor et al., 2009; Kingsford et al., 2011; Pittock and Finlayson, 2011).

1.3   Estuarine evolution and facies models

Estuaries can be categorised into three types: tide-dominated, wave-dominated and intermittently closed, with wave-dominated estuaries further categorised into barrier estuaries, barrier lagoons and inter-barrier estuaries (Roy et al., 2001). Barrier estuaries are known for their well-defined tripartite structure with lithofacies typically presenting a coarse-fine-coarse sequence comprising the marine sands of the barrier complex and flood-tide delta, the clays and silts of the central basin, and the fluvial sands of the bayhead delta and river channel (Figure 1.8; Dalrymple et al., 1992). Typically, the landward extent of the estuary is defined by the tidal limit, with fluvial sedimentation upstream from this point (Figure 1.8). The bayhead delta occupies the upper estuarine zone between the tidal limit and mean sea level (Figure 1.8). Variations in the size, development and progradation of the bayhead delta are highly dependent on sediment availability, with low sediment supply from the up-

stream catchment resulting in a small bayhead delta, or no bayhead delta in extreme cases, and slow rates of seaward progradation (Dalrymple et al., 1992). The central basin is the region of lowest energy and is characterised by the confluence of marine and fluvial influence and deposition of the finest sediment (Figure 1.8). Seaward, the marine influence creates a starkly contrasting geomorphic response with the formation of a barrier complex including washover and flood-tide delta facies which are commonly dominated by coarser-grained sediment derived from the adjacent shelf (Figure 1.8).
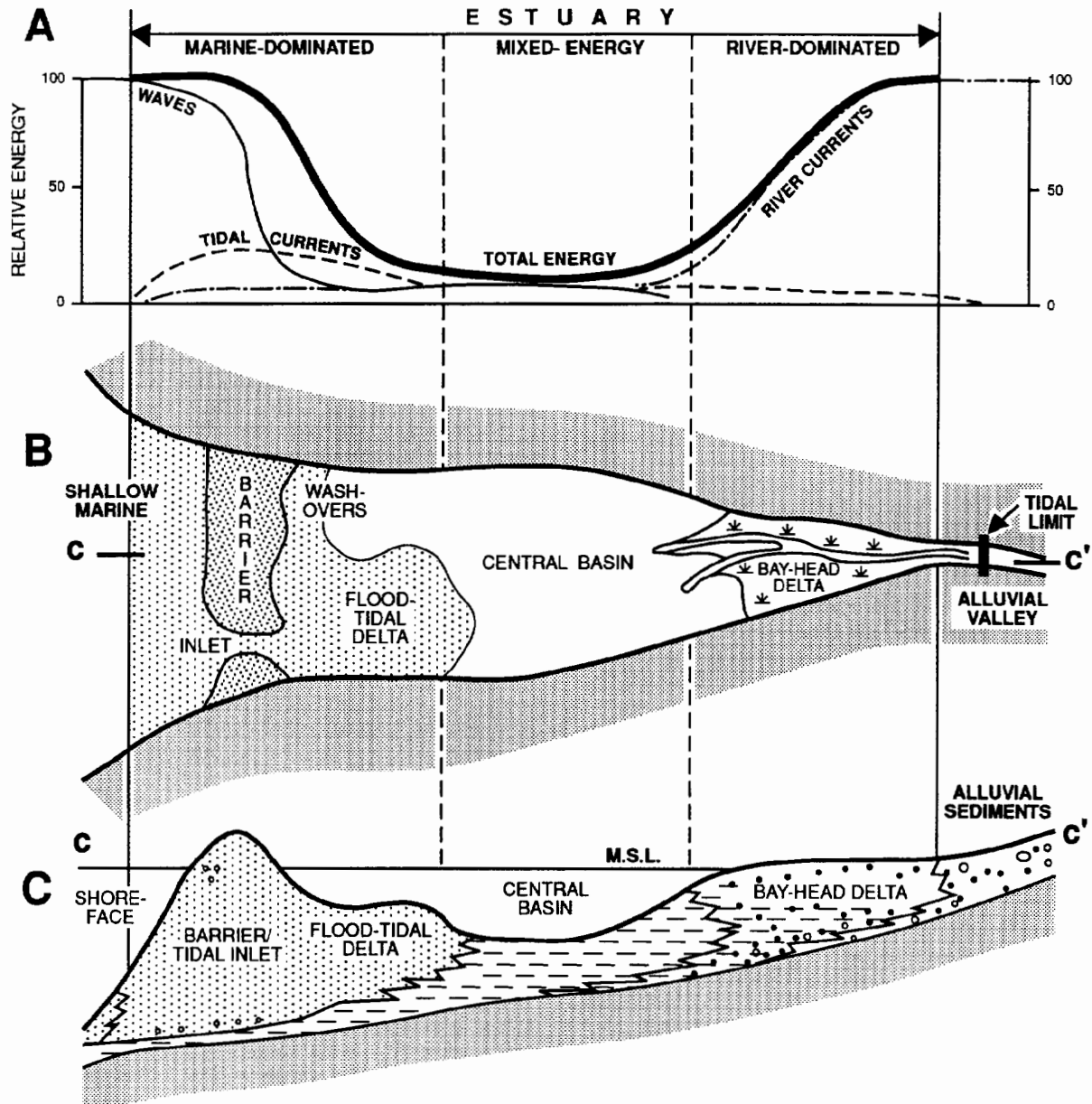
Figure 1.8: An idealised wave-dominated estuary. Showing the distribution of (**a**) energy, (**b**) morphology, and (**c**) sedimentary facies. (after Dalrymple et al., 1992).

Conceptual models provide the framework for generalisations of fluvial responses to changes

in sea level. The onset of relative sea-level fall results in deposition, which transitions the system to valley incision and sediment bypass as sea levels reach lowstands (Blum and Tornqvist, 2000; Posamentier et al., 1988). The contrary is then also expected during marine transgressions and sea level highstands with sediment infilling valleys (Blum and Tornqvist, 2000). Figure 1.9 presents the evolutionary response of an incised valley to the lowstand, transgressive and highstand phases of a complete sea level cycle in plan view, which can be applied when assessing the geomorphic evolution of the LMR and Murray estuary. The lowstand (fan) systems tract (Figure 1.9a) is representative of the response of the palaeo-Murray River as it meandered across the Lacepede shelf and approached the edge of the continental shelf beyond which terrigenous sediment would have deposited in the submarine Murray Canyons (Hill et al., 2009). The lowstand (wedge) systems tract (Figure 1.9b) shows the region comprising the modern day LMR as exhibiting a braided channel morphology, as was suggested by Firman (1966), with the non-incised fluvial portion comprising the modern-day Mallee Region.

The early Holocene was a period of transgression which saw the rapid inundation of the Lacepede Shelf causing the formation and subsequent inundation of barrier complexes in parallel sequence representing estuarine sedimentation on the migrating shoreline (Hill et al., 2009). Indeed, Quaternary sediments on the Lacepede Shelf are a palaeo-analogue of the estuarine system that we see today, with evidence of fluvial facies such as incised palaeo-channels and point bar deposits, as well as the muds and sands that comprise lacustrine and estuarine environments (Hill et al., 2009).

The transgressive phase also saw the development of the modern-day estuary as the rate of sea-level rise began to slow. The barrier complex began its evolution allowing for the development of a central basin and bayhead delta (Figure 1.9c). Finally, as sea levels stabilise the central basin infilled and the bayhead delta prograded seaward leaving in its wake distributary channels, inter-distributary bays, levees and overbank deposits (Figure 1.9d; Nichol et al., 1997; Zaitlin et al., 1994).

Zaitlin et al. (1994) describe the tripartite structure of estuaries as 'segments' with segment 1 constituting the outer incised valley, segment 2 the middle incised valley and segment 3 the inner incised valley (Figure 1.10). The outer incised valley extends from the lowstand shoreline to the highstand stabilised shoreline – i.e. from the edge of the continental shelf to the modern-day Murray Mouth and barrier complex. The landward migration of fluvial, estuarine and marine environments causes a continuing decrease in the depositional gradient resulting in an upward fining sequence within fluvial deposits (Zaitlin et al., 1994). Commonly this results in a transition from high-energy fluvial sands to low-energy mud-dominated sediments indicating a shift from braided to meandering channel morphologies (Zaitlin et al., 1994). The abrupt change in morphology between lowstand and transgression
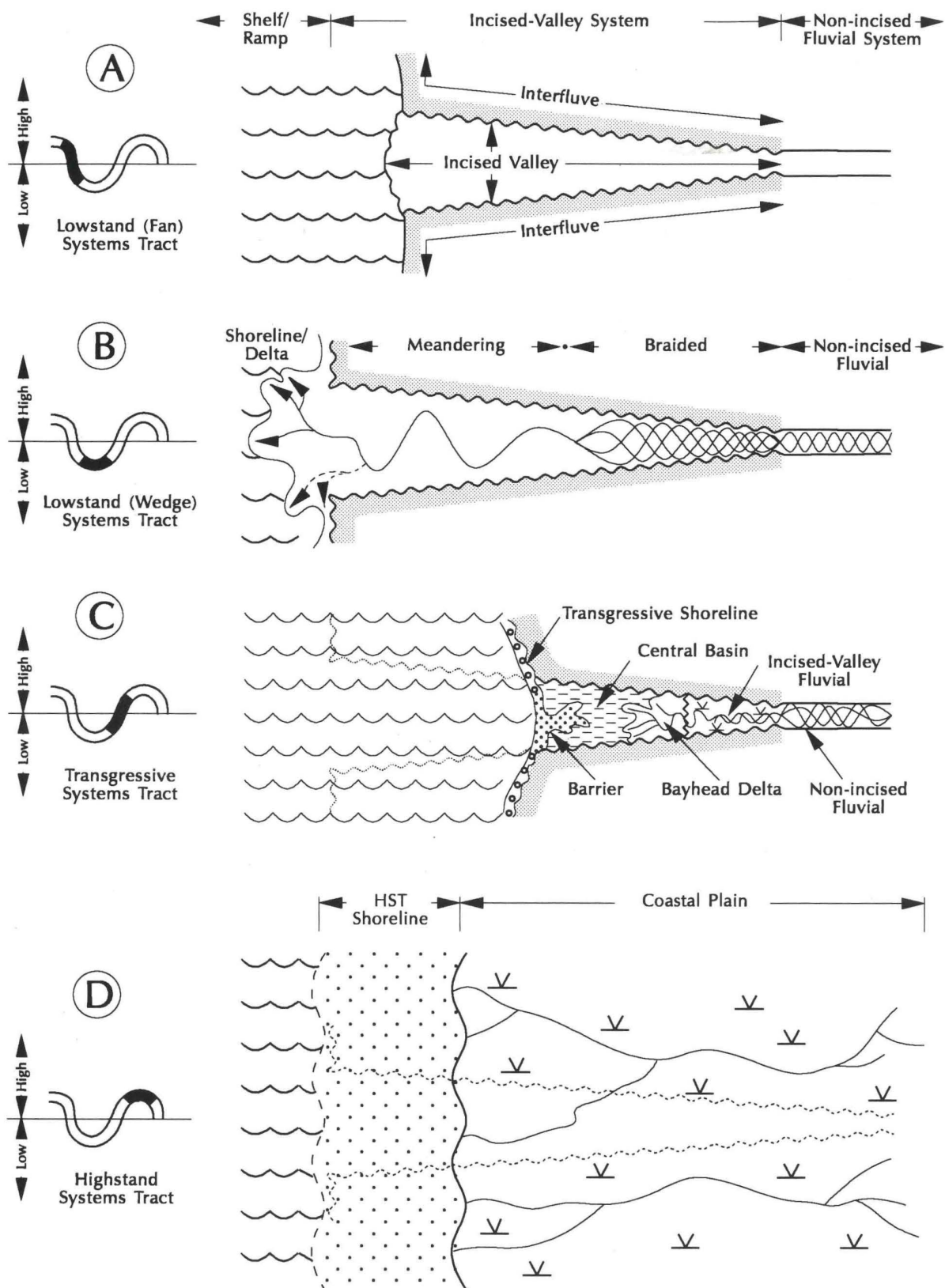
Figure 1.9: An idealised incised valley system in plan view. Idealised evolution of an incised valley system during the course of a complete sea level cycle (after Zaitlin et al., 1994).

is generally inferred to be represented by the sharp transition seen in the LMR's valley fill from the Monoman Formation sands to the Coonambidgal Formation muds.

The middle incised valley segment of this system extends from the highstand or modern day shoreline to the landward estuarine extent at sea-level highstand or at the time of maximum flooding (Zaitlin et al., 1994). Facies within this zone typically depict the sequence boundary of lowstand to transgressive fluvial facies overlain by fine-grained central basin deposits, with an upward coarsening sequence representing a transition to bayhead delta and highstand fluvial deposits (Zaitlin et al., 1994). The landward portion of the middle incised valley is characterised by the absence of central basin deposits, such that the sequence depicts only the sediments of the bayhead delta overlain by highstand fluvial deposits (Zaitlin et al., 1994). The length of this segment is highly variable and is primarily dependent on gradient, as well as the ratio of sediment input to sea-level rise (Dalrymple et al., 1992; Zaitlin et al., 1994).

The final segment of this system, termed the inner incised valley, is entirely fluvial and extends from the landward limit of estuarine influence to the landward limit of valley incision which may be many hundreds of kilometres upstream (Zaitlin et al., 1994). In the case of the LMR the landward limit of this zone, at Overland Corner (rkm 439), is strikingly apparent as the entire character of the river changes as it transitions from the unconfined Mallee Region and into the Murray Gorge (Figure 1.11). Fluctuations in base level and accommodation (and associated erosion and sediment bypass) throughout the sea level cycle will likely result in a thinner sequence of coarse-grained lowstand sediments within this segment. An upward fining sequence may characterise the lowstand and transgressive sediments, while highstand sediments may exhibit an upward coarsening sequence as a result of sea-level stabilisation (Zaitlin et al., 1994).

There are numerous studies on the eastern seaboard of Australia which describe the initiation of Holocene estuaries, their response to the sea-level highstand and their subsequent geomorphic evolution (e.g. Kermode et al., 2013; Nichol et al., 1997; Roy, 1984; Roy et al., 1980; Sloss et al., 2006a). This tectonically stable region that was not subject to widespread glaciation affords preservation of sedimentary sequences therefore allowing for detailed facies designation throughout the estuary. These studies reveal that, even given constricted bedrock valley settings which are common along the east coast of Australia, the Holocene sea-level highstand forced the estuarine limit tens of kilometres upstream within the valley confines (e.g. Kermode et al., 2013; Nichol et al., 1997; Rustomji et al., 2006). Given the low sediment supply characteristic of Australian rivers, the accommodation generated by sea-level rise in the early-Holocene was typically not filled, if it was at all, until the mid- to late-Holocene when sea level stabilised to its present-day level (Sloss et al., 2010).
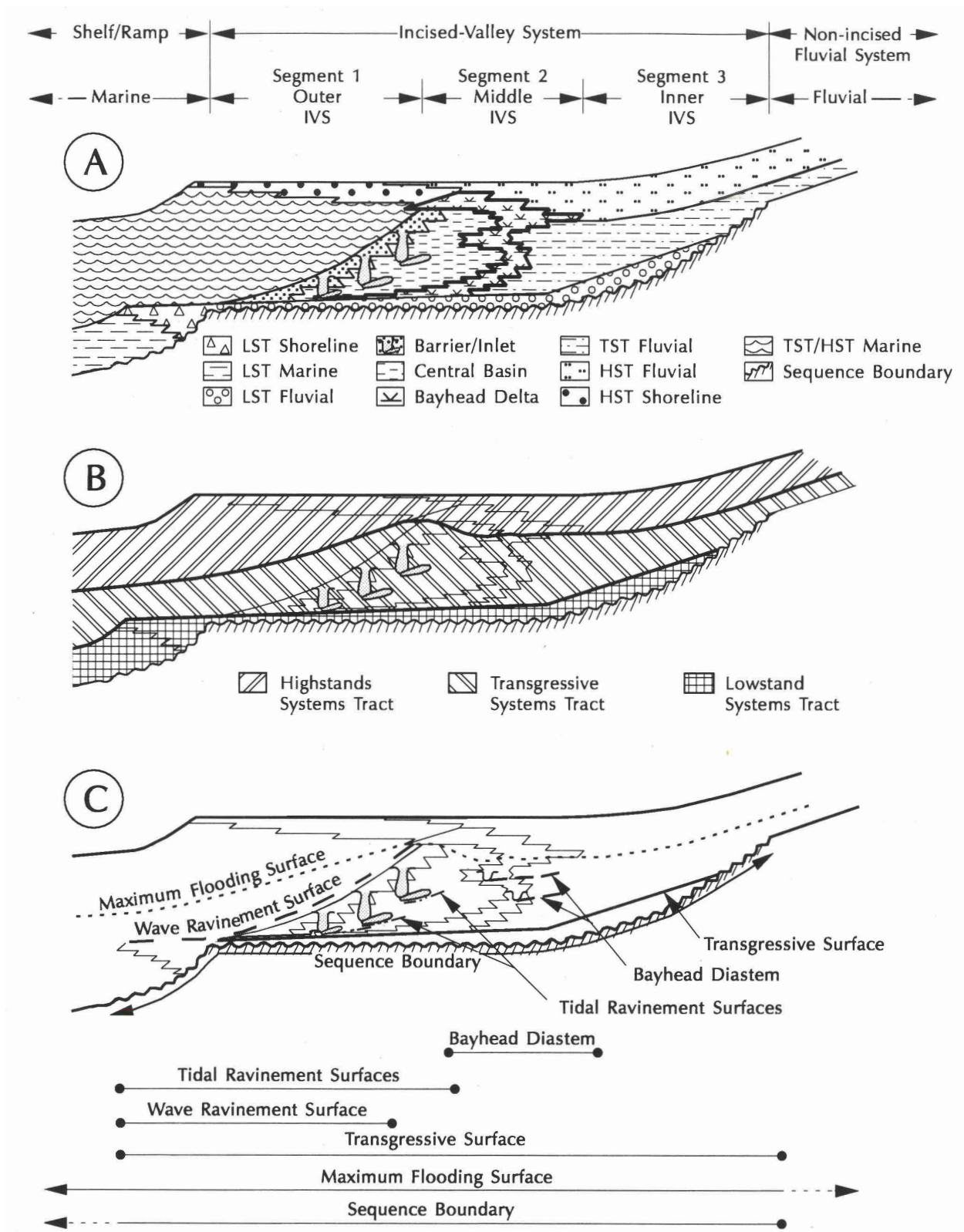
Figure 1.10: An idealised incised valley system in logitudinal view. Conceptual longitudinal model of an incised valley system with distribution of (**a**) depositional environments, (**b**) system tracts, and (**c**) stratigraphic surfaces (after Zaitlin et al., 1994).

Figure 1.11: Satellite imagery showing the upstream extent of the Murray Gorge at Overland Corner. The lower Murray River enters the Murray Gorge at Overland Corner (rkm 439; white line). The dramatic transition in planform brought about by this confinement is strikingly apparent from satellite imagery. Satellite imagery source: Google Earth.

The gradient and width of river valleys are key determinants of available accommodation when valleys are inundated due to sea-level rise (Simms and Rodriguez, 2014). The Murray Gorge is an elongate feature that is relatively narrow, bedrock confined with an extremely low gradient. In addition, the annual discharge is relatively low and the sediment supply tiny. Circumstances such as these are extremely atypical for the terminus of a coastal plain river on the scale of the MDB, which is draining a 1 million km^2 catchment. Normally the relationship between catchment area and valley width is characteristically exponential (Mattheus and Rodriguez, 2011; Simms and Rodriguez, 2014). Consequently, it can be hypothesised that the Holocene sea-level highstand may have exerted an unusually large influence over a significant longitudinal extent of the LMR, with the upstream extent of estuarine palaeo-environments perhaps extending much further inland than normally expected from conventional models of estuarine morphology and development.

1.4 Geomorphic evolution and sedimentary sequences within the LMR and Murray estuary

This section presents a synthesis of publicly available sedimentary data for the region, which has been compiled, analysed and interpreted to produce a geomorphic history for the LMR and Murray estuary. This data has been compiled from a range of sources including historical

geological core logs, historical engineering and geotechnical reports, scientific publications, doctoral theses and historical government-commissioned reports. The geomorphic history presented in this chapter forms the foundation for further analysis within this thesis.

1.4.1   LMR - Blanchetown to Wellington (rkm 282 - 78)

The Murray Gorge is an example of an incised valley which was formed by a relative fall in sea level (Stephenson and Brown, 1989). Sediments within incised valleys clearly depict successive oscillations in sea level (Blum and Törnqvist, 2000), with the LMR's valley fill in the study area comprised of relatively young sediment due to cyclic stripping and subsequent backfilling (Jaksa et al., 2013; Twidale et al., 1978). This is an example of one of two types of incised valleys defined by Dalrymple et al. (1994), with the valley fill comprising sediments of a single cycle of lowstand, transgression and highstand, rather than successive phases of cut and infill. The LMR valley's sedimentary infill comprises two distant facies: (1) the high energy coarse-grained Monoman Formation sands of the lower valley fill, and (2) the low energy fine-grained Coonambidgal Formation clays and silts of the upper valley fill. Firman (1966) described the Monoman Formation a further 300 rkm upstream of Blanchetown where it presents as a braided channel facies, suggesting that these sands were deposited in the initial period of aggradation facilitated by sea-level rise in the late-Pleistocene to early-Holocene. The detailed examination of the Coonambidgal Formation within the Riverine Plain and Mallee Region indicates that these sediments are terraced. The terraces reveal a history of floodplain aggradation and river incision comprising low energy floodplain muds and silts deposited during the mid-Holocene as sea level stabilised to the present-day level (Firman, 1966; 1971; Stone, 2006). Gibson (1958) and Firman (1971a) describe the distinct transition from the lower to upper valley fill as being representative of a time break and climatic change, with some authors suggesting a palaeosol exists at this sequence boundary denoting a transition in channel behaviour and morphology (Clarke et al., 2008; Firman, 1966; Gill, 1978).

In 1931, Taylor and Poole conducted the first comprehensive survey of the swamps that fringe the LMR. Many of the swamps downstream of Mannum (rkm 154) had already been subject to reclamation through levee construction by this time, nevertheless, this account provides a detailed description of the nature of the LMR's floodplain prior to significant anthropogenic modification (Taylor and Poole, 1931). Prior to levee construction, Taylor and Poole (1931) note that the riverbanks between Mannum (rkm 154) and Mypolonga (rkm 130) were typically high creating a natural levee, a feature that was not evident downstream from Mypolonga (rkm 130) to Wellington (rkm 78). Mypolonga (rkm 130) marks the transitional point within the LMR's floodplain from low-lying flats to an unbroken series of swamps (Taylor and Poole, 1931).

Publicly available geological reports obtained from the South Australian Resources Information Gateway (SARIG) database were compiled, analysed and interpreted to provide an overview of the stratigraphy of the LMR. Cross sections were extrapolated from core logs at Blanchetown (rkm 283), Swan Reach (rkm 249), Teal Flat (rkm 179), Murray Bridge (rkm 116), and Monteith (rkm 104; Figure 1.12). At each of these locations, spanning some 179 river kilometres, the upper valley-fill comprises the fine-grained sediments of the Coonambidgal Formation which typically extend across the measured extent of the Murray Gorge. The Coonambidgal Formation is underlain by the lower valley-fill, comprising the Monoman Formation sands, or valley-fringing protrusions of limestone or bedrock. A detailed investigation of the SARIG database and the relevant literature led to the compilation of an extensive dataset of a further 103 sediment cores (SARIG, 2018; Barnett, 1993; Barnett, 1989) and 26 cone penetrometer test soundings (Hubble and De Carli, 2015). Compilation and analysis of this extensive dataset revealed that the Coonambidgal Formation thins markedly with increasing distance upstream with the thalweg of the modern channel incised completely at Blanchetown (rkm 283). The apparent uniformity of the Coonambidgal Formation muds across the valley at these locations suggests a complete absence of fluvial channel sands within the upper valley-fill; any sands present within the top of these cores consist of construction fills placed there for land reclamation or levee construction. The uniformity between locations suggests that these trends in cross-valley stratigraphy may characterise much of the LMR.

The presence of a laminated sequence within the Murray Gorge was first identified by Taylor and Poole (1931) who described alternating layers of grey and black clay throughout the (now reclaimed) backswamps of the LMR from Mannum (rkm 155) to Wellington (rkm 78). The sequence was later described by De Carli and Hubble (2014) within a series of sediment cores obtained on the channel margins between Walker Flat (rkm 212) and Wellington (rkm 78). De Carli and Hubble (2014) interpret an absence of sand lenses within this laminated silt-clay sequence as an indication that this sequence is a depositional feature typical of lacustrine (standing – still water) rather than of fluvial origin. A geomorphic history of the LMR was compiled based on this hypothesis (Figure 1.13; Jaksa et al., 2013), the validity of which will be investigated as part of this study. Specifically, this study will seek to confirm or refute the suggestion that a complete closure of the barrier complex was necessitated for deposition of this laminated sequence. Radiocarbon dates at Mannum (rkm 159, core EFR2) show deposition of the laminated sequence from approx. 6,000 yr BP, and at Monteith (rkm 104, core RG2) from approx. 7,500 yr BP (De Carli et al., 2015). These cores bottom out on laminated mud therefore do not represent the base of the sequence at these locations (De Carli et al., 2015).
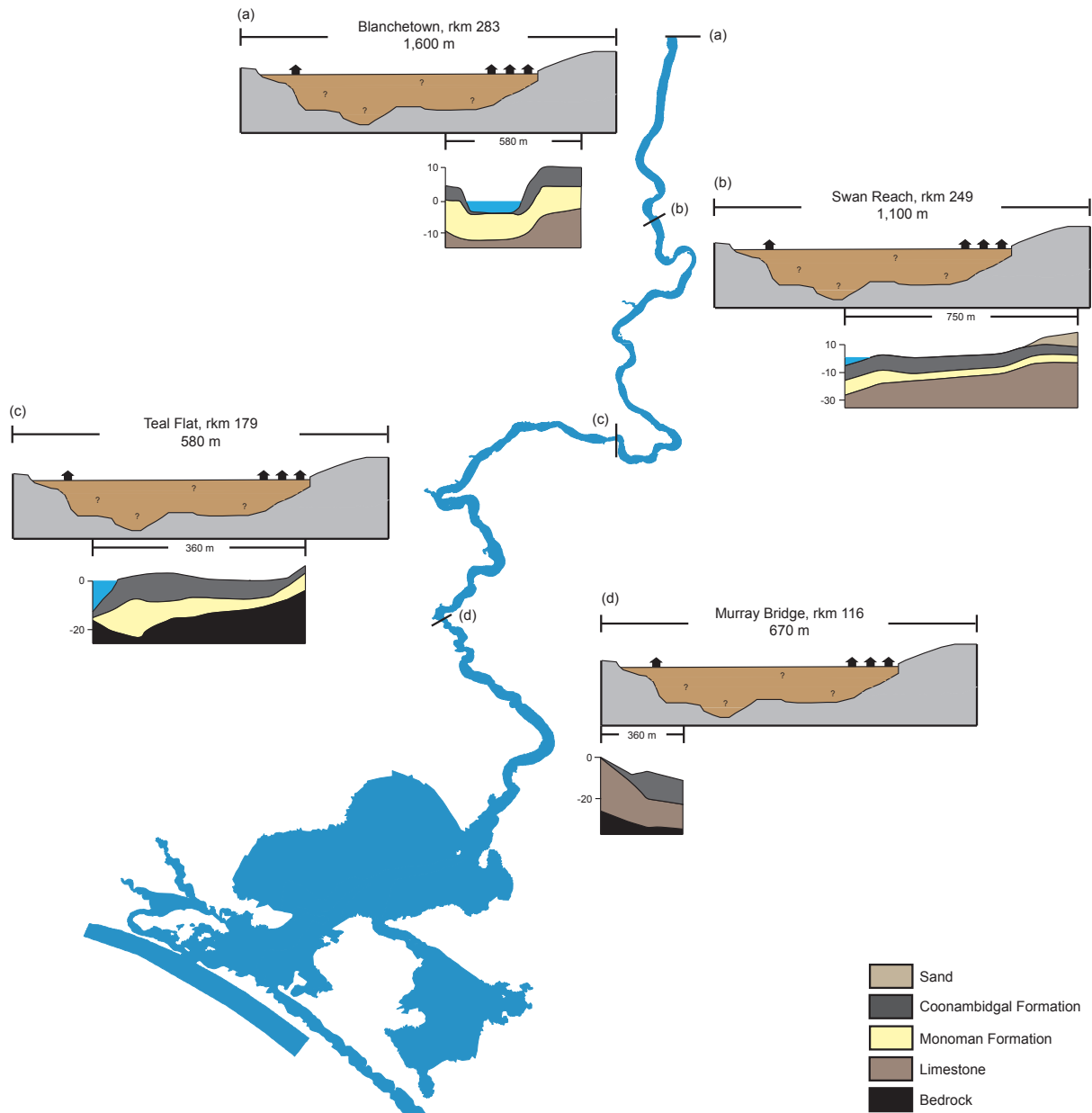
Figure 1.12: Representative geologic cross sections throughout the Murray Gorge. Cross sections, produced from geologic logs of sediment cores on the SARIG database (SARIG, 2019), are given for (**a**) Blanchetown (rkm 283), (**b**) Swan Reach (rkm 249), (**c**) Teal Flat (rkm 179) and (**d**) Murray Bridge (rkm 116). The position of the cross section within the valley is given for reference as cross sections (bottom sub-figure) do not span the entire width of the valley (top sub-figure). The fine-grained sediments of the Coonambidgal Formation characterise the upper valley-fill, with an apparent absence of channel sands evident. Typically, these muds overly the sands of the Monoman Formation, except in the valley fringes were limestone and bedrock protrusions underly the Coonambidgal Formation. Upstream the modern-day channel is incised into the Monoman Formation, with thickness of the overlying Coonambidgal Formation increasing with distance downstream. Cross sections were compiled from sediment cores given in Table 1.1

Table 1.1: Sediment cores used in the creation of geologic cross sections throughout the Murray Gorge. Core logs and geological reports taken from the online SARIG database (SARIG, 2019) were analysed to produce cross sections at Blanchetown (rkm 283), Swan Reach (rkm 249), Teal Flat (rkm 179) and Murray Bridge (rkm 116).

rkm	ID	Name	Easting	Northing	Elevation (m)	Retrieval (m)
283	85831	Blanchetown Bridge 8	372547.0	6198623.0	24.04	19.81
283	85832	Blanchetown Bridge 9	372562.0	6198628.0	14.63	15.24
283	85833	Blanchetown Bridge 1	372577.1	6198633.0	4.56	13.41
283	85835	Blanchetown Bridge 12	372612.0	6198638.0	4.00	30.18
283	85836	Blanchetown Bridge 13	372637.0	6198648.0	4.03	24.38
283	85837	Blanchetown Bridge 2	372677.1	6198653.0	3.07	18.29
283	85876	Blanchetown Bridge 3	372772.0	6198673.0	3.07	14.94
283	85877	Blanchetown Bridge 4	372857.0	6198693.0	3.08	15.24
283	85878	Blanchetown Bridge 10	372882.0	6198698.0	3.12	16.46
283	85879	Blanchetown Bridge 5	372922.0	6198708.0	5.17	24.38
283	85880	Blanchetown Bridge 6	372982.0	6198723.0	10.21	24.38
283	85881	Blanchetown Bridge 11	373142.0	6198758.0	9.97	18.29
249	85459	Swan Reach 2	370984.9	6172001.3	-5.10	30.48
249	85458	Swan Reach 1	371055.9	6172095.2	2.83	30.48
249	85458	Swan Reach 3	371142.9	6172150.2	0.43	27.43
249	85461	Swan Reach 7	371380.9	6172318.2	3.35	18.29
249	85463	Swan Reach 10	371497.9	6172390.2	15.30	21.64
249	85464	Swan Reach 11	371603.9	6172421.2	19.03	26.52
179	85350	Teal Flat PD 17	367001.7	6140188.2	-12.73	3.81
179	85351	Teal Flat PD 16	367006.8	6140173.3	-7.62	4.57
179	85355	Teal Flat PD 15	367011.9	6140158.3	-3.88	17.37
179	85346	Teal Flat PD 19	367016.8	6140148.1	0.73	10.97
179	85362	Teal Flat PD 22	367021.8	6140118.3	2.39	26.06
179	85358	Teal Flat PD 21	367031.9	6140088.2	3.31	23.01
179	85359	Teal Flat PD 22	367042.0	6140058.2	3.24	19.36
179	85356	Teal Flat PD 14	367056.9	6140028.3	1.74	19.81
179	85353	Teal Flat PD 13	367061.9	6139998.2	0.80	14.33
179	85360	Teal Flat PD 12	367086.9	6139938.4	0.16	13.72
179	85352	Teal Flat PD 24	367097.0	6139908.4	0.21	14.17
179	85361	Teal Flat PD 10	367111.9	6139878.3	1.35	10.67
179	85311	Teal Flat PD 26	367116.9	6139848.1	6.42	12.19
116	71353	MB PUMP 6	342697.0	6112971.0	7.99	19.51
116	71352	MB PUMP 5	342737.0	6113023.0	0.36	24.38
116	71350	MB PUMP 4	342770.0	6113018.0	1.14	30.48
116	71348	MB PUMP 2	342824.0	6113068.0	-3.24	12.65

Diagrammatic Sketches - Whole Valley   Time and/or Event

120,000 years ago, interglacial highstand sealevel slightly higher than present day Valley filled with sediment and channel developed similar to present day.

~20,000 years ago, glacial maximum and sealevel is ~120 m lower than present day Valley stripped of alluvial fill - Extremely arid conditions but large winter snow pack on the eastern highlands. Murray drainage confined within bedrock gorge wall.

~15,000 years ago, icesheets begin to break-up and melt, sealevel rises rapidly and climate warms. Lower valley back-filled with coarse sediment. Forests re-establish across much of the Murray-Darling Basin. Braided multi-channel stream & sand plain developed within lower Murray gorges.

~12,000 to 7,000? years ago, sealevel rises from about 50m below present day levels to just above present day levels; a large, long lake develops within lower Murray gorges behind a beach-barrier system that isolates the river from the ocean.

~3,000 years ago, sealevel stable at present day level, the lower Murray lake continues to trap fine sediment - eventually the gorges fill to their current level, producing the present day Lower Murray 'floodplains'.

~1,000 years ago, the lower Murray 'floodplain' formed and exit to ocean re-established. Murray river channel occupies present day position and excavation of the channel commences. Initial channel narrow & shallow.

Present day, landscape modified by Europeans firstly for intensive agriculture and then for residential and recreational use. Channel cross-section wider and deeper, possibly with equilibrium cross-section at the time of the European modifications, more probably river still eroding - note fill placement and levee building.

Figure 1.13: Hubble and De Carli's proposed geomorphic evolution of the LMR and its floodplain over the past 120,000 years. Cross sections represent a generalised interpretation of sedimentation between Mannum (rkm 154) and Murray Bridge (rkm 115; after Jaksa et al., 2013).

1.4.2   Pomanda Embayment (rkm 77-66)

The LMR currently debouches into its terminal lakes, Alexandrina and Albert, at the Pomanda Embayment. The absence of a deltaic complex at the terminus of a channel draining such a large catchment has led some authors to describe it as a 'failed delta' (Murray-Wallace et al., 2010). Instead, there is merely a small digitate delta which has developed at the Pomanda Embayment and indicates the downstream extent of fluvial deposition (Jaksa et al., 2013; Murray-Wallace et al., 2010). The structure has not been investigated in any detail but is generally thought to be a modern feature developed in response to significant anthropogenic modification of the tidal and flow regimes.

1.4.3   Lake Alexandrina (rkm 65-39)

The record of sedimentation in Lake Alexandrina presents the evolution of the estuary as the central basin slowly infilled (Figure 1.14). The LMR's thalweg is apparent both in the modern-day bathymetry and throughout the Holocene stratigraphy, with the laminated sequence thickest within this thalweg and main lake body and absent or less prevalent in the shoreline fringing regions (Figure 1.14; Barnett, 1993). An examination of Barnett's (1993) core logs within Lake Alexandrina suggests that deposition of the laminated sequence was regionally extensive from 5,500 yr BP until present. It is possible that a laminated sequence was deposited in the LMR's palaeo-channel within modern-day Lake Alexandrina prior to 5,500 yr BP as Barnett's (1993) cores within the palaeo-channel bottom out on laminated mud (Figure 1.15).

Estuarine sedimentation within the palaeo-Murray thalweg of Lake Alexandrina commenced prior to the sea-level highstand and became regionally extensive as the rising sea level caused widespread inundation (Barnett, 1993). Deposition prevailed until approximately 2,300 yr BP when a shift from clay to silty deposition and sand pulses indicates a transition to widespread lacustrine sedimentation (Barnett, 1993). Barnett (1993) attributed this shift to the progressive infilling of the lowest lying portions of the central basin environment.

The greatest Holocene extent of Lake Alexandrina is indicated by the Malcolm soil combination which comprises fine grained (up to 70% clay) estuarine and lacustrine sediments (Figure 1.16). de Mooy (1959) attributes the mode of deposition to be estuarine, with isolated areas of lacustrine-like conditions in shallow embayments to the east of Lake Alexandrina. Deposition is thought to have occurred in the relatively sheltered environment afforded by the postulate newly developed barrier complex (de Mooy, 1959). The stratigraphy of the Cooke Plains Embayment suggests that this region was a former extension of Lake Alexandrina at a time when lake levels were higher and the area of inundation larger than today (Figure 1.16). Von der Borch and Altmann (1979) suggested that, at its largest size, Lake Alexan-
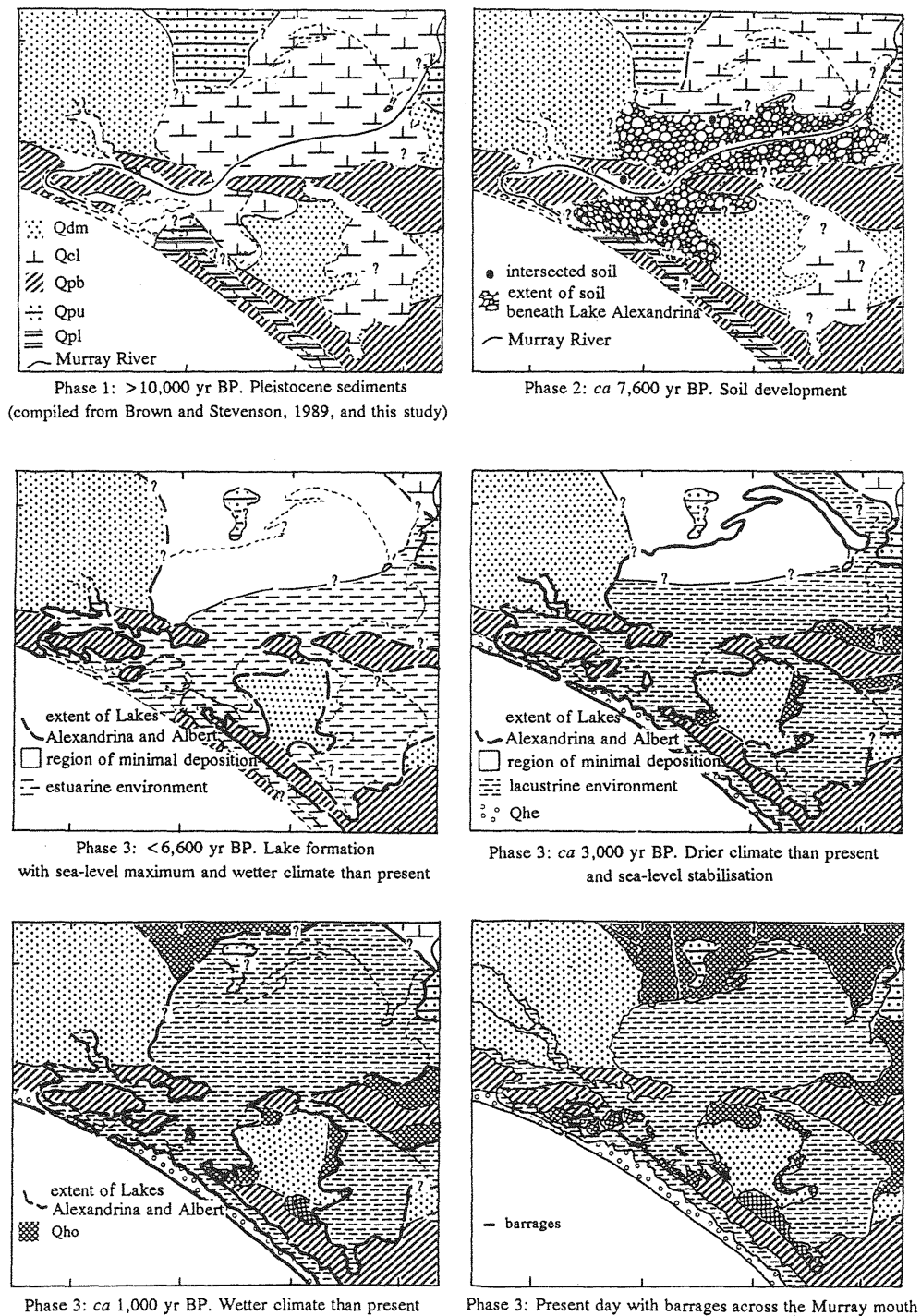
Figure 1.14: Evolution of sedimentary environments within Lake Alexandrina during the Holocene. (**i**) LMR continuing to erode to base level in response to low sea level. (**ii**) Lakes Alexandrina and Albert form in response to a rapidly rising sea level. (**iii**) The Lower Lakes reach their greatest extent at the Holocene sea-level highstand, with Lake Alexandrina inundating the Cook Plains Embayment. (**iv**) Lake levels begin to recede as the climate dries and sea level recedes to present day level. (**v**) A period of greater lake levels in response to wetter climate. (**vi**) Anthropogenic modifications, including the installation of barrages, artificially hold lake levels at 0.75 m, curtailing estuarine sedimentation within the lakes and instead restricting it to the flood tide delta and Coorong lagoon. (after Barnett, 1993).
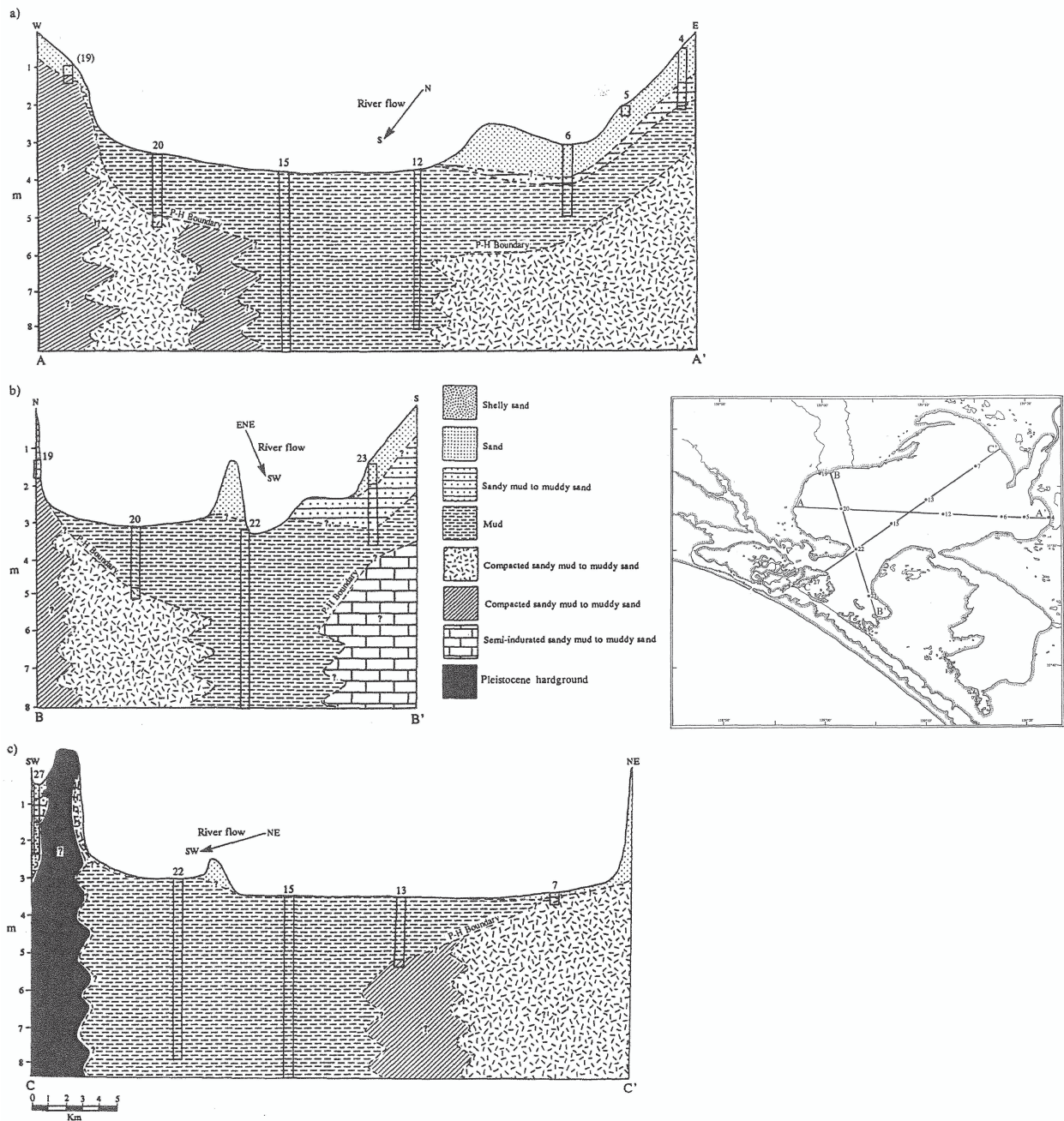
Figure 1.15: Lake Alexandrina sedimentary cross sections. (Cross sections created by combining three transects of sediment cores collected within the main body of Lake Alexandrina. Together they reveal the extent of the laminated mud, with cores bottoming out on this sequence within the palaeo-thalweg. (after Barnett, 1993).

drina occupied the Cooke Plains Embayment during the early- to mid-Holocene. This is attributed to a combination of sea-level highstand backfilling into the region, and fluvial discharges brought on by a worldwide humid pluvial period between 8,000 – 5,000 yr BP (Von der Borch and Altmann, 1979).
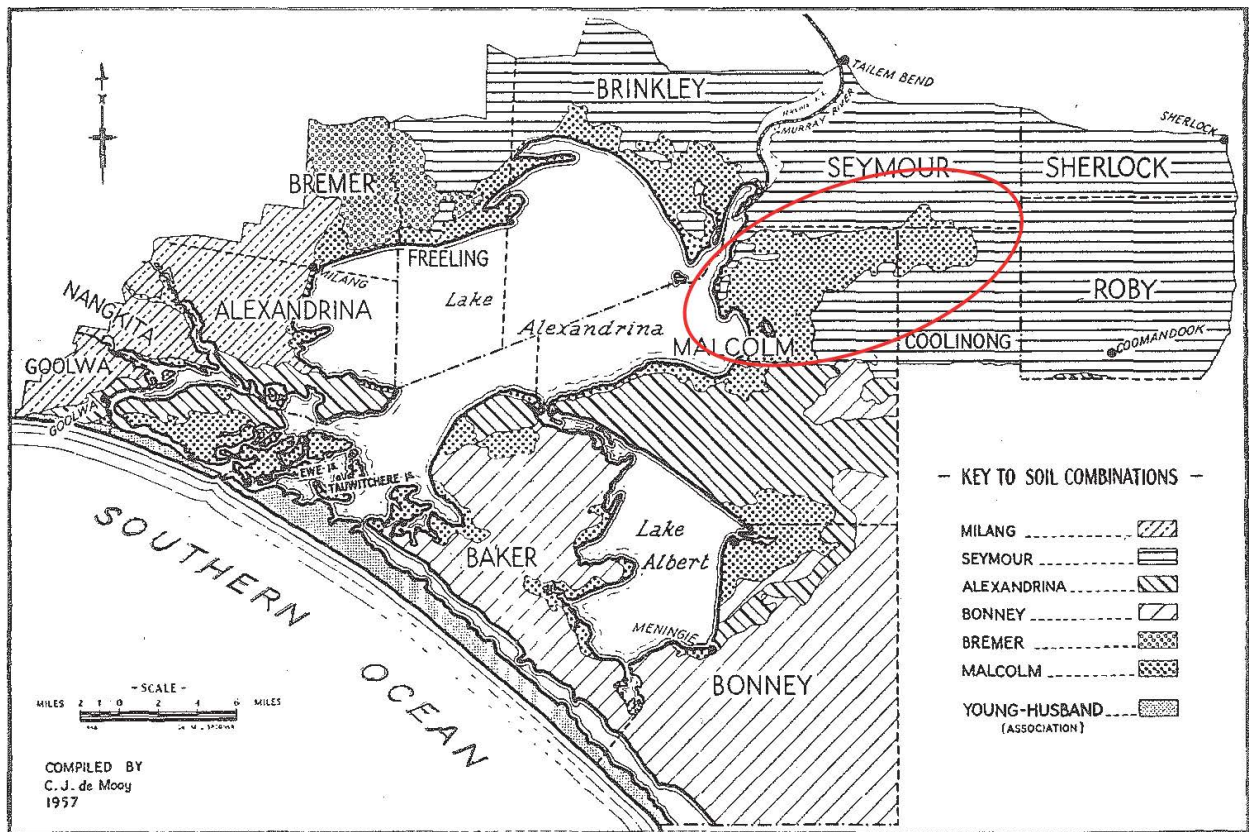
Figure 1.16: Extent of the Malcolm Soil Combination. (The Malcolm soil combination (dotted) is considered indicative of the greatest Holocene extent of Lake Alexandrina. (after de Mooy, 1959).

1.4.4   Murray Mouth, flood tide delta and barrier complex (rkm 38-0)

The Murray estuary's barrier complex began formation in response to a rapidly rising sea level at approximately 8,000 yr BP and is built upon the site of washover facies from a pre-existing, older dune complex developed during the previous highstand (Bourman and Murray-Wallace, 1991). Numerous authors suggest that the present-day barrier evolved from a chain-of-islands into the two unbroken peninsulas that are extant today (Bourman and Murray-Wallace, 1991; de Mooy, 1959; Harvey, 2006; Luebbers, 1982). Bourman and Murray-Wallace (1991) and de Mooy (1959) identify former outlets to the ocean and constrain plausible phases of this chain-of-islands evolution based on stratigraphy, including evidence of a former flood-tide delta, and the distribution and ages of Aboriginal middens (Figure 1.17). Bourman and Murray-Wallace (1991) conclude that the eastern half of Sir Richard Peninsula is significantly younger and may have been the location of a former Murray Mouth. Locations of prior outlets to the ocean have been proposed on Sir Richard Peninsula west of Goolwa Beach and 3.5 km west of the present day Murray Mouth opposite Swan Point, as well as on Younghusband Peninsula opposite Mulloway Point (Bourman and Murray-Wallace, 1991; de Mooy, 1959).
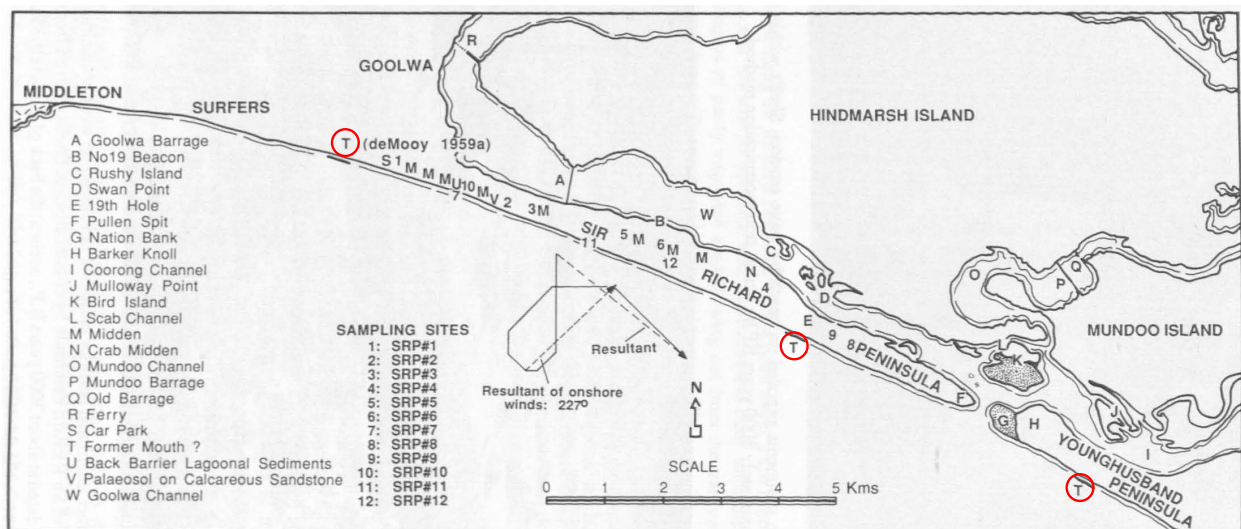
Figure 1.17: Proposed former outlets of the Murray Mouth. (Proposed former outlets of the Murray Mouth (T) from the work of Bourman and Murray-Wallace (1991) and de Mooy (1959; after Bourman and Murray-Wallace, 1991).

Throughout the late-Holocene the Murray Mouth was highly dynamic migrating over 6 km laterally and fluctuating in both width and depth (Bourman and Murray-Wallace, 1991). The dynamic nature of the Murray estuary's flood tide delta and barrier complex may have allowed for the Murray Mouth to have been intermittently opened and closed throughout the late-Holocene as has occurred in recent times, for example, the complete closure in 1981

(Bourman and Harvey, 1983; Bourman and Murray-Wallace, 1991). Closure is facilitated by periods of reduced fluvial discharge and a combination of aeolian drift of material delivered to the shoreface by waves (Bourman and Harvey, 1983; Bourman and Murray-Wallace, 1991; Walker and Jessup, 1992).

1.5   Thesis outline

This thesis investigates the response of the Murray estuary to the Holocene sea-level high-stand through complementary hydrodynamic modelling and sedimentologic studies. This thesis comprises three discrete but closely related research chapters in which each chapter is structured as a manuscript suitable for journal submission. Each of these three core chapters seeks to address the overarching aims and objectives of the thesis and to build upon each other.

This chapter (Chapter 1) provides an introduction to the thesis and outlines the aims of the thesis by contextualising the study through a review of the relevant literature and sedimentary data, which identifies current gaps in understanding. An extensive dataset comprising sedimentary data and records is developed, analysed and interpreted to produce a geomorphic history for the LMR and Murray estuary. Chapters 2, 3 and 4 each contain an introductory section with an additional discussion of the literature relevant to that chapter.

Chapter 2 investigates the response of the Murray estuary to the Holocene sea-level high-stand. This is achieved through a hydrodynamic modelling approach with a sensitivity analysis to constrain the palaeo-environments that prevailed in the mid-Holocene. This chapter also considers potential future responses to climate-change induced sea-level rise on coastal plain estuaries more broadly.

Chapter 3 evaluates the suitability of adopting 2D hydrodynamic models to evaluate real-world estuarine responses by performing a methodological analysis comparing results obtained from a series of 2D and 3D hydrodynamic modelling approaches. A small component of this material was also presented in the supplementary materials for Chapter 2.

Chapter 4 investigates the Holocene geomorphic evolution of the Murray estuary through complementary hydrodynamic modelling and sedimentology. The location chosen for the sedimentary component of this study was informed from the results of hydrodynamic modelling presented in Chapters 2 and 3. Best-estimate mid- to late-Holocene 3D hydrodynamic models are constrained by a well-dated 30 m long sediment core and a valley-wide transect of cone penetrometer soundings taken from the central basin of the Holocene estuary. The extent, nature and development of the Murray estuary is evaluated, and the timing of major

changes in the depositional and hydrological response of the LMR to sea-level change is determined.

Finally, Chapter 5 provides a synthesis of the results from each chapter, drawing together new understanding gained to present conclusions in the context of the thesis as a whole. Suggestions are also given for future work.

Chapter 2

Modelling Holocene analogues of coastal plain estuaries reveals the magnitude of sea-level threat

2.1 Abstract

Hydrodynamic modelling of Australia's lower Murray River demonstrates the response of a large coastal plain estuary to the mid-Holocene (7,000 – 6,000 yr BP) sea-level highstand. The approximately two metre higher-than-present sea level during the highstand forced the estuarine limit upstream generating an extensive central basin environment extending more than 200 kilometres from the river mouth (143 kilometres upstream of the modern tidal limit). The geomorphic history of the region does not conform to conventional estuarine facies models as, for much of the Holocene, the lower Murray River acted as a landward, gorge-confined extension of the Murray estuary. The incredibly low relief of this coastal plain system drove significant saline incursion and limited current velocities across the estuary facilitating deposition of a laminated silt-clay sequence which results suggest may be regionally extensive. Variations to discharge, barrier morphology, or the estuary's bathymetry result in minimal change to the estuarine palaeo-environment. The shift to the present-day fresher water distribution in the Murray estuary requires a fall in sea level to present-day conditions. The dominance of sea level as the controlling factor on this estuarine palaeo-environment highlights the significant potential impact of climate change induced sea-level rise to coastal plain estuaries.

2.2 Introduction

Coastal plains and lowlands are characterised by their low gradient and commonly dense populations, with geomorphic-based risk assessments revealing their significant vulnerability

to future climatic change (Rogers & Woodroffe, 2016). Inundation associated with an increase in mean sea level threatens communities, coastal infrastructure and ecosystems, with estuaries vulnerable to the compounding influences of storm surges and strong winds, along with implications of saline incursion for irrigation and drinking water supply (Reisinger et al., 2014). Indeed, in Australia, flooding is considered the most significant medium-term climate change hazard, with a shift to coastal inundation beyond mid-century (Baynes et al., 2012; Reisinger et al., 2014). There is, however, less emphasis on the consequences of rising sea levels for saline intrusion, particularly for low-gradient coastal plain estuaries.

The Intergovernmental Panel on Climate Change (IPCC) projects that global mean sea level will rise by 0.53 – 0.97 m by 2100 under a high emissions scenario, with these projections likely to be exceeded by at least 10% in Australia (Reisinger et al., 2014). Crucially, even given a stabilisation in temperatures, global mean sea level will continue to rise for several centuries beyond 2100 (Reisinger et al., 2014). Understanding the dominant drivers of environmental change within an estuarine system allows for effective management given uncertainties in future mean sea level, determination of palaeo-environmental responses to the Holocene highstand provides a useful analogue of expected change. There is a pressing need for palaeo-environmental analysis in economically significant regions to direct future natural resource management policies, particularly in intensively managed environmental systems. Developing appropriate management strategies that negate the detrimental impacts forecast in climate change projections is particularly important for lowland coastal plains where rising sea levels will undoubtedly cause problematic inundation and saline intrusion. Applying Holocene analogues to future sea-level rise scenarios is a well-recognised approach to predicting responses of coastal systems to climate change (Blum & Tornqvist, 2000; Woodroffe & Murray-Wallace, 2012). Here the LMR and Murray estuary is used as a case study to demonstrate the utility of understanding Holocene analogues to plan for potential environmental change in coastal plain estuaries.

Understanding fluvial and estuarine responses to sea-level cycles through their associated depositional systems tracts may assist in predicting potential impacts of future sea-level rise. Research has shown that fluvial systems attempt to keep pace with changing base level, with shoreline advance or retreat controlling available accommodation and causing a shift in the nature and location of estuarine processes and depositional environments (Blum & Tornqvist, 2000). There is a significant body of literature detailing the influence of Holocene sea-level change on the sedimentary infill and evolution of estuaries on the east coast of Australia (Roy & Thom, 1981; Sloss et al., 2006a; Sloss et al., 2006b; Sloss et al., 2010; Thom & Roy, 1985; Umitsu et al., 2001), however, few studies specifically examine southern coast Australian estuaries, such as the Murray estuary (e.g. Cann et al., 1999; Belperio et al., 1983; Harvey, 2006). The Murray estuary lies at the terminus of the MDB, Australia's largest and most politically and economically important river basin (Figure 2.1). The geo-

morphic and palaeo-environmental history of the region has been the subject of much debate, driven by the reliance on Holocene climatic and hydrologic reconstructions to guide nationally significant water policy (Mills et al., 2013a). This wave-dominated estuary, comprising the Lower Lakes, Coorong and Murray Mouth, is situated on a low-gradient coastal plain and developed in response to slowing sea-level rise during the transgressive period of the early- to mid-Holocene (Bourman et al., 2000; Fluin et al., 2009; Hill et al., 2009). The Murray estuary's barrier complex, comprising Sir Richard and Younghusband Peninsulas, began formation at approximately 8,000 yr BP, allowing for the development of the central basin lakes, Alexandrina and Albert, prior to the Holocene highstand at 7,000 – 6,000 yr BP (Figure 2.1; Belperio et al., 2002; Bourman et al., 2000; Fluin et al., 2009; Harvey et al., 2002; Hill et al., 2009; Lewis et al., 2013).

Upstream, the LMR is entrenched within the Murray Gorge (from Overland Corner to Wellington, Figure 2.1), with the valley fill comprising sediment of the most recent cycle of lowstand, transgression and highstand only (Blum & Tornqvist, 2000; Twidale et al., 1978). This consists of two distinct facies: 1) the Monoman Formation's coarse-grained sands comprise the lower valley fill, and 2) the Coonambidgal Formation's fine-grained clays and silts comprising the upper valley fill. The Holocene infill of Lake Alexandrina is known as the St Kilda Formation, and is a finely laminated silt-clay sequence (Barnett, 1993; 1994). Deposition of this sequence had commenced by at least 8,000 yr BP (Barnett, 1993; 1994); however, it is probable that deposition within the palaeo-channel that transited through modern-day Lake Alexandrina had commenced prior to 8,000 yr BP as dated cores within this area bottom out on laminated mud. The St Kilda Formation was regionally extensive from 5,500 yr BP and has characterised the sediments of Lake Alexandrina ever since (Barnett, 1993; 1994).

Standing water or very weak current velocities are required for the deposition and preservation of a laminated silt-clay sequence (Schieber & Yawar, 2009). However recent flume studies have demonstrated mud floc deposition as distinct laminae in current velocities up to 0.3 m/s, with laminae accumulation considered possible at higher velocities given particularly high sediment concentrations (Baas et al., 2016; Schieber et al., 2007; Schieber & Southard, 2009). Laminations such as those present throughout Lake Alexandrina are undoubtedly a product of low energies and high sedimentation rates (Allen, 2004), features characteristic of central basin environments (Devoy et al., 1994). Indeed, wave-dominated estuaries are known for their well-defined tripartite zonation of facies assemblages with lithofacies typically presenting a coarse-fine-coarse sequence: the marine sands of the barrier complex and flood-tide delta, the clays and silts of the central basin, and the fluvial sands of the bayhead delta and river channel (Dalrymple et al., 1992). Conventional presentations of estuarine models indicate the point where the river debouches into the lagoon locates the transition to reduced energy and defines the landward extent of the central basin and seaward extent of the bayhead delta. However, the contentious Holocene palaeo-salinities of the Lower Lakes
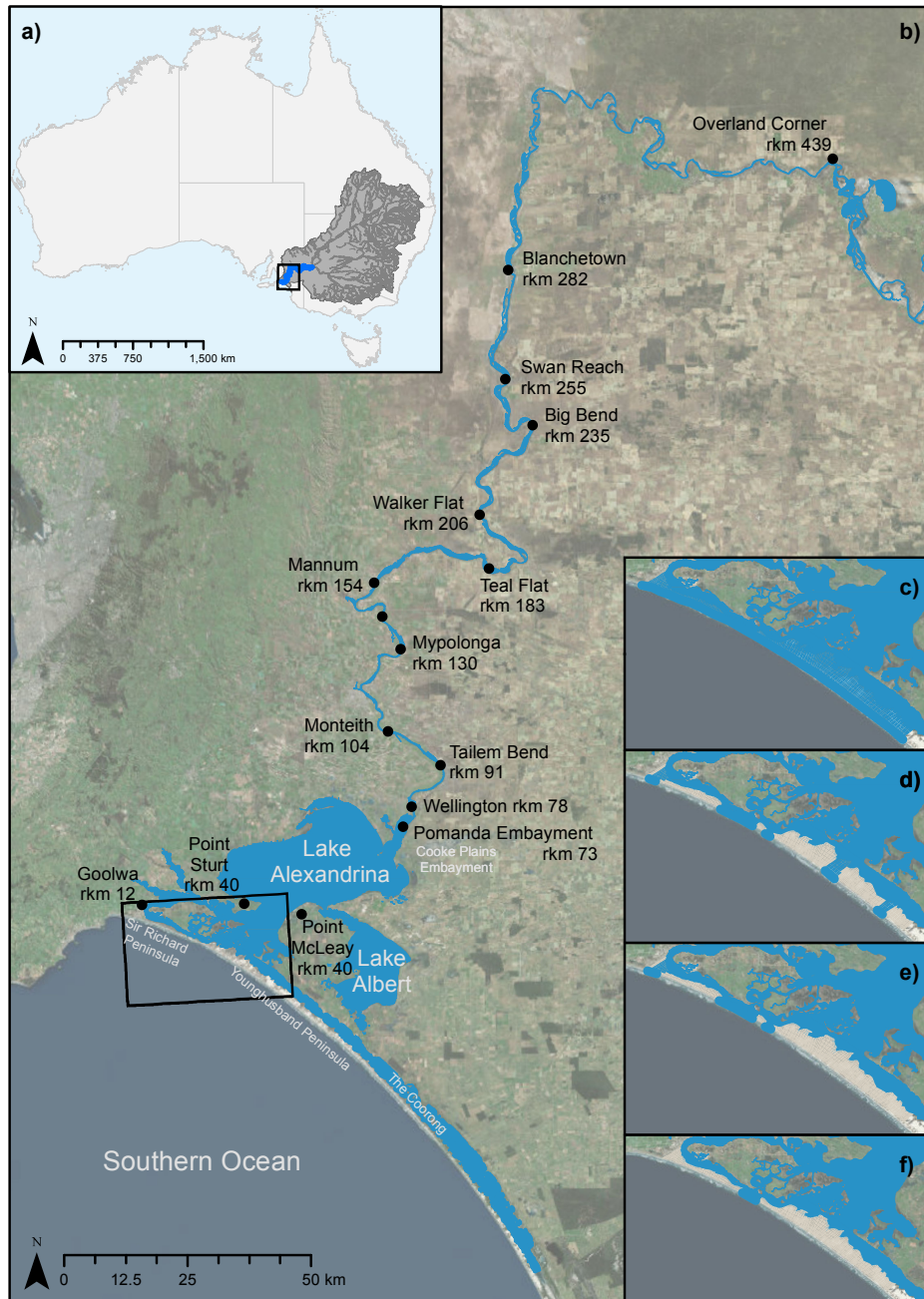
Figure 2.1: Study area and modelled barrier morphologies. (**a**) The Murray Darling Basin (grey) is Australia's largest and most politically and economically important river basin. The Murray Darling Basin comprises the Darling and Murray River catchments, whose major watercourses are shown in dark grey. The lower Murray River (blue) is the final segment of this system flowing from the confluence of the Darling and Murray Rivers at Wentworth, New South Wales to the Murray Mouth at Goolwa, South Australia. (**b**) Within South Australia, the lower Murray River flows through the confines of the Murray Gorge from Overland Corner to Wellington before debouching into Lake Alexandrina at the Pomanda Embayment. The lower Murray River reaches the Southern Ocean at the Murray Mouth between Sir Richard and Younghusband Peninsulas. Collectively, Lakes Alexandrina and Albert are known as the Lower Lakes, and together with the Coorong and Murray Mouth, form the modern-day Murray estuary. The four modelled barrier morphologies, accounting for the chain-of-islands Holocene evolution of Sir Richard and Younghusband Peninsulas (Bourman & Murray-Wallace, 1991; de Mooy, 1959; Harvey, 2006; Luebbers, 1982), are depicted by outlets to the ocean (blue) and barrier formation (brown) in (**c**) B_0; (**d**) B_+; (**e**) B_{++}, with (**f**) B_{mod} representing the modern-day Murray Mouth. Satellite imagery source: Esri.

give rise to debate on the extent and character of the Murray estuary. Some place the up-stream extent of this estuary at the Pomanda Embayment, where the LMR debouches into Lake Alexandrina (rkm 73, Figure 2.1; Hill et al., 2009), with other authors even suggesting that the Lower Lakes were freshwater stilling basins for the duration of the Holocene and cannot be classified as part of this estuarine zone (Fluin et al., 2009).

In this chapter, the range of possible responses of the palaeo-Murray estuary to the Holocene sea-level highstand is evaluated. Specifically, this chapter will:

- Conduct hydrodynamic modelling of the palaeo-Murray estuary and LMR with sensitivity testing for discharge, bathymetric surface and barrier morphology with results analysed for inundation extents, water heights and depths, flow velocity and salinity.

- Assess the palaeo-environment that likely prevailed during the Holocene highstand and correlate model scenarios with geomorphic and sedimentary features of the region to develop a model of estuarine processes zonation and inferred resulting morphology.

- Assess the relative influence of geomorphic and hydrologic drivers on the estuary during the Holocene sea-level highstand.

- Propose the palaeo-Murray estuary, as a possible end-member exemplar of an extremely low-gradient coastal plain estuary, to demonstrate the significant threat of sea-level rise due to climate change on the environmental character of coastal plain estuaries. Particular reference is given to the understated potential impact of climate change-induced saline intrusion on the character and extent of coastal plain estuaries.

2.3   Methodology

2.3.1   Overview of model result categories

The study area encompasses the LMR from Blanchetown (rkm 282) downstream to the barrier complex and modern-day Murray Mouth (Figure 2.1). Using TUFLOW FV, a 2D finite volume numerical model, 72 scenarios are simulated and sensitivity testing is conducted for bathymetric surface (two end members and a best estimate), sea level (Holocene highstand and present-day), discharge (drought, pre-regulation average, and flood), and barrier morphology (four scenarios, ranging from completely open to almost closed, to account for barrier evolution). Results are grouped into six categories based on bathymetric surface and sea level (Table 2.2). The Pleistocene-Holocene stratigraphic boundary and pre-regulation surfaces represent bathymetric end-members to constrain the entire range of plausible bathymetries at the Holocene highstand; these are denoted as S_{low} and S_{up} respectively. A best estimate of bathymetry at the Holocene highstand is given by the S_{mid} surface. Accounting for the approximately 2 m variance in sea level between the Holocene highstand and present day gives

the six modelled categories: $S_{low}WL_2$, $S_{low}WL_0$, $S_{mid}WL_2$, $S_{mid}WL_0$, $S_{up}WL_2$ and $S_{up}WL_0$ (Table 2.2). For each of these six categories, the possible combinations of discharge and barrier morphology were modelled. The three discharge scenarios of drought, pre-regulation average and flood are denoted by D_-, D_{av} and D_+ respectively (Table 2.2). The four barrier morphologies of completely open, two evolutionary phases, and modern-day are denoted by B_0, B_+, B_{++} and B_{mod} respectively (Figure 2.1 c-f; Table 2.2). Inundation extents, water heights and depths, flow velocities and salinities are obtained for the full extent of the LMR and Murray estuary for each of the 72 modelled scenarios.

2.3.2   Numerical model set up

Hydrology is simulated using TUFLOW FV, a 2D finite volume numerical model. The model domain spans some 282 rkm from Lock 1 at Blanchetown to the Murray Mouth and extending 2 km offshore. A base model was provided by BMT WBM and was the subject of vigorous calibration (Hudson, 2010; Supplementary methods: Model calibration). Stitched topography and bathymetry for the region was developed by the Commonwealth Scientific and Industrial Research Organisation (CSIRO; Austin & Gallant, 2010) and provided by the Department of Environment Water and Natural Resources (DEWNR) for use in this study. Outside the extent of this dataset (1956 flood extent), a 1 second Digital Elevation Model (DEM), provided by Geoscience Australia (GA), was applied and the two datasets interpolated together using ArcGIS. This mesh was then modified to extend the model domain to encompass the entire width of the Murray Gorge, as well as the inclusion of the modern-day barrier complex and extension of the Lower Lakes based on the palaeo-maximum inundation shoreline and Holocene estuarine stratigraphy (de Mooy, 1959; Murray-Wallace et al, 2010; Von der Borch & Altmann, 1979). Tides were imposed based on historical data taken from Victor Harbour between 1st January – 28th February 2014 to remove the uncertainties associated with tidal prediction (Figure 2.2). Drought (D_-) and pre-regulation average (D_{av}) scenarios were run for 20 days while flood (D_+) scenarios were run for 31 days, which was a sufficient period for models to run beyond the spin-up phase and reach steady state, as confirmed by a review of hydrograph phasing. An example timeseries for the $S_{mid}WL_2D_+B_{mod}$ scenario is given in Figure 2.3 showing water heights within the upstream (rkm 175) and downstream (rkm 79) portions of the LMR, as well as further through the system within Lake Alexandrina (rkm 39). The timeseries depicts a return to pre-flood water heights demonstrating that the simulation run time is sufficient (Figure 2.3). All models were run at a 5 minute timestep. A comparative analysis of 24 and 1 hour outputs confirmed that the 24 hour outputs were representative and, to save computational time, were applied to all scenarios. Initial salinity was applied at each cell based on salinity data taken from 25 gauging stations throughout the region at the peak of the Millennium drought. This was deemed appropriate as the barrages are in place to curtail saline intrusion and therefore

regional salinities are held fresher than would naturally occur.
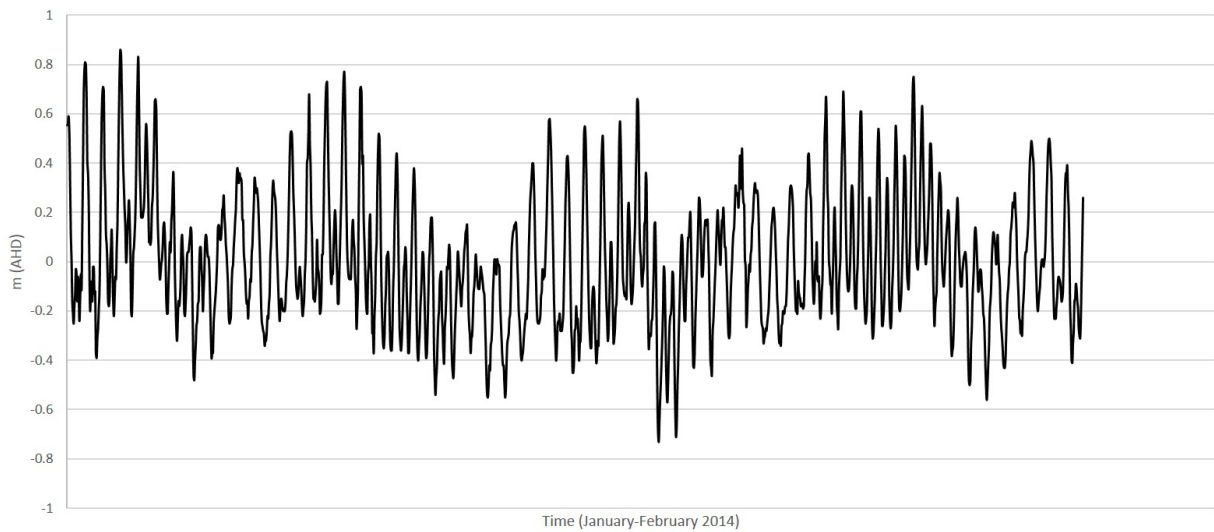
Figure 2.2: Tidal dataset adopted in this study. Data obtained from the Victor Harbour tidal gauge 01/01/2014 – 28/02/2014.
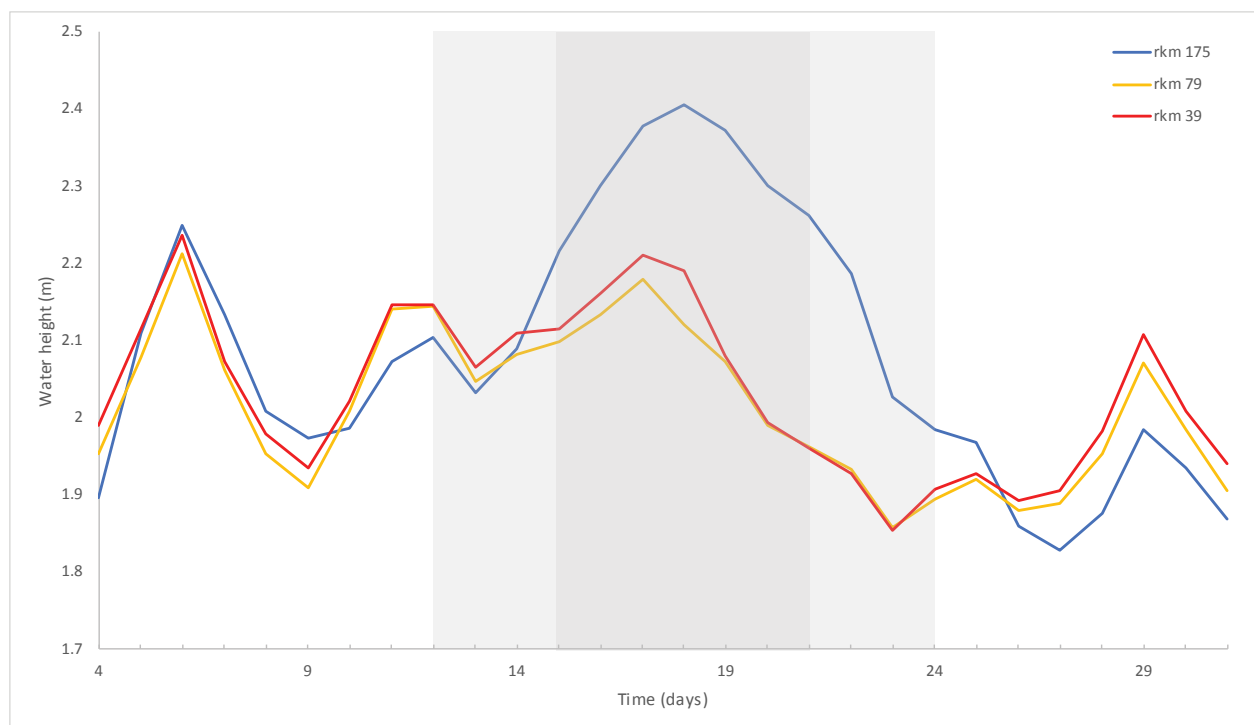
Figure 2.3: An example timeseries for scenario $S_{mid}WL_2D_+B_{mod}$. Dark grey indicates the time period subject to peak flood discharge (D_+), with light grey indicating the lead up from, and return to, D_{av} discharge. Water heights are given both within the upstream portion of the LMR near Teal Flat (blue line, rkm 175) and the downstream portion at Wellington (orange line, rkm 79), as well as further through the system within Lake Alexandrina (red line, rkm 39).

Estuarine stratification can cause a salt wedge at depth which cannot be resolved by a 2D

simulation. The presence of a salt wedge has the potential to alter inferences drawn from estuarine zonation and the likelihood of deposition of a laminated sequence whereby flocculation may be assisted by salinity. The scale of the study area, with the model domain spanning some 282 river kilometres, precluded the use of a 3D model setup without justification as the computational power to run such a simulation is ten times that of its 2D counterpart. Therefore, a representative subset of models were run in 3D to assess the suitability of adopting 2D models for this study. This representative subset of models allowed for a comparative assessment of 2D and 3D results for all bathymetric surfaces ($S_{low}WL_2D_{av}B_{mod}$, $S_{mid}WL_2D_{av}B_{mod}$ and $S_{up}WL_2D_{av}B_{mod}$), both sea level scenarios ($S_{mid}WL_2D_{av}B_{mod}$ and $S_{mid}WL_0D_{av}B_{mod}$), all discharge scenarios ($S_{mid}WL_2D_-B_{mod}$, $S_{mid}WL_2D_{av}B_{mod}$ and $S_{mid}WL_2D_+B_{mod}$) and all barrier morphologies ($S_{mid}WL_2D_{av}B_0$, $S_{mid}WL_2D_{av}B_+$, $S_{mid}WL_2D_{av}B_{++}$ and $S_{mid}WL_2D_{av}B_{mod}$).

3D simulations retained the same model setup with the inclusion of a parametric vertical mixing model with a second order vertical solution and density coupled salinity. A comparative analysis of results suggests that 2D simulations are sufficiently representative of 3D simulations (Figure 2.4). Minor differences in maximum salinity reached across the region does not alter the designation of the palaeo-environment with 2D simulations providing a conservative approximation of 3D results (Figure 2.4a-b). Crucially, the brackish limit (i.e. 1 psu) differed by a maximum of 1 rkm between 2D and 3D depth averaged results, with the exception of the pre-regulation (S_{up}) surface where the 3D simulation captured a salt wedge that penetrated 6 rkm further upstream ($S_{up}WL_2D_{av}B_{mod}$ scenario). A negligible change in the total area conducive to the deposition of a laminated sequence was also observed, with 2D simulations overestimating this area by an average of 4%, demonstrating that 2D approximations of 3D velocity magnitudes are appropriate (Figure 2.4c-d).

Following a significant period of prolonged drought, BMT WBM were commissioned by the MDBA to perform a feasibility study assessing the adoption of a virtual weir at Wellington (rkm 78) to provide an adequate fresh water supply for the region. The study involved the establishment, calibration and validation of a hydrological model encompassing the LMR and Lower Lakes region downstream of Blanchetown (rkm 282, Lock 1). A validation dataset was collected, and the model calibrated for hydrodynamics - including water level, wind and river fluxes – and salinity. Model calibration adequately resolved short term (i.e. a single extreme saline intrusion event) and long term (i.e. entire 17 month dataset) trends.

Owing to the long-term temporal scale of modelling estuarine response to sea level change over the course of the mid- to late-Holocene, simplifications need to be applied based on best estimate assumptions to guide parameters for sensitivity testing. The model set up adopted in this study seeks to apply 'appropriate complexity' balancing a reductionist approach to input data based on geological correlation, to produce outputs which are computationally efficient yet meaningful (de Vriend et al., 1993; French et al., 2016). Model manipulation and
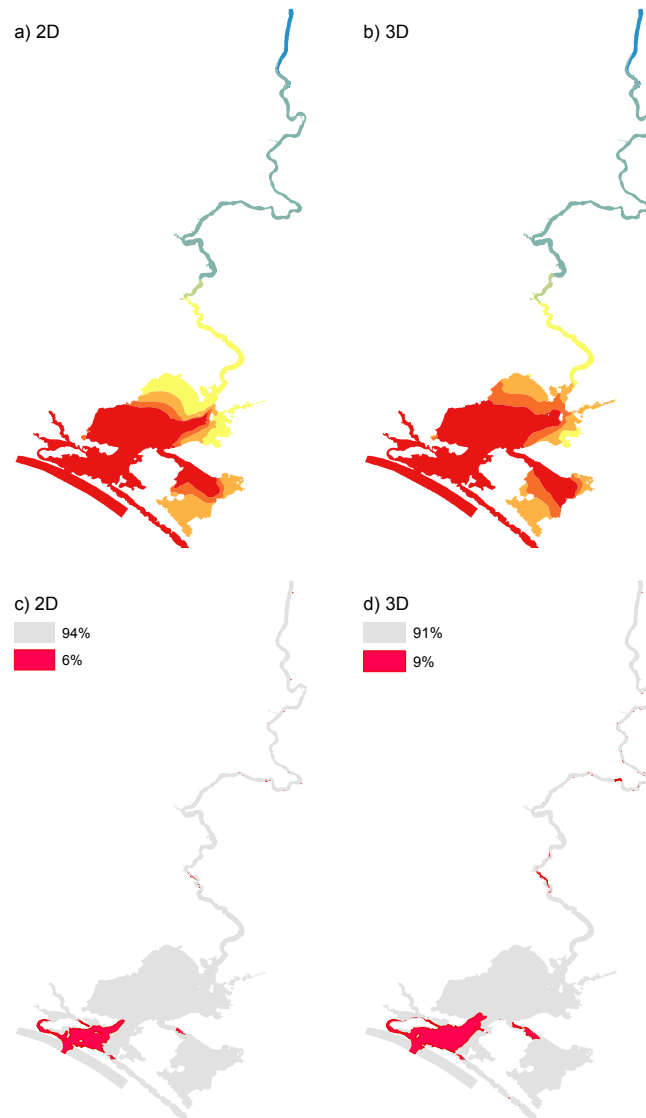
Figure 2.4: Comparison of $S_{mid}WL_2D_{av}B_{mod}$ 2D and 3D key outputs of maximum salinity and velocity magnitude. Maximum salinity reached in a best estimate Holocene highstand (**a**) 2D simulation is comparable to that of a (**b**) 3D simulation such that the classification of estuarine zonation remains consistent. 2D simulations provide a conservative approximation of 3D results. Salinity is measured based on the classification scheme of Tooley (1978). Maximum velocity magnitude in a best estimate Holocene highstand (**c**) 2D simulation and a (**d**) 3D simulation. Areas are shaded red where maximum velocity >0.3 m/s and therefore is not conducive to the deposition of a laminated silt-clay sequence (Baas et al., 2016; Schieber et al., 2007; Schieber & Yawar, 2009). A 3% change in total area demonstrates the negligible difference in velocity magnitude between 2D and 3D simulations.

model scenarios involved a deviation from present day morphology, flow and flow obstructions, sea level and ocean outlet, resulting in models which inherently could not be calibrated against the present day. Instead, results were compared to the Holocene stratigraphic record. Water heights were compared to documented evidence of notches and wave-cut cliffs along the former shoreline of Lake Alexandrina (Luebbers, 1982), and inundation extents correlated with the Malcolm soil combination and sediments of the Cooke Plains Embayment (Cann et al., 2000; de Mooy, 1959).

Wave data was excluded from the model as the primary influence of waves within a wave-dominated estuary is as a driver of morphological change through the formation of a barrier complex at the estuary mouth and this model does not incorporate a sediment transport or morphology component (Dalrymple et al., 1992). Furthermore, although this estuary is wave-dominated at its entrance, owing to the immense scale of this system, areas subject to significant wave energy present a negligible component of the overall model domain (Figure 2.5).

A Manning's coefficient of 0.025 was adopted across the model domain for this study. Applying a varying Manning's coefficient was not actually implementable without a robust understanding of surficial sediments at the Holocene highstand over the entire 282 rkm of the model domain. Given this impracticality, applying a global Manning's coefficient was deemed sensible and, although not an accurate representation of reality, this method nonetheless provides the means for direct comparison between results. The value of 0.025 was selected as it lies within the bounds of appropriate Manning's coefficients given the likely Holocene palaeo-environmental conditions (Ladson et al., 2003). Further, this value was deemed appropriate as sensitivity testing conducted during calibration of the base model provided by BMT WBM revealed that results did not vary significantly given changes in the Manning's coefficient, but the model was best resolved when adopting values between 0.015 and 0.02538 (Hudson, 2010).

2.3.3   Morphology

To best resolve bathymetry and topography at highstand, three surfaces were created. A pre-regulation surface (S_{up}) provided a modern-day end member, the depth to the Monoman – Coonambidgal Formation transition provided a late-Pleistocene – early-Holocene end member (S_{low}), with the third surface a best estimate of highstand bathymetry and topography (S_{mid}). The S_{low} surface is certainly deeper than at Highstand, with the average depth of the body of Lake Alexandrina (between Point Sturt/Point McLeay and Pomanda Embayment) approximately -43 m AHD (Australian Height Datum; approximately mean sea level). By comparison the S_{up} surface has an average of approximately -3 m AHD over the same area,

Figure 2.5: Overview map with site photos demonstrates the immense scale of the Murray estuary and lower Murray River. (**a**) The lower Murray River at Walker Flat (rkm 206) is entrenched in the Murray Gorge. Photo taken from the right bank looking east, main channel width approximately 170 m. (**b**) The lower Murray River exits the Murray Gorge at Wellington (rkm 78). Photo taken from the right bank looking east with the Wellington car ferry shown for scale, main channel width approximately 270 m. (**c**) The main body of Lake Alexandrina is so vast that the opposite shoreline cannot be seen by the naked eye. Photo taken looking east, distance to opposite shoreline approximately 37 km. (**d**) The final segment of the lower Murray River flows through the Goolwa channel (rkm 11) before reaching the Murray Mouth. Photo taken from the right bank looking east, approximate channel width 570 m. (**e**) Sir Richard Peninsula at Goolwa seen from a lookout point facing south east (rkm 12), where the lower Murray River meets the Southern Ocean. (**f**) Goolwa Beach on the Sir Richard Peninsula seen from the lookout point of (**e**) facing north west (rkm 12).

with the S_{mid} best estimate highstand surface at approximately -8 m AHD. Within the LMR, the average of three surfaces is more closely constrained, varying from approximately -15 m to -8 m.

To resolve the S_{up} pre-regulation surface, the lock, barrages (and associated sediment sills), man-made levies and modern flood tide delta were removed from modern day DEMs (Supplementary Figure 15a). To resolve the S_{low} Pleistocene – Holocene surface, depths were

interpreted from over 100 sediment cores, as well as interpretation of data and maps by Barnett (1993) and Von der Borch and Altmann (1979) (Supplementary Figure 15b and Supplementary Table 2). The location and depth of the palaeo-channel within Lake Alexandrina was based on an interpretation of the work of Barnett (1993) and geological maps (Supplementary Figure 15b). The S_{mid} best-estimate highstand surface has the greatest uncertainty as it was resolved by subtracting regional sedimentation rates from the pre-regulation surface (Barnett, 1993; Fluin, 2002) and dated sediment cores (n = 18; Supplementary Figure 15c). Within the LMR and thalweg seaward, a sedimentation rate of 0.69 mm/y was adopted (Barnett, 1993; Fluin, 2002). All other elements were adjusted with a sedimentation rate of 0.16 mm/y (Barnett, 1993; Fluin, 2002).

The spatial interval of the three bathymetric surfaces created is identical to that of the modern-day input dataset as values were adjusted at each individual cell. The cell/element size varies considerably across the model domain with an average of approximately 50 m in cell side length within the LMR, modern flood tide delta (seaward of Point Sturt/Point McLeay, rkm 40) and Lower Lake fringes, and palaeo-Murray thalweg, with a considerably larger cell/element size within the main body of the Lower Lakes.

The chain-of-islands evolution of Sir Richard and Younghusband Peninsulas (Bourman & Murray-Wallace, 1991; de Mooy, 1959; Harvey, 2006; Luebbers, 1982) was the premise behind the series of back barrier morphologies presented in this study. Bourman and Murray-Wallace (1991) and de Mooy (1959) give detailed descriptions and maps of hypothesised former outlets of the LMR to the ocean. These maps were georeferenced and digitised and assessed relative to the modern-day topography of the back barrier system. Furthermore, the presence or absence of Aboriginal middens within the Holocene back barrier (Bourman et al., 2000; Disspain et al, 2011; Harvey et al, 2006; Luebbers, 1978, 1981, 1982) were also mapped and assessed relative to their radiocarbon ages. The data were then combined and analysed to produce a series of best estimates of the morphology of the mouth of the LMR as it evolved throughout the Holocene.

2.3.4   Sensitivity testing

Sensitivity testing for barrier evolution was based on the chain-of-islands model (Harvey, 2006) with the location of possible palaeo-outlets interpreted from Bourman and Murray-Wallace (1991), de Mooy (1959) and Luebbers (1982). Four barrier configurations were tested ranging from the complete removal of Sir Richard and Younghusband Peninsulas to the modern-day Murray Mouth (Figure 2.1c-f; Table 2.2). Three discharge conditions were tested: two held constant at the Millennium drought low flow(D_-; 152 m³/s) and pre-regulation average flow (D_{av}; 419 m³/s), and one variable to simulate a flood, with pre-
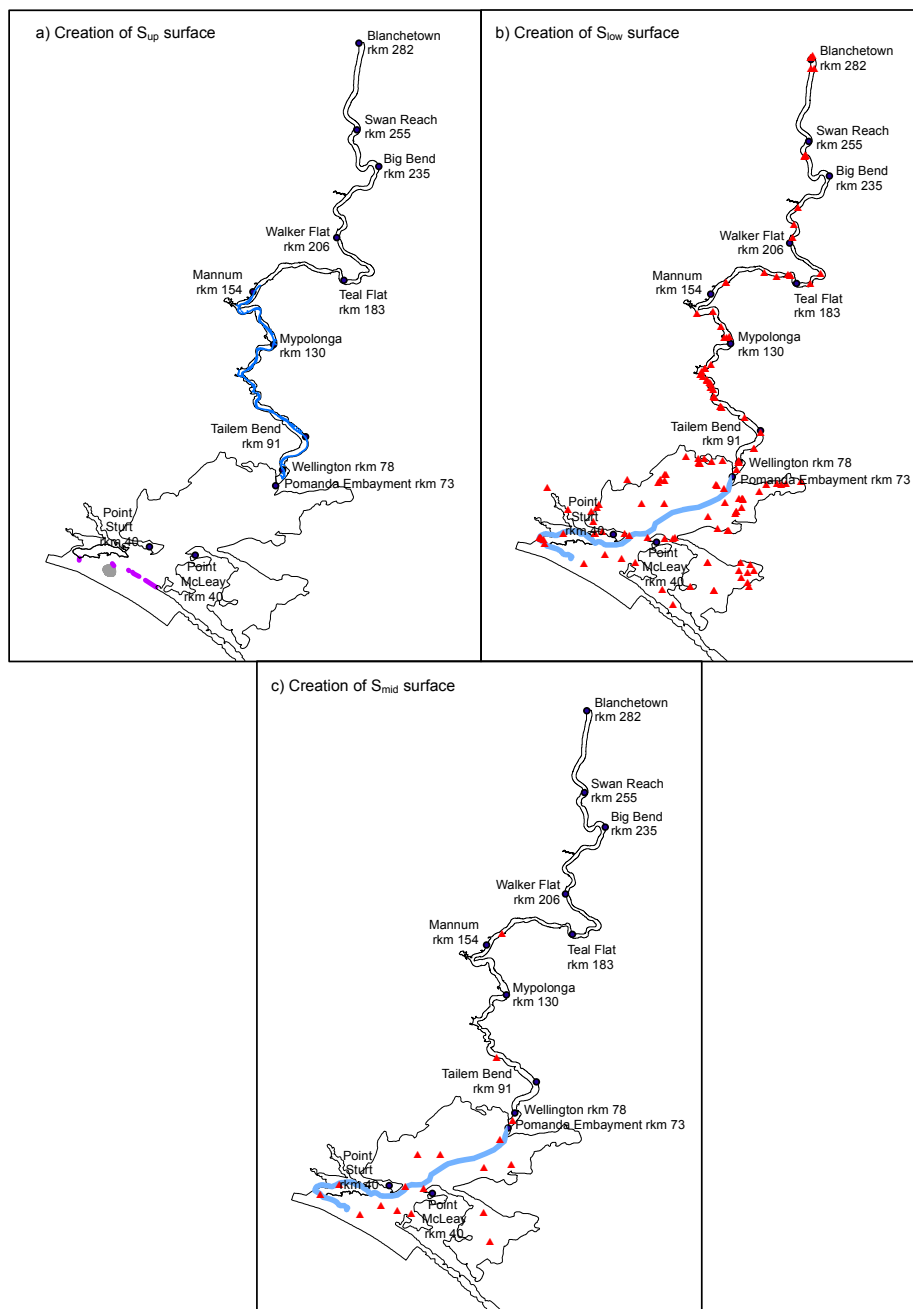
Figure 2.6: Overview of data used in the creation of three bathymetric surfaces. (**a**) Creation of the S_{up} surface involved manipulation of present day DEMs to remove man-made features including artificial levees (blue), Lock 1 at Blanchetown (rkm 282), Goolwa, Mundoo, Boundary Creek, Ewe Island and Tauwitchere barrages (purple), as well as Bird Island (grey), a modern flood tide deltaic island (James et al., 2015). (**b**) Creation of the S_{low} surface involved analysis of depth to the Coonambidgal-Monoman Formation transition, which is considered to mark the Pleistocene-Holocene boundary. Cores and CPTs analysed for creation of this surface (red) are given in Table 2.1. The location of the palaeo-Murray thalweg (blue) was inferred from data presented in Barnett (1993). (**c**) Creation of the S_{mid} surface was resolved by subtracting regional sedimentation rates from the pre-regulation surface (Barnett, 1993; Fluin, 2002) and dated sediment cores (red). Within the LMR and palaeo-Murray thalweg seaward (blue), a sedimentation rate of 0.69 mm/y was adopted (Barnett, 1993; Fluin, 2002). All other elements were adjusted with a sedimentation rate of 0.16 mm/y (Barnett, 1993; Fluin, 2002).

Table 2.1: Sedimentological data used to inform the creation of the S_{low} surface. Core logs (Barnett, 1989; Barnett, 1993; SARIG, 2019) and cone penetrometer tests (Hubble & De Carli, 2015) were analysed for the transition from the Monoman to Coonambidgal formation, which is interpreted to represent the approximate Pleistocene to Holocene boundary (S_{low}). Depths were adjusted relative to present day bathymetry and topography to give elevation in meters AHD.

rkm	X	Y	12K Z (m AHD)	ID	Reference
3	305704	6064588	> 3.6	35	Barnett, 1993
10	300043	6067607	> 3.0	33	Barnett, 1993
18	305738	6069952	> 3.8	32	Barnett, 1993
25	317628	6080376	0.5	19	Barnett, 1993
30	315888	6069243	2.8	25	Barnett, 1993
30	315643	6066463	2.7	26	Barnett, 1993
32	317049	6064273	> 1.9	27	Barnett, 1993
35	321456	6063067	1.7	24	Barnett, 1993
36	325255	6062032	> 2.3	23	Barnett, 1993
39	323598	6069398	> 4.9	22	Barnett, 1993
40	321175	6077118	0.1	11	Barnett, 1993
40	320792	6081178	0.7	18	Barnett, 1993
40	321201	6075823	1.7	20	Barnett, 1993
43	328598	6068940	> 2.1	21	Barnett, 1993
46	335469.7	6068475	> -19.8	Narrung Ferry 3, #70435	SARIG
47	328808	6073753	> 4.8	15	Barnett, 1993
48	326907	6078155	1.3	16	Barnett, 1993
48	324273	6081247	0.4	17	Barnett, 1993
50	335386	6069807	> 0.8	14	Barnett, 1993
52	333115	6078087	1.5	13	Barnett, 1993
53	332968	6086037	1.1	9	Barnett, 1993
54	336659	6074639	> 4.8	12	Barnett, 1993
55	336077	6081656	1.4	10	Barnett, 1993
57	337929	6088161	> 1.3	8	Barnett, 1993
61	344830	6074599	> 2.0	6	Barnett, 1993
61	341063	6082300	0.2	7	Barnett, 1993
64	348312	6074474	> 0.3	5	Barnett, 1993
65	347387	6079188	-41.8	BH 2, #234134	SARIG
65	347477	6079083	> 2.0	3	Barnett, 1993
67	352233	6075279	> 1.5	4	Barnett, 1993
67	347256	6081111	> -20.6	BH 4, #234136	SARIG
69	349244	6082072	> 4.0	2	Barnett, 1993
76	352640	6087305	> 2.7	1	Barnett, 1993
78	353178	6089048	-14.8	Wellington	Hubble & De Carli, 2015
79	353311.8	6089252	-47.4	DEPT H & L G, #71577	SARIG
79	353169.8	6089073	-25.4	DEPT H & L G, #71668	SARIG
79	353346.8	6089207	-11.2	DEPT H & L G, #71581	SARIG
79	353112.8	6088951	-6.0	DEPT H & L G, #71669	SARIG
79	353318.8	6089250	> -35.0	DEPT H & L G, #71578	SARIG
79	353318.8	6089239	> -37.4	DEPT H & L G, #71580	SARIG
79	353318.8	6089239	> -30.7	DEPT H & L G, #71579	SARIG
79	353312	6089252	-48.5	6727-1105	Barnett, 1989
79	353170	6089073	> -22.4	6727-1196	Barnett, 1989
79	353233	6089803	> -2.7	Wellington East Marina	Hubble & De Carli, 2015
85	357350	6093006	> -0.4	Murray view Estates	Hubble & De Carli, 2015
85	357368	6093010	-21.7	Murray view Estates	Hubble & De Carli, 2015
88	358637.8	6093934	-0.6	Tailem Bend Pump 1, #71594	SARIG
92	359155.8	6097151	> -27.2	DEPT H & L G, #71665	SARIG
91.5	359156	6097151	> -27.4	6727-1193	Barnett, 1989
97	354771	6101444	-6.3	Westbrook	Hubble & De Carli, 2015
104	348576	6104196	-14.9	Riverglen Marina	Hubble & De Carli, 2015
104	348214	6104380	-27.2	Riverglen Marina	Hubble & De Carli, 2015
108	346634	6106805	-15.9	Bells Reserve Monteith	Hubble & De Carli, 2015
109	346395.8	6106955	-26.9	Monteith 1, #71337	SARIG
109	346396	6106955	-26.2	6727-865	Barnett, 1989
111	346364.8	6108814	-9.9	Swanport 6, #71336	SARIG
111.5	346365	6108814	-30.0	6727-864	Barnett, 1989
112	345553.8	6109505	-30.0	Swanport 4, #71334	SARIG
112	345554	6109505	> -29.2	6727-862	Barnett, 1989
113	345564	6110662	-3.9	Long Island Marina	Hubble & De Carli, 2015
113	345364	6110811	> -2.7	Long Island Marina	Hubble & De Carli, 2015
114	344665	6111528	-20.3	Long Island	Hubble & De Carli, 2015
114	344634	6111322	-12.7	Long Island Reserve	Hubble & De Carli, 2015
115	343532	6112394	> -1.9	Sturt Reserve, Murray Bridge	Hubble & De Carli, 2015
117	342847	6113083	-12.5	MB PUMP 1, #71347	SARIG
117	342824	6113068	-12.1	MB PUMP 2, #71348	SARIG
117	342807	6113023	-9.7	MB PUMP 3, #71349	SARIG
117	342732	6112903	-0.3	MD PUMP 7, #71354	SARIG
117	342847	6113083	> -20.2	6727-875	Barnett, 1989
117	342807	6113023	> -25.0	6727-877	Barnett, 1989
117	343129	6113921	-10.3	Thiele Reserve	Hubble & De Carli, 2015
119	344090.8	6114680	-21.9	CH2, #70979	SARIG
119	344067.8	6114650	-19.4	CH1, #70978	SARIG
119	344046.8	6114660	-9.7	PTH1, #70980	SARIG
119	344068	6114650	-18.9	6727-498	Barnett, 1989
119	344091	6114680	-21.3	6727-499	Barnett, 1989
119	344047	6114660	-9.4	6727-500	Barnett, 1989
120	345676	6115810	-13.1	Avoca Dell	Hubble & De Carli, 2015
133	350609	6123221	-9.6	6727-2201	Barnett, 1989
133	349935	6123145	-11.9	6727-2205	Barnett, 1989
133	349305	6123011	-19.5	6727-2214	Barnett, 1989
136	348350	6125995	-6.9	Woodlane Reserve	Hubble & De Carli, 2015
142	346193	6130131	-14.2	Wall Flat	Hubble & De Carli, 2015
147	341939	6129444	> -0.3	Neeta Irrigation Area	Hubble & De Carli, 2015
159	349749	6137775	-15.8	East Front Rd	Hubble & De Carli, 2015
160	349204.8	6137915	-11.8	LOWER MURRAY DAM 5 1, #73409	SARIG
161	350989.8	6138882	-4.0	LOWER MURRAY DAM 4 1, #73297	SARIG
172	360167	6140549	-9.2	Younghusband	Hubble & De Carli, 2015
175	363437	6139565	-11.9	Younghusband	Hubble & De Carli, 2015
179	366522	6139908	-10.3	6828-427	Barnett, 1989
180	367076.9	6139963	-12.9	TEAL FLAT PD11, #85363	SARIG
180	367141.8	6139778	-13.5	TEAL FLAT PD28, #85308	SARIG
180	367117	6139848	> -7.8	6828-431	Barnett, 1989
180	367227	6139833	-6.0	6828-434	Barnett, 1989
187	372520	6137668	-7.4	BowHill	Hubble & De Carli, 2015
194	375342	6140438	-15.6	Purnong	Hubble & De Carli, 2015
208	367778	6149959	-4.4	Scrubby Flat	Hubble & De Carli, 2015
213	368198	6153555	-10.5	Walkers Flat	Hubble & De Carli, 2015
221	369210	6158135	-9.8	Wongulla	Hubble & De Carli, 2015
250	371056	6172095	1.1	6828-578	Barnett, 1989
250	370985	6172001	-11.7	6828-579	Barnett, 1989
250	371143	6172150	-7.9	6828-580	Barnett, 1989
250	371381	6172318	-5.6	6828-581	Barnett, 1989
250	371232	6172245	-8.2	6828-582	Barnett, 1989
251	370984.9	6172001	-15.8	Swan Reach 2, #85459	SARIG
251	371142.9	6172150	-11.0	Swan Reach 3, #85458	SARIG
251	370896.9	6171774	-10.4	PH5, #85384	SARIG
251	371055.9	6172095	-8.1	Swan Reach 1, #85458	SARIG
251	371497.9	6172390	-6.1	Swan Reach 10, #85463	SARIG
251	371380.9	6172318	-5.8	Swan Reach 7, #85461	SARIG
251	370896.9	6171774	-3.5	PH6, #85385	SARIG
280	373624	6195800	-3.1	6829-833	Barnett, 1989
280	372657	6195846	7.3	6829-829	Barnett, 1989
284	372922	6198708	-2.5	Blanchetown Bridge 5, #85879	SARIG
284	372612	6198638	0.0	Blanchetown Bridge 12, #85835	SARIG
284	372637	6198688	0.1	Blanchetown Bridge 13, #85836	SARIG
284	372577.1	6198633	0.3	Blanchetown Bridge 1, #85833	SARIG
284	372882	6198698	1.1	Blanchetown Bridge 10, #85878	SARIG
284	372577	6198688	1.2	Blanchetown Bridge 1A, #85834	SARIG
284	372677.1	6198653	2.2	Blanchetown Bridge 2, #85837	SARIG
284	373142	6198758	3.2	Blanchetown Bridge 11, #85881	SARIG
284	372982	6198723	5.1	Blanchetown Bridge 6, #85880	SARIG
284	372562	6198628	9.2	Blanchetown Bridge 9, #85832	SARIG
284	372547	6198628	18.9	Blanchetown Bridge 7, #85831	SARIG
283.5	372577	6198628	3.5	6829-170	Barnett, 1989
283.5	372677	6198653	2.8	6829-173	Barnett, 1989
283.5	372673	6198673	0.2	6829-212	Barnett, 1989
283.5	372922	6198708	6.7	6829-215	Barnett, 1989
284	373148	6199263	> -3.9	6829-1380	Barnett, 1989

regulation average discharge increasing to the peak of the 1974 flood (D_+; 1,883 m^3/s) and decreasing again (Table 2.2; Bloss et al., 2015; Gippel & Blackham, 2002).

There have been numerous sea-level studies across Australia, with the majority stemming from east coast datasets (Lewis et al, 2013; Sloss et al., 2007). As a consequence of iso-static and climatic influences, and localised geomorphology, there is wide variability across the Australian coast in both the magnitude and timing of the Holocene sea-level highstand (Lewis et al., 2013). Highstand estimates must therefore be derived from the regional set-

Table 2.2: The scenarios adopted in this study. Codes identify bathymetric surface (S_{up} = pre-modification condition, S_{mid} = highstand best estimate condition, S_{low} = Pleistocene-Holocene boundary condition), discharge (D_- = drought, D_{av} = pre-regulation average, D_+ = pre-regulation average with a flood event), and barrier morphology (B_0 = no barrier, B_+ and B_{++} = phases of chain-of-islands evolution (Bourman & Murray-Wallace, 1991; de Mooy, 1959; Harvey, 2006; Luebbers, 1982), and B_{mod} = present day). A code and category has been assigned to each scenario to facilitate interpretation. Scenario categories are grouped based on sea-level and bathymetric surface.

Initial sea level at 2 m (with respect to 2014 sea level)					Initial sea level at 0 m (with respect to 2014 sea level)				
Bathymetric Surface	Discharge	Barrier Morphology	Scenario Code	Scenario Category	Bathymetric Surface	Discharge	Barrier Morphology	Scenario Code	Scenario Category
S_{up}	D_-	B_0	$S_{up}WL_2D_-B_0$	$\mathbf{S_{up}WL_2}$	S_{up}	D_-	B_0	$S_{up}WL_0D_-B_0$	$\mathbf{S_{up}WL_0}$
		B_+	$S_{up}WL_2D_-B_+$				B_+	$S_{up}WL_0D_-B_+$	
		B_{++}	$S_{up}WL_2D_-B_{++}$				B_{++}	$S_{up}WL_0D_-B_{++}$	
		B_{mod}	$S_{up}WL_2D_-B_{mod}$				B_{mod}	$S_{up}WL_0D_-B_{mod}$	
	D_{av}	B_0	$S_{up}WL_2D_{av}B_0$			D_{av}	B_0	$S_{up}WL_0D_{av}B_0$	
		B_+	$S_{up}WL_2D_{av}B_+$				B_+	$S_{up}WL_0D_{av}B_+$	
		B_{++}	$S_{up}WL_2D_{av}B_{++}$				B_{++}	$S_{up}WL_0D_{av}B_{++}$	
		B_{mod}	$S_{up}WL_2D_{av}B_{mod}$				B_{mod}	$S_{up}WL_0D_{av}B_{mod}$	
	D_+	B_0	$S_{up}WL_2D_+B_0$			D_+	B_0	$S_{up}WL_0D_+B_0$	
		B_+	$S_{up}WL_2D_+B_+$				B_+	$S_{up}WL_0D_+B_+$	
		B_{++}	$S_{up}WL_2D_+B_{++}$				B_{++}	$S_{up}WL_0D_+B_{++}$	
		B_{mod}	$S_{up}WL_2D_+B_{mod}$				B_{mod}	$S_{up}WL_0D_+B_{mod}$	
S_{mid}	D_-	B_0	$S_{mid}WL_2D_-B_0$	$\mathbf{S_{mid}WL_2}$	S_{mid}	D_-	B_0	$S_{mid}WL_0D_-B_0$	$\mathbf{S_{mid}WL_0}$
		B_+	$S_{mid}WL_2D_-B_+$				B_+	$S_{mid}WL_0D_-B_+$	
		B_{++}	$S_{mid}WL_2D_-B_{++}$				B_{++}	$S_{mid}WL_0D_-B_{++}$	
		B_{mod}	$S_{mid}WL_2D_-B_{mod}$				B_{mod}	$S_{mid}WL_0D_-B_{mod}$	
	D_{av}	B_0	$S_{mid}WL_2D_{av}B_0$			D_{av}	B_0	$S_{mid}WL_0D_{av}B_0$	
		B_+	$S_{mid}WL_2D_{av}B_+$				B_+	$S_{mid}WL_0D_{av}B_+$	
		B_{++}	$S_{mid}WL_2D_{av}B_{++}$				B_{++}	$S_{mid}WL_0D_{av}B_{++}$	
		B_{mod}	$S_{mid}WL_2D_{av}B_{mod}$				B_{mod}	$S_{mid}WL_0D_{av}B_{mod}$	
	D_+	B_0	$S_{mid}WL_2D_+B_0$			D_+	B_0	$S_{mid}WL_0D_+B_0$	
		B_+	$S_{mid}WL_2D_+B_+$				B_+	$S_{mid}WL_0D_+B_+$	
		B_{++}	$S_{mid}WL_2D_+B_{++}$				B_{++}	$S_{mid}WL_0D_+B_{++}$	
		B_{mod}	$S_{mid}WL_2D_+B_{mod}$				B_{mod}	$S_{mid}WL_0D_+B_{mod}$	
S_{low}	D_-	B_0	$S_{low}WL_2D_-B_0$	$\mathbf{S_{low}WL_2}$	S_{low}	D_-	B_0	$S_{low}WL_0D_-B_0$	$\mathbf{S_{low}WL_0}$
		B_+	$S_{low}WL_2D_-B_+$				B_+	$S_{low}WL_0D_-B_+$	
		B_{++}	$S_{low}WL_2D_-B_{++}$				B_{++}	$S_{low}WL_0D_-B_{++}$	
		B_{mod}	$S_{low}WL_2D_-B_{mod}$				B_{mod}	$S_{low}WL_0D_-B_{mod}$	
	D_{av}	B_0	$S_{low}WL_2D_{av}B_0$			D_{av}	B_0	$S_{low}WL_0D_{av}B_0$	
		B_+	$S_{low}WL_2D_{av}B_+$				B_+	$S_{low}WL_0D_{av}B_+$	
		B_{++}	$S_{low}WL_2D_{av}B_{++}$				B_{++}	$S_{low}WL_0D_{av}B_{++}$	
		B_{mod}	$S_{low}WL_2D_{av}B_{mod}$				B_{mod}	$S_{low}WL_0D_{av}B_{mod}$	
	D_+	B_0	$S_{low}WL_2D_+B_0$			D_+	B_0	$S_{low}WL_0D_+B_0$	
		B_+	$S_{low}WL_2D_+B_+$				B_+	$S_{low}WL_0D_+B_+$	
		B_{++}	$S_{low}WL_2D_+B_{++}$				B_{++}	$S_{low}WL_0D_+B_{++}$	
		B_{mod}	$S_{low}WL_2D_+B_{mod}$				B_{mod}	$S_{low}WL_0D_+B_{mod}$	

ting of the study area which, for the Murray estuary, limits data to studies from the Gulf of St Vincent and the Spencer Gulf in South Australia. Immediately prior to the highstand (8,000 – 7,500 yr BP), sea level reached present day levels (Belperio et al., 2002; Bowman & Harvey, 1986; Lewis et al., 2013) with the magnitude of the subsequent highstand ranging from +1 m up to +3 m across the southern Australian coast (Belperio et al., 2002; Lewis et al., 2013). This study adopts a best approximation of a +2 m highstand at 7,000 – 6,000 yr BP (Belperio et al., 2002; Lewis et al., 2013), a value which has been adopted by other studies of the Holocene palaeo-Murray estuary (Bourman et al., 2000). The models were run twice – once using present day tides (WL_0) and again at present day tides plus 2 m to simulate Holocene highstand conditions (WL_2; Table 2.2).

2.3.5   Post-processing

Salinity was classified based on chloride concentration using Tooley's (1978) scheme: fresh <0.1 g Cl/L, fresh-brackish 0.1 – 0.5 g Cl/L, brackish-fresh 0.5 – 1 g Cl/L, brackish 1 – 5 g Cl/L, brackish-marine 5 – 10 g Cl/L, marine-brackish 10 – 17 g Cl/L, and marine >17 g Cl/L. Salinity was assessed using maximum salinities observed post burn-in phase. Maximum rather than average salinity is considered as, due to constraints in computational power giving a 5-fold increase in model run time, salinity is not resolved in 3D therefore results do not account for a salt wedge at depth but rather depict a freshwater plume at the surface. Directional vectors were assessed within the present-day channel (and not fringing swamps) such that a direct comparison could be drawn between the three model surfaces regardless of inundation extent or bathymetrically-controlled primary flow path. Velocity magnitude was considered relative to the critical threshold of 0.3 m/s (Baas et al, 2016; Schieber et al., 2007; Schieber & Yawar, 2009) and representative models were re-run to assess tidal signatures from water levels at 1 hour outputs.

2.4   Results

2.4.1   Model correlation with regional geomorphology and sedimentology

Given the experimental nature of modelling snapshots in geological time, constraining inundation extent to geological features gives an indication of the plausibility of model results. The lacustrine and estuarine clays of the Malcolm soil combination (Figure 2.7a; Table2.3) represent the extent of Lake Alexandrina during the Holocene (de Mooy, 1959). This formation, and recognised Holocene palaeo-shorelines (de Mooy, 1959), are mapped against inundation extent in Figure 2.7. The Malcolm soil combination is well constrained by the $S_{low}WL_2$ scenarios (Figure 2.7d; Table2.2), with the $S_{mid}WL_2$ scenarios proving a reasonable match overall (Figure 2.7c; Table2.2). The $S_{low}WL_2$ scenarios align precisely with the most expansive of the palaeo-shorelines which is consistent with the greatest Holocene extent of Lake Alexandrina (Figure 2.7d; Table2.2; de Mooy, 1959). The S_{mid} scenarios sit at, or beyond, the middle palaeo-shoreline, considered to represent a short stabilisation period during retreat, likely in response to falling sea levels (Figure 2.7c; Table2.2; de Mooy, 1959). The $S_{up}WL_2$ scenarios align with the middle palaeo-shoreline, while the $S_{up}WL_0$ scenarios generate inundation akin to present-day (Figure 2.7d; Table2.2; de Mooy, 1959).

The inundation extent of the 1956 flood, the greatest flood on instrumental record, is also depicted in Figure 2.7. This extent is not as expansive as the Malcolm soil combination within the Lower Lakes region, suggesting that water levels at the Holocene highstand were

Table 2.3: Description of stratigraphic formations and soil combinations within the study area.

Formation Name	Description
Coonambidgal	Holocene alluvial clays and silts comprising the upper valley fill within the LMR
Monoman	Holocene to late-Pleistocene alluvial sands comprising the lower valley fill within the LMR
Saint Kilda	Holocene coastal marine sediment
Bridgewater	Middle-Pleistocene sands
Padthaway	Holocene to early-Pleistocene lacustrine sands, silts and clays
Molineaux Sand	Holocene to late-Pleistocene aeolian sands

Soil Combination Name	Description
Malcolm	Holocene estuarine, alluvial and lacustrine clays demarcating the greatest Holocene inundation extent of Lake Alexandrina

well above maximum historical records. Bank overtopping from fluvial floodwaters during the 1956 flood caused valley-wide inundation within the Murray Gorge which gives insight into the plausible response to the Holocene highstand as the LMR is backfilled. All S_{low} scenarios correlate with the 1956 flood extent and are characterised by valley-wide inundation throughout the Murray Gorge (Figure 2.7d III-IV; Table 2.2). The $S_{mid}WL_2$ scenarios inundate the entire valley, with the exception of two small areas at Big Bend (rkm235) and Swan Reach (rkm255; Figure 2.7c III-IV; Table 2.2). Inundation of these two locations is reduced in the $S_{mid}WL_0$ scenarios along with isolated small dry areas, however, these models remain characterised by valley-wide inundation (Figure 2.7c III-IV; Table 2.2). Conversely, even given Holocene highstand sea levels, the S_{up} scenarios are charactered by a channel with fringing swamps upstream of Mypolonga (rkm 130), as was evident prior to levee construction and land reclamation in the 19th century (Taylor & Poole, 1931); a significant flood (D_+ scenarios) is required to induce valley-wide inundation (Figure 2.7b III-IV; Table 2.2). The results suggest that the period of sea-level fall from highstand in the late-Holocene saw a significant shift in the geomorphic character of the LMR (Figure 2.7c III-IV vs. Figure 2.7b III-IV). Overall, model results are well correlated to regional geomorphology and sedimentology, and are consistent with research into the sedimentary infill and geomorphological evolution of barrier estuaries identified on the east coast of Australia (e.g. Sloss et al., 2006a; Sloss et al., 2006b; Sloss et al., 2006c), therefore, the model is deemed sensible and valid as a basis for further exploratory analysis.
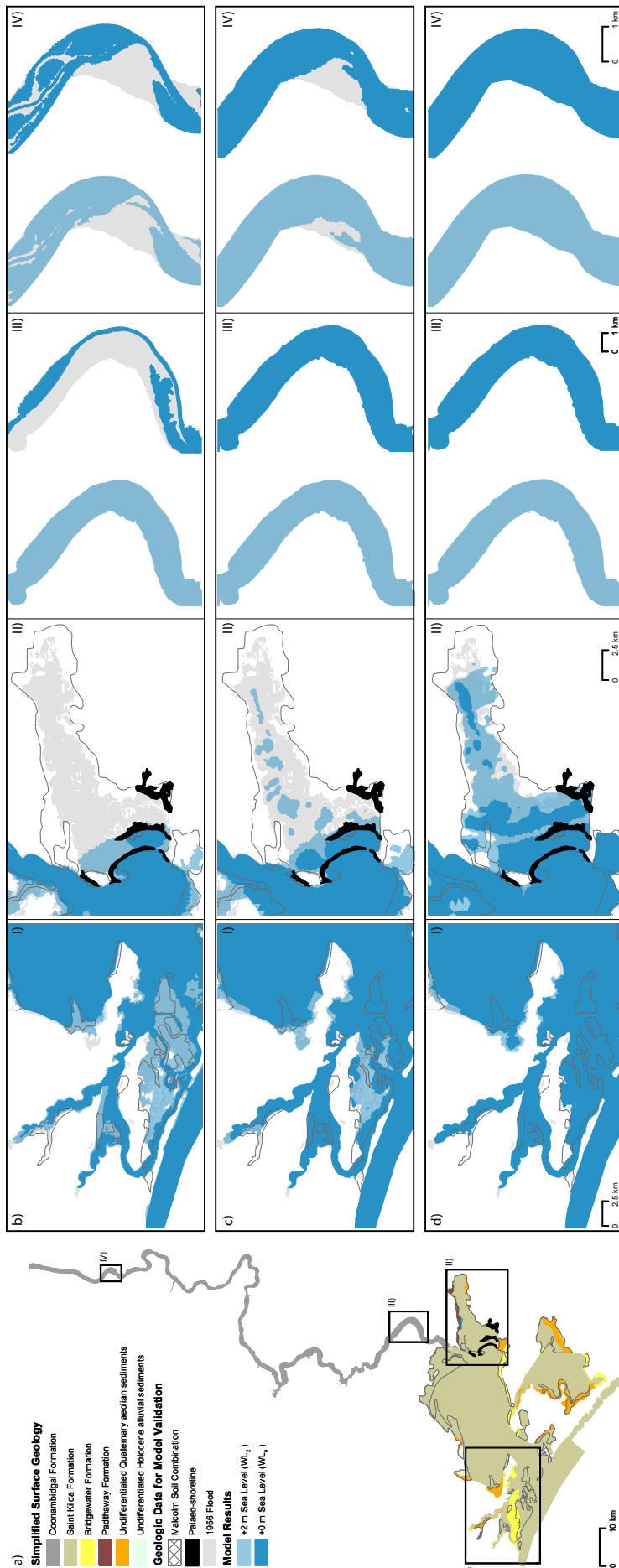
Figure 2.7: Geologic overview of the study area and maps showing maximum inundation extent under $D_{av}B_{mod}$ scenarios. (**a**) Simplified surface geology showing Holocene and Pleistocene stratigraphic formations. Inundation extents are shown for (**b**) S_{up}, (**c**) S_{mid} and (**d**) S_{low} scenarios at $+2$ m sea level (WL$_2$; light blue) and $+0$ m sea level (WL$_0$; dark blue). Panels I and II encompass sub-sections of Lake Alexandrina detailing the flood tide delta and Murray Mouth, and the Cooke Plains Embayment, respectively. Panel III details a 10 rkm representative sub-region of the lower portion of the LMR (centered on Tailem Bend, rkm 91). Panel IV details a 10 rkm representative sub-region of the upper portion of the LMR (centered on Swan Reach, rkm 255). The inundation extent of the 1956 flood (grey) is given as an indicative regional modern-day analogue of the plausible extent of inundation caused by backfilling during the Holocene highstand. The Malcolm soil combination (dark grey outline) represents the maximum Holocene inundation extent of the Lower Lakes (Lakes Alexandrina and Albert; I and II; de Mooy, 1959). Palaeo-shorelines (black) allude to the maximum Holocene extent of Lake Alexandrina and a period of stability following retreat to the present-day shoreline (II; de Mooy, 1959). Maximum inundation extents remain comparable in other model scenarios not depicted here, with non-significant fluctuations in inundation across the Lower Lakes (I and II), with the exception of a significant flood event (D_+ scenarios) which induces valley-wide inundation throughout the LMR (III and IV).

2.4.2   Palaeo-environment at the Holocene highstand

Model results show that the palaeo-environment at the Holocene highstand was likely to have been estuarine throughout the Lower Lakes and well upstream into the LMR (Figures 2.8a I-III & 2.10a; Figure 2.9a-c). All WL_2 highstand scenarios result in an estuarine environment with significant marine incursion in the Lower Lakes, meanwhile all WL_0 scenarios result in a brackish environment within the Lower Lakes, with fluvial discharge supressing significant marine incursion to the barrier and flood tide delta complex (Figure 2.8a & 2.10a; Figure 2.9). This trend is apparent across all scenarios irrespective of discharge, barrier morphology and bathymetric surface (Figures 2.8a & 2.10a; Figure 2.9), with a shift to fresher water dependent upon a fall in sea level to present-day conditions (Figures 2.8a & 2.10a; Figure 2.9). Holocene highstand sea levels also induce valley-wide inundation under Sup morphology, with the S_{mid} and S_{low} morphologies resulting in a significant increase in the areal extent of the Lower Lakes (Figure 2.7). These results demonstrate that sea level is the driving factor controlling the environmental character of the Lower Lakes and LMR. This is apparent through the difference in maximum palaeo-salinities observed with a change in sea level (Figures 2.8a & 2.10a; Figure 2.9) when compared with the near-identical results produced by sensitivity testing for discharge (Figures 2.8b & 2.10a), barrier morphology (Figures 2.8c & 2.10a) or bathymetric surface (Figures 2.8a & 2.10a).

2.4.3   Estuarine processes zonation and inferred resulting morphology

Velocity vectors are used to define the upstream extent of the backwater zone for each scenario (Figures 2.10b & 2.11). The maximum upstream extent in S_{low} scenarios is Blanchetown (rkm 275), regardless of sea level, such that the $S_{low}WL_0$ scenarios present significantly different backwater zones when compared to other WL_0 scenarios (Figures 2.10b & 2.11; Table 2.2). Given that the bathymetry of the S_{low} scenarios is almost certainly not representative of the mid- to late-Holocene when sea levels had receded to present-day, the backwater zone during this period is best constrained by the $S_{mid}WL_0$ and $S_{up}WL_0$ scenarios, confining the backwater zone to the region downstream of Tailem Bend (rkm 91; Figure 2.10b and Figure 2.11; Table 2.2). Under all bathymetric conditions, the backwater zone extended well into the LMR supporting the hypothesis that Lake Alexandrina and the LMR were subject to a single depositional environment that produced a regionally extensive central basin depositional sequence at the Holocene highstand (Figure 2.10b and Figure 2.11). These results suggest that, prior to anthropogenic modifications of the flow regime, this central basin sequence was continuing to accumulate within the entirety of Lake Alexandrina; top-of-core modern dates across the regionally extensive laminated sequence support this contention (Barnett, 1993).
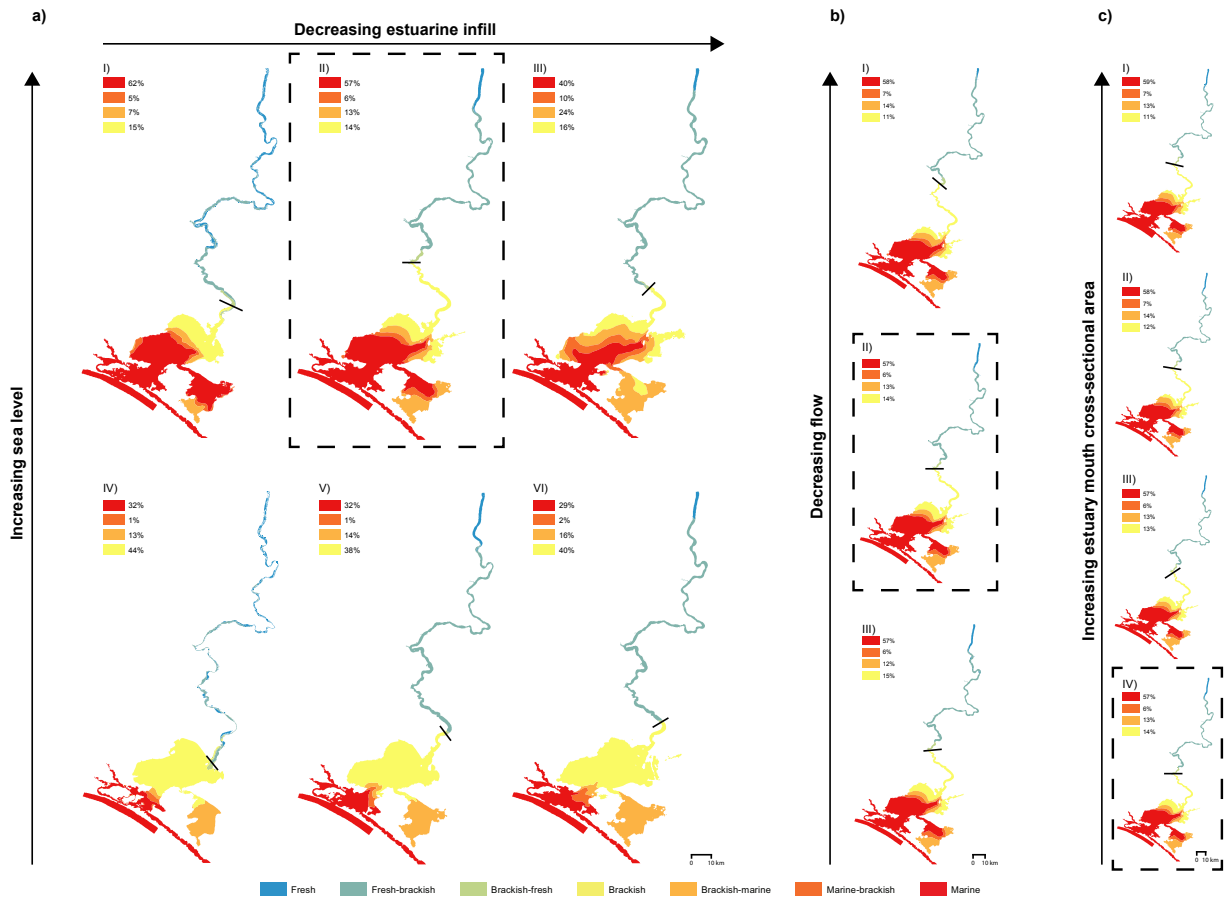
Figure 2.8: Key representative maps comparing maximum salinity reached relative to sea level, bathymetric surface, discharge and barrier morphology. (**a**) An increase in sea level from WL_0 present-day conditions (**IV-VI**) to WL_2 Holocene highstand conditions (**I-III**) significantly increases marine incursion, extending to the upper reaches of Lake Alexandrina and pushing the brackish limit further up the Murray Gorge. There is negligible change to the overall palaeo-environmental character of the region between end-member and best-estimate Holocene bathymetries (**I-III** or **IV-VI**). (**b**) Variance in flow from drought (D_-) to flood (D_+) scenarios (**I-III**) is unable to alter the palaeo-environmental character of the region. (**c**) Variance in barrier morphology from completely open (B_0) to modern-day (B_{mod}) outlet scenarios (**I-IV**) is also unable to alter the palaeo-environmental character of the region. The isohaline delimits the brackish limit (equivalent to 1 psu) with the percentage area of each salinity class seaward of the isohaline given relative to total inundated area. The hatched box highlights the common scenario between the three panels: scenario $S_{mid}WL_2D_{av}B_{mod}$. Within (**a**) all maps shown are pre-regulation average discharge with modern-day barrier morphology scenarios (**I**: scenario $S_{up}WL_2D_{av}B_{mod}$; **II**: scenario $S_{mid}WL_2D_{av}B_{mod}$; **III**: scenario $S_{low}WL_2D_{av}B_{mod}$; **IV**: scenario $S_{up}WL_0D_{av}B_{mod}$; **V**: scenario $S_{mid}WL_0D_{av}B_{mod}$ and **VI**: scenario $S_{low}WL_0D_{av}B_{mod}$; Table 2.2). To demonstrate representative salinities at the Holocene highstand, $S_{mid}WL_2$ scenarios are shown within (**b**) (**I**: scenario $S_{mid}WL_2D_-B_{mod}$; **II**: scenario $S_{mid}WL_2D_{av}B_{mod}$; **III**: scenario $S_{mid}WL_2D_+B_{mod}$) and (**c**) (**I**: scenario $S_{mid}WL_2D_{av}B_0$; **II**: scenario $S_{mid}WL_2D_{av}B_+$; **III**: scenario $S_{mid}WL_2D_{av}B_{++}$; **IV**: scenario $S_{mid}WL_2D_{av}B_{mod}$). Salinity is measured based on the classification scheme of Tooley (1978).
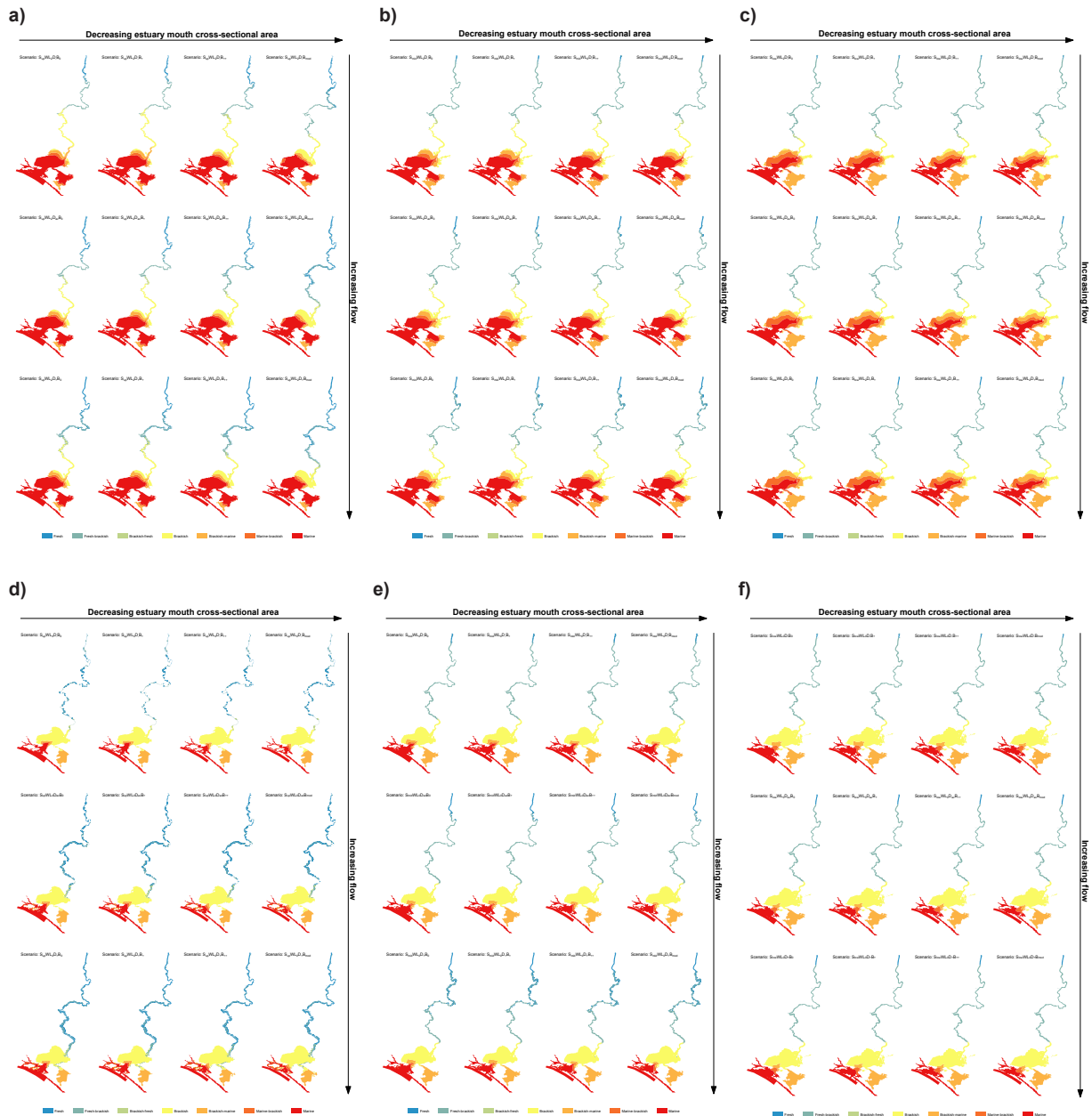
Figure 2.9: Maps of maximum salinity reached for each scenario. Maximum salinity is shown for each (a) $S_{up}WL_2$, (b) $S_{mid}WL_2$, (c) $S_{low}WL_2$, (d) $S_{up}WL_0$, (e) $S_{mid}WL_0$, (f) $S_{low}WL_0$ scenario. Salinity is measured based on the classification scheme of Tooley (1978). Refer to Table 2.2 for scenario descriptions.

The possibility of deposition and preservation of a laminated deposit is limited to regions where the maximum velocity magnitude is <0.3 m/s (Baas et al., 2016; Schieber et al., 2007; Schieber & Yawar, 2009; see grey shaded areas in Figures 2.12 & 2.13), which encompasses a minimum of 82% of the model domain. Suitable conditions for the deposition of a laminated sequence throughout Lake Alexandrina apply in all scenarios (Figure 2.12 and Figure 2.13) and explains the regionally extensive presence of this laminated central basin deposit that has characterised Lake Alexandrina's Holocene stratigraphy since 5,500 yr BP (Barnett, 1993). Variation in barrier morphology (Figure 2.12a-c or d-f) or LMR/Lower Lakes bathymetry (Figure 2.12a & d or b & e or c & f) makes a negligible difference in the regional capacity to generate a laminated central basin deposit (maximum 7% and 3% change respectively).

Overall, the $S_{low}WL_2$ and $S_{mid}WL_2$ scenarios are well constrained by the Malcolm soil combination, and palaeo-shorelines, representing the maximum Holocene inundation extent of the Lower Lakes (de Mooy, 1959) which suggests the suitability of interpolating these results to the palaeo-environment at the Holocene highstand (Figure 2.7; Table 2.2). This result shows that the Holocene highstand probably generated valley-wide inundation within the entirety of the Murray Gorge at least as far upstream as Blanchetown (rkm 282; Figure 2.7), which coincides with the minimum propagation of the tidal limit of the Murray estuary (Figure 2.14). Given this single central basin depositional environment, the presence of a laminated sequence within the valley-wide LMR is inferred, perhaps extending as far upstream as Walker Flat (rkm 206; Figure 2.14). During the late-Holocene, it is suggested that the bay-head delta prograded downstream to Mypolonga (rkm 130), where there is a notable shift in the geomorphic character of the levees and fringing swamps, before anthropogenic modification inhibited further natural estuarine evolution from 1900 onwards (Taylor & Poole, 1931).
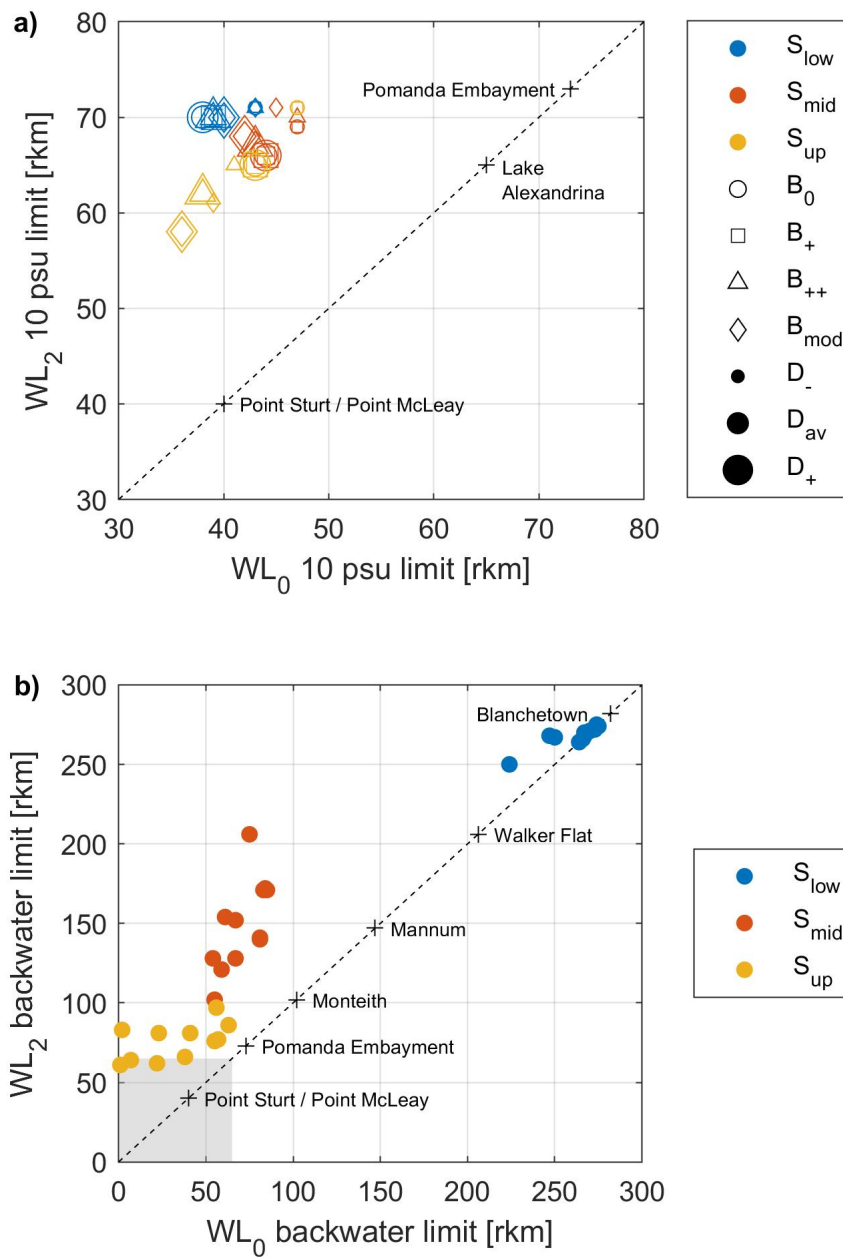
Figure 2.10: Comparison of 10 psu (marine-brackish) and backwater zone limits for all WL_0 and WL_2 paired scenarios. (**a**) An increase in sea level from WL_0 to WL_2 Holocene highstand conditions drives the 10 psu (marine-brackish) limit from the flood tide delta and lower reaches of Lake Alexandrina upstream such that marine or marine-brackish waters occupy the entire body of the lake. This trend is apparent irrespective of bathymetric surface (colours), barrier morphology (shapes) or discharge (sizes) demonstrating that sea level is the primary driver of palaeo-environmental change within this system. (**b**) Velocity vector convergence, taken as the point of convergence of upstream and downstream velocity vectors within the channel thalweg, defines the upstream extent of the backwater zone. Given S_{up} conditions (yellow), the backwater zone is restricted to the main body of Lake Alexandrina (grey shading) and the Pomanda Embayment within WL_0 scenarios, with the higher sea level in WL_2 scenarios driving this limit upstream into the lower reaches of the Murray Gorge. The influence of sea level on the backwater limit is equally apparent given S_{mid} conditions (red), where at the Holocene highstand, an enlarged low energy backwater setting was emplaced up to Walker Flat (rkm 206). By comparison, the S_{low} surface (blue) forces the backwater zone to occupy the entire model domain irrespective of sea level.
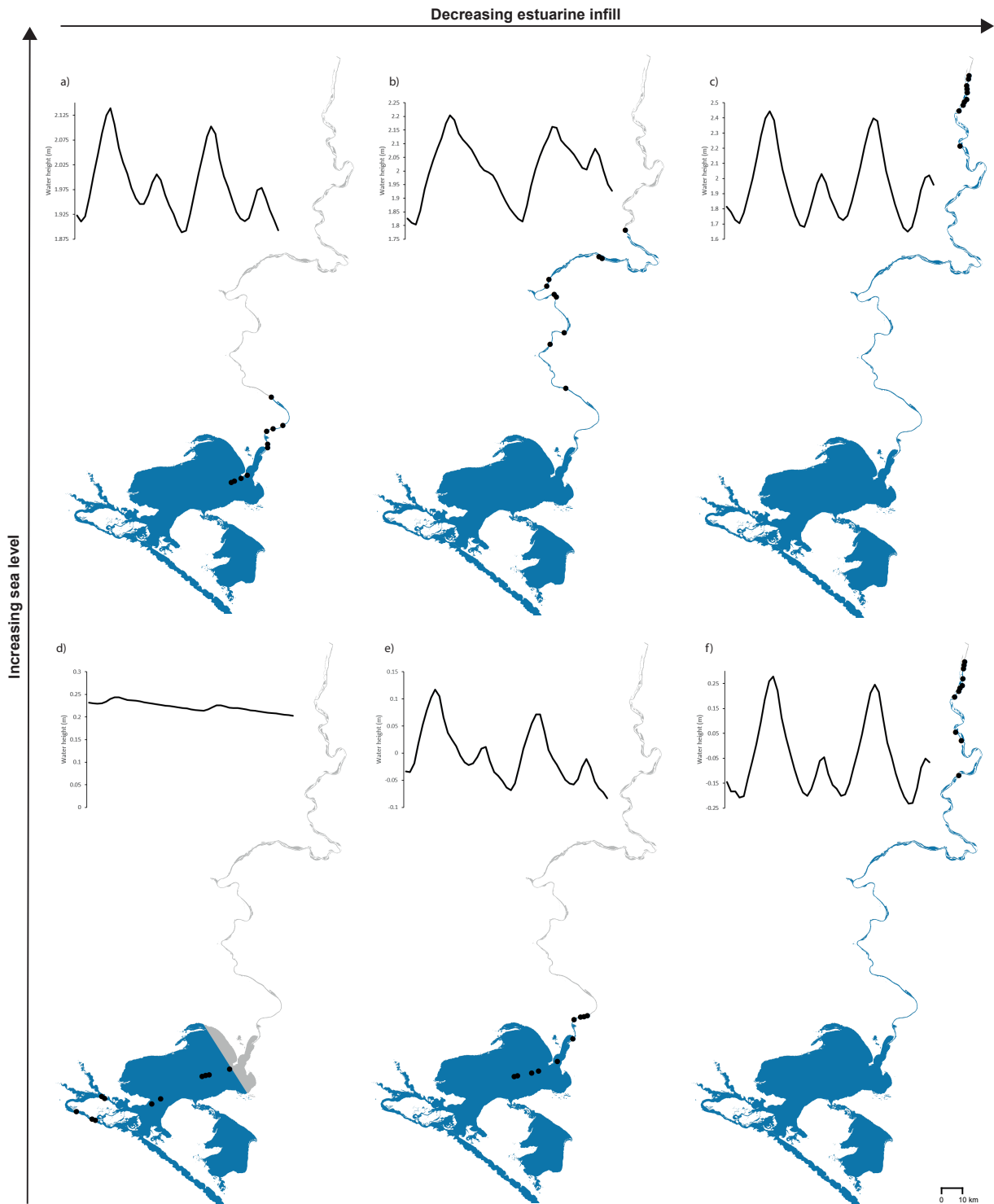
Figure 2.11: Characterisation of backwater zone and key representative tidal signatures. Maps show maximum upstream extent of velocity vector convergence for each scenario (black dots) in scenario category (a) $S_{up}WL_2$, (b) $S_{mid}WL_2$, (c) $S_{low}WL_2$, (d) $S_{up}WL_0$, (e) $S_{mid}WL_0$ and (f) $S_{low}WL_0$. Velocity vector convergence is taken as the point of convergence of upstream and downstream velocity vectors within the channel thalweg. Tidal signatures are given for the final 48 hours at the maximum upstream extent of upstream velocity vectors, in each scenario. Adopting Zaitlin et al.'s (1994) nomenclature, the areas shaded in blue are characterised as the middle incised valley. At the Holocene highstand, an enlarged low-energy backwater setting was emplaced up to Walker Flat (b; rkm 206).

Figure 2.12: Key representative maps comparing maximum velocity magnitude relative to barrier morphology and bathymetric surface. Areas are shaded red where maximum velocity >0.3 m/s and therefore is not conducive to the deposition of a laminated silt-clay sequence (Baas et al., 2016; Schieber et al., 2007; Schieber & Yawar, 2009). Barrier evolution from B_{mod}(**a**: scenario $S_{up}WL_2D_{av}B_{mod}$; **b**: scenario $S_{mid}WL_2D_{av}B_{mod}$; **c**: scenario $S_{low}WL_2D_{av}B_{mod}$; Table 2.2) to B_+(**d**: scenario $S_{up}WL_2D_{av}B_+$; **e**: scenario $S_{mid}WL_2D_{av}B_+$; **f**: scenario $S_{low}WL_2D_{av}B_+$; Table 2.2) has a minimal influence on the area conductive to velocities <0.3 m/s, while variance in bathymetry from S_{low}(**c**: scenario $S_{low}WL_2D_{av}B_{mod}$; **f**: scenario $S_{low}WL_2D_{av}B_+$; Table 2.2) or S_{mid}(**b**: scenario $S_{mid}WL_2D_{av}B_{mod}$; **e**: scenario $S_{mid}WL_2D_{av}B_+$; Table 2.2) to S_{up}(**a**: scenario $S_{up}WL_2D_{av}B_{mod}$; **d**: scenario $S_{up}WL_2D_{av}B_+$; Table 2.2) increases velocities within the back swamps upstream of Teal Flat (rkm 183), with comparable velocities elsewhere in the region. All scenarios shown are WL_2($+2$ m sea level) scenarios, demonstrating representative velocities at the Holocene highstand.
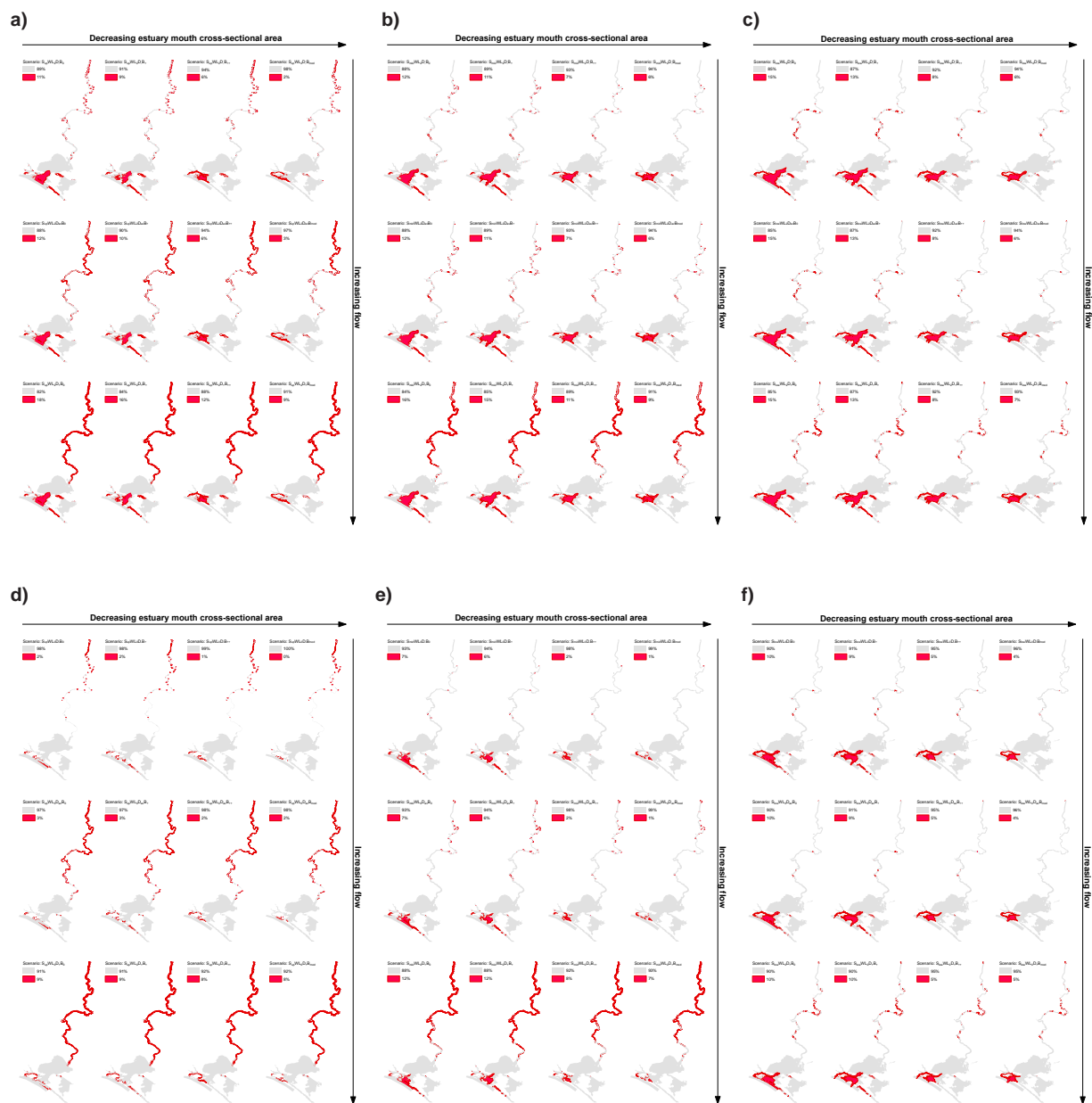
Figure 2.13: Maps of maximum velocity magnitude reached for each scenario. Maximum velocity magnitude is shown for each (a) $S_{up}WL_2$, (b) $S_{mid}WL_2$, (c) $S_{low}WL_2$, (d) $S_{up}WL_0$, (e) $S_{mid}WL_0$, (f) $S_{low}WL_0$ scenario. Areas are shaded red where maximum velocity >0.3 m/s and therefore is not conducive to the deposition of a laminated silt-clay sequence (Baas et al., 2016; Schieber et al., 2007; Schieber & Yawar, 2009). Refer to Table 2.2 for scenario descriptions.
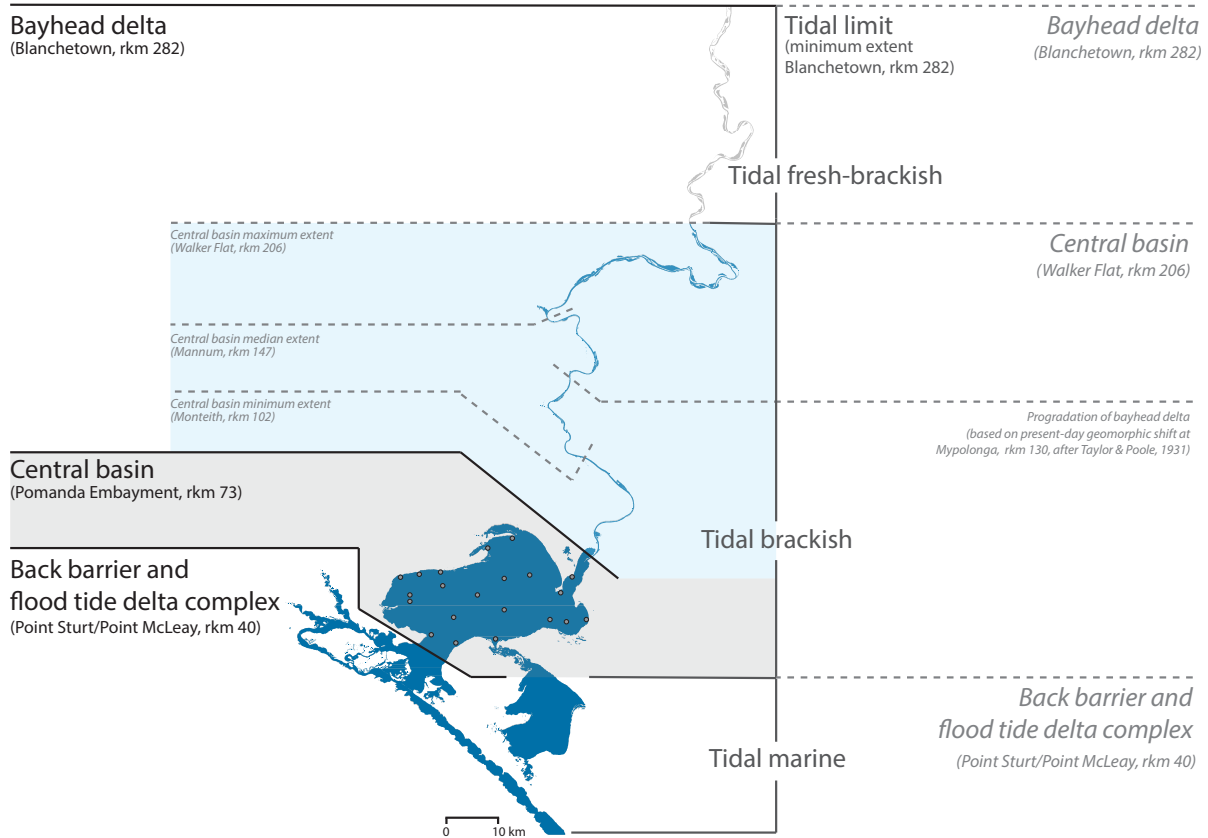
Figure 2.14: Estuarine processes zonation and inferred resulting morphology at the Holocene highstand. Based on $S_{mid}WL_2$ scenarios, estuarine processes can be categorised into three zonations: tidal marine, tidal brackish and tidal fresh-brackish (grey). At the Holocene highstand, the tidal limit propagated beyond the study region, suggesting a minimum tidal limit of Blanchetown (rkm 282). This zonation is extrapolated into inferred resulting morphology at the Holocene highstand (grey italics). The Murray estuary's barrier and flood tide delta complex occupied the region seaward of Point Sturt and Point McLeay (rkm 40). The central basin occupied the entirety of the Lower Lakes, Lakes Alexandrina and Albert, and extended upstream within the Murray Gorge plausibly as far as Walker Flat (rkm 206, minimum Monteith at rkm 102, and median Mannum at rkm 147). Upstream, the bayhead delta occupied a low-energy backwater zone at least as far as Blanchetown (rkm 282). During the late-Holocene, the bayhead delta prograded downstream to Mypolonga (rkm 130). These results are contrasted to conventional barrier estuary facies models (black), which place the upstream limit of the central basin at the point where the river debouches into the lake or lagoon (i.e. Pomanda Embayment, rkm 73). The Murray estuary's laminated central basin deposits have previously been identified in sediment cores (grey points) taken from within the conventional limits of the central basin (grey shaded area; Barnett, 1993; 1994). The results suggest that this laminated sequence characterises the Holocene depositional fill within the Murray Gorge at least as far upstream as Monteith (rkm 102) and plausibly as far as Walker Flat (rkm 206; grey and blue shaded areas).

2.4.4   Sensitivity testing

Examples of the influence of bathymetric surface on maximum palaeo-salinities are shown in Figures 2.8 and 2.10a and on inundation extent in Figure 2.7. The LMR is characterised by a main channel with fringing swamps under S_{up} scenarios, while the S_{mid} and S_{low} scenarios exhibit valley-wide inundation (Figure 2.7; Table 2.2). Within the Lower Lakes, the modelled inundation extent is comparable to present-day shorelines under S_{up} scenarios, with the S_{mid} and S_{low} morphologies extending inundation across the Cooke Plains Embayment (Figure 2.7; Table 2.2). Variation in palaeo-salinities is facilitated by Lake Alexandrina's palaeo-channel within the S_{mid} and S_{low} morphologies, forcing marine influence upstream, pushing the brackish limit well within the Murray Gorge and causing the majority of the LMR to be characterised by brackish-fresh water (Figures 2.8a & 2.10a; Figures 2.9b-c & e-f; Table 2.2). By comparison, the S_{up} scenarios allow for a brackish-fresh channel within the LMR while the fringing swamps largely remain fresh (Figures 2.8a & 2.10a; Figure 2.9a & d; Table 2.2). The presence, or infill of, this palaeo-channel also alters the palaeo-salinity of Lake Albert (Figures 2.8a & 2.9). Overall, variation in bathymetric surface alone is insufficient to alter the palaeo-environment of the region, as demonstrated by comparing the results presented in Figures 2.8a and 2.10a. Despite the uncertainty in the precise location of a S_{mid} surface, the similarity between the results from the two morphological end members (S_{low} and S_{up} scenarios) show that robust conclusions can be drawn irrespective of the validity of the S_{mid} Holocene highstand best-estimate morphology.

Variation in barrier morphology exerts its greatest influence within the barrier and flood tide delta complex and attenuates rapidly; by the mid-section of the Lower Lakes the impact of barrier morphology is negligible (Figures 2.8c & 2.8a). The variety of postulated early- to mid-Holocene chain-of-islands evolution events in the barrier complex does not change the character of the palaeo-environment, as demonstrated by the near identical maximum palaeo-salinities and 10 psu (marine-brackish) limits presented in Figures 2.8c and 2.10a respectively.

Sensitivity testing for discharge reveals that the flood event has a greater influence on palaeo-salinities when compared to drought, however, only under $S_{up}WL_0$ scenarios is a flood sufficient to supress Lake Alexandrina to fresher conditions (Figure 2.10a; Table 2.2). Drought conditions have a more pronounced impact on palaeo-salinities under present-day sea levels when compared to WL_2 scenarios (Figure 2.10a). Overall, variation of discharge has a moderate influence on palaeo-salinities throughout the region, however, as demonstrated by the near-identical maximum palaeo-salinities and 10 psu (marine-brackish) limits presented in Figures 2.8b and 2.10a, discharge alone is unable to alter the palaeo-environmental character of the region.

2.5   Discussion

This chapter has assessed the palaeo-Murray estuary's response to the Holocene highstand exploring the hydrologic and geomorphic influences on the regional palaeo-environment. The experimental hydrodynamic modelling approach adopted in this study allows for the relative importance of drivers of palaeo-environmental change to be determined. Sensitivity testing for sea level, discharge, bathymetry, and barrier morphology indicates sea level to be the determining factor for environmental characterisation of the palaeo-Murray estuary and the probable primary driver of change during the region's Holocene evolution. The experimental hydrodynamic modelling approach used here subjects end-member conditions to a sensitivity analysis giving a range of plausible responses rather than an explicit replication of reality. For instance, the S_{low} (Pleistocene – Holocene boundary) surface is certainly deeper than reality at the Holocene highstand, and the S_{up} (pre-regulation) surface certainly shallower. The negligible difference in results obtained through this end-member approach signifies that the models can in fact be extrapolated to represent a reasonable approximation of reality at the Holocene highstand.

The modelled estuarine environment at highstand is well constrained by global-scale estuary initiation at 8,200 yr BP following a significant meltwater pulse from the Laurentian ice sheet (Rodriguez et al., 2010). This event triggered major coastal change worldwide as the resulting accelerated rise in sea level caused a landward 'jump' in the estuarine zone (Rodriguez et al., 2010). On a local scale, within the Lower Lakes, flood tide delta and barrier complex stratigraphic (Barnett, 1993; de Mooy, 1959; Von der Borch & Altmann, 1979), diatom (Barnett, 1993; Cann et al., 2000) and midden analyses (Luebbers, 1982) support the designation of the regional palaeo-environment as estuarine at the Holocene highstand. However, the results demonstrate that this estuarine palaeo-environment was not limited solely to this region. This study shows that the +2 m Holocene highstand drove the estuarine limit much further upstream causing an enlarged low-energy backwater setting that occupied much of the LMR (tidal limit minimum rkm 282; Figure 2.14). The low relief of this coastal plain facilitated an elongated central basin within the confines of the Murray Gorge, likely extending as far upstream as Walker Flat (rkm 206), where the silt-clay laminated sequence that characterises the central basin deposits within Lake Alexandrina (Barnett, 1993; 1994) are inferred to extend (Figure 2.14). Adopting Zaitlin et al.'s (1994) nomenclature, these results demonstrate that the middle incised valley extends from the modern-day shoreline landward to the estuarine limit at highstand, which these results place between Walker Flat (rkm 206) and Blanchetown (rkm 282; Figures 2.10b & 2.14; Figure 2.11). It is suggested that, at highstand, the fluvial inner incised valley stretched from this estuarine limit landward to Overland Corner (rkm 439) where the river enters the Murray Gorge. Here, the Coonambidgal Formation displays evidence of a declining energy gradient (De Carli & Hubble, 2014), which is not characteristic of the sediments of a meandering river 430 rkm upstream

of its terminus. This unusually extensive backwater zone was a consequence of the unique low relief of this coastal plain system that attenuated flow velocities and forced the limit of coarse-grained fluvial deposition well upstream.

Since European settlement, the region has been subject to significant modification including extensive land reclamation and the construction of levees, locks, and barrages. Prior to this, the riverbanks between Mannum (rkm 154) and Mypolonga (rkm 130) were typically high creating natural levees that separated the channel from low-lying flats; this configuration transitioned to an unbroken series of swamps between Mypolonga (rkm 130) and Wellington (rkm 78; Taylor & Poole, 1931). The shift in channel fringing environment at Mypolonga (rkm 130) is inferred to be the approximate limit of bayhead delta progradation before significant European modification and regulation of the LMR disrupted the natural flow regime (Figure 2.14). A homogenous clay sequence could be expected to overlie the laminated central basin deposit, representing the downstream progradation of the bayhead delta, the precise location of which is to be determined by a subsequent study.

The regionally extensive and continuous nature of the Murray estuary's laminated deposit within Lake Alexandrina from 5,500 yr BP until modern-day (Barnett, 1993; 1994) suggests that the mechanism of deposition and preservation cannot exclusively be attributed to a palaeo-environment that differs to what we see today. The sequence continued to deposit despite the decrease in regional salinity brought about by a fall to present-day sea levels in the late-Holocene (Figures 2.8a and 2.104a). Recent flume studies demonstrate the capacity of laminated silt-clay deposition in much higher velocities than previously thought (Schieber et al., 2007), with the results of this study illustrating a real-world application in a dynamic palaeo-environment subject to marine influence (Figures 2.12 & 2.13) and consistent with the notion that salinity assists, but is not vital, for floc formation and laminae deposition (Schieber & Yawar, 2009). An Australian east coast analogue is present in the Hawkesbury River estuary, where the Holocene estuarine central basin and bayhead delta sediments extend well into the gorge-confined valley, with the Colo River estuarine sequence presenting similar laminations to those described in Lake Alexandrina (Barnett, 1993; 1994; Devoy et al., 1994; Hughes et al 1998; Nichol et al., 1997).

When considering the LMR, or other gorge confined portions of coastal plain estuaries, as an extension of the central basin, the definition adopted is important. Dalrymple et al. (1992) define the central basin not in the geomorphic sense of a lagoon, with which gorge confined regions such as the LMR could not conceivably be considered, but rather on the basis of facies designation. The process-based results from $S_{mid}WL_2$ scenarios are correlated with facies designation to infer the resulting morphology of the Murray estuary at the Holocene highstand (Figure 2.14). The inferred resulting morphology adopts Dalrymple et al.'s (1992) facies rather than a geomorphic definition of the central basin whereby the lower portion of

incised river valleys may exhibit the depositional characteristics of the central basin. Here, the central basin is considered as the region of lowest energy characterised by the confluence of marine and fluvial influence and the deposition of the finest sediment.

Following conventional models of estuarine facies designation, the location where the river debouches into the lagoon is the likely transitional point of the designation of fluvial to estuarine geological formations (Figure 2.14). However, with low relief allowing for elongated estuarine zones at the Holocene highstand, it is suggested that the location of this transition requires review across coastal plain estuaries more broadly. In the case of the Murray estuary, the Holocene stratigraphy of Lake Alexandrina is characterised as the estuarine and coastal-marine sediments of the St Kilda Formation, whereas the LMR is characterised as the Quaternary alluvium of the Coonambidgal Formation (Figure 2.7a; Table 2.3). This transition is currently placed at the Pomanda Embayment (rkm 73; Figures 2.1 & 2.7a), or precisely where the LMR debouches into Lake Alexandrina. By assigning process-based results to inferred resulting morphology, these results suggest a revision of the location of this transition is required to account for the Holocene extension of estuarine sedimentation within the gorge-confined portion of the central basin (Figure 2.14). A sedimentary analysis is currently underway to assess the upstream extent and nature of this deposit, with previous work in the region suggesting the presence of a laminated sequence may be widespread within the LMR (Hubble & De Carli, 2015; Taylor & Poole, 1931).

The key to understanding responses of coastal plain estuaries to future changes in climate requires a knowledge of drivers of change, best explored by an examination of palaeo-responses to such change through representative analogues. This study demonstrates the vulnerability of Australia's largest and most politically and economically significant river basin to future environmental change. A comparison between $S_{up}WL_0$ and $S_{up}WL_2$ scenarios reveal the pronounced shift in environmental character with higher sea levels inducing significant marine incursion to the Lower Lakes, driving the brackish and fresh-brackish water zones as far upstream as Teal Flat (rkm 183; Figure 2.8a I & IV; Figure 2.9a & d). Currently the Murray estuary is a highly regulated system with a series of barrages in place to prevent saline intrusion into the estuary and river system, crucial for maintaining the freshwater resources within the region during 'undesirable' weather events such as prolonged drought. With the pace of future sea-level rise too rapid for barriers to transgress in response, and the results presented here demonstrating a significant change in environmental character regardless of barrier morphology, this study demonstrates the utility of applying a historical analogue to understand the importance of adapting water management to future needs. In the case of the Murray estuary this analysis highlights the future importance of and likely need for reliance on the barrages if the current freshwater resource priorities are to be maintained.

Adopting a hydrodynamic modelling approach to Holocene analogues of coastal plain estu-

aries allows for the significant potential impact of climate change induced sea-level rise to be realised. These results identify sea level as the dominant controlling factor on the environmental character of the Murray estuary, with the approximately 2 m higher-than-present sea level during the Holocene highstand generating an extensive central basin environment characterised by a low-energy backwater and laminated silt-clay deposits. It has been demonstrated that the estuarine limit can extend significantly further inland than expected when evaluating modern-day geomorphology in the context of conventional estuarine facies models. The importance of sea level in controlling the character of the Murray estuary, irrespective of fluvial discharge, bathymetry and barrier morphology, suggests the impacts of future sea-level rise due to climate change on coastal plain estuaries may be underappreciated. These results are broadly applicable to low-gradient coastal plain estuaries with wave-dominated entrances, particularly those with large catchments and low discharges. However, consideration must be applied to the nature of the incised valley and valley fill, dynamics of fluvial discharge and tidal regime, as well as the rate of sea-level rise/fall when transferring these results to other coastal plain estuaries (Roy et al., 1980). The extent and impact of sea-level rise as a driver of environmental change is largely a consequence of the inherently low gradient of these systems. This characteristic low gradient of coastal plain estuaries facilitates the landward extension of the estuarine zone rendering lower portions of the conventionally fluvially dominated zone particularly vulnerable to saline intrusion and potentially unable to support potable water or irrigation supplies. The economic and social implications of these findings to the LMR and Murray estuary, and comparable coastal plain estuaries more broadly, are considerable.

Chapter 3

Simple 2D simulations sufficiently resolve 3D hydrodynamics for assessments of estuarine palaeo-environmental change: A case study of the Holocene Murray estuary

3.1 Abstract

3D hydrodynamic models are complex and computationally expensive, capable of providing a highly accurate representation of the geomorphic and hydrologic behaviour of an estuary. However, for assessments of palaeo-environmental change, such an approach may be beyond the appropriate level of complexity given the inherent uncertainty in modelling past environments. Models of Holocene palaeo-environments cannot be subjected to vigorous calibration against measured events. Rather inputs are validated against evidence in the geological record giving a best-estimate approach which is capable of constraining rather than accurately predicting a system's response to a given variable. Considering this framework, here, this study adopts the lower Murray River and Murray estuary as a case study to demonstrate the utility of applying 2D simulations for assessments of a system's response to palaeo-environmental change during the Holocene. The results demonstrate that despite the inherent inability of 2D models to resolve stratification of an estuary, meaningful proxies can be derived to estimate the upstream extent of the salt wedge at depth resolved in 3D. The 2D to 3D comparison reveals an overall consistency in modelled results for key outputs of salinity and flow velocity magnitude, with 2D simulations providing an appropriate representation of 3D results. Crucially, 2D and 3D estuarine zonation are directly comparable such that 2D simulations provide a simple, efficient and meaningful alternative to 3D hydrodynamic modelling of Holocene estuaries.

3.2   Introduction

2D simulations are significantly more computationally efficient than their 3D counterparts resulting in faster runtimes and simplicity in post-processing. However, the assumption that 2D results are sufficiently indicative of our 3D world is an assumption that is not always tested yet often contested. 2D simulations may not identically mimic intricate flow patterns in complex systems but their results may be sufficiently representative to draw broad conclusions on the behaviour of a system, for instance, when assessing primary drivers of environmental change. Identifying key drivers of palaeo-environmental change is required to better understand how a system behaved under natural conditions, prior to anthropogenic modifications to the flow regime, which is crucial for effective natural resource management (Gell et al., 2009; Mills et al., 2013a). This is particularly important in intensively managed systems where understanding the natural behaviour of a system, and natural responses to change, can be used to help predict system responses to future changes in environmental conditions due to global warming and sea-level rise associated with anthropogenic climate change (Gell et al., 2009; Mills et al., 2013a). Here, the study adopts the LMR and Murray estuary as a case study to evaluate the reliability of 2D simulations compared to 3D simulations when applied to understand palaeo-responses to environmental change during the Holocene. Specifically, this study adopts the +2 m Holocene sea-level highstand (Belperio et al., 2002; Lewis et al., 2013) to assess how well 2D simulations resolve palaeo-environmental change when compared to more complex and computationally expensive 3D simulations.

The LMR and Murray estuary lie at the terminus of Australia's largest river basin, the MDB (Figure 3.1). Flow within the MDB is highly regulated with a series of weirs, dams, locks and barrages. Coupled with extractions for irrigation and drinking water this has resulted in significant alterations to the natural flow regime. Within the Murray estuary, a series of five barrages are in place to prevent saline incursion into the Lower Lakes, Alexandrina and Albert (Figure 3.1). These structures act to significantly curtail the tidal prism in the estuary, by over 85%, and hold the Lower Lakes fresh such that the natural dynamics of vertical mixing or saline stratification within the estuary are not apparent (Harvey, 1996).

Owing to the intensity of water regulation, hydrodynamic modelling is an existing component of natural resource management within the region. A very high resolution and well validated model has been developed to better understand the morphodynamics of the Murray Mouth (Hudson and Wainwright, 2013). The complexity of this model is required to resolve the hydrology of the inlet with enough confidence to guide policy on dredging; a necessity to prevent the Murray Mouth's permanent closure due the magnitude of upstream water extraction (Bourman et al., 2000; Hudson and Wainwright, 2013). Hydrodynamic models
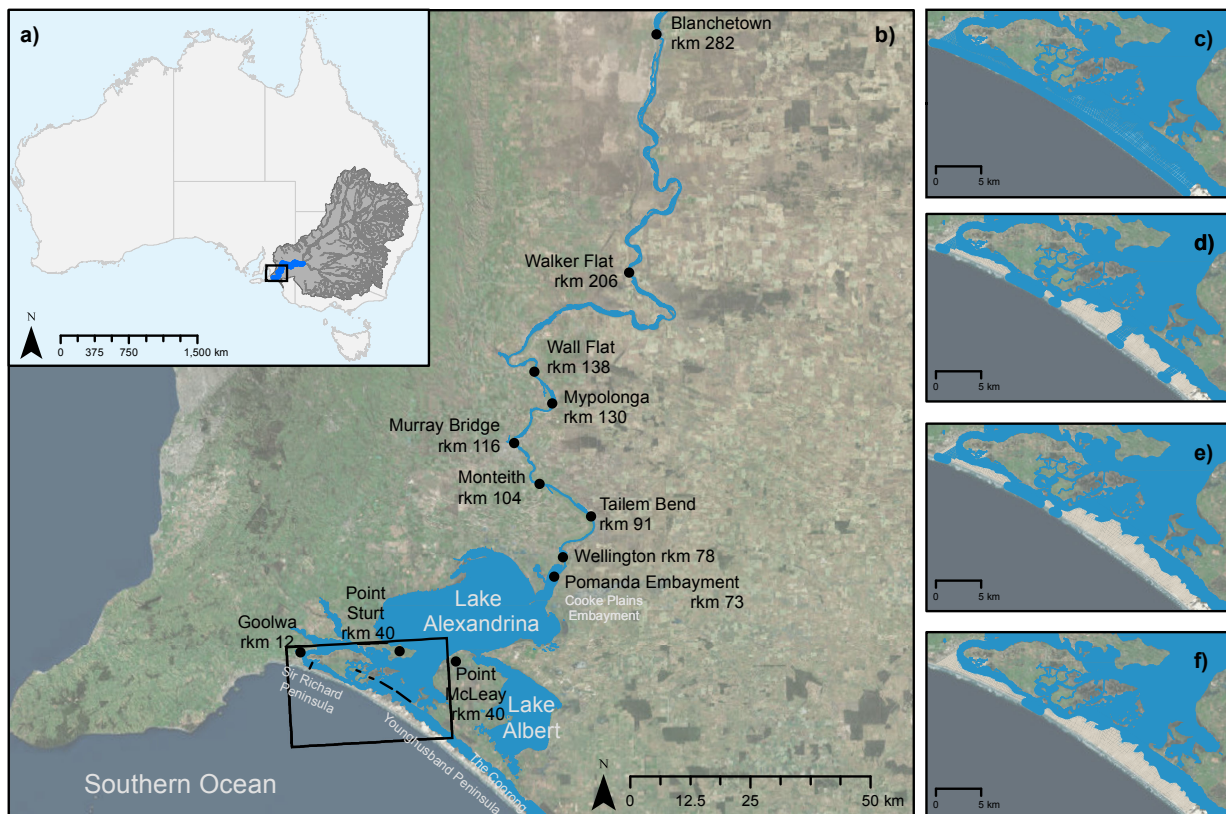
Figure 3.1: Overview of study site. (**a**) The LMR (blue) lies at the terminus of Australia's largest river basin, the MDB (grey), whose major watercourses are shown in dark grey. (**b**) The model domain encompasses the LMR from Lock 1 at Blanchetown (rkm 282) to the outlet to the Southern Ocean at the Murray Mouth between Sir Richard and Younghusband Peninsulas. Collectively, Lake Alexandrina and Lake Albert are known as the Lower Lakes, and, together with the Coorong lagoon, form the Murray estuary. A series of five barrages (black lines) within the flood-tide delta prevent saline incursion into the Lower Lakes and LMR. The morphological evolution of the barrier complex is modelled as four evolutionary phases ranging from completely open (**c**) B_0, two intermediate phases (**d**) B_+ and (**e**) B_{++}, to the modern-day barrier (**f**) B_{mod}.

have also been adopted to guide drought remediation in the region and safeguard against potential vulnerability of water resources given uncertainties due to future climate change. The Wellington Virtual Weir modelling investigation was commissioned by the MDBA after a period of low flow caused significant saline incursion and stratification within the Murray estuary and LMR (Hudson, 2010). The modelling investigated whether sufficient discharge could suppress the formation of a salt wedge and curtail saline ingression which threatened the viability of the extraction of potable water at Tailem Bend (rkm 91) and Murray Bridge (rkm 116) during the Millennium Drought (1997-2011; Hudson, 2010).

Given the need for environmental managers to obtain robust and reliable results from these models, it is no surprise that in both instances modelling was conducted in 3D. When modelling palaeo-environmental responses to change over geological time, however, this level of complexity may not be necessary or possible. Understanding long-term geological scale changes in a system is perhaps best approached by behaviour orientated modelling (Hanson

et al., 2003). This involves identifying and understanding the influence of macro-variables individually and assessing each of these relative to their own spatial and temporal scale (Hanson et al., 2003). Helfensdorfer et al. (2019) developed a suite of 2D models to sensitivity test for palaeo-environmental changes to the LMR and Murray estuary in response to fluctuations in sea level during the Holocene. These models are simplistic in comparison to the 3D simulations described above (i.e. Hudson, 2010; Hudson and Wainwright, 2013), however, the focus of these 2D simulations is a sensitivity analysis of end member and best estimate static configurations of particular variables to constrain, rather than accurately predict, the response of a system to each variable. This approach allows for meaningful results to be derived, in keeping with the premise that the complexity of a given model should be fit for purpose (French et al., 2016). Trends that may be revealed from such exercises are useful to inform 'first-pass' assessments when studying complex, multi-variable systems. For example, modelling exercises are often used to inform the location of fieldwork sites, whereby the identification of highly responsive locations can save significant time and resources.

There is significant disparity in the temporal resolution of physical processes which define the hydrodynamics, morphology and evolution of estuarine systems. Tides and storms can greatly influence the morphology of barrier systems on an hourly scale. Seasonal and decadal climatic drivers cause fluctuation in fluvial discharge, and millennial scale sedimentary infill controls channel planform evolution. Apart from the concerns of computational inefficiency, allowing a sufficient run time to capture natural processes operating at a variety of temporal scales would not produce a valid model, as the dynamic and compounding influences of processes at different scales would induce an unacceptable amount of uncertainty (de Vriend et al., 1993). For example, the short-term influence of tides typically generates trivial amounts of change in the long term (Hanson et al., 2003). Instead, when specifically modelling complex multi-influenced behaviours over large temporal scales, de Vriend et al. (1993) argue that eliminating small scale detail, and focusing instead on broad physical processes, leads to simple yet robust models. Such models remain capable of assessing the relative importance of physical processes which define a system's behaviour (de Vriend et al., 1993).

French et al. (2016) argue that 'appropriate complexity' is achieved when a model sufficiently resolves, and explains, system behaviours to provide a predictive capacity at an adequate temporal and spatial resolution. It follows, then, that the 2D models used by Helfensdorfer et al. (2019) may well assess the response of the Murray estuary to the Holocene sea-level highstand adequately. A key objective of Helfensdorfer et al.'s (2019) study was to determine the palaeo-environmental character of the region by identifying the likely tidal limit, extent of the backwater zone and salinity distribution that prevailed at the Holocene highstand. Maximum flow velocity magnitudes were assessed relative to the critical threshold of 0.3 m/s to determine the likelihood of deposition and preservation of the laminated sequence which characterises the Murray estuary's central basin deposit (Baas et al., 2016; Barnett, 1993;

1994; Helfensdorfer et al., 2019; Schieber and Yawar, 2009; Schieber et al., 2007). Here, a comparative analysis of 2D and 3D simulations is conducted to assess whether Helfensdorfer et al.'s (2019) results in 2D are consistent in 3D. A subset of twelve 2D models from Helfensdorfer et al. (2019) are examined, comprising three bathymetric surfaces (S_{low}, S_{mid} and S_{up}), two sea level scenarios (WL_2 and WL_0), four barrier morphologies (B_0, B_+, B_{++} and B_{mod}) and three discharge scenarios (D_-, D_{av} and D_+; Table 3.1). Each of these twelve models are replicated twice using two different 3D simulations to generate representative 2D to 3D comparisons of the full suite of 2D models presented in Helfensdorfer et al. (2019). Using this set of 36 models this chapter will:

- Evaluate the spatial extent of estuarine facies at the Holocene sea-level highstand;

- Characterise the LMRs Holocene stratigraphy;

- Determine the main events in the Holocene geomorphic evolution of the Murray estuary;

- Identify possible future environmental changes to the LMR and Murray estuary due to climate-change induced sea-level rise.

3.3   Methods

3.3.1   Overview of model result categories

Two bathymetric surfaces represent end-member conditions to constrain the likely bathymetry that prevailed at the Holocene highstand. The Pleistocene-Holocene boundary provides a deep limit, denoted by S_{low}, and the pre-modification surface presents a shallow limit denoted by S_{up}, with a third best-estimate Holocene highstand surface denoted by S_{mid}. Together with the two metre variance in sea level from highstand (denoted by WL_2) to present-day level (denoted by WL_0), this gives six model result categories: $S_{low}WL_2$, $S_{low}WL_0$, $S_{mid}WL_2$, $S_{mid}WL_0$, $S_{up}WL_2$ and $S_{up}WL_0$ (Table 3.1). The Holocene chain-of-islands evolution of the barrier complex is accounted for through four barrier morphologies ranging from completely open (denoted by B_0), through two evolutionary phases (denoted by B_+ and B_{++}), to the modern-day condition (denoted by B_{mod}). The three discharge scenarios range from drought (denoted by D_-), pre-regulation average (denoted by D_{av}) to flood (denoted by D_+). The twelve models assessed in this study represent a subset of the full range of variables tested in Helfensdorfer et al. (2019; Table 3.1). This combination allows each variable to be assessed independently, relative to the best-estimate Holocene highstand scenario ($S_{mid}WL_2D_{av}B_{mod}$), such that the primary drivers of palaeo-environmental change can be evaluated in 3D. For example, the scenario which adopts a combination of the Pleistocene – Holocene surface (S_{low}) with modern-day barrier morphology (B_{mod}) is not indicative of reality, rather this scenario allows for the influence of bathymetric surface to be independently assessed whilst

all other variables are held constant.

Table 3.1: Overview of model scenarios. Codes identify bathymetric surface (S_{up} = pre-modification condition, S_{mid} = highstand best estimate condition, S_{low} = Pleistocene-Holocene boundary condition), discharge (D_- = drought, D_{av} = pre-regulation average, D_+ = pre-regulation average with a flood event), and barrier morphology (B_0 = no barrier, B_+ and B_{++} = phases of chain-of-islands evolution (Bourman and Murray-Wallace, 1991; de Mooy, 1959; Harvey, 2006; Luebbers, 1982), and B_{mod} = present day). A code and category have been assigned to each scenario to facilitate interpretation. Scenario categories are grouped based on sea-level and bathymetric surface. All models were run as 2D, 3D-1 and 3D-2 simulations, with scenario $S_{mid}WL_2D_{av}B_{mod}$ run a fourth time as a 3D-3 simulation (see Supplementary Materials).

Initial sea level at 2 m					Initial sea level at 0 m				
Bathymetric Surface	Discharge	Barrier Morphology	Scenario Code	Scenario Category	Bathymetric Surface	Discharge	Barrier Morphology	Scenario Code	Scenario Category
S_{up}	D_{av}	B_{mod}	$S_{up}WL_2D_{av}B_{mod}$	$\mathbf{S_{up}WL_2}$	S_{up}	D_{av}	B_{mod}	$S_{up}WL_0D_{av}B_{mod}$	$\mathbf{S_{up}WL_0}$
S_{mid}	D-	B_{mod}	$S_{mid}WL_2D_-B_{mod}$	$\mathbf{S_{mid}WL_2}$					
	D_{av}	B_0	$S_{mid}WL_2D_{av}B_0$						
		B_+	$S_{mid}WL_2D_{av}B_+$		S_{mid}	D_{av}	B_{mod}	$S_{mid}WL_0D_{av}B_{mod}$	$\mathbf{S_{mid}WL_0}$
		B_{++}	$S_{mid}WL_2D_{av}B_{++}$						
		B_{mod}	$S_{mid}WL_2D_{av}B_{mod}$						
	D_+	B_{mod}	$S_{mid}WL_2D_+B_{mod}$						
S_{low}	D_{av}	B_{mod}	$S_{low}WL_2D_{av}B_{mod}$	$\mathbf{S_{low}WL_2}$	S_{low}	D_{av}	B_{mod}	$S_{low}WL_0D_{av}B_{mod}$	$\mathbf{S_{low}WL_0}$

3.3.2   Numerical model setup

Hydrology is simulated using the finite volume numerical model TUFLOW FV. The model domain spans some 282 river kilometres encompassing the LMR, downstream of Lock 1 at Blanchetown, and the Murray estuary, including the Lower Lakes, Alexandrina and Albert, Coorong lagoon and Murray Mouth, then extends 2 km offshore. A detailed description of the numerical model set up, including an analysis on the relative influence of morphology, barrier evolution, discharge and sea level performed in 2D is given in Chapter 2.

3.3.3   Sensitivity testing

This study comprises three simulation types: 2D, 3D-1 and 3D-2. 2D simulations are a subset of those presented in Helfensdorfer et al. (2019). Twelve scenarios representing all three bathymetric surfaces (S_{low}, S_{mid} and S_{up}), both sea level scenarios (WL_2 and WL_0), all four barrier morphologies (B_0, B_+, B_{++} and B_{mod}) and all three discharge scenarios (D_-, D_{av} and D_+) are considered to represent the full suite of modelled scenarios (Table 3.1). 3D-1 simulations are a direct scalar of 2D simulations, with the simple addition of vertical layers, while 3D-1 and 3D-2 simulations are differentiated by their vertical momentum and scalar mixing models: 3D-1 simulations adopt the Smagorinsky model, and 3D-2 simulations adopt a parametric model. The parametric turbulence model calculates a parabolic eddy viscosity/diffusivity profile and adopts the Munk and Anderson (1948) stability formula to

represent stratification and is therefore expected to generate a more realistic vertical solution. The 3D-1 simulations also adopt a first order scheme compared to a second order scheme for 3D-2 simulations. Second order schemes typically resolve a more realistic solution as they perform linear reconstructions between each cell which accommodates sharp gradients more effectively. As a direct scalar from 2D, the 3D-1 simulations model salinity without density coupling, while 3D-2 simulations model salinity as density coupled. Finally, both 3D-1 and 3D-2 simulations adopt hybrid z-sigma vertical layers with 6 z-layers and 2 surface sigma layers. For all 3D simulations calculations are reverted to 2D at the threshold water depth of 0.5 m. To assess the influence of additional vertical layers, a single 3D-3 simulation was run, mirroring the 3D-2 simulation type but with double the number of vertical layers; refer to the Supplementary Materials for this analysis.

3.3.4   Post processing

The salinity classification scheme of Tooley (1978) was adopted and applied to maximum salinities observed post burn-in phase. 3D depth averaged outputs provide a direct comparison to 2D results. In addition, 3D netCDF output data was visualised and processed using MATLAB to assess the vertical distribution of representative maximum salinity outputs to account for any stratification within the estuary. Flow velocity vectors within the channel thalweg were assessed such that comparisons could be drawn between the three bathymetric surfaces irrespective of morphology. The critical threshold of 0.3 m/s was adopted when assessing maximum flow velocity magnitudes (Baas et al., 2016; Schieber and Yawar, 2009; Schieber et al., 2007).

3.4   Results

3.4.1   Depth averaged maximum salinity

When comparing post burn-in maximum salinities there is no significant change between 2D models and simple 3D (3D-1) models (Figure 3.2). However, the change in the vertical mixing model as well as coupling salinity and density (from 3D-1 to 3D-2) does cause some divergence of results. The marine-brackish (10 psu) limit ingresses further upstream in 3D-2 models compared to 3D-1 models, with the degree of change dependent on bathymetric surface (Figures 3.2 & 3.3a-b). The simplistic trapezoidal-like representation of the LMR within S_{low} scenarios causes the most significant change in apparent saline ingression approximately doubling the marine-brackish (10 psu) limit when compared with 2D and 3D-1 models (Figure 3.2), driving marine conditions well upstream into the Murray Gorge (Figure 3.3a-b). The presence of a defined palaeo-channel traversing Lake Alexandrina within the S_{low} surface
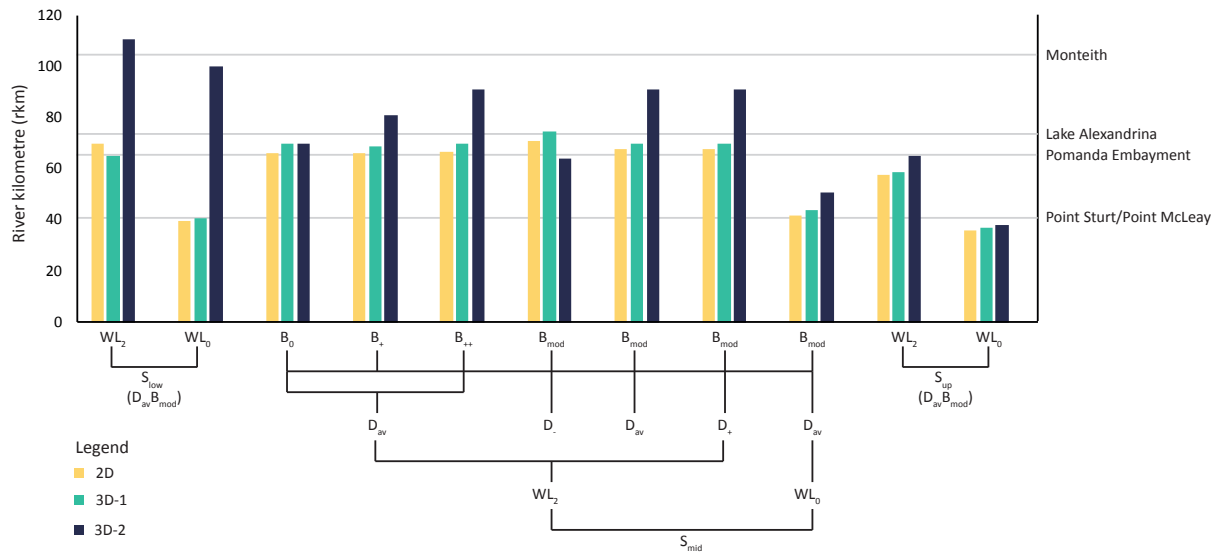
Figure 3.2: Maximum limit of marine-brackish incursion (10 psu) by simulation type relative to sea level, bathymetric surface, discharge and barrier morphology. Overall, 2D and 3D-1 simulations provide a conservative measure of the limit of marine-brackish incursion (10 psu) when compared with 3D-2 simulations. The influence of simulation type is most pronounced given variation in bathymetric surface with S_{low} scenarios producing significantly different brackish limits under 3D-2 simulations. Variation in surface from S_{mid} to S_{up}, or any variation in sea level, discharge or barrier morphology produces consistent trends between simulation type. The 3D-2 simulation of scenario $S_{mid}WL_2D_-B_{mod}$ is represented at a single timestep rather than the post burn in maximum due to an error causing the apparent inconsistency in trend depicted here.

funnels marine influence up into the LMR whilst keeping the comparatively shallow main body of Lake Alexandrina brackish-marine to brackish (Figure 3.3a-b). This phenomenon is best resolved by 3D-2 simulations, with 2D simulations and the simplistic mixing models of 3D-1 simulations unable to adequately resolve the influence of bathymetry on saline incursion (Figure 3.2). The magnitude of this change is greatly diminished in S_{mid} scenarios causing a maximum change in marine-brackish (10 psu) limit of 21 rkm (scenarios: $S_{mid}WL_2D_{av}B_{++}$, $S_{mid}WL_2D_{av}B_{mod}$ and $S_{mid}WL_2D_+B_{mod}$) and no change in others (scenario: $S_{mid}WL_2D_{av}B_0$; Figure 3.2; Table 3.1). Finally, given S_{up} morphology, where the marine-brackish (10 psu) limit is constrained to the comparatively shallow, infilled main body of Lake Alexandrina, the difference between 2D, 3D-1 and 3D-2 results is negligible (Figures 3.2 & 3.3a-b). The relative influence of sea level is comparable between 2D and 3D-2 simulations such that a +2 m increase from present-day WL_0 to Holocene highstand WL_2 scenarios converts the Lower Lakes from brackish waterbodies to almost fully marine (Figure 3.3a-b). Despite the increased proportion of marine-brackish waters within the lower lakes given 3D-2 simulations, a change in discharge from drought (D_-), pre-regulation average (D_{av}) to flood (D_+) scenarios is insufficient to alter the palaeo-salinity distribution of the region, which is in agreement with 2D simulation trends (Figure 3.3c-d). Similarly, sensitivity testing for all four barrier morphologies reveals a consistent palaeo-environment given both 2D and 3D-2 simulations (Figure 3.3e-f).

3.4.2   2D vs 3D maximum salinity

Curtain plots derived from 3D-2 simulations reveal that some stratification of the estuary is apparent under most conditions (Figure 3.4). The magnitude of stratification varies considerably by bathymetric surface with the relatively infilled S_{up} surface preventing the development of a salt wedge and holding the marine-brackish (10 psu) limit to within the main body of Lake Alexandrina (Figure 3.4a). Pronounced stratification is facilitated by the palaeo-channel which traverses Lake Alexandrina and the LMR within both the S_{mid} and S_{up} surfaces (Figure 3.4a). This bathymetric feature causes the marine-brackish limit to ingress well upstream into the Murray Gorge at least as far as Monteith (rkm 100) under Holocene highstand (WL_2) conditions (Figure 3.4a). Given the S_{low} surface, a fall in sea level to present-day conditions (WL_0) reduces marine influence but, owing to the trapezoidal-like channel within the LMR, significant marine-brackish (10 psu) incursion is maintained; the comparative infill of the S_{mid} surface limits these conditions to the main body of Lake Alexandrina (Figure 3.4a).

A comparison of 2D to 3D maximum salinity results indicate that a 2D proxy of the upstream limit of the marine-brackish (10 psu) salt wedge can be developed relative to bathymetric surface. Under S_{low} conditions, the limit of marine-brackish (10 psu) conditions at depth is equivalent to the 2D brackish-fresh (0.5 psu) limit (Figures 3.2 & 3.4). Under S_{mid} conditions this 2D proxy is best defined by the 2.5 psu limit, with the 3.5 psu limit under S_{up} conditions (Figures 3.2 & 3.4).

3.4.3   Depth averaged maximum flow velocity magnitude

Under all scenarios, 3D-1 simulations overestimate flow velocities, both within Lake Alexandrina and the flood-tide delta, and within the LMR (Figure 3.5). In comparison, 2D and 3D-2 simulations are very well constrained under most conditions such that 2D simulations provide an appropriate estimation of 3D-2 trends (Figure 3.5). 2D simulations accurately capture 3D-2 maximum flow velocities relative to the study's critical threshold of 0.3 m/s, with a slight deviation within Lake Alexandrina under S_{low} conditions, however this does not significantly alter palaeo-environmental interpretation (Figure 3.5). Under best estimate Holocene highstand conditions ($S_{mid}WL_2D_{av}B_{mod}$) 2D simulations afford an accurate representation of 3D-2 results, with 3D-1 simulations marginally overestimating the area with a maximum flow velocity magnitude above 0.3 m/s (Figure 3.6).
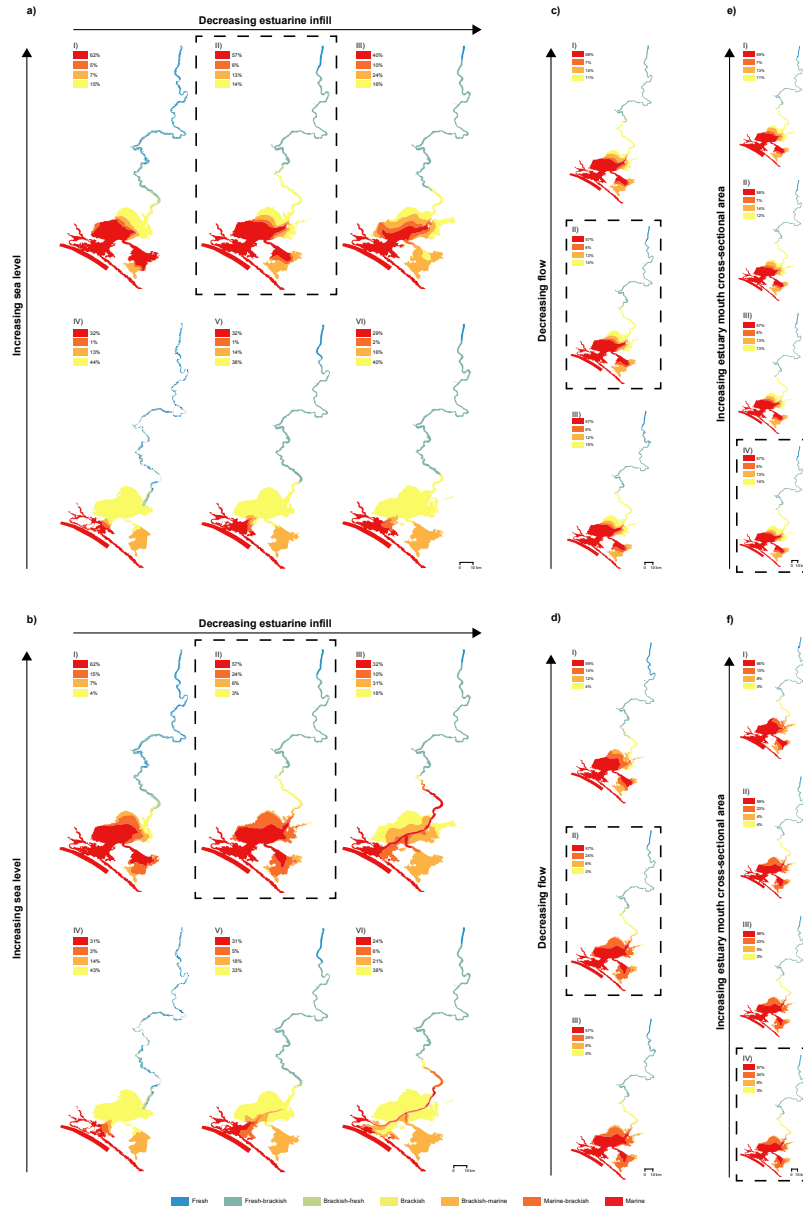
Figure 3.3: Key representative maps comparing depth averaged maximum salinity reached given 2D and 3D-2 simulations relative to sea level, bathymetric surface, discharge and barrier morphology. Under both (**a**) 2D and (**b**) 3D-2 simulations, an increase in sea level from WL_0 present-day conditions (IV-VI) to WL_2 Holocene highstand conditions (I-III) significantly increases marine incursion, with the brackish limit comparable regardless of simulation type. 3D-2 models more accurately resolve flow dynamics within the palaeo-channel that traversed through Lake Alexandrina, increasing the relative area subject to marine and marine-brackish conditions when compared to 2D simulations. This influence is most apparent under S_{low} conditions where Lake Alexandrina's palaeo-channel is deepest (**a**III and VI or **b**III and VI). The influence of discharge on the palaeo-environmental character of the region is negligible under both (**c**) 2D and (**d**) 3D-2 simulations, despite 3D-2 simulations resulting in comparatively greater marine influence throughout the Lower Lakes. These same trends are upheld when accounting for variance in barrier morphology between (**e**) 2D and (**f**) 3D-2 simulations. The hatched box highlights the common scenario between the six panels: scenario $S_{mid}WL_2D_{av}B_{mod}$. Within (**a**) and (**b**) all maps shown are pre-regulation average discharge with modern-day barrier morphology scenarios (I: scenario $S_{up}WL_2D_{av}B_{mod}$; II: scenario $S_{mid}WL_2D_{av}B_{mod}$; III: scenario $S_{low}WL_2D_{av}B_{mod}$; IV: scenario $S_{up}WL_0D_{av}B_{mod}$; V: scenario $S_{mid}WL_0D_{av}B_{mod}$ and VI: scenario $S_{low}WL_0D_{av}B_{mod}$; Table S1). To demonstrate representative salinities at the Holocene highstand, $S_{mid}WL_2$ scenarios are shown within (**c**) and (**d**) (I: scenario $S_{mid}WL_2D_{-}B_{mod}$; II: scenario $S_{mid}WL_2D_{av}B_{mod}$; III: scenario $S_{mid}WL_2D_{+}B_{mod}$) and (**e**) and (**f**) (I: scenario $S_{mid}WL_2D_{av}B_0$; II: scenario $S_{mid}WL_2D_{av}B_{+}$; III: scenario $S_{mid}WL_2D_{av}B_{++}$; IV: scenario $S_{mid}WL_2D_{av}B_{mod}$). The 3D-2 simulation of scenario SmidWL2D-Bmod (**c**I and **d**I) is represented at a single timestep rather than the post burn in maximum due to a saving error. Salinity is measured based on the classification scheme of Tooley (1978).
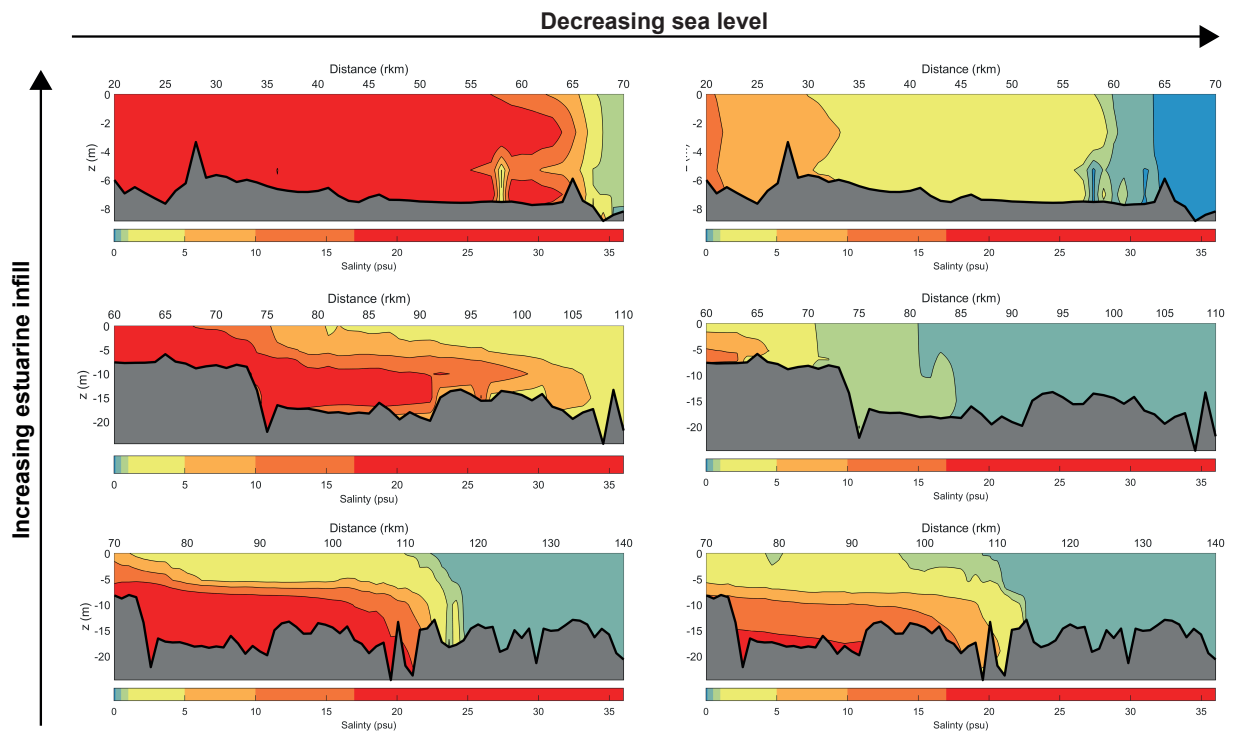
Figure 3.4: Curtain plots representing maximum saline incursion as resolved by 3D-2 simulations. Variation in bathymetric surface has a pronounced influence on both the magnitude of stratification and the upstream limit of saline ingression, with variation in sea level effecting only the length of the salt wedge. Data was derived from timestep 11 which is representative of maximum salinity penetration across the model run time. Salinity is measured based on the classification scheme of Tooley (1978).

3.4.4   Near-bed maximum flow velocity magnitude

When considering the potential for deposition and preservation of a laminated sequence the critical velocity threshold of 0.3 m/s should more accurately be considered within the immediate vicinity of the bed. Maximum flow velocity magnitudes were extracted from the bottom metre of the water column in 3D-1 and 3D-2 simulations and are shown in Figure 3.7 relative to 2D results. Overall, 2D simulations provide a conservative estimate of 3D results, by resolving marginally greater maximum flow velocities throughout the model domain (Figure 3.7). When compared to 3D-2 results, 3D-1 simulations marginally underestimate near-bed maximum flow velocity (Figure 3.7). 2D simulations sufficiently represent 3D-2 flow velocity magnitudes throughout the model domain under all scenarios, especially given the critical threshold of 0.3 m/s, such that these results can be considered meaningful estimations of conditions at the near-bed (Figure 3.7). Overall, 3D depth averaged results do not significantly differ from measured near-bed maximum velocity magnitudes (Figures 3.5 vs 3.7).

3.4.5   Estuarine processes zonation and inferred resulting morphology

Applying velocity vectors to define the upstream extent of the backwater zone allows comparisons to be drawn between inferred extent of the central basin for each simulation type (2D/3D-1/3D-2). The influence of simulation type is demonstrated through $S_{mid}WL_2D_{av}B_{mod}$ scenarios in Figure 3.8. 2D simulations indicate the modelled central basin extent to Mypolonga (rkm 128), which is nearly identical to the results of the 3D-2 simulations (extent: Mypolonga, rkm 129; Figure 3.8), such that the addition of an advanced 3D model set up does not change the designation of the central basin extent. However, 3D-1 scenarios place this limit slightly further upstream at Wall Flat (rkm 139; Figure 3.8). The tidal limit remains consistent across all simulation types with tidal influence propagating beyond the upstream extent of the model domain at Blanchetown (rkm 282; Figure 3.8). These results demonstrate that simple 2D simulations accurately resolve estuarine processes zonation and inferred resulting morphology for the Murray estuary.
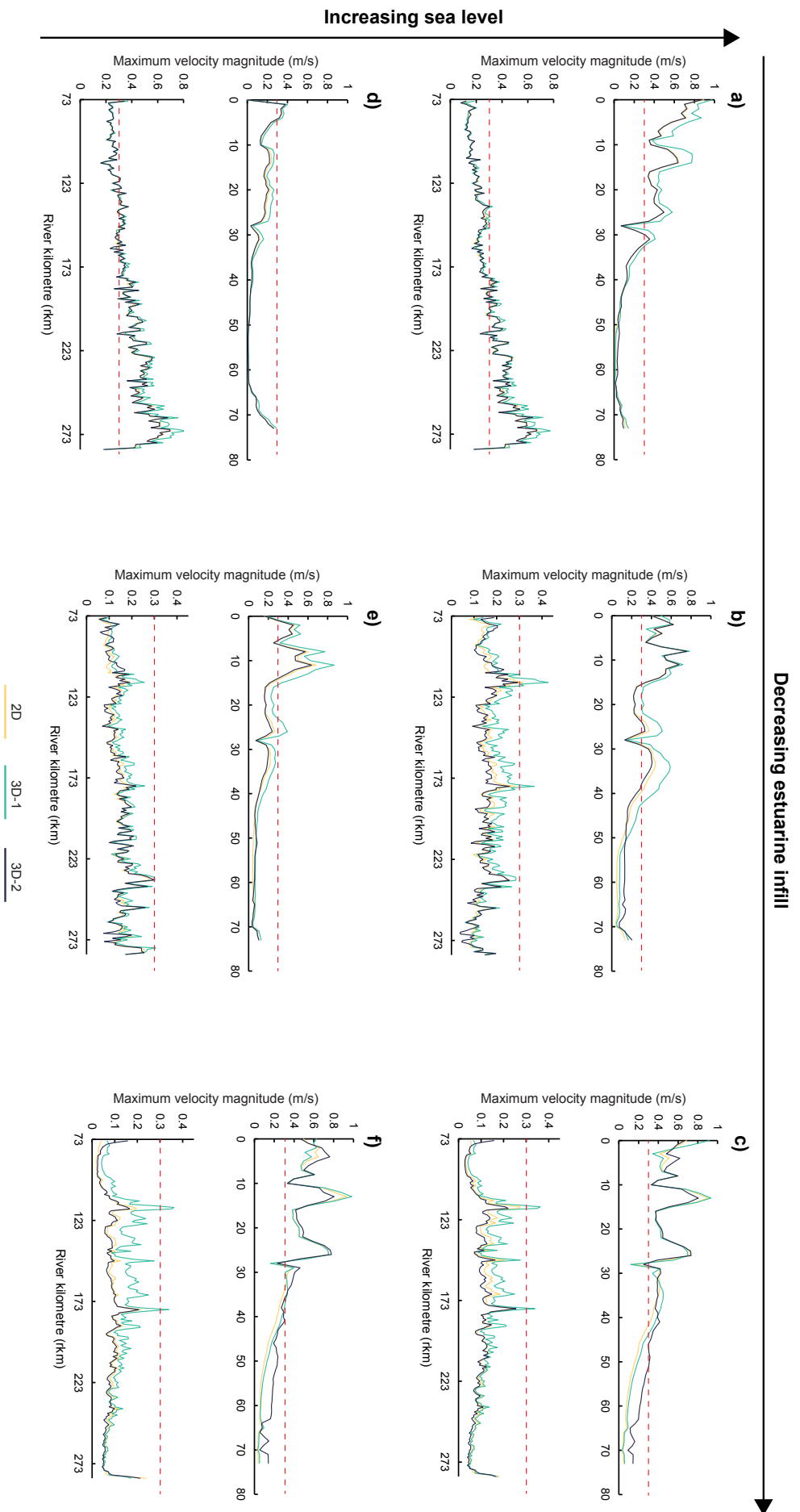
Figure 3.5: Depth averaged maximum flow velocity magnitude by simulation type relative to sea level and bathymetric surface. Overall, 3D-1 simulations overestimate velocity flow magnitude, when compared with 2D and 3D-2 simulations, irrespective of sea level or bathymetric surface. 2D simulations are well constrained by 3D-2 results, typically providing a marginal overestimation. The upper reaches of Lake Alexandrina (rkm 40–73) under S_{low} bathymetry present the only deviation to these trends with 3D-2 scenarios producing a different and increased maximum flow velocity magnitude profile. Panels are split at the Pomanda Embayment (rkm 73) with the Murray Mouth, flood-tide delta and Lake Alexandrina shown above, and the LMR shown below. 0.3 m/s is the critical velocity threshold conducive to the deposition of a laminated sequence (red dash; Baas et al., 2016; Schieber and Yawar, 2009; Schieber et al., 2007). (a: scenario $S_{up}WL_2D_{av}B_{mod}$; b: scenario $S_{mid}WL_2D_{av}B_{mod}$; c: scenario $S_{low}WL_2D_{av}B_{mod}$; d: scenario $S_{up}WL_0D_{av}B_{mod}$; e: scenario $S_{mid}WL_0D_{av}B_{mod}$ and f: scenario $S_{low}WL_0D_{av}B_{mod}$).
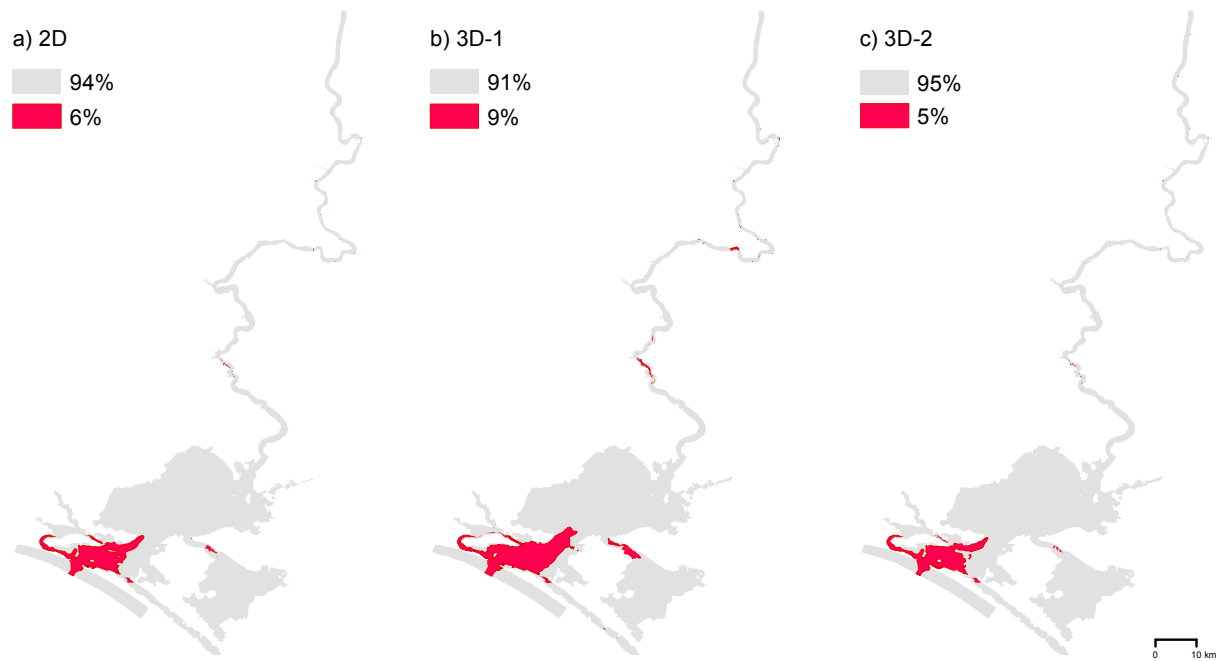
Figure 3.6: Comparison of depth averaged maximum flow velocity magnitudes relative to simulation type for scenario $S_{mid}WL_2D_{av}B_{mod}$. Areas are shaded red where maximum flow velocity >0.3 m/s and is therefore not conducive to the deposition of a laminated sequence (Baas et al., 2016; Schieber and Yawar, 2009; Schieber et al., 2007). The flood-tide delta is the only region where maximum flow velocity exceeds 0.3 m/s in (**a**) 2D and (**c**) 3D-2 simulations, with these simulation types producing near identical results, while (**b**) 3D-1 simulations result in a marginal overestimate of flow velocity magnitudes within both the LMR and Lower Lakes.
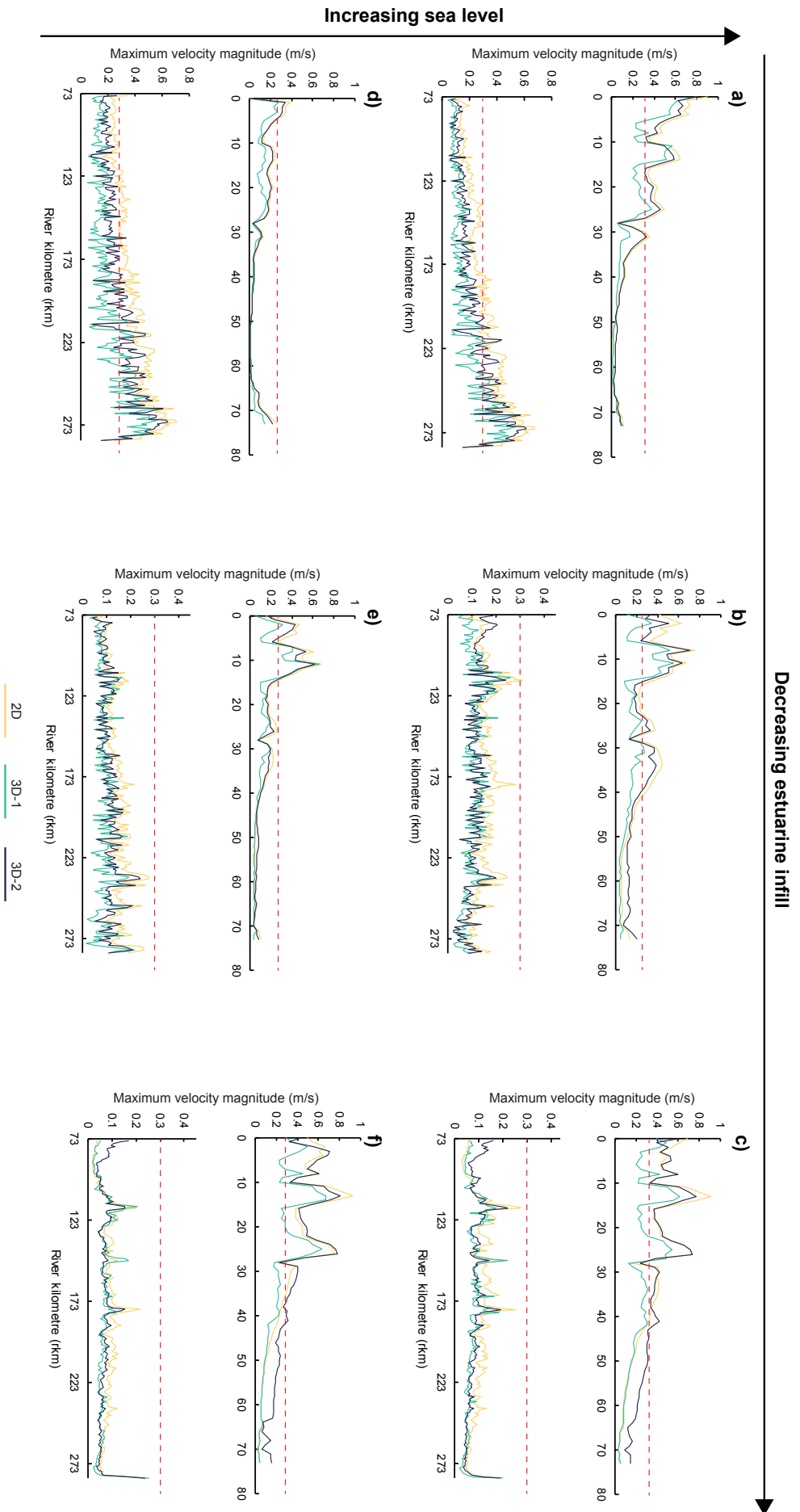
Figure 3.7: Maximum flow velocity magnitude at the near-bed by simulation type relative to sea level and bathymetric surface. Velocity is measured for the bottom meter of the water column for 3D-1 and 3D-2 simulations. Overall, 2D simulations provide an overestimate of maximum flow velocity magnitudes at the near-bed, with the magnitude of this overestimation greater in the LMR (bottom panels) compared to the Murray Mouth, flood-tide delta and Lake Alexandrina (top panels). 2D simulations adequately capture 3D-1 and 3D-2 trends irrespective of sea level or bathymetric surface. Panels are split at the Pomanda Embayment (rkm 73) with the Murray Mouth, flood-tide delta and Lake Alexandrina shown above, and the LMR shown below. 0.3 m/s is the critical velocity threshold conductive to the deposition of a laminated sequence (red dash; Baas et al., 2016; Schieber and Yawar, 2009; Schieber et al., 2007). (a: scenario $S_{up}WL_2D_{av}B_{mod}$; b: scenario $S_{mid}WL_2D_{av}B_{mod}$; c: scenario $S_{low}WL_2D_{av}B_{mod}$; d: scenario $S_{up}WL_0D_{av}B_{mod}$; e: scenario $S_{mid}WL_0D_{av}B_{mod}$ and f: scenario $S_{low}WL_0D_{av}B_{mod}$).

Figure 3.8: Influence of simulation type on resolving estuarine processes zonation and inferred resulting morphology at the Holocene highstand for scenario $S_{mid}WL_2D_{av}B_{mod}$. Applying the tidal limit and maximum extent of velocity vector convergence to infer resulting morphology suggests that the barrier and flood-tide delta complex occupied the region seaward of Point Sturt and Point McLeay (rkm 40) and the central basin extended upstream to Mypolonga (rkm 128) with the bayhead delta occupying the region upstream of this point given 2D simulations (black text). Resolving this in 3D (grey text) maintains the minimum tidal limit at Blanchetown (rkm 282) with the limit of the central basin palaeo-environment dependent on simulation type. Simple 3D-1 simulations overestimate the central basin's extent placing this division at Wall Flat (rkm 139), while 3D-2 simulations are very well constrained by 2D results suggesting the central basin extended 129 rkm upstream of the Murray Mouth.

3.5   Discussion

This chapter has assessed the suitability of applying simple and efficient 2D models to assess the relative influence of drivers of palaeo-environmental change by evaluating results against more complex and computationally expensive 3D simulations of the Holocene palaeo-Murray estuary. The results demonstrate that 2D simulations adequately resolve the key outputs of salinity and flow velocity magnitude obtained in 3D such that estuarine process zonation and inferred morphology resulting from 2D and 3D simulations is virtually identical (Figure 3.8). These results demonstrate that applying practical, simple and computationally efficient 2D simulations is a suitable approach for 'first-pass' assessments of estuarine environmental change.

When assessing the suitability of modelling in 2D versus 3D, the most notable consideration is the inverse relationship between predicted model accuracies and runtime – 2D simulations are expected to provide the least certainty but are computationally efficient, while 3D-2 simulations are expected to produce the most accurate result at the expense of a considerable increase in model run time, with 3D-1 simulations providing a middle ground. Here, this balance has been assessed in the context of understanding estuarine palaeo-environmental change where model input parameters are, inherently, subject to uncertainty. It has been demonstrated that, when assessing relative responses to change in the geological past, the increased accuracy of 3D results is unjustified as simple and computationally efficient 2D simulations afford a sufficient representation of 3D model trends.

The influence of 3D model complexity is apparent in the difference between 3D-1 and 3D-2 results. 3D-1 simulations typically give conservative depth averaged salinity, as first order schemes cannot accurately resolve saline stratification (Figure 3.2). 3D-1 simulations also overestimate depth averaged flow velocity magnitude while producing conservative values at the near-bed (Figure 3.5 vs. 3.7). The discrepancy in salinity and velocity trends between 3D-1 and 3D-2 simulations demonstrates the requirement for a second order solution, a more complex turbulent mixing model and density coupled salinity when scaling hydrodynamic models up from 2D to 3D. All 3D-1 and 3D-2 simulations had an average run time between 45-50 hours on a specially built 16-core 16 GB RAM server, with surprisingly little variance in computational expense by spatial order scheme. Given this unexpected result, there is no justification for the use of 3D-1 simulations in lieu of more appropriately complex 3D-2 simulations. By contrast, 2D equivalents were significantly less computationally expensive with an average run time of less than half their 3D-2 counterpart at 15-20 hours, supporting the preference of simple and efficient 2D simulations given sufficiently comparable key outputs.

The significant contrast in maximum salinity reached, and the location of the marine-brackish (10 psu) limit between 2D and 3D-2 results given S_{low} and S_{mid} or S_{up} surfaces, highlights

the importance of morphology when considering whether simple and efficient 2D simulations can provide an adequate representation of an estuary (Figures 3.2 & 3.3a-b). Overall, 2D simulations underestimate the relative importance of bathymetric surface in controlling the palaeo-environmental character of the region, with the increased complexity of vertical mixing models in 3D-2 scenarios more accurately resolving the influence of Lake Alexandrina's palaeo-channel in driving saline incursion up into the Murray Gorge (Figures 3.2 & 3.3a-b). This is particularly apparent under S_{low} conditions, where the presence of a deep palaeo-channel facilitates the development of a significant salt wedge driving the marine-brackish (10 psu) limit twice as far upstream when compared to 2D results (Figures 3.2 & 3.4). However, given that this palaeo-channel is certainly deeper than that at the Holocene sea-level highstand (Helfensdorfer et al., 2019), the suitability of 2D simulations in resolving 3D-2 trends under S_{mid} or S_{up} conditions is crucial when assessing Holocene palaeo-environmental change within the Murray estuary. Given this comparison only, the 2D simulations are considered to provide a reasonable estimation of 3D-2 results (Figures 3.2 & 3.3a-b).

The purpose of model reduction is to increase computational efficiency while maintaining meaningful outputs. A key approach to model reduction is to increase the morphological timestep and constrain variables to within justified ranges (de Vriend et al., 1993). The utility of this reductionist approach has been demonstrated through an assessment of the Holocene evolution of the Murray estuary's barrier complex. The addition of a morphological component to the model would have served to resolve wave (short-term) and storm (event-based) dominated morphological change to the barrier complex, processes which do not operate on the geological scale required for a study of a Holocene palaeo-estuary. Instead, by increasing the morphological timestep through an assessment of static phases of chain-of-islands barrier evolution (Bourman and Murray-Wallace, 1991; de Mooy, 1959; Harvey, 2006; Luebbers, 1982), the relative influence of barrier morphology on the palaeo-environment can be assessed. No present morphological model could sufficiently resolve and model morphological evolution on this timescale whilst also accurately resolving hydrodynamics in order to identify estuarine zonation; the approach demonstrated here provides the most appropriate solution. The same reductionist principles can be applied when considering the suitably of assessing the influence of barrier morphology in 2D as oppose to 3D. Given that the complexities of 3D morphological change are principally relevant when assessing short-term or event-based changes in morphology, this resolution becomes redundant when upscaling to understanding drivers of Holocene palaeo-environmental change. A comparison of maximum salinity between 2D and 3D-2 simulations reveals that, despite an increase in the areal extent of Lower Lakes subject to marine-brackish conditions, 2D simulations accurately convey 3D trends whereby the evolution of the barrier is unable to change the palaeo-environmental character of the region (Figure 3.3e-f).

The ability to resolve potential saline stratification is likely the most meaningful advantage

of scaling an estuarine hydrodynamic model from 2D to 3D. Stratification is dependent on the strength of tides (with spring-neap variations common), the horizontal salinity gradient (which is itself dependent on both the strength of tidal inflows and fluvial outflows) and, to a lesser degree, estuarine circulation (Geyer, 2010). Subject to the morphology of the estuary, a salt wedge typically occurs when the strength of freshwater fluvial flow overwhelms vertical mixing by the tides causing stratification of lighter freshwater and denser salt water (Geyer and Ralston, 2011). It follows, then, that this condition prevails in estuaries with particularly weak tidal conditions (Geyer and Ralston, 2011). As the series of the barrages within the flood-tide delta significantly curtail the tidal prism and act to keep the Lower Lakes fresh, a field based assessment of how prone the Murray estuary is to saline stratification under natural conditions cannot be conducted. However, even under average present-day conditions some saline stratification is evident, with periods of low flow providing an indication as to what extent this may occur under natural conditions if the barrages were not in place (Aldridge et al., 2009). Aldridge et al. (2009) demonstrate that sheltered areas, such as the Goolwa channel, exhibit greater stratification when compared to the open main body of Lake Alexandrina. This trend is apparent as far upstream as the sheltered Pomanda Embayment under low flow conditions (Aldridge et al., 2009). Significant stratification, presently confined to the Goolwa channel due to the presence of the barrages, may serve as an indication of what the Lower Lakes and lower reaches of the LMR experienced prior to regulation of the flow regime, as, presently, salinity can be over five times higher in the hypolimnion compared to the epilimnion (Aldridge et al., 2009).

It follows, then, that 2D simulations may not accurately represent the palaeo-environmental character of the Murray estuary as this evidenced saline stratification cannot be resolved. Given depth averaged results, 2D simulations provide a predictively conservative measure of preferred 3D (3D-2 simulation) results with the limit of marine-brackish (10 psu) incursion held seaward of the Pomanda Embayment (rkm 73) rather than propagating up into the lower reaches of the Murray Gorge under most Holocene highstand scenarios (Figure 3.2). A comparison of 2D and 3D maximum salinity demonstrates that the 2D 3 psu limit can be used as a proxy for the maximum ingression of the marine-brackish (10 psu) salt wedge under Holocene highstand conditions (Figure 3.4). Overall, the considerable influence of the +2 m Holocene highstand (WL_2) in altering the palaeo-environmental character of the Murray estuary, and the dominance of this factor when compared to variance in bathymetric surface, discharge or barrier morphology, is a trend which is maintained irrespective of 2D or 3D-2 simulations (Figure 3.3). Crucially, when combining these salinity results with flow velocity magnitude results to infer estuarine process zonation and morphology the suitability of 2D simulations is immediately apparent (Figure 3.8).

3.6   Conclusion

The discrepancy in overall results of 3D-1 simulations compared to 3D-2 simulations suggest that the simplistic nature of these 3D models produces inaccuracies which, given comparative model runtimes, precludes further comparison. Therefore, a comparison between 2D and 3D-2 simulations is favoured. Overall, a comparison between results derived from these two simulation types demonstrate that critical parameters for determining palaeo-environmental conditions within the Murray estuary were sufficiently resolved in 2D. 2D depth averaged maximum flow velocity magnitudes are well constrained by 3D-2 results (Figure 3.5), and, when assessed relative to 3D-2 results at the near-bed, provide a conservative estimate of velocity conditions (Figure 3.7) such that the area conductive to the deposition and preservation of a laminated sequence is virtually identical (Figure 3.6). Inherently, 2D simulations cannot resolve the salt wedge which penetrated into the Murray Gorge under average flow conditions throughout the Holocene prior to the installation of the barrages (Figure 3.4). Given this stratification, 2D simulations are unable to resolve the influence of the simple trapezoidal bathymetry of the S_{low} surface in driving saline incursion up into the LMR (Figures 3.2 & 3.3a-b & 3.4a). Nonetheless, Helfensdorfer et al.'s (2019) conclusion developed in 2D – that variation in sea level was the most significant driver of palaeo-environmental change within the Murray estuary during the Holocene – is sufficiently upheld by 3D-2 simulations. This suggestion is validated by an assessment of estuarine processes zonation where 2D simulations produce near identical placements of the inferred resulting morphology at the Holocene sea-level highstand (Figure 3.8). This result demonstrates that the predictive skill of 2D simulations is not sufficiently different from 3D-2 simulations such that results of 2D simulations are deemed an appropriate estimation of 3D palaeo-environmental conditions within the LMR and Murray estuary.

This chapter has adopted the LMR and Murray estuary as a case study to demonstrate the utility of applying simple and computationally efficient 2D simulations as a sufficient 'first-pass' assessment of 3D estuarine change. The precision of 3D results is forgone for increased efficiency and simplicity of 2D simulations, however, given inherent uncertainties of modelling in geological time, this approach is deemed fit for purpose. This approach is applicable to palaeo-environmental studies of estuaries more broadly, particularly those with gradational changes in bathymetry. The results of this study suggest that 2D simulations are a simple and effective means of sufficiently resolving estuarine palaeo-environmental change particularly when applied as a 'first-pass' assessment to guide further study.

Chapter 4

Atypical responses of a large catchment river to the Holocene sea-level highstand: The Murray River, Australia

4.1   Abstract

Three-dimensional hydrodynamic modelling of the lower Murray River and Murray estuary indicates the approximately 2 m higher-than-present sea level during the Holocene highstand generated an extensive central basin environment within the confines of the Murray Gorge at least 140 kilometres upstream from the river mouth. Analysis of sediment present in a 30 m core (Monteith-A), sited 104 kilometres upstream from the river mouth, indicate a shift in deposition to a silt-clay laminated sequence at 8,518 cal yr BP and the initiation of estuarine conditions. A transect of cone penetrometer soundings demonstrates that the Murray estuary's central basin deposit occupied the entire width of the several kilometre-wide Murray Gorge. The accommodation space provided within this extremely low gradient, backwater environment captured the river's sediment discharge and essentially prevented the delivery of the Murray's terrigenous sediment load to the offshore marine environment between 8,518 and 5,067 cal yr BP. The existence of this previously unrecognised natural sediment trap located upstream of the point of discharge to the ocean suggests that mid-Holocene climate reconstructions based on fluctuations of terrigenous sediment in marine cores taken offshore of the Murray's Mouth should be re-evaluated.

4.2   Introduction

Effective natural resource management benefits from a thorough understanding of how a system functioned prior to anthropogenic modification. Palaeo-climatic data is often used to inform natural resource management, with sequences of Holocene sediments providing a record that constrains a system's predicted response to a changing climate and sea level (Mills et al., 2013a). The political, economic and environmental ramifications of natural resource allocation decisions will become increasingly contentious in coming decades as the consequences of a changing climate become more apparent (Gell et al., 2009; Mills et al., 2013a). Managers will become increasingly reliant on high quality palaeo-climatic data to inform their policies (Gell et al., 2009; Mills et al., 2013a). This is particularly the case for intensively managed river systems, such as Australia's MDB, that support large-scale agriculture whilst also being important ecological refuges (Figure 4.1). The MDB comprises the Murray and Darling sub-catchments which drain over 1 million km^2 and is Australia's most economically important agricultural region. At the terminus of the MDB, the gorge-confined LMR debouches into Lake Alexandrina and then flows through the Murray Mouth to the Southern Ocean (Figure 4.1). The Murray's barrier estuary developed in response to a rapidly rising sea level during the Holocene with the formation of Sir Richard and Younghusband peninsulas and the development of the central basin lakes Alexandrina and Albert (Bourman et al., 2000; Hill et al., 2009) (Figure 4.1).

The MDB has been increasingly managed since 1900 to accommodate the competing needs of irrigation and drinking water supply for development while maintaining environmental flows in a hydroclimate that is prone to long-term droughts (Mills et al., 2013a). Given the challenges of a warming and drying climate (Reisinger et al., 2014) the successful management of this system and its water allocation policy will be informed by an improved understanding of southeastern Australia's Holocene climate.

The Holocene climate of southeastern Australia is typically characterised by wetter than present-day conditions during the early- to mid-Holocene, before a shift to increased climatic variability and an overall trend to aridity in the late-Holocene (Gingele et al., 2007; Gouramanis et al., 2013; Kemp et al., 2012). Within the MDB, approximately 90% of flow is derived from the Murray River and its tributaries (Walker, 2006), with the annual snow melt on the southeast Australian highstands producing significant seasonal flow variability within this sub-catchment. Murray sub-catchment annual rainfall and flow variability is currently dominated by the El Nino-Southern Oscillation (ENSO), which generates inter-annual variability, and the Pacific Decadal Oscillation (PDO) driving decadal to centurial variability (Gell et al., 2009; Gouramanis et al., 2013; McGowan et al., 2009). The semi-arid Darling sub-catchment receives its most significant flows from the Inter-Tropical Convergence Zone (ITCZ) summer monsoon (Gell et al., 2009; Gouramanis et al., 2013; McGowan et al., 2009).
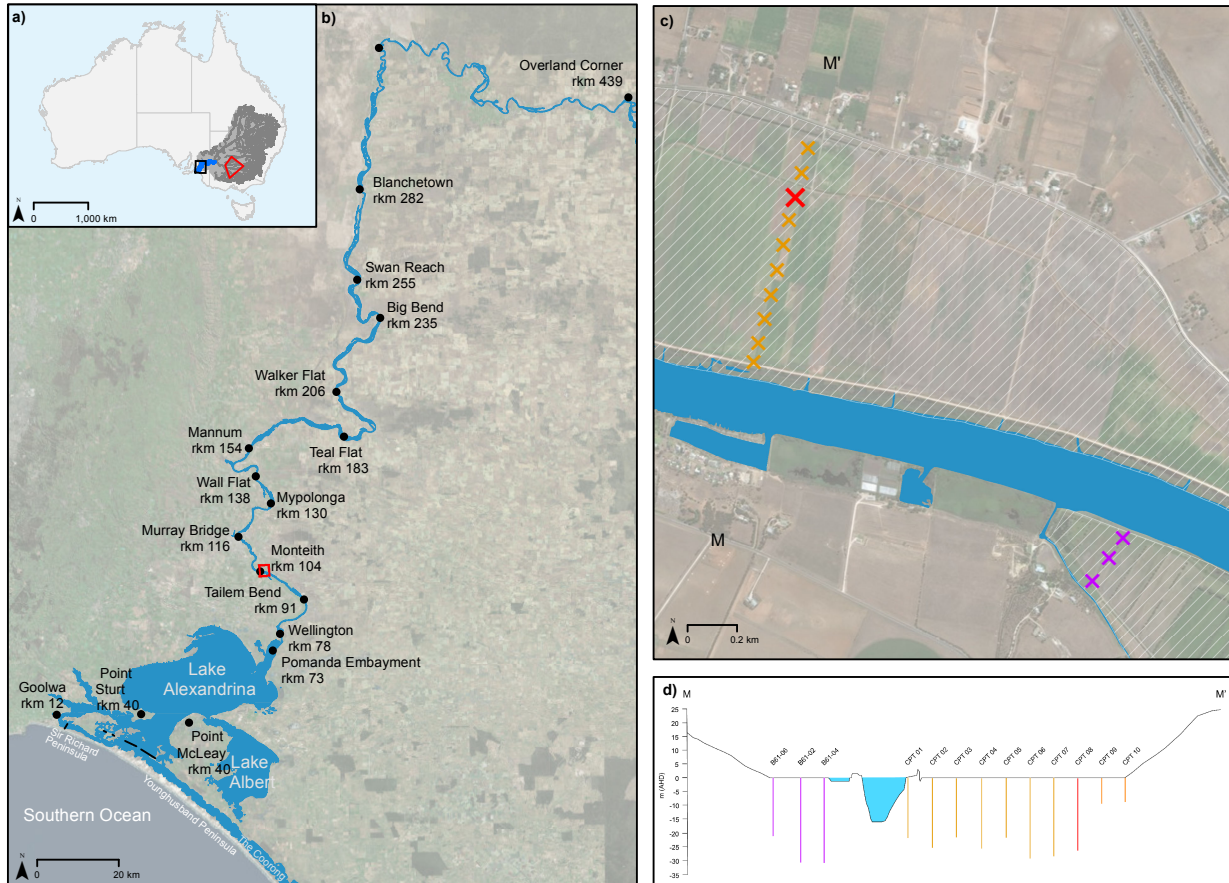
Figure 4.1: Overview of study sites. (**a**) The Murray-Darling Basin (grey) drains the twin Murray and Darling catchments, whose major watercourses are shown in dark grey. The confluence of the Murray and Darling Rivers marks the upstream extent of the lower Murray River (blue) which flows to the Southern Ocean in South Australia. The extent of the Riverine Plain is given in red (see Discussion for context). (**b**) The lower Murray River enters the Murray Gorge at Overland Corner (rkm 439) and remains confined until debouching into Lake Alexandrina at Wellington (rkm 78). The modern-day estuary comprises the Lower Lakes, Alexandrina and Albert, together with the Coorong lagoon. The lower Murray River flows through the Murray Mouth into the Southern Ocean between Younghusband and Sir Richard Peninsulas. A series of five barrages (black) regulate saline incursion into the estuary. (**c**) Fieldwork was conducted at Monteith (rkm 104) on grazing land comprising a reclaimed backswamp (white hatch) situated behind an artificial levee on the left bank of the river. Ten CPTs were taken at 100 m spacing commencing 100 m from the channel (orange crosses), with core Monteith-A extruded at the same site as CPT08 (red crosses). Three CPTs collected as part of an alternate study completes the transect on the right bank of the river (purple crosses). (**d**) Elevation profile of transect M-M' showing the position of each CPT relative to the width of the Murray Gorge. CPTs were pushed until refusal with penetration depths reaching beyond 20 m in all but two at the valley margins. Satellite imagery source: Esri.

Analyses of a record of uninterrupted sediment deposition preserved in marine cores MD03-2611 and MD03-2607, taken offshore from the Murray's Mouth on the Lacepede Shelf, has been used to generate the only available and commonly cited palaeo-climatic reconstruction derived from sediment captured from the entire MDB (Gell et al., 2009; Gingele et al., 2007; Gingele et al., 2004). Analyses of the terrigenous sediment flux within these cores led Gingele et al. (Gingele et al., 2007; 2004) to conclude that, except for a brief dry period from 9,000 – 8,000 yr BP, humid conditions prevailed throughout the early- to mid-Holocene. This was followed by a shift to increasingly arid conditions reaching conditions akin to the present-day by 5,500 yr BP (Gingele et al., 2007; Gingele et al., 2004).

As sea level rose rapidly in the early-Holocene, river valleys were drowned and formed the precursor of the modern-day estuary and the river valleys of southeastern Australia's stable craton (Rodriguez et al., 2010; Roy et al., 1980). Increased availability of marine sediment saw the development of the Murray estuary's barrier complex from approximately 8,000 yr BP, prior to the +2 m Holocene highstand at 7,000 – 6,000 yr BP (Belperio et al., 2002; Bowman and Harvey, 1986; Hill et al., 2009; Lewis et al., 2013; Roy et al., 1980). World-wide, landward migration of fluvial, estuarine, and marine environments caused a continuing decrease in the depositional gradient of coastal plain rivers which typically resulted in the deposition of an upward fining sequence within fluvial deposits in coastal incised valleys (Zaitlin et al., 1994). This commonly presents as a transition from high-energy fluvial sands to low-energy mud-dominated sediments (Zaitlin et al., 1994). This is also evident in the LMR where the valley-fill transitions from the braid plain sands of the Monoman Formation to the low-energy clays and silts of the Coonambidgal Formation (Firman, 1966). With their ample accommodation space, young estuaries were very efficient sediment traps, which sequestered terrigenous and marine sediment as they infilled (Dalrymple et al., 1992; Roy et al., 1980; Thom and Roy, 1985). The estuarine fill in the main body of Lake Alexandrina is characterised by a laminated silt-clay central basin deposit, known as the St Kilda Formation, which began accumulating by at least 8,000 yr BP and was well-established and regionally extensive by 5,500 yr BP (Barnett, 1993; 1994).

A previous assessment of the extent of the palaeo-Murray estuary demonstrated that the +2 m higher-than-present sea level of the mid-Holocene highstand generated an estuarine environment throughout the Lower Lakes and well upstream into the LMR (Helfensdorfer et al., 2019). The rapid rise in sea level inundated the entire width of the several kilometre-wide Murray Gorge and extended upstream at least to Blanchetown (rkm 282), creating a single, continuous, body of water quite unlike the present-day channel and fringing swamps (Helfensdorfer et al., 2019). At highstand, the flooded Murray Gorge presented an extensive backwater zone with an enlarged central basin environment that occupied Lake Alexandrina and the lower reaches of the LMR at least as far upstream as Monteith (rkm 104) and possibly upstream to Walker Flat (rkm 206; Helfensdorfer et al., 2019).

Here, this chapter evaluates the findings of 3D hydrodynamic modelling of the Murray estuary during the Holocene highstand (Helfensdorfer et al., 2019) against a well dated core and sediment data to understand the Holocene geomorphic evolution of the LMR and Murray estuary. Specifically, this chapter will:

- Establish the lateral extent of the water body that occupied the Murray Gorge at the Holocene highstand by correlating thirteen closely spaced cone penetrometer soundings, taken along a transect perpendicular to the modern-day channel, with an undisturbed 30 m sediment core (Monteith-A) taken at Monteith, 104 rkm upstream of the Murray Mouth;

- Conduct a sedimentary analysis on core Monteith-A, with analyses for grainsize, moisture content, bulk density, total organic carbon, and radiocarbon dating (to establish a chronology and sedimentation rates), to determine sedimentary units and assign facies designation constraining the timing and nature of geomorphic evolution;

- Further confirm Helfensdorfer et al.'s (2019) best-estimate Holocene highstand and pre-anthropogenic 2D hydrodynamic model in 3D to resolve the potential influence of estuarine stratification; and

- Assess to what extent the Murray estuary propagated upstream into the confines of the Murray Gorge at the Holocene highstand and independently verify, through the combination of 3D modelling and sedimentology, the conclusion of Helfensdorfer et al. (2019) that the palaeo-Murray's central basin, characterised by a laminated silt-clay sequence as described by Barnett (1993; 1994), extended from Lake Alexandrina at least as far upstream as Monteith (rkm 104).

4.3   Methodology

4.3.1   Hydrodynamic model

Best-estimate Holocene highstand and late-Holocene models from Helfensdorfer et al. (2019) were replicated in 3D using TUFLOW FV, a finite volume numerical model. From the conclusions of Helfensdorfer et al. (2019) the most appropriate scenarios that adequately captured the transition in palaeo-environmental character from the Holocene highstand to the pre-anthropogenic condition required a change in bathymetric surface and sea level only. The best-estimate Holocene highstand scenario adopts an inferred mid-Holocene bathymetry (S_{mid}) with modern-day barrier morphology (B_{mod}; Helfensdorfer et al., 2019). The average discharge prior to anthropogenic modification of the flow regime (D_{av}) is applied at Blanchetown (rkm 282), while +2 m is superimposed on a modern-day tidal dataset to represent sea level at the Holocene highstand (WL$_2$; Belperio et al., 2002; Helfensdorfer et al.,

2019; Lewis et al., 2013). Together, this set of variables corresponds to Helfensdorfer et al.'s (2019) scenario $S_{mid}WL_2D_{av}B_{mod}$. The corresponding late-Holocene scenario, depicting the natural system prior to anthropogenic alteration to the flow regime, differs only by the adoption of pre-regulation bathymetry (S_{up}) and a modern-day tidal dataset at present-day sea level (WL_2), corresponding to Helfensdorfer et al.'s (2019) scenario $S_{up}WL_0D_{av}B_{mod}$.

The 3D models presented here used hybrid z-sigma coordinates with a total of 8 vertical layers – 6 z-layers and 2 surface sigma layers – and a second order vertical solution, parametric vertical mixing model, and density coupled salinity. All other aspects of the model set up were held constant to those of Helfensdorfer et al. (2019). Details on the numerical model set up, morphology and sensitivity testing are given in Helfensdorfer et al. (2019).

Under present day conditions, with artificially high lake levels and supressed marine influence, wind-waves are the primary driver of sediment resuspension within the Lower Lakes (Aldridge et al., 2009). The temporally and spatially extensive deposition of a laminated sequence throughout the main body of Lake Alexandrina during the mid- to late-Holocene (Barnett, 1993; 1994) suggests that salinity-assisted flocculation sufficiently counteracted the influence of wind-waves. The results of this study support this contention suggesting that the Lower Lakes were subject to significant marine influence at the Holocene highstand. The presence of this salt wedge at depth would have assisted floc formation and settling of fine suspended sediment (Sutherland et al., 2015). Previous studies into the influence of wind-generated waves on saline incursion have demonstrated that the dominant south-westerly wind direction results in wind-waves driving backflow events into the LMR (Ellicott and Hudson, 2010). With wind-waves absent from the model adopted in this study, modelled saline incursion results reflect calm conditions and could therefore be considered conservative estimates when compared to likely conditions under the dominant wind regime.

4.3.2   Fieldwork

Monteith was chosen as the most suitable fieldwork site along the LMR as sensitivity testing of hydrodynamic models by Helfensdorfer et al. (2019) indicated that this location marks the minimum upstream extent of the Murray estuary's central basin at the Holocene highstand. The study site, located at rkm 104, is situated within the Monteith Irrigation Management Zone and, as such, has been subject to artificial levee construction, land reclamation and laser levelling allowing access to naturally inundated land. For this study, ten CPTs were collected in a transect perpendicular to the channel at 100 m spacing, commencing 100 m from the left bank, using a 22 t 6x6 specialist CPT truck. To provide a whole-of-valley analysis, results of three CPTs taken on the opposite side of the channel at 100 m spacing, and employing the same specialist CPT truck, were acquired for analysis. For each of the thirteen

CPTs, cone resistance (q_c), sleeve friction (f_s), dynamic pore pressure (u_2), inclination (I), friction ratio (R_f) and corrected cone resistance (q_t) were collected at 1 cm resolution in real time. The 30 m sediment core, Monteith-A, was taken at the location of CPT08 (Figure 4.1) using a Commachio MC900 Multi-Sonic drilling rig, split at the time of extrusion into 1 m sections and placed immediately into cold storage.

4.3.3   Chronology

Five samples of >63 µm charcoal fragments and 4 samples of fibrous organic fragment were submitted for AMS ^{14}C radiocarbon dating (lab ID: UBA) and calibrated using Calib 7.0.4 applying the SHCal13 calibration curve (Stuiver and Reimer, 1993). Macro-organic material is the prefered target material for AMS ^{14}C radiocarbon dating due to the likelihood of being deposited in situ, however only four samples were found in core Monteith-A at a suitable sample interval to develop a meaningful chronology. To suppliment this, charcoal samples were wet seived to isolate the >63 µm fraction and reduce the liklihood of selecting charcoal which has been transported. An age-depth model was developed in R using Bacon 2.3.3 (Blaauw and Christen, 2011). Assuming the surface to be modern, there is a significantly different sediment accumulation rate above the youngest age, which is unrealistic particularly given the potential of disturbance of the near surface due to agricultural activities. To account for this, a hiatus was input into the model directly above the shallowest ^{14}C date at 2.10 m.

4.3.4   Sedimentary analyses

Core Monteith-A was subsampled at 10 cm resolution for sedimentary analyses. Grain-size samples were subject to 35 H_2O_2 to oxidise the organic material, then disaggregated by adding hexametaphosphate 50 g/L and rotating samples for 12 hours prior to analysis. Grainsize analyses were conducted using a Malvern Mastersizer 2000 and statistical analyses conducted using GRADISTAT 8.0 (Blott and Pye, 2001) adopting the classification scheme of Folk and Ward (Folk and Ward, 1957). Moisture content, unit weight and bulk density were assessed by subsampling sediment into rings of a known weight and volume and oven drying overnight at 60 °C. Subsequently, these dried samples were crushed and placed into a furnace at 550 °C to ascertain a crude measure of the organic content of the sediment through loss on ignition (LOI).

4.3.5   Interpretation of cone penetrometer soundings

The high resolution, fast testing rate and low cost makes the CPT a novel and desirable method of interpreting sequence stratigraphy at a site (Lafuerza et al., 2005; Styllas, 2014). The use of CPT data to infer sequence stratigraphy is particularly robust when calibrated against a sediment core taken at the same or adjacent location. CPT08 was calibrated against the particle size distribution of core Monteith-A to assess the suitability of extrapolating results to infer sedimentary units from the thirteen CPTs obtained across the valley. The two key parameters are: the cone tip resistance (q_c), which is considered indicative of the density and consistency of the sediment; and, the friction ratio (R_f), which is considered indicative of sediment grainsize and texture (Lafuerza et al., 2005; Robertson, 2010; Styllas, 2014). Together these parameters are plotted using Robertson's (2010) q_c/R_f classification chart to determine the soil behaviour type (SBT).

Previous studies which have used CPT soundings to determine estuarine stratigraphy typically attribute the bounds and average q_c/R_f values of each sediment facies in the calibrated CPT to the soundings across the valley to develop a whole-of-valley analysis (e.g. Amorosi and Marchi, 1999; Kyungsik and Ju Hyong, 2006; Lafuerza et al., 2005; Styllas, 2014). Here, this methodology is enhanced by adopting a k-medoids clustering analysis (Kaufman and Rousseeuw, 2009) in Matlab on the calibrated CPT soundings (CPT08). The 1 cm resolution soundings were averaged in 10 cm intervals so as to be directly comparable to the grainsize sampling resolution of core Monteith-A. Due to the incredibly low strength of the Coonambidgal Formation muds, negative friction values were recorded within CPTs B61-02, B61-04 and CPT05; these were excluded from the analysis. A k-medoids clustering analysis adopting a squared Euclidean distance metric was performed on $\log_{10}$ transformed q_c/R_f data for CPT08 (and cross referenced relative to depth, to assess whether the facies divisions identified in core Monteith-A were correctly captured through the SBT analysis). The elbow and average silhouette methods were adopted to determine the optimal number of clusters. Both approaches suggested two clusters was optimal, which differentiated the Monoman Formation sands and the Coonambidgal Formation muds. This was, however, insufficient for the identification of sequence stratigraphy. Both methods returned six clusters as the second most optimal number of clusters. Each of the remaining twelve CPT soundings were then assessed in turn by attributing each individual soundings to the nearest medoid of each of the six clusters identified in CPT08 also using a squared Euclidean distance measure (Figure 4.2). The results of this clustering analysis were then plotted relative to depth and distance across the valley to infer sequence stratigraphy (Figure 4.3).
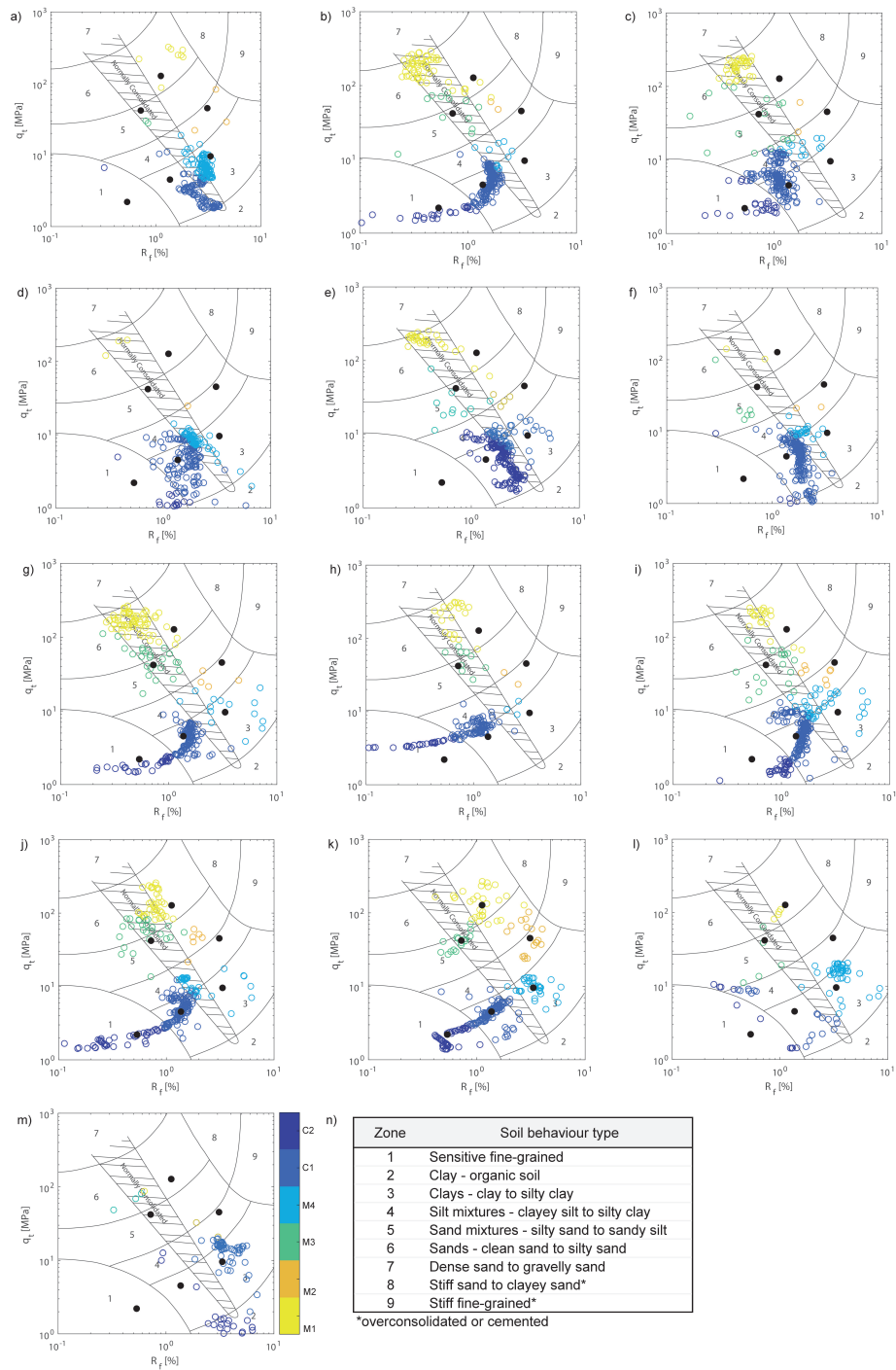
Figure 4.2: q_c/R_f plots for each CPT giving Robertson's (2010) SBT coloured by cluster relative to the six clusters identified within CPT08. (**a**) B61-06; (**b**) B61-02; (**c**) B61-04; (**d**) CPT01; (**e**) CPT02; (**f**) CPT03; (**g**) CPT04; (**h**) CPT05; (**i**) CPT06; (**j**) CPT07; (**k**) CPT08; (**l**) CPT09; (**m**) CPT10; (**n**) description of soil behaviour type given by each of Robertson's (2010) nine zones. Black points denote the medoid of each cluster identified for CPT08, with the cluster legend given in panel (**m**). Clusters M1-M4 comprise sediments of the Monoman Formation, while clusters C1-C2 comprise sediments of the Coonambidgal Formation.
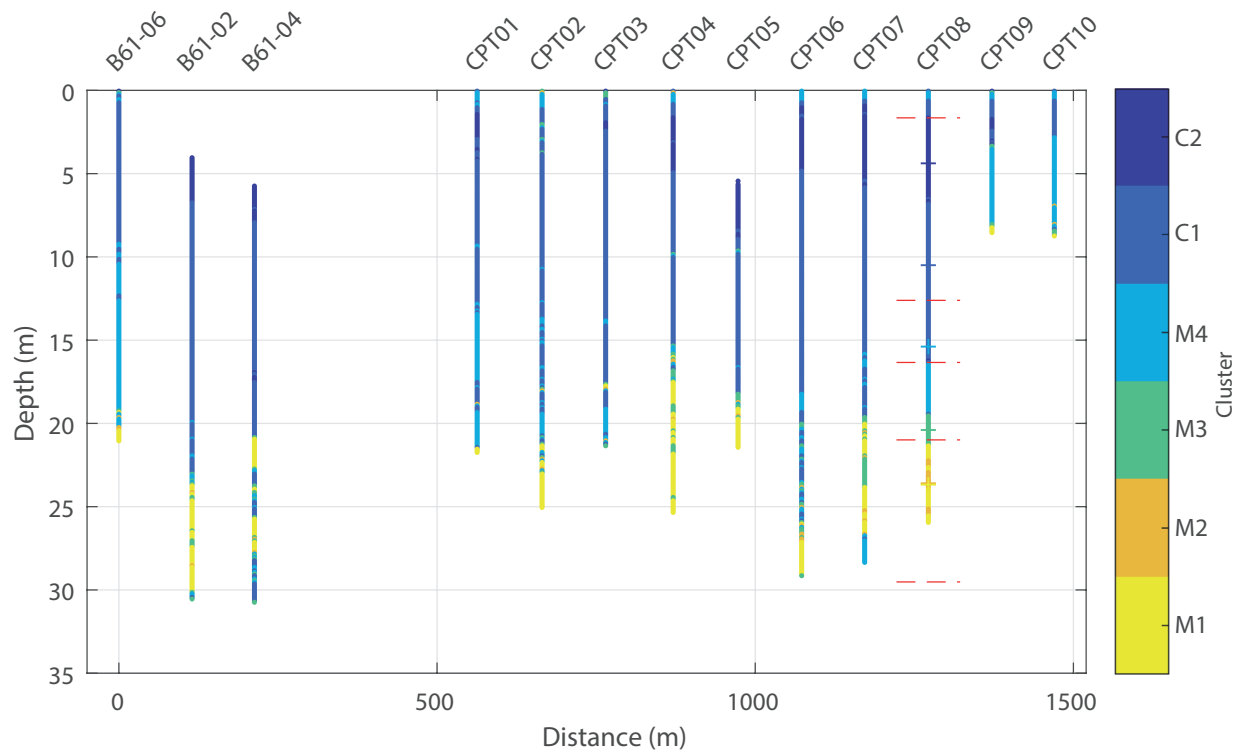
Figure 4.3: CPT cluster analysis by depth. Plotting the results of individual clustering analyses (Figure 4.2) by depth and relative position across the valley reveals vertical and lateral trends in sediment geotechnical properties. The median depth of each cluster in CPT08 is denoted by a cross, with the red hatched line indicating the depth of each sedimentary unit identified within core Monteith-A. Negative sleeve friction values prevented q_c/R_f analysis for the top few meters of sediment within B61-02, B61-04 and CPT05. Data displayed here was used to inform the creation of the cross section in Figure 4.9b.

4.4   Results

4.4.1   Hydrodynamic modelling

A best-estimate 3D Holocene highstand scenario (model scenario code: $S_{mid}WL_2D_{av}B_{mod}$) supports and extends the 2D model results of Helfensdorfer et al. (2019), which showed that the +2 m sea level of the Holocene highstand generated an estuarine palaeo-environment throughout the Lower Lakes and upstream into the lower reaches of the LMR (Figure 4.4a). This high-resolution 3D model suggests that the lower Murray Gorge flooded completely, with the depth-averaged marine-brackish (10 psu) limit penetrating upstream as far as Tailem Bend (rkm 91; Figure 4.4a). The tidal limit extended beyond the model extent (minimum Blanchetown, rkm 282; Figure 4.4a). A central basin environment occupied the region upstream of Point Sturt and Point McLeay (rkm 40) up into the Murray Gorge to Wall Flat (rkm 140; Figure 4.4a), correlating well with the median extent given by the suite of 2D models in Helfensdorfer et al. (2019; median Mannum, rkm 147). At highstand, maximum flow velocities were <0.3 m/s for 95% of the model domain, consistent with generating an environment conducive to the deposition of a laminated silt-clay sequence (Baas et al., 2016; Schieber and Yawar, 2009; Schieber et al., 2007). Significant areas subject to velocities exceeding 0.3 m/s were only extant seaward of Point Sturt/Point McLeay (rkm 40, within the flood-tide delta; Figure 4.4a).

Estuarine infill and a decline in sea level to present-day levels, representative of modern pre-modification conditions (model scenario code: $S_{up}WL_0D_{av}B_{mod}$), significantly reduced saline incursion to the Lower Lakes and limited marine influence to the flood-tide delta region, with the brackish limit propagating only as far upstream as Wellington (rkm 85; Figure 4.4b). Under these conditions, the central basin is inferred to be restricted to the Lower Lakes with the upstream limit remaining within the upper reaches of Lake Alexandrina at the Pomanda Embayment (rkm 72; Figure 4.4b). Maximum flow velocities are reduced, enabling conditions suitable for the deposition of a laminated silt-clay sequence throughout almost the entire model domain (99%; Figure 4.4b).

4.4.2   Analyses of core Monteith-A

4.4.2.1   Chronology

The chronology for core Monteith-A was determined with five ^{14}C radiocarbon dates with ages that span the early- to mid-Holocene from 10,249 – 10,506 cal yr BP to 6,509 – 6,636 cal yr BP (Table 4.1). These dates present an increasing age with depth, with two ages 2.18 m apart (at 7.36 m and 9.54 m) returning near identical calibrated ages of 7,966 – 8,169 and 7,927 – 8,162 cal yr BP respectively (Table 4.1). Assuming the surface is modern, the top
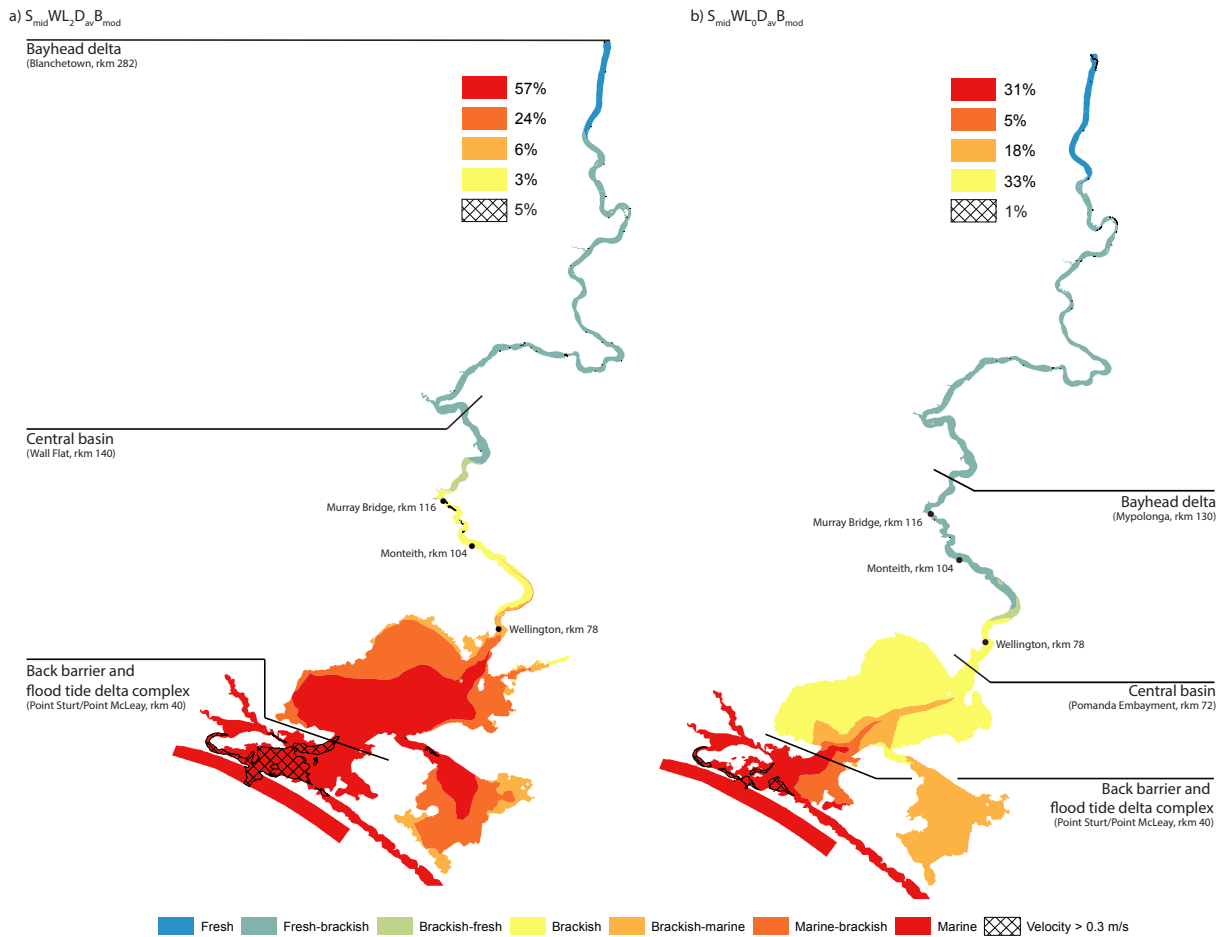
Figure 4.4: Modelled maximum salinity and velocity magnitude and inferred resulting morphological zonation. (**a**) 3D depth-averaged maximum salinity reached from a best-estimate Holocene highstand scenario ($S_{mid}WL_2D_{av}B_{mod}$) demonstrates that the Lower Lakes were subject to significant marine incursion driving the brackish limit beyond Murray Bridge (rkm 118). The flood-tide delta is the only region where maximum velocity magnitudes exceed the limit for deposition of a laminated sequence over significant areas (Baas et al., 2016; Schieber and Yawar, 2009; Schieber et al., 2007). (**b**) The reduction of sea level in the late Holocene (modelled as scenario $S_{mid}WL_0D_{av}B_{mod}$) causes a significant change in the palaeo-environmental character of the region restricting the brackish limit to Wellington (rkm 85) and suppressing marine incursion to the flood tide delta. Salinity categorisation is based on the classification scheme of Tooley (1978).

2.10 m (above the youngest date) has a markedly different sediment accumulation rate of 0.03 cm/yr (Figure 4.5). Given the potential for disturbance of the near surface by agricultural activities, this top-most 2.1 m section of the core was excluded from further chronological analysis. For the period spanning the five radiocarbon ages (20.65 m), the age-depth model is very well constrained with a linear regression of $R^2 = 0.997$, such that depth in the core is considered to be a valid approximation of age (Figure 4.5). The model returns a mean sediment accumulation rate of 0.60 cm/yr (Figure 4.5), with minor variations from the mean rate that correspond to the rise of sea level during the period of deposition. The period 8,516 - 7,750 cal yr BP marks the most rapid sediment accumulation in the core, with an average of 0.77 cm/yr, and is likely a consequence of the rapid rise in sea level caused by the melting of the Laurentide ice sheet at approx. 8,200 yr BP (Figure 4.6; Hijma and Cohen, 2010; Rodriguez et al., 2010). The worldwide initiation of Holocene estuaries has been attributed to this event and this chronology demonstrates that the response of the LMR is consistent with the world's other major river systems (Hijma and Cohen, 2010; Rodriguez et al., 2010). Sediment accumulation rates are slowest at highstand with an average of 0.48 cm/yr between 7,750 - 6,543 cal yr BP (Figure 4.6).

Table 4.1: Conventional and calibrated ages for core Monteith-A ^{14}C samples. Nine charcoal or fibrous organic samples were taken from the top 23 m of core and analysed at lab UBA. Calibrated ages with the greatest probability are referred herein.

Lab ID	Depth (m)	^{14}C date (yr BP ± 1 σ)	Material	Calibrated age (2 σ) (cal. yr BP)	Probability (%)	Median calibrated age (2 σ) (cal. yr BP)
UB-38709	2.11	5,761 ± 43	> 63 µm charcoal fragments	6,409 - 6,636	100	6,513
UBA-38326	5.06	6,413 ± 45	> 63 µm charcoal fragments	7,241 - 7,421	93.9	7,308
				7,178 - 7,214	6.1	
UBA-38765	7.36	7,282 ± 49	> 63 µm charcoal fragments	7,966 - 8,169	100	8,062
UBA-38710	9.54	7,221 ± 58	fibrous organic fragment	7,927 - 8,162	96.0	7,998
				7,871 - 7,895	4.0	
UBA-38325	12.60	7,748 ± 44	> 63 µm charcoal fragments	8,411 - 8,583	100	8,490
UBA-36739	15.17	8,006 ± 37	charred fibrous organic fragment	8,691 - 8,992	93.6	8,839
				8,649 - 8,678	5.4	
				8,683 - 8,689	1.0	
UBA-38766	18.33	8,757 ± 44	> 63 µm charcoal fragments	9,548 - 9,824	94.1	9,671
				9,843 - 9,869	3.4	
				9,872 - 9,887	2.0	
				9,827 - 9,831	0.5	
UBA-38186	19.91	8,884 ± 54	charred fibrous organic fragment	9,701 - 10,165	100	9,929
UBA-38187	22.76	9,256 ± 44	charred fibrous organic fragment	10,249 - 10,506	100	10,374

4.4.2.2   Sediment grainsize and characteristics

High resolution optical imagery and radiographs of the Holocene sediments of core Monteith-A (up to 24.12 m) are presented in Figure 4.7. The weathered claystone basal unit (Unit 1; 30.12 – 29.52 m) underlies the Monoman Formation, which, in this core, presents as two distinct units: Unit 2 and Unit 3. Unit 2 (29.52 – 20.99 m) is comprised of fine and medium sands with an average mean grainsize of 186.6 µm and a clay:silt:sand (C:S:S) ratio
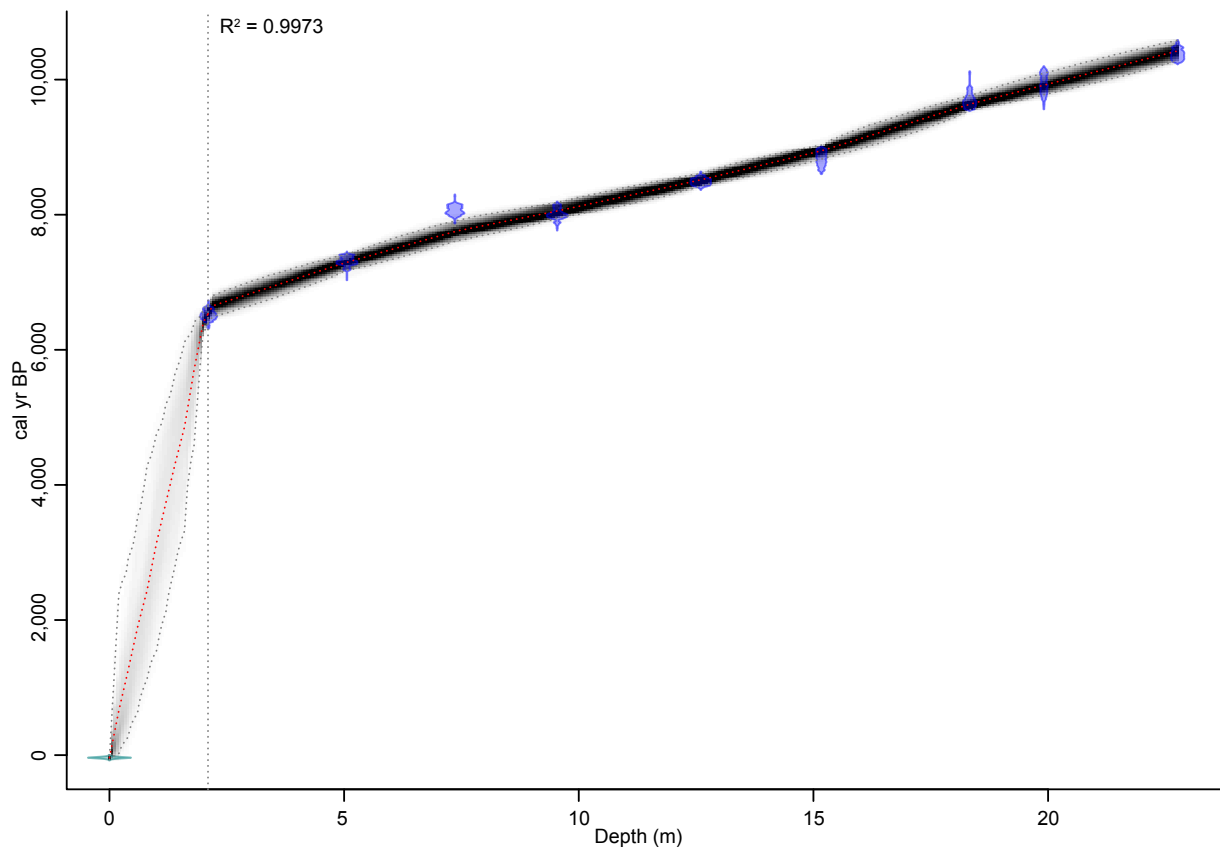
Figure 4.5: Bacon age-depth model produced from core Monteith-A dates. The model is very well constrained for the period between the youngest and oldest dates (6,513 – 10,374 yr BP; $R^2 = 0.997$), giving an average sediment accumulation rate of 0.14 cm/yr for this 20.65 m range. Assuming the surface of the core is modern, the model gives an average sediment accumulation rate of 0.03 cm/yr for the top 2.10 m. The model returns all calibrated ^{14}C dates (purple), the 'best' model based on the mean age for each depth (red dashed line) and the 95% confidence interval (grey dashed lines), with the degree of shading between the 95% confidence intervals representing the likelihood of the calendar age.

Figure 4.6: Sedimentary analysis of core Monteith-A relative to sea level and key proxies from offshore marine cores MD03-2611 and MD03-2607. Calibrated ages together with the grainsize distribution, moisture content, dry bulk density, TOC and sediment accumulation rate from basal weathered clay (Unit 1) to lowstand braided fluvial facies (Unit 2), and transgressive single-thread fluvial (Unit 3), transitional fluvial bayhead delta (Unit 4) and central basin facies (Unit 5). The top 1.65 m is potentially disturbed due to agricultural activities at the site. Fluctuations in the clay/silt ratio and illite percentage are given for offshore marine cores MD03-2607 and MD03-2611 respectively (Gingele et al., 2007; Gingele et al., 2004). The timing of the Holocene sea-level highstand (7,000 – 6,000 yr BP) is demarcated by blue shading (Belperio et al., 2002; Lewis et al., 2013), and the 8,500 – 8,200 yr BP worldwide estuarine initiation event by green shading (Cohen and Hijma, 2014; Hijma and Cohen, 2010; Hori and Saito, 2007; Rodriguez et al., 2010).

of 3:18:79 (Figure 4.6). The boundary between Units 2 and 3 (20.99 m; 10,112 cal yr BP) is marked by an abrupt change from very poorly sorted grey (7.5Y 5/1) sands to banded finer greenish grey (5G 5/1) to coarser grey (7.5Y 5/1) sands (Figure 4.7) and a sharp increase in moisture content and TOC (Figure 4.6). Unit 3 (20.99 – 16.34 m) presents a decrease in average mean grainsize to 136.6 µm and a C:S:S of 14:23:63 (Figure 4.6). The two sand units also differ in their physical properties with an increase in average moisture content and TOC and decrease in average dry bulk density from 20 to 36%, 1.21 to 4.36% and 1,775 to 1,448 kg/m^3 between Units 2 and 3 respectively (Figure 4.6). A 3.73 m thick transitional sequence (16.34 – 12.61 m) comprising mottled fine and medium silts (Unit 4) separates the Monoman Formation sands and the Coonambidgal Formation muds with its basal boundary (9,200 cal yr BP) marked by a distinct colour and textural change (Figure 4.7). Unit 4 has an average mean grainsize of 19.1 µm and a C:S:S of 30:59:11 (Figure 4.6). The transition out of this mottled grey (7.5Y 5/1), greenish grey (5G 5/1) and dark greenish grey (5G 3/1) sequence is gradational in colour and texture but presents a small incremental increase in TOC and moisture content and decrease in dry bulk density at 12.61 m (8,518 cal yr BP; Figure 4.6). Units 4 and 5 differ in average moisture content, TOC and dry bulk density by 90 to 110%, 11.33 to 10.00% and 838 to 738 kg/m^3 respectively. Unit 5 presents alternating 0.5 to 2 mm thick dark-coloured grey (7.5Y 4/1) laminations comprising fine to medium silts (average grainsize of 8.6 µm and C:S:S of 31:61:8) and light-coloured greenish grey (5G 6/1) laminations comprised of clay to very fine silt (average grainsize of 1.8 µm and C:S:S of 65:33:2). Moisture content, dry bulk density and TOC averages of 104%, 766 kg/m^3 and 10% respectively, with the significant increase in TOC in the near surface material (0 – 0.7 m) due to the presence of roots (Figure 4.6).

4.4.2.3   Cone penetrometer soundings profile

Interpretation of CPT results using Robertson's (Robertson, 2010) SBT identifies a clear distinction between two sedimentary sequences in all CPTs beyond the valley margins (i.e. with the exception of B61-06, CPT09 and CPT10): an upper sequence comprising clays and sensitive fine-grained sediments (Figure 4.2 clusters C1-C2), and an underlying sequence comprising silts and sands (Figure 4.2 clusters M1-M4). This cross-valley uniformity demonstrates a valley-wide transition from the coarse-grained Monoman Formation to the fine-grained Coonambidgal Formation which is consistent with previous accounts of the Murray Gorge's valley fill (Brown and Stephenson, 1991; Firman, 1966). At the study site, this near horizontal transition from lower to upper valley fill occurs at a depth of approximately 14-19 m across the 1,200 m width of the drowned river valley, which is reflected in the mean grainsize of Units 2 and 3 when compared with Units 4 and 5 within core Monteith-A (Figure 4.6).

The simple division between the Monoman and Coonambidgal Formations has been con-
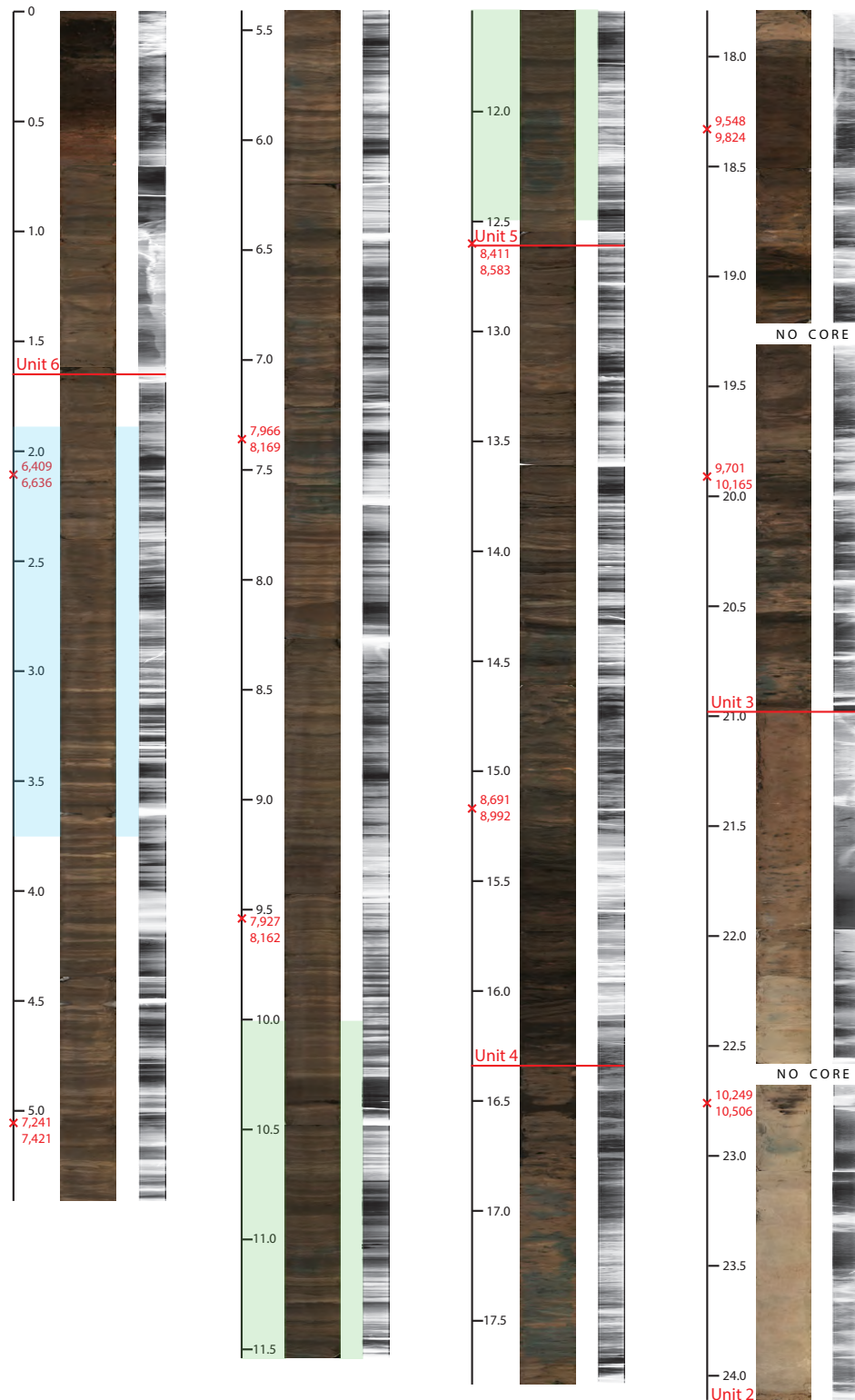
Figure 4.7: Core Monteith-A imagery. Optical imagery and radiographs of 24.12 m of core Monteith-A showing locations of ^{14}C dates and calibrated ages (in cal yr BP). Unit boundaries (red), worldwide estuary initiation event (green) and sea-level highstand (blue) are given as per Figure 4.6. Scale is depth in meters.

firmed and further extrapolated to identify the sedimentary units across the valley through a correlation with core Monteith-A. A k-medoids clustering analysis (Kaufman and Rousseeuw, 2009) of Robertson's (2010) SBT data obtained from the CPT collected adjacent to the sediment core (CPT08) identifies six clusters (see methodology) which, when plotted relative to depth, allows clusters to be linked to the facies identified in core Monteith-A (Figure 4.8). Unit 2 presents in CPT08 as silt mixtures to sands (clusters M1 and M2) with the sequence boundary to Unit 3 correctly placed (Figure 4.8). The distinction between the lowstand and transgressive sand facies (Unit 2 to 3) is marked by a reduction in consolidation (Figure 4.8); however, the clustering analysis suggests Unit 3 is better represented as two distinct units (clusters M3 and M4), with a sequence boundary at -19.5 m (9,844 cal yr BP). This division, which was not identified through analysis of core Monteith-A, is interpreted as illustrating the highly transitional nature of the transgressive system during this period. The boundary between Units 3 and 4 is also correctly placed at -16.34 m (clusters M4 and C1; Figure 4.8), however, a limitation is that the SBT analysis cannot distinguish between Units 3 and 2, but rather identifies both these units as typically comprising clays and sensitive fine-grained sediments (Figure 4.8). The clustering analysis suggests a division at -6.3 m, which is not reflected through the analysis of core Monteith-A. Rather, it is suggested that this is an artefact of drying during the Millennium drought (1997-2011) when the significant lowering of the water table caused clays of the reclaimed swamps, such as those at the study site, to crack to depths in excess of 3.5 m (Fitzpatrick et al., 2017). This is consistent with the maximum depth of the sub-cluster (circled in Figure 4.8a) of 4.35 m. Overall, the correlation of CPT08 with core Monteith-A confirms that the division of units assigned based on the visual log (Figure 4.7) and sedimentary data (Figure 4.6) can also be identified by the geotechnical properties of the sediment (Figure 4.8). This calibration validates the use of CPT soundings to extrapolate the sedimentary units identified in core Monteith-A across the width of the valley.

A cross-valley profile generated from the thirteen cone penetrometer soundings demonstrates the presence of a uniform valley-fill sequence consisting of a 14-19 m thick layer of muds (clays and sensitive fine-grained sediments) that overlies an interlayered sequence of sand mixtures and clays before reaching consolidated silts and sands (Figure 4.9b). Aside from the valley-fringes (B61-06, CPT09 & 10), each sounding presents an almost identical vertical trace with consistent and very low cone resistance within the upper mud layer (Units 4 and 5; 0.13 – 0.80 Mpa), a notable increase within Unit 3 (0.59 – 4.60 Mpa) and high, variable oscillating cone resistance typical of coarse to fine sands and coarse silts within Unit 2 (2.35 – 31.36 Mpa; Figures 4.9b, 4.2 & 4.3). Soundings within Unit 5 are punctuated by brief, sharp increases in q_t at -9.5 m, most prominently within CPTs 01, 04, 05, 07 and B61-06, which is interpreted to represent a slightly coarse-grained lens of sandy silt. This corresponds to a sharp increase in grainsize and dry bulk density and a decrease in moisture content and TOC at the same depth in core Monteith-A (7,998 cal yr BP) further validating the cross-valley
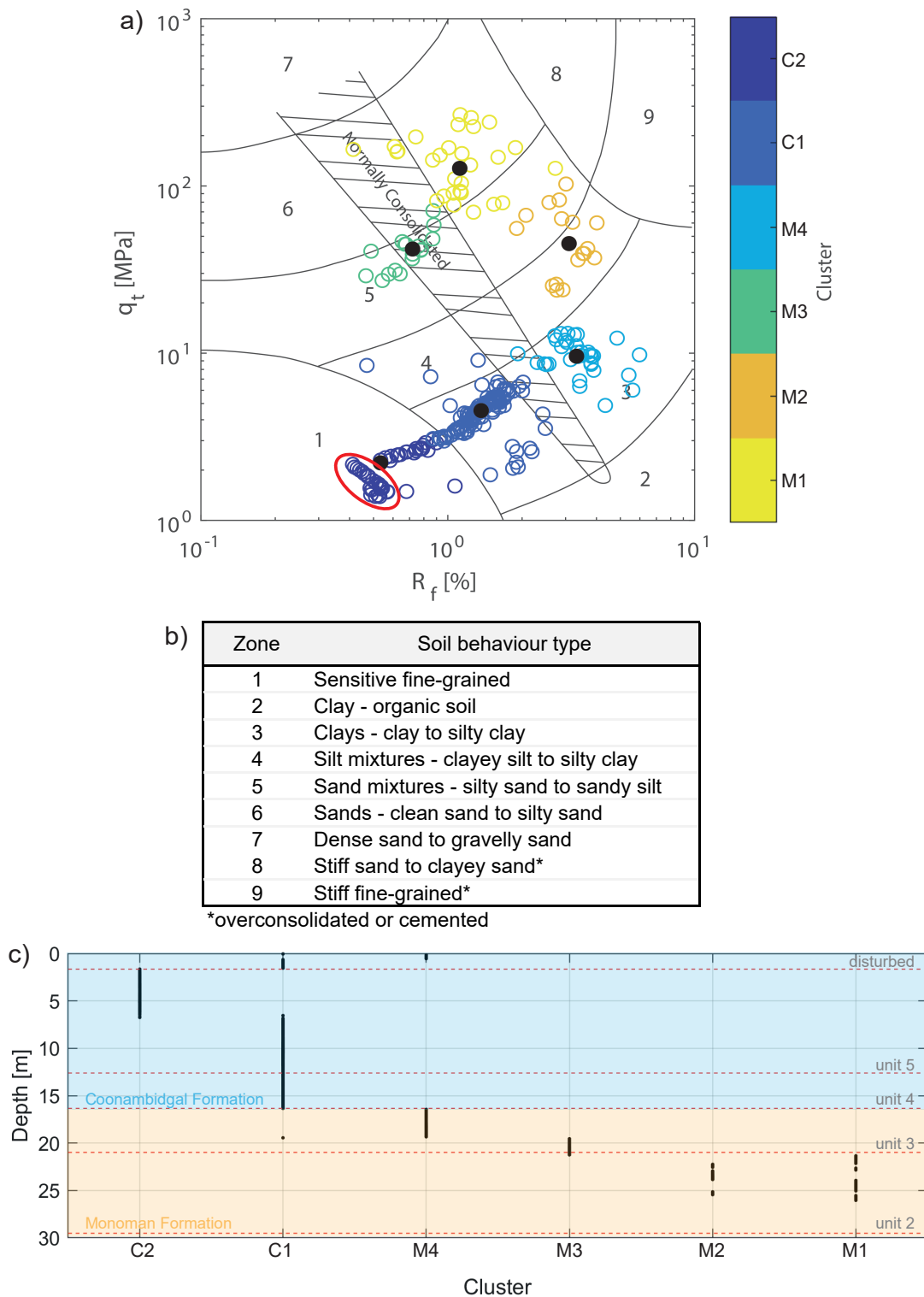
Figure 4.8: Correlation of facies identified in core Monteith-A to results of CPT08 applying Robertson's (2010) SBT. (**a**) Plotting CPT08 on Robertson's (2010) q_c/R_f plot and performing a k-medoids clustering analysis reveals six distinct clusters. A sub-cluster within cluster 1 (circled in red) comprises drought-affected surficial and shallow sediment. (**b**) Robertson's (2010) SBT provides a description of sediment based on nine zones distinguished through CPT results q_c and R_f. **c** Plotting clusters relative to depth facilitates comparison with sedimentary units identified within core Monteith-A (red dashed lines). Sedimentary unit boundaries within core Monteith-A correlate well with the clustering analysis of q_c/R_f for CPT08.

uniformity. Each of the ten CPTs away from the valley margins reach a much stronger, denser, underlying coarse-grained sand (Unit 2) which prevented further safe operational penetration of the cone and rods. The significant increase in material resistance due to the stiffness of the compacted sands present in the lower portions of Unit 2 prevented penetration to rock basement in most CPTs; this is a typical depth limiter of the CPT method when assessing Pleistocene-Holocene sequences (Lafuerza et al., 2005; Styllas, 2014). The upper surface of this underlying consolidated sand layer varies between approximately -25 m and -19 m across the entire valley extent (Figures 4.9b & 4.3). Limestone and underlying weathered bedrock are abruptly encountered at the margins of the valley at a depth of approximately -10 m within B61-06 and -8 m within CPTs 09 and 10 (Figures 4.9b & 4.3).

4.4.2.4   Depositional history - system tract identification

The basal sequence boundary presented in core Monteith-A is marked by a transition from weathered claystone to fluvial sands (Unit 1 to 2). Deposition of this unit is inferred to have commenced at approximately 20,000 – 18,000 yr BP contemporaneous with the last glacial maximum (Belperio et al., 1995; Hill et al., 2009). Unit 2 is interpreted to be a component of the lowstand systems tract (Zaitlin et al., 1994) and likely represent aggradation of braided fluvial channels (as suggested by Firman (1966)), comprising medium to fine sands, in response to a rising base level in the early stages of sea-level rise (Figures 4.6 & 4.7). This lower sand deposit is 8.5 m thick and presents its upper surface at 20.99 m depth in core Monteith-A which marks the fluvial transgressive surface and a probable shift from braided to single-thread morphology at 10,112 cal yr BP (Figure 4.7; Firman, 1966). This event presents as a transition from very poorly sorted medium sands to alternating bands of silts and silty fine sands in core Monteith-A (Unit 3; Figures 4.6 & 4.7). This is contrasted by the identified braided to meandering morphological transition exhibited upstream within the Riverine Plain (Figure 4.1), which is evidenced by an upward fining sequence, crevasse splay and point bar deposits (Brown and Stephenson, 1991). Similar sedimentary structures are absent in core Monteith-A (Figure 4.7) suggesting that the rapidly declining energy gradient within the lower Murray Gorge during the transgressive phase of the early-Holocene prevented the development of a meandering channel at the study site.

The presence of cross-lamination, shell lenses and a sharp increase in TOC marks a transitional phase with deposition of a transitional facies from 16.34 m (9,200 cal yr BP; Unit 4) in response to continued base level rise (Figures 4.6 & 4.7). The unique characteristics of this coastal plain system - the incredibly low gradient, discharge and sediment yield - caused a significant reduction in energy at the study site which accounts for the similarity in appearance (sediment colour, composition and texture) between Units 4 and 3, with the reduction in TOC a consequence of increased depth and salinity due to backfilling from marine
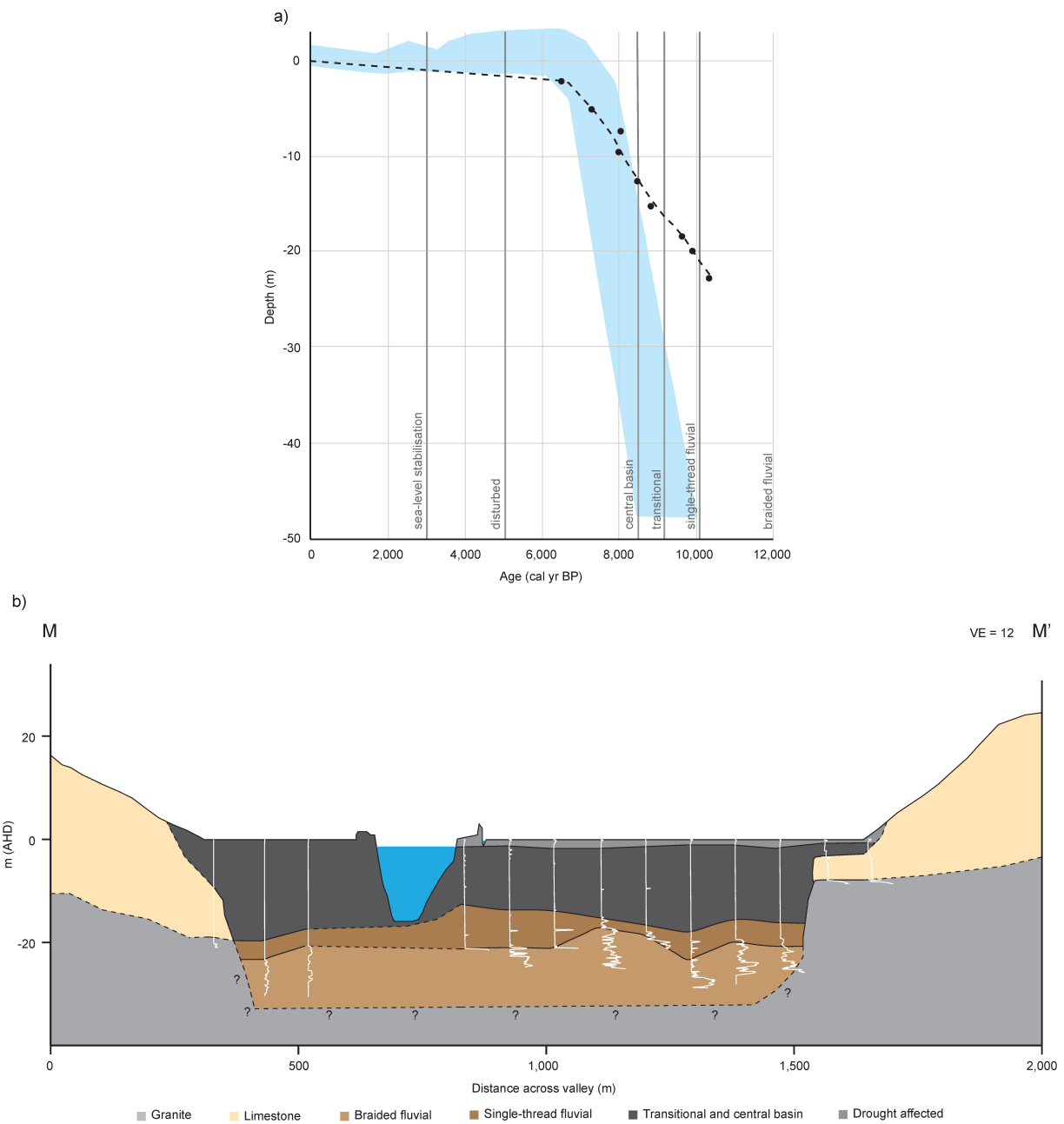
Figure 4.9: Core Monteith-A sedimentary facies relative to sea level and valley-wide cross section extrapolated from CPTs collected in transect. (**a**) The Bacon age-depth plot for core Monteith-A is plotted, relative to facies designation, against the Holocene sea-level envelope for the Southern Australian coast (Belperio et al., 2002). The inception of the Murray estuary, and commencement of deposition of the central basin sequence, is synchronous with the onset of marine flooding at this location. Calibrated ^{14}C ages are denoted by black points, with the approximate timing of sea-level stabilisation to the present-day level shown as 3,500 yr BP (Bourman et al., 2000; Cann et al., 2000; Fluin, 2002; Luebbers, 1982). (**b**) A valley-wide cross section at Monteith (rkm 104; transect M-M' given in Figure 1c-d) developed from SBT analysis of thirteen CPTs reveals that the central basin (Unit 5) is uninterrupted across the whole width of the valley. The underlying single-thread fluvial (Unit 3) and braided fluvial (Unit 2) facies are interrupted only by limestone and bedrock outcrops at the extent of the valley. Dashed lines indicate uncertainty with question marks denoting uncertainty at depth.

flooding (Figures 4.6 & 4.7). A transition to a laminated silt-clay sequence at 12.61 m (8,518 cal yr BP; Unit 5) marks the establishment of the mid-Holocene palaeo-Murray estuary and widespread deposition of a central basin facies (Figures 4.6 & 4.7). The timing of transition between depositional styles correlates with numerous accounts globally of back stepping events and estuary initiation as a response to the melting of the Laurentian ice sheet (e.g. Cohen and Hijma, 2014; Hijma and Cohen, 2010; Hori and Saito, 2007; Rodriguez et al., 2010). The laminated silt-clay sequence is 11 m thick and indicates continuous uninterrupted mud laminae deposition between 8,518 – 5,067 cal yr BP. Finally, the radiographs suggest that the top 1.65 m of core Monteith-A may be anthropogenically disturbed which hampers interpretation in this core (Figure 4.7). Consequently, the transition from highstand central basin to stillstand deposits beyond 5,067 cal yr BP cannot be confidently identified.

4.5   Discussion

The sedimentary facies identified in core Monteith-A record a sequence of deposition from lowstand, through transgression, to highstand. These facies demonstrate an example of the response of a stable cratonic river system to the progressive flooding of an incised valley by a rising sea level (Figures 4.6 & 4.10; Dalrymple et al., 1992; Nichol et al., 1994; Zaitlin et al., 1994). This particular presentation of Zaitlin et al.'s (1994) middle incised valley facies association located 104 rkm upstream of the present-day river mouth is an atypical response to sea-level rise during the Holocene. This remarkable example of inland estuarine deposition is attributed to the incredibly low relief, the fine-grained sediment load comprised almost exclusively of silt and clay, and to the large size of this semi-arid catchment. The unusually low energy of this system, indicated by modelled current velocities of <0.3 m/s (Figure 4.4), enabled the formation of a condensed sedimentary section where the full transition from braided fluvial to central basin deposition occurred in approximately 1,600 years (10,112 – 8,518 cal yr BP). This transition is presented in core Monteith-A by an upward fining section of sands and muds (Units 3 and 4; Figures 4.6 & 4.7). The energy available within this system was too low to produce the range of depositional conditions normally expected within the middle incised valley facies association such that a continuous condensed section is instead apparent. This has allowed for the depositional response to a full sea level cycle within the 30 m of sediment captured in core Monteith-A. These results have been summarised to produce a revised geomorphic history of the LMR, shown in Figure 4.10.

Three-dimensional hydrodynamic models confirm the conclusions drawn from 2D scenarios (Helfensdorfer et al., 2019) which demonstrate that, at the Holocene highstand, the Murray estuary's central basin extended 140 rkm upstream from the present-day river mouth, well into the confines of the Murray Gorge (Figure 4.10a). The 11 m thick central basin deposit presented within core Monteith-A (Figure 4.6) confirms that a central basin facies was de-

~ 120,000 yr BP
Sea level was slightly higher than present at the interglacial sea-level highstand. A succession of coarse-grained fluvial deposits would have underlain finer-grained fluvial deposits through which a single-thread channel would have begun to incise.

~ 20,000 - 18,000 yr BP
At the peak of the glacial maximum, sea level was about 120 m lower than present. The Murray Gorge was completely stripped of its valley fill exposing the weathered clay below.

~ 18,000 - 10,000 yr BP
A warming climate caused melting of ice sheets and associated rapid sea-level rise. A series of braid plain channels formed in response to this change in base level and deposited coarse-grained fluvial sediments.

~ 10,000 - 9,200 yr BP
Sea level continued to rise rapidly causing the braid plain channels to transition into a single-thread channel. This reduction in energy gradient brought about by a rising base level resulted in the deposition of finer-grained fluvial sediments.

~9,200 - 8,500 yr BP
Sea level continued to rise rapidly causing a further reduction in the energy gradient and deposition of fine-grained fluvial sediments. Flow velocity was significantly reduced allowing for the growth of channel fringing and aquatic vegetation.

~ 8,500 - 4,000 yr BP
A stepwise jump in sea level preceding the Holocene sea-level highstand backfilled the lower Murray Gorge creating a central basin environment which occupied the entire width of the valley. This ample accommodation and reduction in energy allowed a finely laminated silt-clay sequence to rapidly deposit.

~ 4,000 yr BP to 1900
Sea level receded to the present-day level causing the bayhead delta to prograde forming a single-thread channel with levees and fringing swamps. The channel begun incising into the underlying soft central basin muds.

~ 1900 - present day
Significant modification to the landscape and flow regime with European influences. Construction of levees and land reclamation infilled channel fringing swamps. The channel continued to incise into the underlying soft central basin muds.

Figure 4.10: Revised geomorphic history of the LMR. The combination of results derived from hydrodynamic models and sedimentologic data allows for the development of a revised model of sedimentary infilling of the lower Murray Gorge. These results validate and modify some aspects of Jaksa et al.'s (2013) model, while invalidating others, and serve as a complementary upstream counterpart to the Holocene geomorphic history of Lake Alexandrina presented by Barnett (1994).

posited at least as far upstream as Monteith (rkm 104) during the mid-Holocene (8,518 –
5,067 cal yr BP). The transect of CPT profiles indicate that this central basin was deposited
across the entire width of the Murray Gorge at this location (Figure 4.9b). Temporally
and spatially, this sequence is contiguous with Lake Alexandrina's central basin deposit and
presents comparable mean grainsize, moisture content and TOC content to cores within the
main body and palaeo-thalweg of Lake Alexandrina (Barnett, 1993; 1994). This single, con-
tinuous depositional environment in the LMR and Lake Alexandrina confirms Helfensdorfer
et al.'s (2019) suggestion that the LMR's Coonambidgal Formation and Lake Alexandrina's
St Kilda Formation should be considered equivalent units. The existence of this elongate
estuary that was extant throughout the mid-Holocene should be considered when applying
our understanding of Holocene palaeo-environments to assist in the development of manage-
ment policies for the region.

In the intensively managed MDB, water use, policy and planning decisions are guided by
the accuracy and quality of our knowledge of pre-anthropogenic conditions. A recent debate
about the long-term variation in salinity of the Lower Lakes has been dominated by the
need to maintain a freshwater supply for irrigation and environmental flows (Fluin et al.,
2009; Fluin et al., 2007; Gell, 2019). The Lower Lakes are held fresh by closing a series of
barrages within the flood tide delta, even during periods of extreme drought (Figure 4.1).
The impetus to maintain these lakes as bodies of fresh water is strengthened by the Ramsar
listing of the Coorong and Lakes Alexandrina and Albert wetland, which declared the wa-
ters landward of the Goolwa barrage (Figure 4.1) to be fresh, and imposes an international
obligation to maintain them in this condition (Pittock et al., 2010). There are numerous,
and serious, consequences of this policy, which were demonstrated during the Millennium
drought (1997-2011) when water levels within the Lower Lakes dropped to a record -1.05 m
Australian Height Datum (AHD; i.e. below mean sea level) exposing acid sulphate soils to
a major sub-areal oxidation event as well as causing extensive property and infrastructure
damage due to riverbank collapse (Hubble and De Carli, 2015; Job et al., 2018). Opening
the barrages would have probably prevented the oxidisation event and bank failure but at
the cost of salinising the water in the Lower Lakes and downstream reaches of the LMR.
The combination of the modelling results and the sedimentary sequences identified in core
Monteith-A support the body of literature (see Gell 2019) which suggests that the Lower
Lakes were estuarine central basins subject to significant marine incursion at the Holocene
highstand. A shift to a fresher water distribution within the Lower Lakes required a fall in
sea level to present-day levels (Figure 4.4b).

Applying the highly accurate chronology ($R^2 = 0.997$) to the facies designation of core
Monteith-A allows Belperio et al.'s (2002) sea level envelope to be constrained at the ter-
minus of Australia's largest river. Initially, the older limit of the envelope is supported,
with marine influence first reaching Monteith (rkm 104) at 8,518 yr BP (Figure 4.9a). Core

Monteith-A's sediment accumulation rate then supports a trend to the younger limit of Belperio et al.'s (2002) envelope over the following 2,000 years (Figure 4.9a). The location and age of shells, middens, and diatom assemblages in the Murray estuary's flood tide delta constrains the timing of sea-level stabilisation to the present-day level and the coincident shift to fresher water distribution to approximately 3,500 yr BP (Bourman et al., 2000; Cann et al., 2000; Fluin, 2002; Luebbers, 1982).

Laminations that are planar in orientation, such as those deposited within the central basin of the Murray estuary, traditionally indicate that the suspended sediment settled in water that was still or almost stationary (Zaleha, 1997b). However, recent studies on the deposition of mud flocs have demonstrated that the deposition and preservation of a distinctly laminated sequence can occur at current velocities up to 0.3 m/s (Baas et al., 2016; Schieber and Yawar, 2009; Schieber et al., 2007). The modelling results of this study demonstrate that this condition was extant over a minimum of 95% of the LMR and Murray estuary at the Holocene highstand (Figure 4.4). Indeed, rhythmites or banded grainsize couplets are not uncommon in the transitional environment of the central basin of low energy estuaries and commonly record seasonal (winter/summer) variation in fluvial suspended sediment load (Allen, 2004; Lanier et al., 1993; Reineck and Singh, 1980). It is hypothesised that the Murray estuary's central basin deposit comprises such couplets as the present-day flow (which is dominantly derived from the Murray sub-catchment) is distinctly seasonal due to the annual spring/summer melting of the winter snow pack that develops on the Australian Alps. Evidence for such a pronounced seasonality within the LMR during the mid- to late-Holocene has previously been described through fluctuating palaeo-salinities identified in fish otoliths located immediately upstream from the study site (rkm 110 – 125; Disspain et al., 2011).

The Holocene provides a useful analogue of potential future change to assist in the adaptation of natural resource management policies to the changing climate and rising sea level. Variation in the Holocene palaeo-climate of the MDB has been inferred from sedimentary analyses of two marine sediment cores collected from the Lacepede Shelf offshore from the Murray Mouth (MD03-2611 and MD03-2607; Gingele et al., 2007; Gingele et al., 2004). Several previous studies have used these high resolution, continuous sedimentary records, located at the terminus of the MDB, to constrain climatic conditions for the MDB during the Holocene (Gell et al., 2009). Climatic interpretation of cores MD03-2611 and MD03-2607 rely on the clay/silt-ratio, as a proxy for fluvial/aeolian terrigenous input, and illite concentration, as a proxy for sediments derived from the Murray sub-catchment (Figure 4.6; Gingele et al., 2007; Gingele et al., 2004). However, this study demonstrates that a large natural sediment trap was extant in the lower Murray Gorge and Lake Alexandrina for much of the Holocene where the extensive central basin intercepted and likely prevented the delivery of terrigenous sediment derived from the MDB to the Southern Ocean and Lacepede Shelf. Other studies have demonstrated that the significant accommodation space provided

by coastal plain estuaries, particularly during initial stages of estuarine development in the early- to mid-Holocene, can result in up to 95% of fluvial sediment being prevented from reaching the continental shelf (Meade, 1982; Phillips and Slattery, 2006). The LMR is an extreme example of this phenomenon as this coastal plain river presents a particularly low gradient which significantly limits stream power (Gill, 1978). It follows therefore that there should have been significant terrigenous sediment sequestration within the Holocene sedimentary record of the young estuary – which these results demonstrate – and a consequential reduction in the delivery of terrigenous sediment and deposition in the sedimentary record immediately offshore.

Given the results presented here, an alternate and more plausible interpretation to the palaeo-climate signal presented in Gingele et al. (2007; 2004) is suggested. The results of this study suggest that the transitional point marked by a sudden decrease in the clay/silt-ratio and a trend to decreasing illite concentrations from 8,500 – 8,300 yr BP (Figure 4.6; Gingele et al., 2007; Gingele et al., 2004) is better explained by the inception and widespread development of the Murray estuary. This development of the central basin and estuary within the lower Murray Gorge is another example of the response of a large incised-valley river system to the melting of the Laurentian ice sheet and associated sudden increase in sea level between 8,500 – 8,200 yr BP that initiated estuaries globally (Cohen and Hijma, 2014; Hijma and Cohen, 2010; Rodriguez et al., 2010). This elongate central basin afforded ample accommodation space for the sequestration of terrigenous sediments within the LMR and Lower Lakes. The timing of reduced clay/silt-ratios in MD03-2607 corresponds exactly with the transition from fluvial to estuarine deposits in core Monteith-A and is also contemporaneous with the commencement of deposition of the central basin laminated silt-clay sequence at 8,518 cal yr BP (Figures 4.6 & 4.9a). Gingele et al.'s (2007; 2004) continued trend of apparent increasing aridity culminating in the commencement of arid conditions from 5,500 yr BP corresponds to the rapid deposition of an 11 m uninterrupted laminated sequence spanning from 8,518 – 5,067 cal yr BP in core Monteith-A (Figure 4.6). Similarly, the sharp decrease in clay/silt-ratio and illite concentration that marks a transitional point in the sedimentary record within marine cores MD03-2607 and MD03-2611 (Gingele et al., 2007; Gingele et al., 2004) corresponds to the Holocene sea-level highstand of +2 m between 7,000 – 6,000 yr BP (Belperio et al., 2002; Lewis et al., 2013). At this time, the incursion of central basin conditions into the lower Murray Gorge was at its maximum and likely presented over a 100 rkm section of Lake Alexandrina and the lower Murray Gorge to trap sediment (Figure 4.6).

This study demonstrates the response of an extreme end-member (low discharge, low sediment load, low gradient, and large catchment) coastal plain system to a rising sea level during the Holocene, revealing valley-wide sequences from lowland, through transgression to highstand (Figure 4.9). A novel approach to assessing palaeo-environmental change is adopted by independently verifying best-estimate Holocene highstand and late-Holocene 3D

hydrodynamic models with sedimentary analyses, an approach which, to date, has not been conducted. These results confirm and extend the conclusions of Helfensdorfer et al. (2019) and show that the Holocene sea-level highstand induced an extensive estuarine environment in the LMR, driving the tidal and brackish limits well upstream into the Murray Gorge (Figure 4.4). These results support the contention that the Lower Lakes developed as part of the Murray estuary and therefore could not have been freshwater bodies for the duration of the Holocene. The results of this study demonstrate that the mid-Holocene sea-level highstand created a single, vast central basin environment throughout the Lower Lakes and upstream to Wall Flat (rkm 140; Figure 4.4), that was characterised by a finely laminated silt-clay sequence, as previously described within Lake Alexandrina by Barnett (1993; 1994). A 30 m sediment core (Monteith-A) and transect of CPT soundings independently verify the modelling in demonstrating that this deposit is valley-wide throughout the lower reaches of the LMR. This is consistent with previous accounts of the upper valley-fill as comprising the Coonambidgal Formation muds without evidence of coarse-grained channel sediments (Firman, 1966). The presence of an uninterrupted, valley-wide 11 m central basin deposit (8,518 – 5,067 cal yr BP) suggests that the rising sea level would have strongly supressed deposition of terrigenous sediment on the Lacepede Shelf and may have prevented the offshore delivery of terrestrial sediment entirely. Instead, this sediment was trapped within the young estuary and deposited in discrete laminations within the Lake Alexandrina and the lower reaches of the Murray Gorge. This finding suggests that palaeo-climatic inferences drawn from the terrigenous flux signal within marine cores MD03-2611 and MD03-2607 presented elsewhere may not be valid and that Holocene palaeo-climatic reconstructions which rely on conclusions drawn from the Lacepede Shelf cores should be re-evaluated and reconsidered. Further investigation of the record of sedimentation preserved in core Monteith-A has the potential to provide a detailed, reliable, high-resolution palaeo-climate signal for the MDB during the mid-Holocene.

Chapter 5

Synthesis

5.1   Outline

This study has investigated the geomorphic response of the LMR and Murray estuary to sea-level fluctuations during the Holocene using a combination of hydrodynamic modelling, sedimentological and chronological techniques. In chapter two, sensitivity testing for sea level, bathymetric surface, discharge and barrier morphology through a suite of 2D hydrodynamic models identified the probable response of the LMR and Murray estuary to the Holocene sea-level highstand and subsequent late-Holocene recession to present-day sea level. Chapter three furthered the outcomes of the 2D models using 3D modelling and validated the 2D approach demonstrating the utility of using simpler 2D simulations for investigating palaeo-environmental change. Chapter four presented best estimate 3D Holocene highstand and late-Holocene models that were constrained and validated against the chronology of facies changes presented in core Monteith-A. A sedimentary analysis of core Monteith-A, taken 104 rkm upstream of the Murray Mouth at Monteith, has determined the timing, nature and extent of sedimentary facies successions from lowstand, through transgression to highstand. An analysis of a transect of CPT soundings calibrated against core Monteith-A has allowed for the sedimentary facies successions to be extrapolated out to the entire width of the Murray Gorge at Monteith (rkm 104). This complementary approach of modelling validated with geologic data has established the LMRs Holocene stratigraphy and has enabled the timing of major geomorphic events in the evolution of the hydrology of the LMR to be robustly established. This chapter synthesises the results of this thesis, drawing together and highlighting its key findings. Suggestions for future research are also presented.

5.2 Revised geomorphic history of the LMR and Murray estuary

The combination of results derived from hydrodynamic models and sedimentologic data presented in this thesis allows for the development of a revised model of sedimentary infilling of the lower Murray Gorge (Figure 5.1). These results validate and modify some aspects of Jaksa et al.'s (2013) model and extends and complements the Holocene geomorphic history of Lake Alexandrina presented by Barnett (1994) which receives the LMRs discharge.

5.2.1 ~20,000 – 18,000 yr BP

During the last glacial maxima, it is probable that the Murray Gorge was completely stripped of its valley fill (Figure 5.1). This is supported by the presence of weathered clay at the base of core Monteith-A which is directly overlain by early transgressive fluvial deposits (Figure 4.6). This erosional surface is the only sedimentary hiatus present in core Monteith-A, with the remaining 29.5 m of sediment representing a complete and uninterrupted sequence of deposition (Figure 4.6). This confirms that the Murray Gorge's valley fill comprises sediments derived from a single cycle of lowstand, transgression and highstand only.

5.2.2 ~18,000 – 10,000 yr BP

Sedimentary analyses of core Monteith-A supports previous accounts of the Murray Gorge's lower valley fill comprising coarse-grained sediments derived from braid plain channels (Figures 5.1 & 4.6; e.g. Firman, 1966; Jaksa et al., 2013). These sands, from 21.0 m to 29.5 m in core Monteith-A, were deposited in response to the early phase of sea-level rise in the late-Pleistocene to early-Holocene.

5.2.3 ~10,000 – 9,200 yr BP

The continued rapid rise in sea level caused a change in base level and resulting transitional fluvial depositional sequence (Figures 5.1 & 4.6). The transitional nature of the palaeo-environment resulted in deposition of thin alternating layers of sands and silts present in core Monteith-A from 16.3 m to 21.0 m (Figure 4.7).

~ 120,000 yr BP
Sea level was slightly higher than present at the interglacial sea-level highstand. A succession of coarse-grained fluvial deposits would have underlain finer-grained fluvial deposits through which a single-thread channel would have begun to incise.

~ 20,000 - 18,000 yr BP
At the peak of the glacial maximum, sea level was about 120 m lower than present. The Murray Gorge was completely stripped of its valley fill exposing the weathered clay below.

~ 18,000 - 10,000 yr BP
A warming climate caused melting of ice sheets and associated rapid sea-level rise. A series of braid plain channels formed in response to this change in base level and deposited coarse-grained fluvial sediments.

~ 10,000 - 9,200 yr BP
Sea level continued to rise rapidly causing the braid plain channels to transition into a single-thread channel. This reduction in energy gradient brought about by a rising base level resulted in the deposition of finer-grained fluvial sediments.

~9,200 - 8,500 yr BP
Sea level continued to rise rapidly causing a further reduction in the energy gradient and deposition of fine-grained fluvial sediments. Flow velocity was significantly reduced allowing for the growth of channel fringing and aquatic vegetation.

~ 8,500 - 4,000 yr BP
A stepwise jump in sea level preceding the Holocene sea-level highstand backfilled the lower Murray Gorge creating a central basin environment which occupied the entire width of the valley. This ample accommodation and reduction in energy allowed a finely laminated silt-clay sequence to rapidly deposit.

~ 4,000 yr BP to 1900
Sea level receded to the present-day level causing the bayhead delta to prograde forming a single-thread channel with levees and fringing swamps. The channel begun incising into the underlying soft central basin muds.

~ 1900 - present day
Significant modification to the landscape and flow regime with European influences. Construction of levees and land reclamation infilled channel fringing swamps. The channel continued to incise into the underlying soft central basin muds.
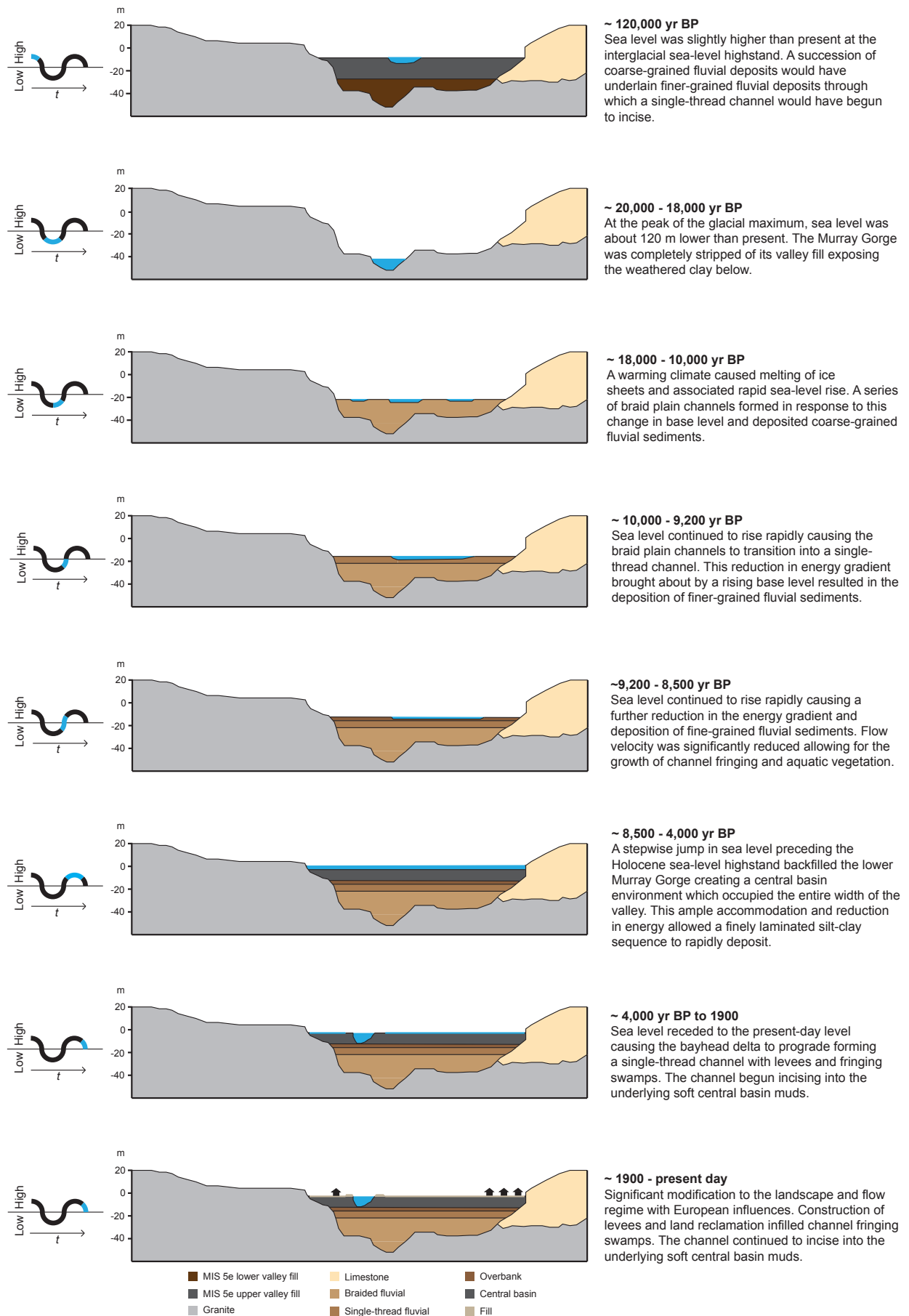
Figure 5.1: A revised model of the sedimentary infill of the Murray Gorge. Developed from a whole-of-valley sedimentary analysis at Monteith (rkm 104) in conjunction with hydrodynamic modelling of the LMR and Murray estuary.

5.2.4   ~9,200 − 8,500 yr BP

A transition to the deposition of cross bedded sandy-muds with high TOC contents from 12.6 m to 16.3 m in core Monteith-A (Figure 4.6). These materials identify as a discrete group in the clustering analysis conducted on CPT soundings and indicate that a further reduction in energy with continued sea-level rise resulted in the deposition of a very low-energy fine-grained estuarine-fluvial transitional sequence including abundant aquatic and channel fringing plants (Figure 5.1 & 4.8 & 4.2).

5.2.5   ~8,500 − 4,000 yr BP

A stepwise 'jump' in sea level at approximately 8,200 yr BP (Hijma and Cohen, 2010; Rodriguez et al., 2010) initiated an extremely elongate estuary which generated low energy backwater conditions throughout the Murray Gorge (Figure 4.6). This produced a central basin environment within the Lower Lakes and lower reaches of the Murray Gorge, with 3D hydrodynamic modelling indicating the central basin was extant upstream as far as Wall Flat (rkm 140; Figures 5.1 & 5.2 & 4.4a). In core Monteith-A this is exhibited as an approximately 11 m (1.65 –12.61 m) finely laminated silt-clay sequence which deposited from 8,518 –5,067 cal yr BP and is contiguous with the central basin deposit within Lake Alexandrina described by Barnett (1993; 1994; Figure 4.6). The combination of hydrodynamic modelling and sedimentologic results presented in this study demonstrates that a single central basin depositional environment extended from Point Sturt/Point McLeay into the Murray Gorge at least as far upstream as Wall Flat (rkm 140; Figures 5.2 & 4.4).

Despite small amounts of saline ingression by barrage overtopping in the present-day modified condition, density stratification causes anoxic conditions within the Lower Lakes (Aldridge et al., 2009) which supports the development of widespread laminations described in cores taken from Lake Alexandrina and the LMR. Anoxia facilitates the preservation of laminated sequences by limiting or preventing bioturbation, which may explain the lack of bioturbation in Barnett's (1993; 1994) Lake Alexandrina cores, as well as within core Monteith-A, and the very well-preserved nature of this uninterrupted central basin deposit (Figure 4.7).

Barnett's (1993; 1994) palaeo-limnological analysis confirms the presence of marine influence throughout the Holocene which refutes the sustained isolation from the ocean proposed by Jaksa et al. (2013). As does the presence of flaser bedding within the flood-tide delta and a laminated silt-clay sequence within the main body of Lake Alexandrina throughout the mid-Holocene (Barnett, 1993; 1994). Jaksa et al.'s (2013) hypothesis that the laminated sequence within the LMR originates from a freshwater palaeo-lake extant behind a closed barrier complex cannot be sustained. Sensitivity testing the chain-of-islands evolution of the barrier complex through hydrodynamic modelling demonstrates that an elevated sea level

was sufficient to establish very low-energy estuarine conditions throughout LMR with substantial periods of the mid-Holocene subject to backwater conditions irrespective of barrier morphology (Figures 2.10b and 2.11). Landward of the flood-tide delta, the remarkably low modelled maximum flow velocity magnitudes under all scenarios indicates that a low energy environment was likely sustained throughout the Holocene (Figures 3.5 & 3.7 & 4.4). This is attributed to the unique set of characteristics that define this coastal plain system, namely the system's extremely low gradient, discharge and sediment yield, which generate conditions where maximum flow velocity magnitudes are below the critical threshold of 0.3 m/s required for the deposition and preservation of a laminated clay-silt sequence (Baas et al., 2016; Schieber and Yawar, 2009; Schieber et al., 2007). The closed barrier envisioned by Jaksa et al. (2013) was not required for the deposition and preservation of a finely laminated sequence.
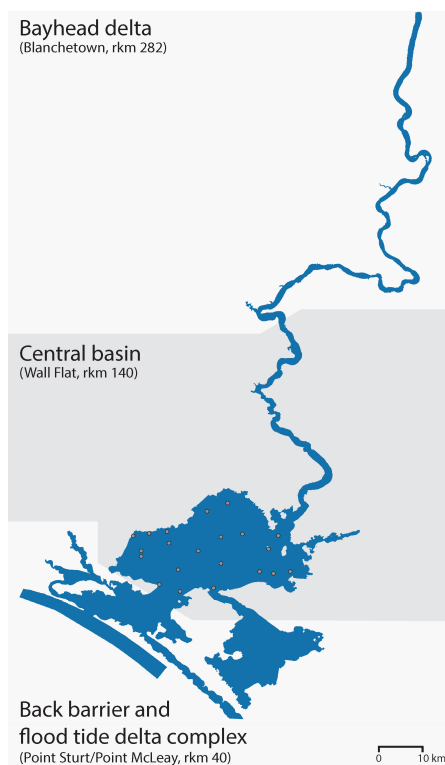
Figure 5.2: Morphological zonation of the Murray estuary at the Holocene highstand. A 3D best-estimate Holocene highstand scenario ($S_{mid}WL_2D_{av}B_{mod}$) demonstrates that the flood-tide delta was restricted seaward of Point Sturt and Point McLeay (rkm 40). Modelling results were validated by sedimentary analyses of core Monteith-A and cores previously collected within Lake Alexandrina (grey points; Barnett, 1993; 1994) to demonstrate that a single central basin environment was extant from Point Sturt/Point McLeay (rkm 40) at least as far upstream as Wall Flat (rkm 140) at the Holocene highstand. Upstream, the bayhead delta occupied the Murray Gorge at least up to Blanchetown (rkm 282). The areal extent of the LMR and Murray estuary (blue) depicts maximum inundation of scenario $S_{mid}WL_2D_{av}B_{mod}$.

5.2.6   ~4,000 yr BP − 1900

Late-Holocene hydrodynamic models suggest that significant marine influence was restricted to the flood-tide delta once sea level had receded to present-day levels (Figures 2.8a & 3.3a-b & 4.4b). Despite the potentially disturbed nature of the near surface in core Monteith-A, the sedimentary record indicates that significant sediment accumulation had ceased by this time as the accommodation space in the Murray Gorge and Lower Lakes was infilled. The timing of sea-level stabilisation to the present-day level, at approximately 3,500 yr BP, has been constrained by the location and age of shells and middens as well as diatom assemblages in the Murray estuary's flood-tide delta (Cann et al., 2000; Fluin, 2002; Luebbers, 1982). This is also evident from the shift in composition of diatoms from species tolerant to diverse salinity gradients between 7,000 − 5,000 yr BP, to predominately freshwater species post 5,000 yr BP and indicates a reduction in marine influence within Lake Alexandrina as sea level receded 2 m from highstand (Barnett, 1993; 1994). Sedimentary infill caused progradation of the bayhead delta and instigated the process of channel incision in the Murray Gorge, creating the incised channel, scour holes, levees and backswamps of the present-day LMR (Figure 5.1).

5.2.7   ~1900 − present day

Significant alterations to the flow regime, including flow regulation and significant water extraction for irrigation and drinking water supplies, was enabled by the construction of locks, weirs, dams and barrages, combined with alterations to the landscape through levee construction, land reclamation and laser levelling (Figure 5.1). Natural geomorphic evolution of the LMR and Murray estuary has been interrupted by these anthropogenic interventions.

5.2.8   Present day − future

The response of the LMR and Murray estuary to sea-level rise during the Holocene can be used as an analogue to predict the system's vulnerability to future environmental change due to climate-change induced sea-level rise. When considering estuarine responses to future sea-level rise, there is an important distinction in the range of responses between young, newly initiated, Holocene estuaries and the managed and regulated estuaries of today (Kermode et al., 2013). The significant amount of accommodation space generated by a rapid rise in sea level some 130 m during the late-Pleistocene to mid-Holocene is entirely different to the comparatively subtle rise of between 0.53 −0.97 m by 2100 projected by the IPCC, provided the rate of sea-level rise could be constrained beyond this point (Reisinger et al., 2014). However, the morphological response is affected by not just the magnitude of the change but also the rate of sea-level rise whereby projected future changes are comparable to rates during the late-Pleistocene and early-Holocene. It follows, then, that direct compar-

isons cannot be made from a depositional standpoint, nevertheless responses to the Holocene sea-level highstand provide a useful analogue of potential environmental change (Kermode et al., 2013).

Hydrodynamic modelling of the LMR and Murray estuary reveals the considerable influence of a 2 m higher-than-present sea level (Figures 2.8 & 2.10 & 3.3 & 4.4). Irrespective of bathymetry, discharge or barrier morphology, the Holocene sea-level highstand caused a pronounced shift in the palaeo-environmental character of the region driving saline incursion well upstream into the Murray Gorge (Figures 2.8 & 2.10 & 3.3). The presence of an estuarine central basin deposit 104 rkm upstream from the Murray Mouth within core Monteith-A independently verifies the extent of estuarine influence. The significant marine influence within the Lower Lakes and lower reaches of the LMR under a +2 m sea level scenario gives insight into the plausible response of the system to a future rise in sea level. The considerable change in palaeo-environmental character between + 0 m (WL_0) and +2 m (WL_2) scenarios constrains the limit of plausible change and suggests that even a 0.53 – 0.97 m rise in sea level (Reisinger et al., 2014) will likely result in an estuarine environment at least within the Lower Lakes (Figures 2.14 & 4.4). Of course, these results represent a natural, 'do nothing' scenario, with the barrages currently in place to separate the system from the ocean. These results, therefore, highlight the increased future reliance on the barrages to maintain the freshwater character of the LMR and Lower Lakes for irrigation and drinking water supply, as well as the 'dry-land' nature of the low-lying floodplain areas adjacent to the LMR channel which would become saturated and boggy, if not submerged in places.

5.3   Conceptual models of incised valley systems and the unique case of the LMR

The findings of this thesis serve as a point of comparison to traditional estuarine models, framing the palaeo-Murray estuary as an end-member example of a coastal plain estuary's response to sea level fluctuations during the Holocene. At the terminus of an immense 1 million km^2 catchment, the LMR and Murray estuary present a unique set of characteristics, with an extremely low gradient, low discharge and low sediment yield. The influence of these unique characteristics on the deposits formed in the LMR contrasts distinctly with the distribution of lithofacies in an idealised wave-dominated estuary as proposed by Dalrymple et al. (1992; Figure 5.3). Core Monteith-A was collected from an equivalent location to C4 in the Dalrymple model (Figure 5.3; Dalrymple et al., 1992), however, it does not present the idealised sequence of fluvial-estuarine-fluvial lithofacies (Figure 4.6). In contrast, core Monteith-A exhibits a similar sequence of lowstand and transgressive fluvial deposits, however, proportionately, the central basin deposit dominates and there is no equivalent pro-

grading fluvial material within core Monteith-A as the central basin deposit is not overlain
by bayhead delta and alluvial sequences as is expected from Dalrymple et al.'s (1992) model
(Figures 5.3 & 4.6). This absence of the fluvial highstand depositional material is unusual
and demonstrates the depositional response of a very low-gradient system which is relatively
'starved' of sediment.
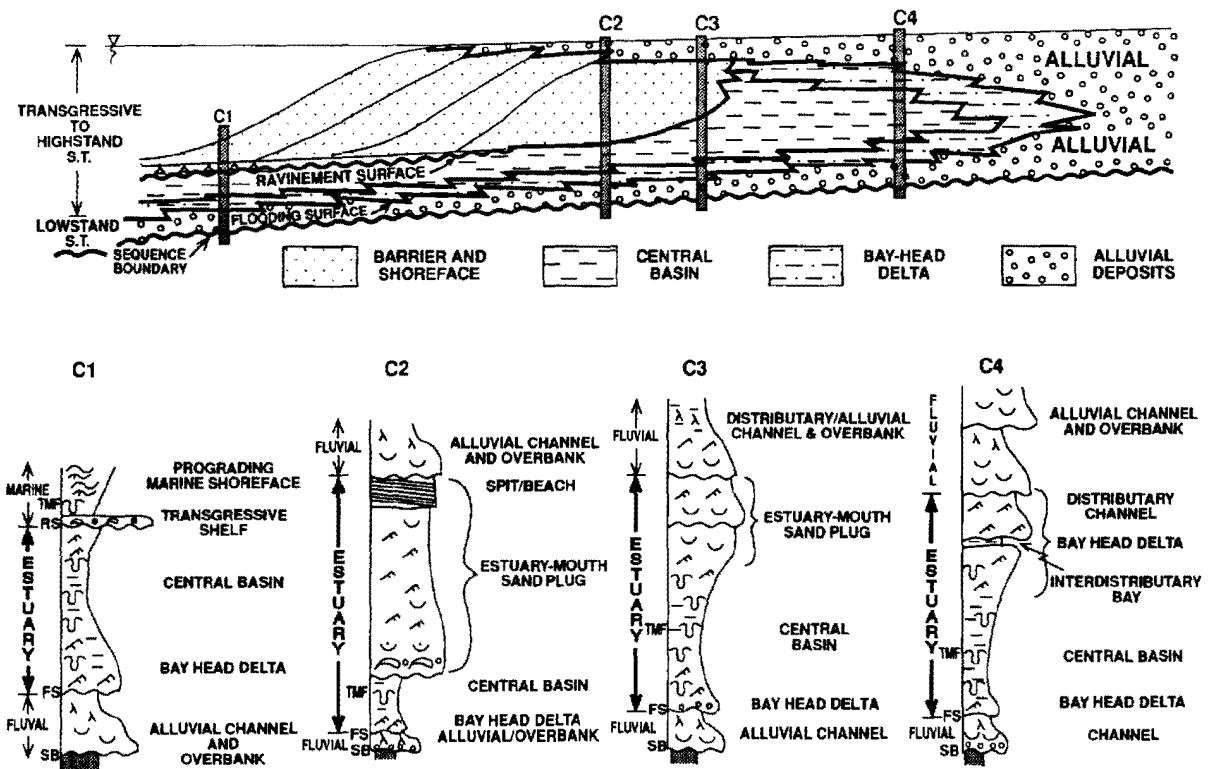
Figure 5.3: Distribution of lithofacies in an idealised wave-dominated estuary. The section through C4
represents an idealised sedimentary sequence at an equivelent location in the estuary to core Monteith-A
(after Dalrymple et al., 1992).

Similarly, comparisons can be drawn between the sedimentary infill of the Murray Gorge
as depicted in core Monteith-A and the conceptual longitudinal model of an incised valley
system developed by Zaitlin et al. (1994). Conventionally, incised valley systems exhibit a
coarsening upward sequence in response to sea-level stabilisation (Figure 1.10). However,
owing to the low flow and low gradient of this system, core Monteith-A presents a relative
absence of a conventional highstand system tract deposit with very little sedimentation above
the maximum flooding surface (Figure 1.10). The results of this study demonstrate that the
Murray Gorge's valley fill comprises a highly modified presentation of Zaitlin et al.'s (1994)
overall model in a landward location.

5.4   Future research

This study has described the geomorphic evolution of LMR at Monteith (rkm 104), with a robust chronology constraining this evolution to demonstrate the response of the Murray estuary to sea level fluctuations during the Holocene. A key recommendation for future research, therefore, is to replicate the sedimentary components of this study – analyses of a sediment core and transect of CPT soundings – to other key locations within the palaeo-Murray estuary. The hydrodynamic model results of best-estimate Holocene highstand and late-Holocene scenarios presented in this study facilitates the choice of suitable future field-work locations. It is suggested that fieldwork be undertaken in the vicinity of Wall Flat (rkm 140), where a thin succession of central basin deposits should be overlain by the prograding bayhead delta, which is absent at Monteith (rkm 104). The bayhead delta is inferred to have prograded downstream to Mypolonga (rkm 130) prior to significant anthropogenic alteration to the flow regime which prevented further natural geomorphic evolution (Taylor and Poole, 1931). Given this assertion, the vicinity of Mypolonga (rkm 130) would also be a suitable location for future fieldwork. Finally, a sedimentary analysis at the Pomanda Embayment (rkm 72) would provide the crucial link between the work of Barnett (1993; 1994) in Lake Alexandrina and analyses within the Murray Gorge presented here. Together, a whole-of-valley sedimentary analysis at these three additional locations would allow for the model of Holocene estuarine evolution proposed by the suite of hydrodynamic models presented herein to be further validated.

The finely laminated sequence revealed within core Monteith-A is inferred to be comprised of annually deposited seasonal rhythmites. This hypothesis forms the basis of a critical area of future research which, if proven, may allow for the development of a mid-Holocene palaeo-climate record for the entire MDB. The mode of deposition could be confirmed through an analysis of thin sections from core Monteith-A, with a palaeo-climate record extracted from x-ray fluorescence elemental profiles. The sedimentary record within core Monteith-A demonstrates significant Holocene deposition within the Murray Gorge between 8,518 and 5,067 cal yr BP which essentially prevented terrigenous sediment delivery to the offshore marine environment during this period. This finding suggests that Holocene climatic inferences derived from fluctuations of terrigenous sediment in marine cores collected directly offshore from the Murray Mouth should be re-evaluated (Gingele et al., 2007; Gingele et al., 2004). If a palaeo-climate record could indeed be extracted from core Monteith-A, it would represent the first uninterrupted Holocene climate record capturing the entire MDB. This is a highly significant area of future research which has the potential to inform nationally significant water policy, particularly given future uncertainties in the MDB's response to changes in sea level and climate with anthropogenic climate change.

5.5   Concluding remarks

A suite of 2D hydrodynamic models has constrained the plausible response of the LMR and Murray estuary to the Holocene sea-level highstand and has shown that sea level was the primary driver of palaeo-environmental change during the Holocene. A sensitivity analysis has demonstrated that variation of bathymetric surface, discharge or barrier morphology alone is insufficient to alter the regional palaeo-environment. Through this suite of models this study has identified, for the first time, that the limit of the Murray estuary propagated well upstream into the confines of the Murray Gorge during the Holocene.

Palaeo-climatic data provides a context for current and projected variability in climate, and has an important role in contextualising whether variabilities in climate currently seen are artefacts of the current climatic regime or can be considered to be an imposed variability due to anthropogenic climate change (Mills et al., 2013b). Accurate palaeo-data is required for the designation of the natural, pre-anthropogenic condition of a region, as a baseline for effective natural resource management, while understanding the response of a system to palaeo-climatic changes is crucial to direct policy to curtail the potential impacts of future climate change and sea-level rise (Gell et al., 2009). Water management within the MDB is highly contentious, with politically motivated policies driving allocations for irrigation and environmental flows (Walker, 2019). One highly contented issue is the palaeo-salinity of the Lower Lakes, with a diverse range of Holocene palaeo-salinities interpreted, even by the same authors, with some suggesting that studies on the palaeo-environment of these lakes has been manipulated to drive a particular policy outcome (Fluin, 2002; Fluin et al., 2009; Gell, 2019). This study independently verifies, through hydrodynamic modelling and sedimentary analyses, that the Lower Lakes could not have been freshwater bodies for the entire duration of the Holocene, with the Holocene sea-level highstand driving the estuarine limit well upstream into the Murray Gorge (likely as far as Wall Flat, rkm 140) and generating significant marine influence throughout Lake Alexandrina and Lake Albert.

This study has contrasted the results of simple and efficient 2D simulations with complex and computationally expensive 3D simulations. This analysis has considered the appropriate level of complexity required when adopting hydrodynamic models for studies of palaeo-environmental change. Inherently, 3D simulations allow for a more robust analysis of salinity dynamics within the estuary, resolving the presence of a salt wedge at depth, with 2D simulations providing a more conservative estimate. However, when assessed relative to estuarine zonation and morphology, it was shown that a 2D model of the LMR and Murray estuary sufficiently resolves 3D trends and produced closely similar results and environmental conditions. The 2D-3D comparison provided in this study demonstrates the suitability of adopting simple and efficient 2D simulations for 'first-pass' assessments of estuarine systems.

Finally, best-estimate Holocene highstand and late-Holocene 3D models were independently validated against analyses of a 30 m sediment core (Monteith-A) and valley-wide transect of CPT soundings at Monteith (rkm 104). The revised geomorphic history developed through this analysis demonstrates the sedimentary response of a large coastal plain system to the full cycle of lowstand, transgression and highstand. The LMR and Murray estuary's response to fluctuations in sea level during the Holocene is constrained by the highly accurate (R^2 = 0.9973) chronology developed from core Monteith-A. As a consequence of a unique set of characteristics – an extremely low gradient, low discharge and low sediment yield, combined with an immense 1 million km^2 catchment – the LMR and Murray estuary can be considered an end-member coastal plain system. The lower Murray Gorge's Holocene sedimentary infill has been characterised, for the entire width of the valley, and a facies designation developed, that demonstrates a highly modified presentation of Zaitlin et al.'s (1994) model in a landward location. The finely laminated silt-clay sequence that comprises the Murray estuary's central basin deposit confirms the timing and nature of estuarine influence at Monteith (rkm 104) and demonstrates that a single depositional environment existed within Lake Alexandrina and the lower reaches of the Murray Gorge during the mid-Holocene. This finding demonstrates that Lake Alexandrina's St Kilda Formation and the LMR's Coonambidgal Formation are equivalent units such that the location of the division of these two stratigraphic units could be discarded.

Chapter 6

References

Aldridge, K. T., Deegan, B. M., Lamontagne, S., Bissett, A., & Brookes, J. D. (2009). Spatial and temporal changes in water quality and sediment character in Lake Alexandrina and Lake Albert during a period of rapid water level drawdown. CSIRO: Water for a Healthy Country National Research Flagship, Canberra. ISSN: 1835-095X.

Allen, J. R. L. (2004). Annual textural banding in Holocene estuarine silts, Severn Estuary Levels (SW Britain): patterns, cause and implications. The Holocene, 14(4), 536-552.

Amorosi, A., & Marchi, N. (1999). High-resolution sequence stratigraphy from piezocone tests: an example from the Late Quaternary deposits of the southeastern Po Plain. Sedimentary Geology, 128(1), 67-81.

Austin, J. M., & Gallant, J. C. (2010). Stitching elevation and bathymetry data for the Murray River and Lower Lakes, South Australia. CSIRO: Water for a Healthy Country National Research Flagship. 76 pp.

Baas, J. H., Best, J. L., & Peakall, J. (2016). Predicting bedforms and primary current stratification in cohesive mixtures of mud and sand. Journal of the Geological Society, 173(1), 12-45.

Barnett, E. J. (1993). Recent Sedimentary History of Lake Alexandrina and the Murray Estuary. (Doctor of Philosophy), The Flinders University of South Australia.

Barnett, E. J. (1994). A Holocene paleoenvironmental history of Lake Alexandrina, South Australia. Journal of Paleolimnology, 12, 259-268.

Barnett, S. R. (1989). The hydrogeology of the Murray Basin in South Australia with special reference to the alluvium of the River Murray floodplain. (M.Sc.), Flinders University.

Baynes, T., Herr, A., Langston, A., & Schandl, H. (2012). Coastal Climate Risk Project Milestone 1 Final Report to the Australian Department of Climate Change and Energy Efficiency. DCCEE, Canberra, ACT, Australia.

Belperio, A. P., Hails, J. R., & Gostin, V. A. (1983). A review of Holocene sea levels in South Australia. In D. Hopley (Ed.), Australian sea levels in the last 15 000 years: a review (Occasional Paper 3 ed.). James Cook University.

Belperio, A. P., Harvey, N., & Bourman, R. P. (2002). Spatial and temporal variability in the Holocene sea-level record of the South Australian coastline. Sedimentary Geology, 150(1), 153-169.

Belperio, A. P., Murray-Wallace, C. V., & Cann, J. H. (1995). The last interglacial shoreline in southern Australia: Morphostratigraphic variations in a temperate carbonate setting. Quaternary International, 26(0), 7-19.

Blaauw, M., & Christen, J. A. (2011). Flexible Paleoclimate Age-Depth Models Using an Autoregressive Gamma Process. Bayesian Analysis, 6, 457-474.

Bloss, C., Montazeri, M., & Eckert, G. (2015). Flood mapping of the River Murray floodplain in South Australia. DEWNR Technical report 2015/57, Government of South Australia, through Department of Environment, Water and Natural Resources, Adelaide.

Blott, S. J., & Pye, K. (2001). GRADISTAT: a grain size distribution and statistics package for the analysis of unconsolidated sediments. Earth Surface Processes and Landforms, 26, 1237-1248.

Blum, M. D., & Törnqvist, T. E. (2000). Fluvial responses to climate and sea-level change: a review and look forward. Sedimentology, 47, 2-48.

Bourman, B., & Harvey, N. (1983). The murray mouth flood tidal delta. Australian Geographer, 15(6), 403-406.

Bourman, B., & Murray-Wallace, C. V. (1991). Holocene evolution of a sand spit at the mouth of a large river system: Sir Richard Peninsular and the Murray Mouth, South Australia. Zeitschrift für Geomorphologie Supplementband, 81, 63-83.

Bourman, R. P., & Barnett, E. J. (1995). Impacts of River Regulation on the Terminal Lakes and Mouth of the River Murray, South Australia. Australian Geographical Studies, 33(1), 101-115.

Bourman, R. P., Murray-Wallace, C. V., Belperio, A. P., & Harvey, N. (2000). Rapid coastal geomorphic change in the River Murray Estuary of Australia. Marine Geology, 170, 141-168.

Bowman, G., & Harvey, N. (1986). Geomorphic Evolution of a Holocene Beach-Ridge Complex, LeFevre Peninsula, South Australia. Journal of Coastal Research, 2(3), 345-362.

Brown, C. M., & Stephenson, A. E. (1991). Geology of the Murray Basin, Southeastern Australia. Canberra: Australian Government Publishing Service. Bulletin 235. IBSN 0644137827.

Cai, W., & Cowan, T. (2008). Evidence of impacts from rising temperature on inflows to the Murray-Darling Basin. Geophysical Research Letters, 35(7), L07701.

Cann, J. H., Bourman, R. P., & Barnett, E. J. (2000). Holocene Foraminifera as Indicators of Relative Estuarine-Lagoonal and Oceanic Influences in Estuarine Sediments of the River Murray, South Australia. Quaternary Research, 53(3), 378-391.

Cann, J. H., Murray-Wallace, C. V., Belperio, A. P., & Brenchley, A. J. (1999). Evolution of Holocene coastal environments near Robe, southeastern South Australia. Quaternary International, 56, 81-97.

Christensen, J. H., Hewitson, B., Busuioc, A., Chen, A., Gao, X., Held, R., Dethloff, K. (2007). Regional Climate Projections. Climate change 2007: The physical science basis. Contribution of Working Group I to the Fourth Assessment Report of the Intergovernmental Panel on Climate Change. 847-940.

Clarke, J. D. A., Pain, C. F., Gibson, D., Wong, V., & Apps, H. (2008). Remote sensing of fluvial architecture of the Murray River, southern Australia. Geophysical Research Abstracts, 10.

Cohen, K. M., & Hijma, M. P. (2014). The Transgressive Early–Middle Holocene Boundary: The Case for a GSSP at Rotterdam, Rhine Delta, North Sea Basin. In R. Rocha, J. Pais, J. C. Kullberg, & S. Finney (Eds.), STRATI 2013: First International Congress on Stratigraphy At the Cutting Edge of Stratigraphy (pp. 925-929). Cham: Springer International Publishing.

Cohen, T. J., & Nanson, G. C. (2007). Mind the gap: an absence of valley-fill deposits identifying the Holocene hypsithermal period of enhanced flow regime in southeastern Australia. The Holocene, 17(3), 411-418.

Connor, J., Schwabe, K., King, D., Kaczan, D., & Kirby, M. (2009). Impacts of climate change on lower Murray irrigation. Australian Journal of Agricultural and Resource Economics, 53(3), 437-456.

Dalrymple, R. W., Boyd, R., & Zaitlin, B. A. (1994). History of research, types and internal organization of incised-valley systems: Introduction to the volume. In R.

W. Dalrymple, R. Boyd, & B. A. Zaitlin (Eds.), Incised-valley systems: Origin and sedimentary sequences (pp. 3-10): SEPM, Special Publication.

Dalrymple, R. W., Zaitlin, B. A., & Boyd, R. (1992). Estuarine facies models; conceptual basis and stratigraphic implications. Journal of Sedimentary Research, 62(6), 1130-1146.

Davis, P. S. (1978). Man and the Murray. Kensington, Australia. New South Wales University Press.

De Carli, E., Hubble, T., Penny, D., Petley, D., Clarke, S., Hamilton, R., Brand, H. (2015). Discovery of a palaeolake at the terminus of the Murray-Darling Basin: a Holocene record of southeastern Australia's hydroclimate and implications for current palaeoclimate reconstructions. Paper presented at the INQUA Congress, Nagoya, Japan.

De Carli, E., & Hubble, T. C. T. (2014). Morphological Characteristics of Riverbank Failure on the Lower River Murray, South Australia. Paper presented at the Proceedings of the 7th Australian Stream Management Conference, Townsville, Queensland.

de Mooy, C. J. (1959). Notes on the geomorphic history of the area surrounding Lakes Alexandrina and Albert. Transactions of the Royal Society of South Australia, 82, 99-118.

de Vriend, H. J., Capobianco, M., Chesher, T., de Swart, H. E., Latteux, B., & Stive, M. J. F. (1993). Approaches to long-term modelling of coastal morphology: A review. Coastal Engineering, 21(1), 225-269.

Devoy, R. J., Dodson, J. R., Thom, B. G., & Nichol, S. (1994). Holocene environments in the Hawkesbury valley, new South Wales: A comparison of terrestrial and marine records. Quaternary Science Reviews, 13(3), 241-256.

Disspain, M., Wallis, L. A., & Gillanders, B. M. (2011). Developing baseline data to understand environmental change: a geochemical study of archaeological otoliths from the Coorong, South Australia. Journal of Archaeological Science, 38(8), 1842-1857.

Ellicott, L., & Hudson, R. (2010). Modelling investigations into the Wellington 'Virtual Weir' concept: Phase 3 water level, wind data and wind setup analyses (including TUFLOW-FV wind design simulations). Prepared For: Murray Darling Basin Authority.

Firman, J. B. (1966). Stratigraphy of the Chowilla Area in the Murray Basin. Quarterly Geological Notes, 20.

Firman, J. B. (1971). Riverine and Swamp Deposits in the Murray River Tract, South Australia. Quarterly Geological Notes, 40.

Fitzpatrick, R. W., Mosley, L. M., & Cook, F. J. (2017). Understanding and managing irrigated acid sulfate and salt-affected soils: A handbook for the Lower Murray Reclaimed Irrigation Area. Adelaide, Australia. University of Adelaide Press.

Fluin, J. (2002). A diatom-based palaeolimnological investigation of the lower Murray River (south east Australia). (Doctor of Philosophy), Monash University.

Fluin, J., Gell, P., Haynes, D., Tibby, J., & Hancock, G. (2007). Palaeolimnological evidence for the independent evolution of neighbouring terminal lakes, the Murray Darling Basin, Australia. Hydrobiologia, 591(1), 117-134.

Fluin, J., Haynes, D., & Tibby, J. (2009). An Environmental History of the Lower Lakes and the Coorong. A report for the Department of Environment and Heritage, South Australia. University of Adelaide, 22 pp.

Folk, R. L., & Ward, W. C. (1957). Brazos River bar: a study in the significance of grain size parameters. Journal of Sedimentary Petrology, 27, 3-26.

French, J., Payo, A., Murray, B., Orford, J., Eliot, M., & Cowell, P. (2016). Appropriate complexity for the prediction of coastal and estuarine geomorphic behaviour at decadal to centennial scales. Geomorphology, 256, 3-16.

Gallant, A. J. E., Kiem, A. S., Verdon-Kidd, D. C., Stone, R. C., & Karoly, D. J. (2012). Understanding hydroclimate processes in the Murray-Darling Basin for natural resources management. Hydrology and Earth System Sciences, 16(7), 2049-2068.

Gell, P., Gergis, J., Mills, K., Baker, P. J., De Deckker, P., Finlayson, M., Tibby, J. (2009). Palaeoclimate studies relevant to natural resource management in the Murray-Darling Basin. A report for the Murray-Darling Basin Authority.

Gell Peter, A. (2019). Watching the tide roll away – contested interpretations of the nature of the Lower Lakes of the Murray Darling Basin. Pacific Conservation Biology - https://doi.org/10.1071/PC18085.

Geyer, W. R. (2010). Estuarine salinity structure and circulation. In A. Valle-Levinson (Ed.), Contemporary Issues in Estuarine Physics (pp. 12-26). Cambridge: Cambridge University Press.

Geyer, W. R., & Ralston, D. (2011). The Dynamics of Strongly Stratified Estuaries. In E. Wolanski & D. McLusky (Eds.), Treatise on Estuarine and Coastal Science (Vol. 2: Water and fine sediment circulation, pp. 37-51).

Gill, E. D. (1978). The Murray-Darling River System. Paper presented at the Proceedings of Royal Society of Victoria, Melbourne, Australia.

Gingele, F., De Deckker, P., & Norman, M. (2007). Late Pleistocene and Holocene climate of SE Australia reconstructed from dust and river loads deposited offshore the River Murray Mouth. Earth and Planetary Science Letters, 255(3-4), 257-272.

Gingele, F. X., De Deckker, P., & Hillenbrand, C.-D. (2004). Late Quaternary terrigenous sediments from the Murray Canyons area, offshore South Australia and their implications for sea level change, palaeoclimate and palaeodrainage of the Murray–Darling Basin. Marine Geology, 212(1-4), 183-197.

Gippel, C. J., & Blackham, D. (2002). Review of environmental impacts of flow regulation and other water resource developments in the River Murray and Lower Darling River system. Final Report by Fluvial Systems Pty Ltd, Stockton, to Murray-Darling Basin Commission, Canberra, ACT.

Gouramanis, C., De Deckker, P., Switzer, A. D., & Wilkins, D. (2013). Cross-continent comparison of high-resolution Holocene climate records from southern Australia — Deciphering the impacts of far-field teleconnections. Earth-Science Reviews, 121, 55-72.

Hanson, H., Aarninkhof, S., Capobianco, M., Jimenez, J. A., Larson, M., Nicholls, R. J., Plant, N. G., Southgate, H. N., Steetzel, H. J., Stive M. J. F., & de Vriend, H. J. (2003). Modelling of Coastal Evolution on Yearly to Decadal Time Scales. Journal of Coastal Research, 19(4), 790-811.

Harle, K., Etheridge, D., Barbetti, M., Jones, R., Brooke, B., Whetton, P., Haberle, S. (2007). Building a future on knowledge from the past: what palaeo-science can reveal about climate change and its potential impacts in Australia. A research brief for the Australian Greenhouse Office prepared by CSIRO in association with scientifi c collaborators. Australian Greenhouse Office, Department of the Environment and Water Resources, Commonwealth of Australia.

Harvey, N. (1996). The Significance of Coastal Processes for Management of the River Murray Estuary. Australian Geographical Studies, 34(1), 45-57.

Harvey, N. (2006). Holocene Coastal Evolution: Barriers, Beach Ridges, and Tidal Flats of South Australia. Journal of Coastal Research, 90-99.

Harvey, N., Belperio, A., Bourman, R., & Mitchell, W. (2002). Geologic, isostatic and anthropogenic signals affecting sea level records at tide gauge sites in southern Australia. Global and Planetary Change, 32(1), 1-11.

Harvey, N., Bourman, R., & Kris, J. (2006). Evolution of the Younghusband Peninsula, South Australia: New evidence from the northern tip. South Australian Geographical Journal, 105, 37-50.

Helfensdorfer, A. M., Power, H. E., & Hubble, T. C. T. (2019). Modelling Holocene analogues of coastal plain estuaries reveals the magnitude of sea-level threat. Scientific Reports, 9(1), 2667.

Hesse, P. P., Magee, J. W., & van der Kaars, S. (2004). Late Quaternary climates of the Australian arid zone: a review. Quaternary International, 118-119, 87-102.

Hijma, M. P., & Cohen, K. M. (2010). Timing and magnitude of the sea-level jump preluding the 8200 yr event. Geology, 38(3), 275-278.

Hill, P. J., De Deckker†, P., von der Borch, C., & Murray-Wallace, C. V. (2009). Ancestral Murray River on the Lacepede Shelf, southern Australia: Late Quaternary migrations of a major river outlet and strandline development. Australian Journal of Earth Sciences, 56(2), 135-157.

Hori, K., & Saito, Y. (2007). An early Holocene sea-level jump and delta initiation. Geophysical Research Letters, 34(18).

Hotzel, G., & Croome, R. (1996). Population dynamics of Aulacoseira granulata (EHR) SIMMONSON (Bacillariophyceae, Centrales), the dominant algae in the Murray River, Australia. Arch Hydrobiol, 136, 191-215.

Hubble, T. C. T., & De Carli, E. (2015). Mechanisms and Processes of the Millennium Drought River Bank Failures: Lower Murray River, South Australia. Goyder Institute for Water Research Technical Report Series No. 15/5, Adelaide, South Australia.

Hudson, R. (2010). Modelling Investigation into the Wellington 'Virtual Weir' Concept: Project summary report. Prepared by BMT WBM Pty Ltd on behalf of Murray Darling Basin Authority.

Hudson, R., & Wainwright, D. (2013). Hydrodynamic and morphological modelling to enhance ecosystem recovery of the Coorong, Lower Lakes and Murray Mouth region. Paper presented at the Coasts and Ports 2013: 21st Australasian Coastal and Ocean Engineering Conference and the 14th Australasian Port and Harbour Conference. , Sydney, NSW.

Jaksa, M. B., Hubble, T. C. T., Kuo, Y. L., De Carli, E., & Liang, C. (2013). Riverbank Collapse Along the Lower River Murray - Literature Review, Goyder Institute for Water Research Technical Report Series No. 13/15, Adelaide, South Australia.

James, K. F., Robert P. Bourman, & Harvey, N. (2015). Rapid Evolution of a Flood Tidal Deltaic Island in the River Murray Estuary, South Australia: A Canary in the Cage of River Management. Journal of Coastal Research, 1103-1119.

Job, T., Penny, D., & Hua, Q. (2018). Metal enrichment in estuarine sediments proximal to acid sulfate soils as a novel palaeodrought proxy. Science of the Total Environment, 612, 247-256.

Kaufman, L., & Rousseeuw, P. J. (2009). Finding Groups in Data: An introduction to cluster analysis. Hoboken, New Jersey: John Wiley & Sons, Inc.

Kemp, J., Radke, L. C., Olley, J., Juggins, S., & De Deckker, P. (2012). Holocene lake salinity changes in the Wimmera, southeastern Australia, provide evidence for millennial-scale climate variability. Quaternary Research, 77(1), 65-76.

Kermode, S. J., Gibling, M. R., Jones, B. G., Cohen, T. J., Price, D. M., & Daley, J. S. (2013). Determining the impact of the Holocene highstand at the coastal-fluvial interface, Shoalhaven River, south-eastern Australia. Earth Surface Processes and Landforms, 38(13), 1481-1495.

Kiem, A. S. (2013). Drought and water policy in Australia: Challenges for the future illustrated by the issues associated with water trading and climate change adaptation in the Murray–Darling Basin. Global Environmental Change, 23(6), 1615-1626.

Kiem, A. S., Franks, S. W., & Kuczera, G. (2003). Multi-decadal variability of flood risk. Geophysical Research Letters, 30(2).

Kingsford, R. T., Walker, K. F., Lester, R. E., Young, W. J., Fairweather, P. G., Sammut, J., & Geddes, M. C. (2011). A Ramsar wetland in crisis – the Coorong, Lower Lakes and Murray Mouth, Australia. Marine and Freshwater Research, 62(3), 255-265.

Kirby, J. M., Connor, J., Ahmad, M. D., Gao, L., & Mainuddin, M. (2014). Climate change and environmental water reallocation in the Murray–Darling Basin: Impacts on flows, diversions and economic returns to irrigation. Journal of Hydrology, 518, 120-129.

Knox, J. C. (1993). Large increases in flood magnitude in response to modest changes in climate. Nature, 361(6411), 430-432.

Kyungsik, C., & Ju Hyong, K. (2006). Identifying late Quaternary coastal deposits in Kyonggi Bay, Korea, by their geotechnical properties. Geo-Marine Letters, 26(2), 77-89.

Ladson, A., Lang, S., Anderson, B., & Rutherfurd, I. D. (2003). An Australian Handbook of Stream Roughness Coefficients. Paper presented at the 28th Hydrology and Water Resources Symposium, Wollongong.

Lafuerza, S., Canals, M., Casamor, J. L., & Devincenzi, J. M. (2005). Characterization of deltaic sediment bodies based on in situ CPT/CPTU profiles: A case study on the Llobregat delta plain, Barcelona, Spain. Marine Geology, 222-223, 497-510.

Lanier, W. P., Feldman, H. R., & Archer, A. W. (1993). Tidal sedimentation from a fluvial to estuarine transition, Douglas Group, Missourian-Virgilian, Kansas. Journal of Sedimentary Research, 63(5), 860-873.

Leblanc, M., Tweed, S., Van Dijk, A., & Timbal, B. (2012). A review of historic and future hydrological changes in the Murray-Darling Basin. Global and Planetary Change, 80–81, 226-246.

Lewis, S. E., Sloss, C. R., Murray-Wallace, C. V., Woodroffe, C. D., & Smithers, S. G. (2013). Post-glacial sea-level changes around the Australian margin: a review. Quaternary Science Reviews, 74, 115-138.

Luebbers, R. A. (1981). The Coorong Report: An archaeological survey of the Southern Younghusband Peninsula. Prepared for the Southern Australian Department for the Environment and Planning.

Luebbers, R. A. (1982). The Coorong Report: An archaeological survey of the Northern Coorong. Prepared for the South Australian Department for Environment and Planning.

Mackay, N., & Eastburn, D. (Eds.). (1990). The Murray. Canberra, Australia: Murray-Darling Basin Commission.

Marx, S. K., Kamber, B. S., McGowan, H. A., & Denholm, J. (2011). Holocene dust deposition rates in Australia's Murray-Darling Basin record the interplay between aridity and the position of the mid-latitude westerlies. Quaternary Science Reviews, 30(23–24), 3290-3305.

Marx, S. K., McGowan, H. A., & Kamber, B. S. (2009). Long-range dust transport from eastern Australia: A proxy for Holocene aridity and ENSO-type climate variability. Earth and Planetary Science Letters, 282(1–4), 167-177.

Mattheus, C. R., & Rodriguez, A. B. (2011). Controls on late Quaternary incised-valley dimension along passive margins evaluated using empirical data. Sedimentology, 58(5), 1113-1137.

Mayewski, P. A., Rohling, E. E., Curt Stager, J., Karlén, W., Maasch, K. A., Meeker, L. D., Steig, E. J. (2004). Holocene climate variability. Quaternary Research, 62(3), 243-255.

McGowan, H., Marx, S., Denholm, J., Soderholm, J., & Kamber, B. (2009). Reconstructing annual inflows to the headwater catchments of the Murray River, Australia, using the Pacific Decadal Oscillation. Geophysical Research Letters, 36(6).

McIntosh, M. (1949). The River Murray Barrages. Journal of Agriculture, 425-429.

Meade, R. H. (1982). Sources, Sinks, and Storage of River Sediment in the Atlantic Drainage of the United States. The Journal of Geology, 90(3), 235-252.

Mills, K., Gell, P., Hesse, P. P., Jones, R., Kershaw, P., Drysdale, R., & McDonald, J. (2013a). Paleoclimate studies and natural-resource management in the Murray-Darling Basin I: past, present and future climates. Australian Journal of Earth Sciences, 60(5), 547-560.

Munk, W. H., & Anderson, E. R. (1948). Notes on a theory of the thermocline. Journal of Marine Research, 7, 276-295.

Murray-Wallace, C. V., Bourman, R. P., Prescott, J. R., Williams, F., Price, D. M., & Belperio, A. P. (2010). Aminostratigraphy and thermoluminescence dating of coastal aeolianites and the later Quaternary history of a failed delta: The River Murray mouth region, South Australia. Quaternary Geochronology, 5(1), 28-49.

Nanson, G. C., Cohen, T. J., Doyle, J., & Price, D. M. (2003). Alluvial evidence of Late-Quaternary climate and flow-regime changes on the coastal rivers of New South Wales, Australia. In K. J. Gregory & G. Benito (Eds.), Palaeohydrology: Understanding Global Change (pp. 233-258). Chichester: Wiley.

Nichol, S. L., Boyd, R., & Penland, S. (1994). Stratigraphic Response of Wave-Dominated Estuaries to Different Relative Sea-Level and Sediment Supply Histories: Quaternary Case Studies from Nova Scotia, Louisiana and Eastern Australia. In R. W. Dalrymple, R. Boyd, & B. A. Zaitlin (Eds.), Incised-Valley Systems: Origin and Sedimentary Sequences: SEPM Society for Sedimentary Geology.

Nichol, S. L., Zaitlin, B. A., & Thom, B. G. (1997). The upper Hawkesbury River, New South Wales, Australia: a Holocene example of an estuarine bayhead delta. Sedimentology, 44(2), 263-286.

Petherick, L., Bostock, H., Cohen, T. J., Fitzsimmons, K., Tibby, J., Fletcher, M. S., Dosseto, A. (2013). Climatic records over the past 30 ka from temperate Australia – a synthesis from the Oz-INTIMATE workgroup. Quaternary Science Reviews, 74, 58-77.

Phillips, J. D., & Slattery, M. C. (2006). Sediment storage, sea level, and sediment delivery to the ocean by coastal plain rivers. Progress in Physical Geography, 30(4), 513-530.

Pittock, J., & Finlayson, C. M. (2011). Australia's Murray–Darling Basin: freshwater ecosystem conservation options in an era of climate change. Marine and Freshwater Research, 62(3), 232-243.

Pittock, J., Finlayson, C. M., Gardner, A., & McKay, C. (2010). Changing character: the Ramsar Convention on wetlands and climate change in the Murray-Darling Basin, Australia. Environmental and Planning Law Journal, 27, 401-425.

Posamentier, H. W., Jervey, M. T., & Vail, P. R. (1988). Eustatic Controls on Clastic Deposition I - Conceptual Framework. In C. K. Wilgus, B. S. Hastings, C. G. S. C. Kendall, H. W. Posamentier, C. A. Ross, & J. C. Van Wagoner (Eds.), Sea-level changes: an integrated approach (Vol. Sepcial Publication No. 42). Oklahoma, USA: Society of Economic Paleontologists and Mineralogists.

Reineck, H.-E., & Singh, I. B. (1980). Depositional sedimentary environments: with reference to terrigenous clastics (Second ed.). Berlin: Springer-Verlag.

Reisinger, A., Kitching, R. L., Chiew, F., Hughes, L., Newton, P. C. D., Schuster, S. S., Whetton, P. (2014). 2014: Australasia. In V. R. Barros, C. B. Field, D. J. Dokken, M. D. Mastrandrea, K. J. Mach, T. E. Bilir, M. Chatterjee, K. L. Ebi, Y. O. Estrada, R. C. Genova, B. Girma, E. S. Kissel, A. N. Levy, S. MacCracken, P. R. Mastrandrea, & L. L. White (Eds.), Climate Change 2014: Impacts, Adaptation, and Vulnerability. Part B: Regional Aspects. Contribution of Working Group II to the Fifth Assessment Report of the Intergovernmental Panel on Climate Change (pp. 1371-1438). Cambridge, United Kingdom and New York, NY, USA: Cambridge University Press.

Robertson, P. K. (2010). Soil behaviour type from the CPT: an update. 2nd International Symposium on Cone Penetration Testing, Huntington Beach, CA, USA. Volume 2&3: Technical Papers, Session 2: Interpretation, Paper No. 56.

Rodriguez, A. B., Simms, A. R., & Anderson, J. B. (2010). Bay-head deltas across the northern Gulf of Mexico back step in response to the 8.2 ka cooling event. Quaternary Science Reviews, 29(27–28), 3983-3993.

Rogelj, J., den Elzen, M., Hohne, N., Fransen, T., Fekete, H., Winkler, H., Meinshausen, M. (2016). Paris Agreement climate proposals need a boost to keep warming well below 2 degrees C. Nature, 534, 631.

Rogers, K., & Woodroffe, C. D. (2016). Geomorphology as an indicator of the biophysical vulnerability of estuaries to coastal and flood hazards in a changing climate. Journal of Coastal Conservation, 20(2), 127-144.

Roy, P. S. (1984). Holocene sedimentation histories of estuaries in southeastern Australia. Paper presented at the Estuarine Environments of the Southern Hemisphere: Papers presented at a symposium, Man's Impact on the Estuarine Environment held at the 53rd Congress of the Australian and New Zealand Association for the Advancement of Science in conjunction with the Australian Marine Sciences Association, Perth.

Roy, P. S., Thom, B. G., & Wright, L. D. (1980). Holocene sequences on an embayed high-energy coast: an evolutionary model. Sedimentary Geology, 26(1), 1-19.

Roy, P. S., Williams, R. J., Jones, A. R., Yassini, I., Gibbs, P. J., Coates, B., Nichol, S. (2001). Structure and Function of South-east Australian Estuaries. Estuarine, Coastal and Shelf Science, 53(3), 351-384.

Rustomji, P., Olley, J., & Chappell, J. (2006). Holocene valley aggradation driven by river mouth progradation: examples from Australia. Earth Surface Processes and Landforms, 31(12), 1510-1524.

South Australian Resources Information Gateway (SARIG). (2019). Department of State Development, the Government of South Australia. Drillholes: All mineral drillholes. Https://map.sarig.sa.gov

Schieber, J., Southard, J., & Thaisen, K. (2007). Accretion of Mudstone Beds from Migrating Floccule Ripples. Science, 318(5857), 1760-1763.

Schieber, J., & Yawar, Z. (2009). A new twist on mud deposition - mud ripples in experiment and rock record. The Sedimentary Record, 7(2), 4-8.

Simms, A. R., & Rodriguez, A. B. (2014). Where do coastlines stabilize following rapid retreat? Geophysical Research Letters, 41(5), 1698–1703.

Sloss, C. R., Jones, B. G., McClennen, C. E., De Carli, J., & Price, D. M. (2006b). Mid- to late Holocene sedimentation in a coastal lagoon: Burrill Lake, NSW, Australia. Journal of Sedimentary Geology, 187, 229-249.

Sloss, C. R., Jones, B. G., McClennen, C. E., de Carli, J., & Price, D. M. (2006c). The geomorphological evolution of a wave-dominated barrier estuary: Burrill Lake, New South Wales, Australia. Sedimentary Geology, 187(3–4), 229-249.

Sloss, C. R., Jones, B. G., Switzer, A. D., Nichol, S., Clement, A. J. H., & Nicholas, A. W. (2010). The Holocene infill of Lake Conjola, a narrow incised valley system on the southeast coast of Australia. Quaternary International, 221(1–2), 23-35.

Sloss, C. R., Murray-Wallace, C. V., & Jones, B. G. (2006a). Aminostratigraphy of Two Holocene Wave-Dominated Barrier Estuaries in Southeastern Australia. Journal of Coastal Research, 113-136.

Sloss, C. R., Murray-Wallace, C. V., & Jones, B. G. (2007). Holocene sea-level change on the southeast coast of Australia: a review. The Holocene, 17(7), 999-1014.

Stephenson, A. E., & Brown, C. M. (1989). The Ancient Murray River System. BMR Journal of Australian Geology & Geophysics, 11, 387-395.

Stone, T. (2006). The late-Holocene origin of the modern Murray River course, southeastern Australia. The Holocene, 16(5), 771-778.

Stuiver, M., & Reimer, P. J. (1993). Extended 14C data base and revised CALIB 3.0 14C age calibration program. Radiocarbon, 35(1), 215-230.

Styllas, M. (2014). A simple approach to define Holocene sequence stratigraphy using borehole and cone penetration test data. Sedimentology, 61(2), 444-460.

Sutherland, B., Barrett, K., & Gingras, M. (2015). Clay settling in fresh and salt water. Environmental Fluid Mechanics, 15(1), 147-160.

Sweet, W. V., Kopp, R. E., Weaver, C. P., Obeysekera, J., Horton, R. M., Thieler, E. R., & Zervas, C. (2017). Global and regional sea level rise scenarios for the United States. NOAA Technical Report NOS CO-OPS 083. Silver Spring, Maryland.

Taylor, J. K., & Poole, H. G. (1931). A soil survey of the swamps of the lower Murray River. Melbourne: C.S.I.R.

Thom, B. G., & Roy, P. S. (1985). Relative sea-levels and coastal sedimentation in southeast Australia in the Holocene. Journal of Sedimentary Petrology, 55, 257-264.

Tooley, M. J. (1978). Sea-level Changes: Northwest England during the Flandrian stage: Oxford: Clarendon Press.

Twidale, C. R., Lindsay, J. M., & Bourne, J. A. (1978). Age and Origin of the Murray River and Gorge in South Australia. Paper presented at the Proceedings of Royal Society of Victoria, Melbourne, Australia.

Umitsu, M., Buman, M., Kawase, K., & Woodroffe, C. D. (2001). Holocene palaeoecology and formation of the Shoalhaven River deltaic-estuarine plains, southeast Australia. The Holocene, 11(4), 407-418.

Von der Borch, C., & Altmann, M. (1979). Holocene stratigraphy and evolution of the Cooke Plains Embayment, a former extension of Lake Alexandrina, South Australia. Transactions of the Royal Society of South Australia, 103(3), 69-78.

Walker, B. (2019). South Australia, Murray-Darling Basin Royal Commission, Report.

Walker, D. J., & Jessup, A. (1992). Analysis of the Dynamic Aspects of the River Murray Mouth, South Australia. Journal of Coastal Research, 8(1), 71-76.

Walker, K. (2006). Serial weirs, cumulative effects: the Lower River Murray, Australia. In Kingsford, R.T. (Ed.) The Ecology of Desert Rivers, Cambridge University Press (pp. 248-279).

Woodroffe, C. D., & Murray-Wallace, C. V. (2012). Sea-level rise and coastal change: the past as a guide to the future. Quaternary Science Reviews, 54, 4-11.

Zaitlin, B. A., Dalrymple, R. W., & Boyd, R. (1994). The stratigraphic organization of incised-valley systems associated with relative sea-level change. In R. W. Dalrymple, R. Boyd, & B. A. Zaitlin (Eds.), Incised-Valley Systems: Origin and Sedimentary Sequences (Vol. Special Publication No. 51, pp. 45-60). Tulsa, Oklahoma, U.S.A.: SEPM (Society for Sedimentary Geology).

Zaleha, M. J. (1997b). Fluvial and lacustrine palaeoenvironments of the Miocene Siwalik Group, Khaur area, northern Pakistan. Sedimentology, 44(2), 349-368.

Appendix A

SCIENTIFIC REP⬡RTS

OPEN

Modelling Holocene analogues of coastal plain estuaries reveals the magnitude of sea-level threat

Anna M. Helfensdorfer[1,2], Hannah E. Power [2] & Thomas C. T. Hubble [1]

Hydrodynamic modelling of Australia's lower Murray River demonstrates the response of a large coastal plain estuary to the mid-Holocene (7,000–6,000 yr BP) sea-level highstand. The approximately two metre higher-than-present sea level during the highstand forced the estuarine limit upstream generating an extensive central basin environment extending more than 200 kilometres from the river mouth (143 kilometres upstream of the modern tidal limit). The geomorphic history of the region does not conform to conventional estuarine facies models as, for much of the Holocene, the lower Murray River acted as a landward, gorge-confined extension of the Murray estuary. The incredibly low relief of this coastal plain system drove significant saline incursion and limited current velocities across the estuary facilitating deposition of a laminated silt-clay sequence which our results suggest may be regionally extensive. Variations to discharge, barrier morphology, or the estuary's bathymetry result in minimal change to the estuarine palaeo-environment. The shift to the present-day fresher water distribution in the Murray estuary requires a fall in sea level to present-day conditions. The dominance of sea level as the controlling factor on this estuarine palaeo-environment highlights the significant potential impact of climate change induced sea-level rise to coastal plain estuaries.

Coastal plains and lowlands are characterised by their low gradient and commonly dense populations, with geomorphic-based risk assessments revealing their significant vulnerability to future climatic change[1]. Inundation associated with an increase in mean sea level threatens communities, coastal infrastructure and ecosystems, with estuaries vulnerable to the compounding influences of storm surges and strong winds, along with implications of saline incursion for irrigation and drinking water supply[2]. Indeed, in Australia, flooding is considered the most significant medium-term climate change hazard, with a shift to coastal inundation beyond mid-century[2,3]. There is, however, less emphasis on the consequences of rising sea levels for saline intrusion, particularly for low-gradient coastal plain estuaries.

The Intergovernmental Panel on Climate Change (IPCC) projects that global mean sea level will rise by 0.53–0.97 m by 2100 under a high emissions scenario, with these projections likely to be exceeded by at least 10% in Australia[2]. Crucially, even given a stabilisation in temperatures, global mean sea level will continue to rise for several centuries beyond 2100[2]. Understanding the dominant drivers of environmental change within an estuarine system allows for effective management given uncertainties in future mean sea level, and determining palaeo-environmental responses to the Holocene highstand provides a useful analogue of expected change. There is a pressing need for palaeo-environmental analysis in economically significant regions to direct future natural resource management policies, particularly in intensively managed environmental systems. Developing appropriate management strategies that negate the detrimental impacts forecast in climate change projections is particularly important for lowland coastal plains where rising sea levels will undoubtedly cause problematic inundation and saline intrusion. Applying Holocene analogues to future sea-level rise scenarios is a well-recognised approach to predicting responses of coastal systems to climate change[4,5]. Here, we use the lower Murray River (LMR) and Murray estuary as a case study to demonstrate the utility of understanding Holocene analogues to plan for potential environmental change in coastal plain estuaries.

Understanding fluvial and estuarine responses to sea-level cycles through their associated depositional systems tracts may assist in predicting potential impacts of future sea-level rise. Research has shown that fluvial systems attempt to keep pace with changing base level, with shoreline advance or retreat controlling available

[1]School of Geosciences, The University of Sydney, Sydney, NSW, 2006, Australia. [2]School of Environmental and Life Sciences, The University of Newcastle, Callaghan, NSW, 2308, Australia. Correspondence and requests for materials should be addressed to A.M.H. (email: anna.helfensdorfer@sydney.edu.au)

and Younghusband Peninsulas, began formation at approximately 8,000 yr BP, allowing for the development of the central basin lakes, Alexandrina and Albert, prior to the Holocene highstand at 7,000–6,000 yr BP[16–21] (Fig. 1).

Upstream, the LMR is entrenched within the Murray Gorge (from Overland Corner to Wellington, Fig. 1), with the valley fill only comprising sediment of the most recent cycle of lowstand, transgression and highstand[5,22]. This consists of two distinct facies: (1) the Monoman Formation's coarse-grained sands comprise the lower valley fill, and (2) the Coonambidgal Formation's fine-grained clays and silts comprising the upper valley fill. The Holocene infill of Lake Alexandrina is known as the St Kilda Formation, and is a finely laminated silt-clay sequence[23,24]. Deposition of this sequence had commenced by at least 8,000 yr BP[23,24]; however, it is probable that deposition within the palaeo-channel that transited through modern-day Lake Alexandrina had commenced prior to 8,000 yr BP as dated cores within this area bottom out on laminated mud[23,24]. The St Kilda Formation was regionally extensive from 5,500 yr BP and has characterised the sediments of Lake Alexandrina since[23,24].

Standing water or very weak current velocities are required for the deposition and preservation of a laminated silt-clay sequence[25]. However, recent flume studies have demonstrated mud floc deposition as distinct laminae in current velocities up to 0.3 m/s, with laminae accumulation considered possible at higher velocities given particularly high sediment concentrations[26,27]. Laminations, such as those present throughout Lake Alexandrina, are undoubtedly a product of low energies and high sedimentation rates[28], features characteristic of central basin environments[29]. Indeed, wave-dominated estuaries are known for their well-defined tripartite zonation of facies assemblages with lithofacies typically presenting a coarse-fine-coarse sequence: the marine sands of the barrier complex and flood-tide delta, the clays and silts of the central basin, and the fluvial sands of the bayhead delta and river channel[30]. Conventional presentations of estuarine models indicate that the point where the river debouches into the lagoon locates the transition to reduced energy and defines the landward extent of the central basin and seaward extent of the bayhead delta. However, the contentious Holocene palaeo-salinities of the Lower Lakes give rise to debate on the extent and character of the Murray estuary. Some place the upstream extent of this estuary at the Pomanda Embayment, where the LMR debouches into Lake Alexandrina[16] (river kilometre (rkm) 73, Fig. 1), with other authors even suggesting that the Lower Lakes were freshwater stilling basins for the duration of the Holocene and cannot be classified as part of this estuarine zone[17].

In this paper, we evaluate the range of possible responses of the palaeo-Murray estuary to the Holocene sea-level highstand. Specifically, we:

a) Conduct hydrodynamic modelling of the palaeo-Murray estuary and LMR with sensitivity testing for discharge, bathymetric surface and barrier morphology with results analysed for inundation extents, water levels and depths, flow velocity and salinity.
b) Assess the palaeo-environment that likely prevailed during the Holocene highstand and correlate model scenarios with geomorphic and sedimentary features of the region to develop a model of estuarine process-es zonation and inferred resulting morphology.
c) Assess the relative influence of geomorphic and hydrodynamic drivers on the estuary during the Holocene sea-level highstand.
d) Propose the palaeo-Murray estuary, as a possible end-member exemplar of an extremely low-gradient coastal plain estuary, to demonstrate the significant threat of sea-level rise due to climate change on the environmental character of coastal plain estuaries. Particular reference is given to the understated potential impact of climate change-induced saline intrusion on the character and extent of coastal plain estuaries.

Results

Here, we model the inundation extents, water depths, flow velocities and salinities for the full extent of the LMR and Murray estuary as a function of four key morphologic and hydrodynamic forcings: (1) bathymetric surface (two end members and a best estimate), (2) sea level (Holocene highstand and present-day), (3) discharge (drought, pre-regulation average, and flood), and (4) barrier morphology (four scenarios, ranging from completely open to almost closed, to account for barrier evolution). Results are grouped into six categories based on bathymetric surface and sea level: $S_{low}WL_2$, $S_{low}WL_0$, $S_{mid}WL_2$, $S_{mid}WL_0$, $S_{up}WL_2$ and $S_{up}WL_0$ (see *Methodology - Overview of model result categories* and Table S1 for further information).

Model correlation with regional geomorphology and sedimentology. Given the experimental nature of modelling snapshots in geological time, constraining inundation extent to geological features gives an indication of the plausibility of model results. The lacustrine and estuarine clays of the Malcolm soil combination (Fig. 2a; Table S2) represent the extent of Lake Alexandrina during the Holocene[31]. This formation, and recognised Holocene palaeo-shorelines[31], are mapped against inundation extent in Fig. 2. The Malcolm soil combination is well constrained by the $S_{low}WL_2$ scenarios (Fig. 2d; Table S1), with the $S_{mid}WL_2$ scenarios proving a reasonable match overall (Fig. 2c; Table S1). The $S_{low}WL_2$ scenarios align precisely with the most expansive of the palaeo-shorelines which is consistent with the greatest Holocene extent of Lake Alexandrina[31] (Fig. 2d; Table S1). The S_{mid} scenarios sit at, or beyond, the middle palaeo-shoreline, considered to represent a short stabilisation period during retreat, likely in response to falling sea levels[31] (Fig. 2c; Table S1). The $S_{up}WL_2$ scenarios align with the middle palaeo-shoreline, while the $S_{up}WL_0$ scenarios generate inundation akin to present-day[31] (Fig. 2b; Table S1).

The inundation extent of the 1956 flood, the greatest flood on instrumental record, is also depicted in Fig. 2. This extent is not as expansive as the Malcolm soil combination within the Lower Lakes region, suggesting that water levels at the Holocene highstand were well above maximum historical records. Bank overtopping from fluvial floodwaters during the 1956 flood caused valley-wide inundation within the Murray Gorge which gives insight into the plausible response to the Holocene highstand as the LMR is backfilled. All S_{low} scenarios correlate
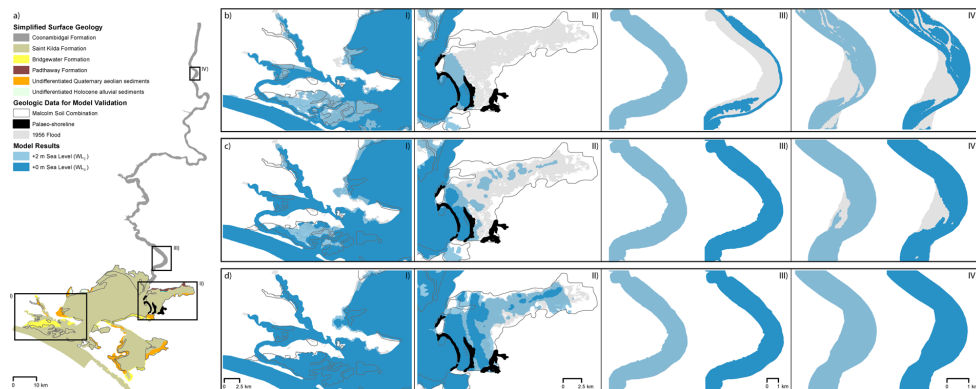
Figure 2. Geologic overview of the study area and maps showing maximum inundation extent under average discharge and modern-day barrier conditions ($D_{av}B_{mod}$ scenarios). (**a**) Simplified surface geology showing Holocene and Pleistocene stratigraphic formations. Inundation extents are shown for (**b**) S_{up}, (**c**) S_{mid} and (**d**) S_{low} scenarios at $+2$ m sea level (WL_2; light blue) and $+0$ m sea level (WL_0; dark blue). Panels I and II encompass sub-sections of Lake Alexandrina detailing the flood tide delta and Murray Mouth, and the Cooke Plains Embayment respectively. Panel III details a 10 rkm representative sub-region of the lower portion of the LMR (centered on Tailem Bend, rkm 91). Panel IV details a 10 rkm representative sub-region of the upper portion of the LMR (centered on Swan Reach, rkm 255). The inundation extent of the 1956 flood (grey) is given as an indicative regional modern-day analogue of the plausible extent of inundation caused by backfilling during the Holocene highstand. The Malcolm soil combination (dark grey outline) represents the maximum Holocene inundation extent of the Lower Lakes (Lakes Alexandrina and Albert; I and II)[31]. Palaeo-shorelines (black) allude to the maximum Holocene extent of Lake Alexandrina and a period of stability following retreat to the present-day shoreline (II)[31]. Maximum inundation extents remain comparable in other model scenarios not depicted here, with non-significant fluctuations in inundation across the Lower Lakes (I and II), with the exception of a significant flood event (D_+ scenarios) which induces valley-wide inundation throughout the LMR (III and IV), consistent with 1956 flood extents.

with the 1956 flood extent and are characterised by valley-wide inundation throughout the Murray Gorge (Fig. 2d III-IV; Table S1). The $S_{mid}WL_2$ scenarios inundate the entire valley, with the exception of two small areas at Big Bend (rkm235) and Swan Reach (rkm255; Fig. 2c III-IV; Table S1). Inundation of these two locations is reduced in the $S_{mid}WL_0$ scenarios along with isolated small dry areas, however, these models remain characterised by valley-wide inundation (Fig. 2c III-IV; Table S1). Conversely, even given Holocene highstand sea levels, the S_{up} scenarios are charactered by a channel with fringing swamps upstream of Mypolonga (rkm 130), as was evident prior to levee construction and land reclamation in the 19th century[32]. A significant flood (D_+ scenarios) is required to induce valley-wide inundation (Fig. 2b III-IV; Table S1). Our results suggest that the period of sea-level fall from highstand in the late-Holocene saw a significant shift in the geomorphic character of the LMR (Fig. 2c III-IV vs. 2b III-IV). Overall, model results are well correlated to regional geomorphology and sedimentology, and are consistent with research into the sedimentary infill and geomorphological evolution of barrier estuaries identified on the east coast of Australia (e.g[7,8,33].), therefore, the model is deemed sensible and valid as a basis for further exploratory analysis.

Palaeo-environment at the Holocene highstand. Our results show that the palaeo-environment at the Holocene highstand was likely to have been estuarine throughout the Lower Lakes and well upstream into the LMR (Figs 3a I–III, 4a and S1a–c). All WL_2 scenarios result in an estuarine environment with significant marine incursion in the Lower Lakes, meanwhile all WL_0 scenarios result in a brackish environment within the Lower Lakes, with fluvial discharge supressing significant marine incursion to the barrier and flood tide delta complex (Figs 3a, 4a and S1). This trend is apparent across all scenarios irrespective of discharge, barrier morphology and bathymetric surface (Figs 3, 4a and S1), with a shift to fresher water dependent upon a fall in sea level to present-day conditions (Figs 3a, 4a and S1). Holocene highstand sea levels also induce valley-wide inundation under S_{up} morphology, with the S_{mid} and S_{low} morphologies resulting in a significant increase in the areal extent of the Lower Lakes (Fig. 2). These results demonstrate that sea level is the driving factor controlling the environmental character of the Lower Lakes and LMR. This is apparent through the difference in maximum palaeo-salinities observed with a change in sea level (Figs 3a, 4a and S1) when compared with the near-identical results produced by sensitivity testing for discharge (Figs 3b and 4a), barrier morphology (Figs 3c and 4a) or bathymetric surface (Figs 3a and 4a).

Estuarine processes zonation and inferred resulting morphology. Flow velocity vectors are used to define the upstream extent of the backwater zone for each scenario (Figs 4b and S2). The maximum upstream
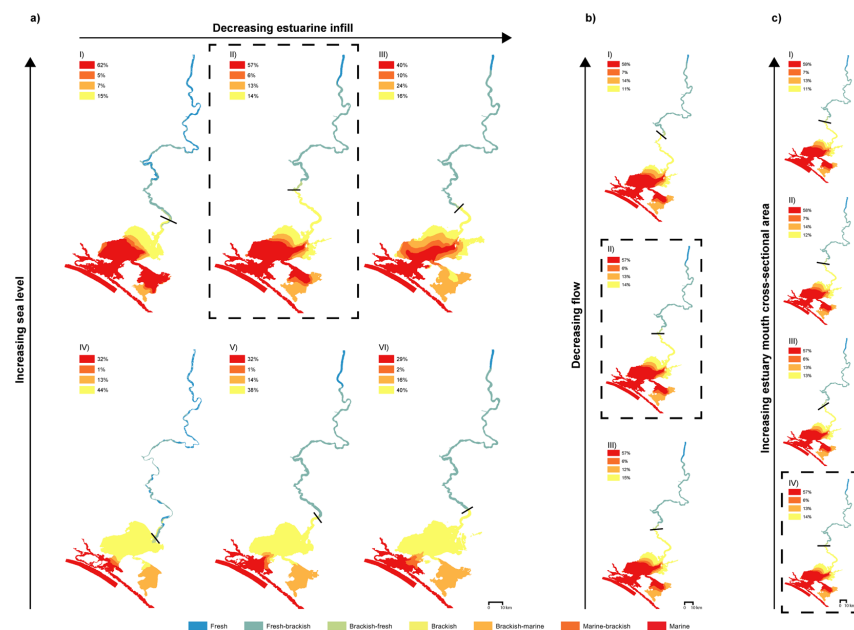
Figure 3. Key representative maps comparing maximum salinity reached relative to sea level, bathymetric surface, discharge and barrier morphology. (**a**) An increase in sea level from WL_0 present-day conditions (IV–VI) to WL_2 Holocene highstand conditions (I–III) significantly increases marine incursion, extending to the upper reaches of Lake Alexandrina and pushing the brackish limit further up the Murray Gorge. There is negligible change to the overall palaeo-environmental character of the region between end-member and best-estimate Holocene bathymetries (I–III or IV–VI). (**b**) Variance in flow from drought (D_-) to flood (D_+) scenarios (I–III) is unable to alter the palaeo-environmental character of the region. (**c**) Variance in barrier morphology from completely open (B_0) to modern-day (B_{mod}) outlet scenarios (I–IV) is also unable to alter the palaeo-environmental character of the region. The isohaline (black line) delimits the brackish limit (equivalent to 1 psu) with the percentage area of each salinity class seaward of the isohaline given relative to total inundated area. The hatched box highlights the common scenario between the three panels: scenario $S_{mid}WL_2D_{av}B_{mod}$. Within (**a**) all maps shown are pre-regulation average discharge with modern-day barrier morphology scenarios (I: scenario $S_{up}WL_2D_{av}B_{mod}$; II: scenario $S_{mid}WL_2D_{av}B_{mod}$; III: scenario $S_{low}WL_2D_{av}B_{mod}$; IV: scenario $S_{up}WL_0D_{av}B_{mod}$; V: scenario $S_{mid}WL_0D_{av}B_{mod}$ and VI: scenario $S_{low}WL_0D_{av}B_{mod}$; Table S1). To demonstrate representative salinities at the Holocene highstand, $S_{mid}WL_2$ scenarios are shown within (**b**) (I: scenario $S_{mid}WL_2D_-B_{mod}$; II: scenario $S_{mid}WL_2D_{av}B_{mod}$; III: scenario $S_{mid}WL_2D_+B_{mod}$) and (**c**) (I: scenario $S_{mid}WL_2D_{av}B_0$; II: scenario $S_{mid}WL_2D_{av}B_+$; III: scenario $S_{mid}WL_2D_{av}B_{++}$; IV: scenario $S_{mid}WL_2D_{av}B_{mod}$). Salinity is measured based on the classification scheme of Tooley[51].

extent in S_{low} scenarios is Blanchetown (rkm 275), regardless of sea level, such that the $S_{low}WL_0$ scenarios present significantly different backwater zones when compared to other WL_0 scenarios (Figs 4b and S2; Table S1). Given that the bathymetry of the S_{low} scenarios is almost certainly not representative of the mid- to late-Holocene when sea levels had receded to present-day, the backwater zone during this period is best constrained by the $S_{mid}WL_0$ and $S_{up}WL_0$ scenarios, confining the backwater zone to the region downstream of Tailem Bend (rkm 91; Figs 4b and S2; Table S1). Under all bathymetric conditions, the backwater zone extended well into the LMR supporting the hypothesis that Lake Alexandrina and the LMR were subject to a single depositional environment that produced a regionally extensive central basin depositional sequence at the Holocene highstand (Figs 4b and S2). We suggest that, prior to anthropogenic modifications of the flow regime, this central basin sequence was continuing to accumulate within the entirety of Lake Alexandrina; top-of-core modern dates across the regionally extensive laminated sequence support this hypothesis[23].

The possibility of deposition and preservation of a laminated sequence is limited to regions where the maximum flow velocity magnitude is <0.3 m/s[25–27] (see grey shaded areas in Figs 5 and S3), which encompasses a minimum of 82% of the model domain. Suitable conditions for the deposition of a laminated sequence throughout Lake Alexandrina apply in all scenarios (Figs 5 and S23) and explain the regionally extensive presence of this laminated central basin deposit that has characterised Lake Alexandrina's Holocene stratigraphy since 5,500 yr BP[23]. Variation in barrier morphology (Fig. 5a–c or d–f) or LMR/Lower Lakes bathymetry (Fig. 5a,d or b,e or c,f) makes a negligible difference in the regional capacity to generate a laminated central basin deposit (maximum 7% and 3% change respectively).
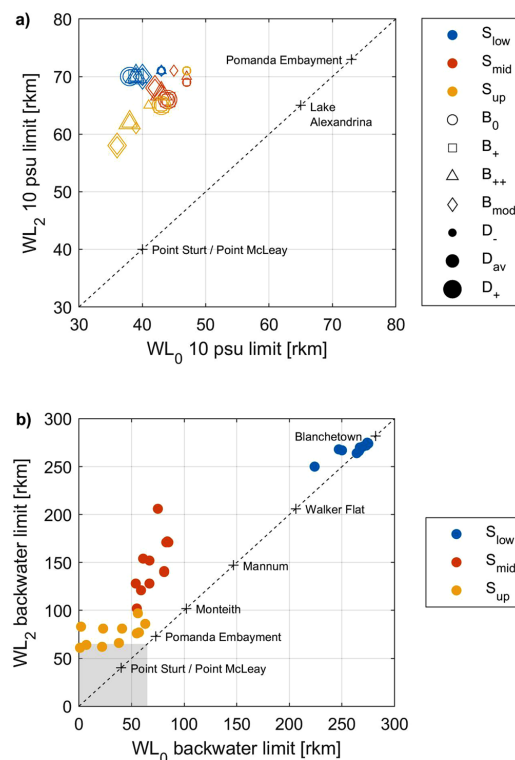
Figure 4. Comparison of 10 psu (marine-brackish) and backwater zone limits for all WL_0 and WL_2 paired scenarios. (**a**) An increase in sea level from WL_0 to WL_2 Holocene highstand conditions drives the 10 psu (marine-brackish) limit from the flood tide delta and lower reaches of Lake Alexandrina upstream such that marine or marine-brackish waters occupy the entire body of the lake. This trend is apparent irrespective of bathymetric surface (marker colours), barrier morphology (marker shapes) or discharge (marker sizes) demonstrating that sea level is the primary driver of palaeo-environmental change within this system. (**b**) Velocity vector convergence, taken as the point of convergence of upstream and downstream velocity vectors within the channel thalweg, defines the upstream extent of the backwater zone. Given S_{up} conditions (yellow), the backwater zone is restricted to the main body of Lake Alexandrina (grey shading) and the Pomanda Embayment within WL_0 scenarios, with the higher sea level in WL_2 scenarios driving this limit upstream into the lower reaches of the Murray Gorge. The influence of sea level on the backwater limit is equally apparent given S_{mid} conditions (red), where at the Holocene highstand, an enlarged low energy backwater setting was emplaced up to Walker Flat (rkm 206). By comparison, the S_{low} surface (blue) forces the backwater zone to occupy nearly the entire model domain irrespective of sea level.

Overall, the $S_{low}WL_2$ and $S_{mid}WL_2$ scenarios are well constrained by the Malcolm soil combination, and palaeo-shorelines, representing the maximum Holocene inundation extent of the Lower Lakes[31] which suggests the suitability of interpolating these results to the palaeo-environment at the Holocene highstand (Fig. 2; Table S1). These results show that the Holocene highstand probably generated valley-wide inundation within the entirety of the Murray Gorge at least as far upstream as Blanchetown (rkm 282; Fig. 2), which coincides with the minimum propagation of the tidal limit of the Murray estuary (Fig. 6). Given this single central basin depositional environment, we infer the presence of a laminated sequence within the valley-wide LMR perhaps extending as far upstream as Walker Flat (rkm 206; Fig. 6), a hypothesis that will be tested by a complementary sedimentary analysis in a subsequent study. During the late-Holocene, we suggest that the bayhead delta prograded downstream to Mypolonga (rkm 130), where there is a notable shift in the geomorphic character of the levees and fringing swamps, before anthropogenic modification inhibited further natural estuarine evolution from 1900 onwards[32].

Sensitivity testing. Examples of the influence of bathymetric surface on maximum palaeo-salinities are shown in Figs 3 and 4a and on inundation extent in Fig. 2. The LMR is characterised by a main channel with fringing swamps under S_{up} scenarios, while the S_{mid} and S_{low} scenarios exhibit valley-wide inundation (Fig. 2; Table S1). Within the Lower Lakes, the modelled inundation extent is comparable to present-day shorelines under
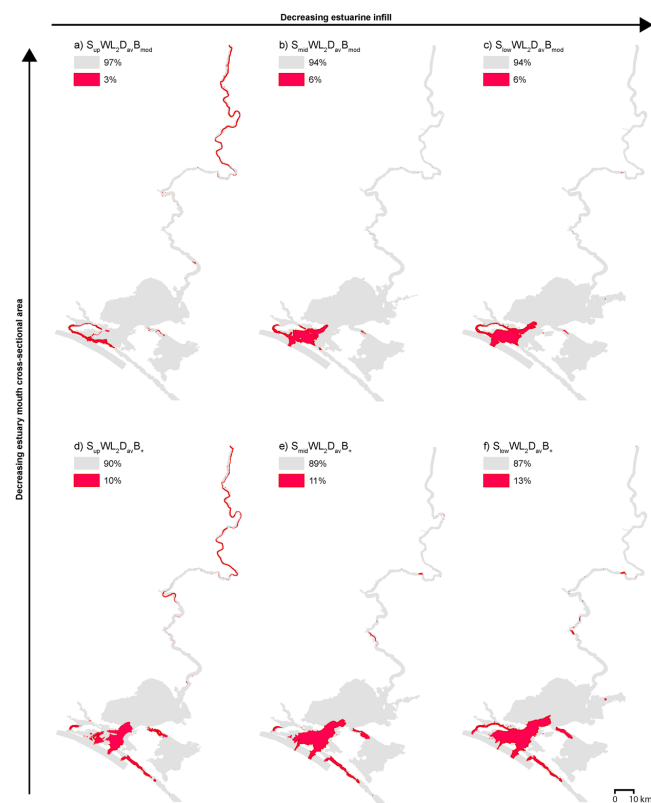
Figure 5. Key representative maps comparing maximum flow velocity magnitude relative to barrier morphology and bathymetric surface. Areas are shaded red where maximum velocity >0.3 m/s and conditions are therefore not conducive to the deposition of a laminated silt-clay sequence[25–27]. Barrier evolution from B_{mod} to B_+ (a–c to d–f respectively) has a minimal influence on the area conductive to velocities <0.3 m/s, while variance in bathymetry from S_{low} (c and f), or S_{mid} (b and e) to S_{up} (a and d) increases velocities within the back swamps upstream of Teal Flat (rkm 183), with comparable velocities elsewhere in the model domain. All scenarios shown are WL_2 (+2 m sea level) scenarios, demonstrating representative velocities at the Holocene highstand: (**a**) scenario $S_{up}WL_2D_{av}B_{mod}$; (**b**) scenario $S_{mid}WL_2D_{av}B_{mod}$; (**c**) scenario $S_{low}WL_2D_{av}B_{mod}$; (**d**) scenario $S_{up}WL_2D_{av}B_+$; (**e**) scenario $S_{mid}WL_2D_{av}B_+$; (**f**) scenario $S_{low}WL_2D_{av}B_+$.

S_{up} scenarios, with the S_{mid} and S_{low} morphologies extending inundation across the Cooke Plains Embayment (Fig. 2; Table S1). Variation in palaeo-salinities is facilitated by Lake Alexandrina's palaeo-channel within the S_{mid} and S_{low} morphologies, forcing marine influence upstream, pushing the brackish limit well within the Murray Gorge and causing the majority of the LMR to be characterised by brackish-fresh water (Figs 3a, 4a and S1b–c,e–f; Table S1). By comparison, the S_{up} scenarios allow for a brackish-fresh channel within the LMR while the fringing swamps largely remain fresh (Figs 3a, 4a and S1a,d; Table S1). The presence, or infill of, this palaeo-channel also alters the palaeo-salinity of Lake Albert (Figs 3a and S1). Overall, however, variation in bathymetric surface alone is insufficient to alter the palaeo-environment of the region, as demonstrated by comparing the results presented in Figs 3a and 4a. Despite the uncertainty in the precise location of a S_{mid} surface, the similarity between the results from the two morphological end members (S_{low} and S_{up} scenarios) show that robust conclusions can be drawn irrespective of the validity of the S_{mid} Holocene highstand best-estimate morphology.

Variation in barrier morphology exerts its greatest influence within the barrier and flood tide delta complex and attenuates rapidly; by the mid-section of the Lower Lakes the impact of barrier morphology is negligible (Figs 3c and 4a). The variety of postulated early- to mid-Holocene chain-of-islands evolution events in the barrier complex does not change the character of the palaeo-environment, as demonstrated by the near identical maximum palaeo-salinities and 10 psu (marine-brackish) limits presented in Figs 3c and 4a respectively.

Sensitivity testing for discharge reveals that the flood event has a greater influence on palaeo-salinities when compared to drought, however, only under $S_{up}WL_0$ scenarios is a flood sufficient to supress Lake Alexandrina to fresher conditions (Fig. 4a; Table S1). Drought conditions have a more pronounced impact on palaeo-salinities
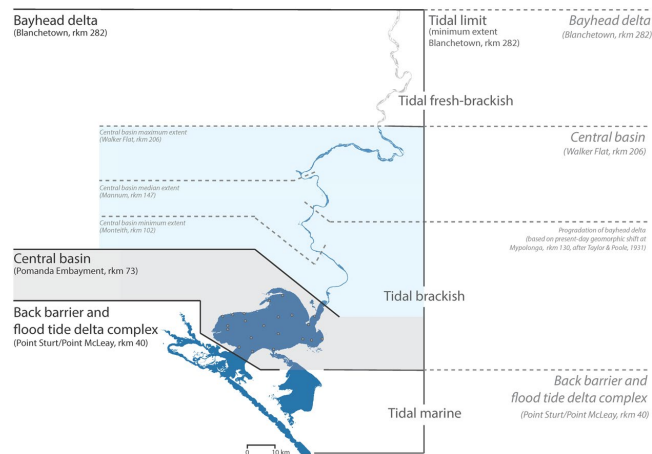
Figure 6. Estuarine processes zonation and inferred resulting morphology at the Holocene highstand. Based on $S_{mid}WL_2$ scenarios, estuarine processes can be categorised into three zonations: tidal marine, tidal brackish and tidal fresh-brackish (grey text). At the Holocene highstand, the tidal limit propagated beyond the study region, suggesting a minimum tidal limit of Blanchetown (rkm 282). This zonation is extrapolated into inferred resulting morphology at the Holocene highstand (grey italicised text). The Murray estuary's barrier and flood tide delta complex occupied the region seaward of Point Sturt and Point McLeay (rkm 40). The central basin occupied the entirety of the Lower Lakes, Lakes Alexandrina and Albert, and extended upstream within the Murray Gorge plausibly as far as Walker Flat (rkm 206, minimum Monteith at rkm 102, and median Mannum at rkm 147). Upstream, the bayhead delta occupied a low-energy backwater zone at least as far as Blanchetown (rkm 282). During the late-Holocene, the bayhead delta prograded downstream to Mypolonga (rkm 130). Our results contrast conventional barrier estuary facies models (black text), which place the upstream limit of the central basin at the point where the river debouches into the lake or lagoon (i.e., Pomanda Embayment, rkm 73). The Murray estuary's laminated central basin deposits have previously been identified in sediment cores (grey points) taken from within the conventional limits of the central basin (grey shaded area)[23,24]. Our results suggest that this laminated sequence characterises the Holocene depositional fill within the Murray Gorge at least as far upstream as Monteith (rkm 102) and plausibly as far as Walker Flat (rkm 206; grey and blue shaded areas).

under present-day sea levels (WL_0) when compared to WL_2 scenarios (Fig. 4a). Overall, variation of discharge has a moderate influence on palaeo-salinities throughout the region, however, as demonstrated by the near-identical maximum palaeo-salinities and 10 psu (marine-brackish) limits presented in Figs 3b and 4a, discharge alone is unable to alter the palaeo-environmental character of the region.

Discussion

Here, we assess the palaeo-Murray estuary's response to the Holocene highstand exploring the hydrologic, hydro-dynamic and geomorphic influences on the regional palaeo-environment. The experimental hydrodynamic modelling approach adopted in this study allows for the relative importance of drivers of palaeo-environmental change to be determined. Sensitivity testing for sea level, discharge, bathymetry and barrier morphology indicates sea level to be the determining factor for environmental characterisation of the palaeo-Murray estuary and the probable primary driver of change during the region's Holocene evolution. The experimental hydrodynamic modelling approach used here subjects end-member conditions to a sensitivity analysis giving a range of plausible responses rather than an explicit replication of reality. For instance, the S_{low} (Pleistocene-Holocene boundary) surface is certainly deeper than reality at the Holocene highstand, and the S_{up} (pre-regulation) surface certainly shallower. The negligible difference in results obtained through this end-member approach signifies that our models can in fact be extrapolated to represent a reasonable approximation of reality at the Holocene highstand.

The modelled estuarine environment at highstand is well constrained by global-scale estuary initiation at 8,200 yr BP following a significant meltwater pulse from the Laurentian ice sheet[34]. This event triggered major coastal change worldwide as the resulting accelerated rise in sea level caused a landward 'jump' in the estuarine zone[34]. On a local scale, within the Lower Lakes, flood tide delta and barrier complex stratigraphic[23,31,35], diatom[23,36] and midden analyses[37] support the designation of the regional palaeo-environment as estuarine at the Holocene highstand. However, our results demonstrate that the estuarine palaeo-environment was not limited solely to this region. We show that the +2 m Holocene highstand drove the estuarine limit much further upstream causing an enlarged low-energy backwater setting that occupied much of the LMR (minimum tidal limit rkm 282; Fig. 6). The low relief of this coastal plain facilitated an elongated central basin within the confines of the Murray Gorge, likely extending as far upstream as Walker Flat (rkm 206), where the silt-clay laminated sequence that characterises the central basin deposits within Lake Alexandrina[23,24] are inferred to extend (Fig. 6).

Adopting Zaitlin et al.'s[38] nomenclature, our results demonstrate that the middle incised valley extends from the modern-day shoreline landward to the estuarine limit at highstand, which we place between Walker Flat (rkm 206) and Blanchetown (rkm 282; Figs 4b, 6 and S2). We suggest that, at highstand, the fluvial inner incised valley stretched from this estuarine limit landward to Overland Corner (rkm 439) where the river enters the Murray Gorge. Here, the Coonambidgal Formation displays evidence of a declining energy gradient[39], which is not characteristic of the sediments of a meandering river 430 rkm upstream of its terminus. This unusually extensive backwater zone was a consequence of the unique low relief of this coastal plain system that attenuated flow velocities and forced the limit of coarse-grained fluvial deposition well upstream.

Since European settlement, the region has been subject to significant modification including extensive land reclamation and the construction of levees, locks, and barrages. Prior to this, the riverbanks between Mannum (rkm 154) and Mypolonga (rkm 130) were typically high creating natural levees that separated the channel from low-lying flats; this configuration transitioned to an unbroken series of swamps between Mypolonga (rkm 130) and Wellington (rkm 78)[32]. This shift in channel fringing environment at Mypolonga (rkm 130) is inferred to be the approximate limit of bayhead delta progradation before significant European modification and regulation of the LMR disrupted the natural flow regime (Fig. 6). A homogenous clay sequence could be expected to overlie the laminated central basin deposit, representing the downstream progradation of the bayhead delta, the precise location of which will be determined by a subsequent study.

The regionally extensive and continuous nature of the Murray estuary's laminated deposit within Lake Alexandrina from 5,500 yr BP until modern-day[23,24] suggests that the mechanism of deposition and preservation cannot exclusively be attributed to a palaeo-environment that differs to what we see today. The sequence continued to deposit despite the decrease in regional salinity brought about by a fall to present-day sea levels in the late-Holocene (Figs 3a and 4a). Recent flume studies demonstrate the capacity of laminated silt-clay deposition in much higher velocities than previously thought[26], with our results illustrating a real-world application in a dynamic palaeo-environment subject to marine influence (Figs 5 and S3) and consistent with the notion that salinity assists, but is not vital, for floc formation and laminae deposition[25]. An Australian east coast analogue is present in the Hawkesbury River estuary, where the Holocene estuarine central basin and bayhead delta sediments extend well into the gorge-confined valley, with the Colo River estuarine sequence presenting similar laminations to those described in Lake Alexandrina[23,24,29,40].

When considering the LMR, or other gorge confined portions of coastal plain estuaries as an extension of the central basin, the definition adopted is important. Dalrymple et al.[30] define the central basin not in the geomorphic sense of a lagoon, with which gorge confined regions such as the LMR could not conceivably be considered, but rather on the basis of facies designation. We correlate the process-based results from $S_{mid}WL_2$ scenarios with facies designation to infer the resulting morphology of the Murray estuary at the Holocene highstand (Fig. 6). Our inferred resulting morphology adopts Dalrymple et al.'s[30] facies rather than a geomorphic definition of the central basin whereby the lower portion of incised river valleys may exhibit the depositional characteristics of the central basin. Here we consider the central basin as the region of lowest energy characterised by the confluence of marine and fluvial influence and the deposition of the finest sediment.

Following conventional models of estuarine facies designation, the location where the river debouches into the lagoon is the likely transitional point of the designation of fluvial to estuarine geological formations (Fig. 6). However, with low relief allowing for elongated estuarine zones at the Holocene highstand, we suggest that the location of this transition requires review across coastal plain estuaries more broadly. In the case of the Murray estuary, the Holocene stratigraphy of Lake Alexandrina is characterised as the estuarine and coastal-marine sediments of the St Kilda Formation, whereas the LMR is characterised as the Quaternary alluvium of the Coonambidgal Formation (Fig. 2a; Table S2). This transition is currently placed at the Pomanda Embayment (rkm 73; Figs 1 and 2a), or precisely where the LMR debouches into Lake Alexandrina. By assigning our process-based results to inferred resulting morphology, we suggest a revision of the location of this transition is required to account for the Holocene extension of estuarine sedimentation within the gorge-confined portion of the central basin (Fig. 6). A sedimentary analysis is currently underway to assess the upstream extent and nature of this deposit, with previous work in the region suggesting the presence of a laminated sequence may be widespread within the LMR[32,41].

The key to understanding responses of coastal plain estuaries to future changes in climate requires a knowledge of drivers of change, best explored by an examination of palaeo-responses to such change through representative analogues. Here we demonstrate the vulnerability of Australia's largest and most politically and economically significant river basin to future environmental change. A comparison between $S_{up}WL_0$ and $S_{up}WL_2$ scenarios reveal the pronounced shift in environmental character with higher sea levels inducing significant marine incursion to the Lower Lakes and driving the brackish and fresh-brackish water zones as far upstream as Teal Flat (rkm 183; Figs 3a I,IV and S1a,d). Currently, the Murray estuary is a highly regulated system with a series of barrages in place to prevent saline intrusion into the estuary and river system, crucial for maintaining the freshwater resources within the region during 'undesirable' weather events such as prolonged drought. With the pace of future sea-level rise too rapid for barriers to transgress in response, and our results demonstrating a significant change in environmental character regardless of barrier morphology, we demonstrate the utility of applying a historical analogue to understand the importance of adapting water management to future needs. In the case of the Murray estuary, this analysis highlights the future importance of and likely need for reliance on the barrages if the current freshwater resource priorities are to be maintained.

Adopting a hydrodynamic modelling approach to Holocene analogues of coastal plain estuaries allows for the significant potential impact of climate change induced sea-level rise to be realised. Our results identify sea level as the dominant controlling factor on the environmental character of the Murray estuary, with the approximately 2 m higher-than-present sea level during the Holocene highstand generating an extensive central basin environment characterised by a low-energy backwater and laminated silt-clay deposits. We demonstrate that

the estuarine limit can extend significantly further inland than expected when evaluating modern-day geomorphology in the context of conventional estuarine facies models. The importance of sea level in controlling the character of the Murray estuary, irrespective of fluvial discharge, bathymetry and barrier morphology, suggests the impacts of future sea-level rise due to climate change on coastal plain estuaries may be underappreciated. Our results are broadly applicable to low-gradient coastal plain estuaries with wave-dominated entrances, particularly those with large catchments and low discharges. However, consideration must be applied to the nature of the incised valley and valley fill, dynamics of fluvial discharge and tidal regime, as well as the rate of sea-level rise/fall when transferring these results to other coastal plain estuaries[6]. The extent and impact of sea-level rise as a driver of environmental change is largely a consequence of the inherently low gradient of these systems. This characteristic low gradient of coastal plain estuaries facilitates the landward extension of the estuarine zone rendering lower portions of the conventionally fluvially dominated zone particularly vulnerable to saline intrusion and potentially unable to support potable water or irrigation supplies. The economic and social implications of our findings to the LMR and Murray estuary, and comparable coastal plain estuaries more broadly, are considerable.

Methodology

Overview of model result categories.   The study area encompasses the LMR from Blanchetown (rkm 282) downstream to the barrier complex and modern-day Murray Mouth (Fig. 1). Using TUFLOW FV, a 2D finite volume numerical model, we simulate 72 scenarios and conduct sensitivity testing for bathymetric surface (two end members and a best estimate), sea level (Holocene highstand and present-day), discharge (drought, pre-regulation average, and flood), and barrier morphology (four scenarios, ranging from completely open to almost closed, to account for barrier evolution). Results are grouped into six categories based on bathymetric surface and sea level (Table S1). The Pleistocene-Holocene stratigraphic boundary and pre-regulation surfaces represent bathymetric end-members to constrain the entire range of plausible bathymetries at the Holocene highstand. These are denoted as S_{low} and S_{up} respectively. A best estimate of bathymetry at the Holocene highstand is given by the S_{mid} surface. Accounting for the approximately 2 m variance in sea level between the Holocene highstand and present day gives the six modelled categories: $S_{low}WL_2$, $S_{low}WL_0$, $S_{mid}WL_2$, $S_{mid}WL_0$, $S_{up}WL_2$ and $S_{up}WL_0$ (Table S1). For each of these six categories, all possible combinations of discharge and barrier morphology were modelled. The three discharge scenarios of drought, pre-regulation average and flood are denoted by D_-, D_{av} and D_+ respectively (Table S1). The four barrier morphologies of completely open, two evolutionary phases, and modern-day are denoted by B_0, B_+, B_{++} and B_{mod} respectively (Fig. 1c–f; Table S1). We obtain inundation extents, water heights and depths, flow velocities and salinities for the full extent of the LMR and Murray estuary for each of the 72 modelled scenarios.

Numerical model set up.   Hydrology is simulated using TUFLOW FV, a 2D finite volume numerical model. The model domain spans some 282 rkm from Lock 1 at Blanchetown to the Murray Mouth and extending 2 km offshore. A base model was provided by BMT WBM and was the subject of vigorous calibration[42] (Supplementary methods: Model calibration). Stitched topography and bathymetry for the region was developed by the Commonwealth Scientific and Industrial Research Organisation (CSIRO)[43] and provided by the South Australian Department of Environment Water and Natural Resources (DEWNR) for use in this study. Outside the extent of this dataset (1956 flood extent), a 1 second Digital Elevation Model (DEM), provided by Geoscience Australia (GA), was applied and the two datasets interpolated together using ArcGIS. This mesh was then modified to extend the model domain to encompass the entire width of the Murray Gorge, as well as the inclusion of the modern-day barrier complex and extension of the Lower Lakes based on the palaeo-maximum inundation shoreline and Holocene estuarine stratigraphy[31,35,44]. Tides were imposed based on historical data taken from Victor Harbour between 1st January – 28th February 2014 to remove the uncertainties associated with tidal prediction (Fig. S4). Drought (D_-) and pre-regulation average (D_{av}) scenarios were run for 20 days while flood (D_+) scenarios were run for 31 days, which was a sufficient period for models to run beyond the spin-up phase and reach steady state, as confirmed by a review of hydrograph phasing. All models were run at a 5 minute timestep. A comparative analysis of 24 and 1 hour outputs confirmed that the 24 hour outputs were representative and, to save computational time, were subsequently applied to all scenarios. Initial salinity was applied at each cell based on salinity data taken from 25 gauging stations throughout the region at the peak of the Millennium drought. This was deemed appropriate as the barrages are in place to curtail saline intrusion and therefore regional salinities are held fresher than would naturally occur. Due to the potential influence of stratification of the estuary a representative subset of models were run in 3D to assess the suitability of adopting computationally efficient 2D models for this study. Refer to Supplementary methods: Comparison of 2D and 3D simulations for further information. The bottom drag model adopted for this study is the Manning's coefficient, with a global value of 0.025 applied to the entire model domain. This value is supported by sensitivity testing and calibration performed by BMT WBM on the base model provided for this study[42], and aligns with sensible values given hypothesised Holocene regional palaeo-environmental conditions[45]. Refer to Supplementary methods: Model calibration for further information.

Morphology.   To best resolve bathymetry and topography at highstand, three surfaces were created: (1) a pre-regulation surface (S_{up}) provided a modern-day end member, (2) the depth to the Monoman – Coonambidgal Formation transition provided a Late Pleistocene – Early Holocene end member (S_{low}), and (3) a best estimate of highstand bathymetry and topography (S_{mid}). Details on the creation of the three bathymetric surfaces, and chain-of-islands evolution of Sir Richard and Younghusband Peninsulas used to inform the four modelled barrier morphologies are given in Supplementary methods: Morphology.

Sensitivity testing.   Sensitivity testing for barrier evolution was based on the chain-of-islands model[13] with the location of possible palaeo-outlets interpreted from Bourman and Murray-Wallace[46], de Mooy[31] and

Luebbers[37]. Four barrier configurations were tested ranging from the complete removal of Sir Richard and Younghusband Peninsulas to the modern-day Murray Mouth (Fig. 1c–f; Table S1). Three discharge conditions were tested: two held constant at the Millennium drought low flow (D_; 152 m³/sec) and pre-regulation average flow (D_{av}; 419 m³/sec), and one variable to simulate a flood, with pre-regulation average discharge (D_{av}) increasing to the peak of the 1974 flood (D_{+}; 1,883 m³/sec) and decreasing again[47,48] (Table S1).

There have been numerous sea-level studies across Australia, with the majority stemming from east coast datasets[19,49]. As a consequence of isostatic and climatic influences, and localised geomorphology, there is wide variability across the Australian coast in both the magnitude and timing of the Holocene sea-level highstand[19]. Highstand estimates must therefore be derived from the regional setting of the study area which, for the Murray estuary, limits data to studies from the Gulf of St Vincent and the Spencer Gulf in South Australia. Immediately prior to the highstand (8,000–7,500 yr BP), sea level reached present day levels[19,20,50] with the magnitude of the subsequent highstand ranging from +1 m up to +3 m across the southern Australian coast[19,20]. This study adopts a best approximation of a +2 m highstand at 7,000–6,000 yr BP[19,20], a value which has been adopted by other studies of the Holocene palaeo-Murray estuary[18]. Our models were run twice – once using present day tides (WL_0) and again at present day tides plus 2 m to simulate Holocene highstand conditions (WL_2; Table S1).

Post-processing.   Salinity was classified based on chloride concentration using Tooley's[51] scheme: fresh <0.1 g Cl/L, fresh-brackish 0.1–0.5 g Cl/L, brackish-fresh 0.5–1 g Cl/L, brackish 1–5 g Cl/L, brackish-marine 5–10 g Cl/L, marine-brackish 10–17 g Cl/L, and marine >17 g Cl/L. Salinity was assessed using maximum salinities observed post model burn-in phase. We considered maximum rather than average salinity as, due to constraints in computational power giving a 5-fold increase in model run time, salinity is not resolved in 3D therefore results do not account for a salt wedge at depth but rather depict a freshwater plume at the surface. Directional vectors were assessed within the present-day channel (and not fringing swamps) such that a direct comparison could be drawn between the three model surfaces regardless of inundation extent or bathymetrically-controlled primary flow path. Velocity magnitude was considered relative to the critical threshold of 0.3 m/s[25–27] and representative models were re-run to assess tidal signatures from water levels at 1 hour outputs.

References

1. Rogers, K. & Woodroffe, C. D. Geomorphology as an indicator of the biophysical vulnerability of estuaries to coastal and flood hazards in a changing climate. *J. Coast. Conserv.* **20**, 127–144 (2016).
2. Reisinger, A. *et al*. In *Climate Change 2014: Impacts, Adaptation, and Vulnerability. Part B: Regional Aspects*. [Barros, V. R. *et al*., (eds)] Contribution of Working Group II to the Fifth Assessment Report of the Intergovernmental Panel on Climate Change pp. 1371–1438 (Cambridge University Press 2014).
3. Baynes, T., Herr, A., Langston, A. & Schandl, H. Coastal Climate Risk Project Milestone 1 Final Report to the Australian Department of Climate Change and Energy Efficiency. Prepared for the Department of Climate Change and Energy Efficiency (DCCEE) by the Commonwealth Scientific and Industrial Research Organisation (CSIRO) (DCCEE 2012).
4. Woodroffe, C. D. & Murray-Wallace, C. V. Sea-level rise and coastal change: the past as a guide to the future. *Quat. Sci. Rev.* **54**, 4–11 (2012).
5. Blum, M. D. & Törnqvist, T. E. Fluvial responses to climate and sea-level change: a review and look forward. *Sedimentology* **47**, 2–48 (2000).
6. Roy, P. S., Thom, B. G. & Wright, L. D. Holocene sequences on an embayed high-energy coast: an evolutionary model. *Sediment. Geol.* **26**, 1–19 (1980).
7. Sloss, C. R., Murray-Wallace, C. V. & Jones, B. G. Aminostratigraphy of Two Holocene Wave-Dominated Barrier Estuaries in Southeastern Australia. *J. Coast. Res.*, 113–136 (2006).
8. Sloss, C. R., Jones, B. G., McClennen, C. E., De Carli, J. & Price, D. M. Mid- to late Holocene sedimentation in a coastal lagoon: Burrill Lake, NSW, Australia. *Journal of Sedimentary Geology* **187**, 229–249 (2006).
9. Sloss, C. R. *et al*. The Holocene infill of Lake Conjola, a narrow incised valley system on the southeast coast of Australia. *Quat. Int.* **221**, 23–35 (2010).
10. Thom, B. G. & Roy, P. S. Relative sea-levels and coastal sedimentation in southeast Australia in the Holocene. *J. Sediment. Petrol.* **55**, 257–264 (1985).
11. Umitsu, M., Buman, M., Kawase, K. & Woodroffe, C. D. Holocene palaeoecology and formation of the Shoalhaven River deltaic-estuarine plains, southeast Australia. *The Holocene* **11**, 407–418 (2001).
12. Cann, J. H., Murray-Wallace, C. V., Belperio, A. P. & Brenchley, A. J. Evolution of Holocene coastal environments near Robe, southeastern South Australia. *Quat. Int.* **56**, 81–97 (1999).
13. Harvey, N. Holocene Coastal Evolution: Barriers, Beach Ridges, and Tidal Flats of South Australia. *J. Coast. Res.* 90–99 (2006).
14. Belperio, A. P., Hails, J. R. & Gostin, V. A. A review of Holocene sea levels in South Australia, Occasional Paper 3. [Hopley, D. (ed.)] Australian sea levels in the last 15 000 years: a review (James Cook University 1983).
15. Mills, K. *et al*. Paleoclimate studies and natural-resource management in the Murray-Darling Basin I: past, present and future climates. *Aust. J. Earth Sci.* **60**, 547–560 (2013).
16. Hill, P. J., De Deckker, P., von der Borch, C. & Murray-Wallace, C. V. Ancestral Murray River on the Lacepede Shelf, southern Australia: Late Quaternary migrations of a major river outlet and strandline development. *Aust. J. Earth Sci.* **56**, 135–157 (2009).
17. Fluin, J., Haynes, D. & Tibby, J. An Environmental History of the Lower Lakes and the Coorong. Report commissioned by the South Australian Department of Envrionment and Heritage, Adelaide (2009).
18. Bourman, R. P., Murray-Wallace, C. V., Belperio, A. P. & Harvey, N. Rapid coastal geomorphic change in the River Murray Estuary of Australia. *Mar. Geol.* **170**, 141–168 (2000).
19. Lewis, S. E., Sloss, C. R., Murray-Wallace, C. V., Woodroffe, C. D. & Smithers, S. G. Post-glacial sea-level changes around the Australian margin: a review. *Quat. Sci. Rev.* **74**, 115–138 (2013).
20. Belperio, A. P., Harvey, N. & Bourman, R. P. Spatial and temporal variability in the Holocene sea-level record of the South Australian coastline. *Sediment. Geol.* **150**, 153–169 (2002).
21. Harvey, N., Belperio, A., Bourman, R. & Mitchell, W. Geologic, isostatic and anthropogenic signals affecting sea level records at tide gauge sites in southern Australia. *Global Planet. Change* **32**, 1–11 (2002).
22. Twidale, C. R., Lindsay, J. M. & Bourne, J. A. Age and origin of the Murray River and Gorge in South Australia [Warren, J. W. (ed.)] Proceedings of Royal Society of Victoria, pp. 27–42 (The Royal Society of Victoria 1978).
23. Barnett, E. J. Recent Sedimentary History of Lake Alexandrina and the Murray Estuary. The Flinders University of South Australia (1993).

24. Barnett, E. J. A Holocene paleoenvironmental history of Lake Alexandrina, South Australia. *J Paleolimnol* **12**, 259–268 (1994).
25. Schieber, J. & Yawar, Z. A new twist on mud deposition - mud ripples in experiment and rock record. *The Sedimentary Record* **7**, 4–8 (2009).
26. Schieber, J., Southard, J. & Thaisen, K. Accretion of Mudstone Beds from Migrating Floccule Ripples. *Science* **318**, 1760–1763 (2007).
27. Baas, J. H., Best, J. L. & Peakall, J. Predicting bedforms and primary current stratification in cohesive mixtures of mud and sand. *J. Geol. Soc.* **173**, 12–45 (2016).
28. Allen, J. R. L. Annual textural banding in Holocene estuarine silts, Severn Estuary Levels (SW Britain): patterns, cause and implications. *The Holocene* **14**, 536–552 (2004).
29. Devoy, R. J., Dodson, J. R., Thom, B. G. & Nichol, S. Holocene environments in the Hawkesbury valley, new South Wales: A comparison of terrestrial and marine records. *Quat. Sci. Rev.* **13**, 241–256 (1994).
30. Dalrymple, R. W., Zaitlin, B. A. & Boyd, R. Estuarine facies models; conceptual basis and stratigraphic implications. *J. Sediment. Res.* **62**, 1130–1146 (1992).
31. de Mooy, C. J. Notes on the geomorphic history of the area surrounding Lakes Alexandrina and Albert. *Trans. Roy. Soc. S. Aust.* **82**, 99–118 (1959).
32. Taylor, J. K. & Poole, H. G. A soil survey of the swamps of the lower Murray River, S. Council for, R. Industrial, Eds., Bulletin (Council for Scientific and Industrial Research (Australia)); no. 51. (C.S.I.R, Melbourne 1931).
33. Sloss, C. R., Jones, B. G., McClennen, C. E., de Carli, J. & Price, D. M. The geomorphological evolution of a wave-dominated barrier estuary: Burrill Lake, New South Wales, Australia. *Sediment. Geol.* **187**, 229–249 (2006).
34. Rodriguez, A. B., Simms, A. R. & Anderson, J. B. Bay-head deltas across the northern Gulf of Mexico back step in response to the 8.2 ka cooling event. *Quat. Sci. Rev.* **29**, 3983–3993 (2010).
35. Von der Borch, C. & Altmann, M. Holocene stratigraphy and evolution of the Cooke Plains Embayment, a former extension of Lake Alexandrina, South Australia. *Trans. Roy. Soc. S. Aust.* **103**, 69–78 (1979).
36. Cann, J. H., Bourman, R. P. & Barnett, E. J. Holocene Foraminifera as Indicators of Relative Estuarine-Lagoonal and Oceanic Influences in Estuarine Sediments of the River Murray, South Australia. *Quat. Res.* **53**, 378–391 (2000).
37. Luebbers, R. A. The Coorong Report: An archaeological survey of the Northern Coorong, Prepared for the South Australian Department for Environment and Planning (1982).
38. Zaitlin, B. A., Dalrymple, R. W. & Boyd, R. The stratigraphic organization of incised-valley systems associated with relative sea-level change, [Dalrymple, R. W., Boyd, R. & Zaitlin, B. A., (eds)] Incised-Valley Systems: Origin and Sedimentary Sequences, Special Publication No. 51, pp. 45–60 (SEPM (Society for Sedimentary Geology), Tulsa, Oklahoma, U.S.A. 1994).
39. De Carli, E. & Hubble, T. C. T. Morphological characteristics of riverbank failure on the lower River Murray, South Australia, [Vietz, G., Rutherfurd, I. D. & Hughes, R., (eds)] Proceedings of the 7th Australian Stream Management Conference, pp. 255–261 (Townsville, Queensland 2014).
40. Nichol, S. L., Zaitlin, B. A. & Thom, B. G. The upper Hawkesbury River, New South Wales, Australia: a Holocene example of an estuarine bayhead delta. *Sedimentology* **44**, 263–286 (1997).
41. Hubble, T. C. T. & De Carli, E. Mechanisms and Processes of the Millennium Drought River Bank Failures: Lower Murray River, South Australia, *Goyder Institute for Water Research Technical Report* (Adelaide, South Australia, 2015).
42. Hudson, R. Modelling Investigation into the Wellington 'Virtual Weir' Concept: Project summary report, BMT WBM, Prepared for the Murray Darling Basin Authority (MDBA) (MDBA 2010).
43. Austin, J. M. & Gallant, J. C. Stitching elevation and bathymetry data for the Murray River and Lower Lakes, South Australia, CSIRO: Water for a Healthy Country National Research Flagship (CSIRO 2010).
44. Murray-Wallace, C. V. *et al.* Aminostratigraphy and thermoluminescence dating of coastal aeolianites and the later Quaternary history of a failed delta: The River Murray mouth region, South Australia. *Quat. Geochronol.* **5**, 28–49 (2010).
45. Ladson, A., Lang, S., Anderson, B. & Rutherfurd, I. D. An Australian Handbook of Stream Roughness Coefficients, paper presented at the 28th Hydrology and Water Resources Symposium, Wollongong, 10–14 November (2003).
46. Bourman, B. & Murray-Wallace, C. V. Holocene evolution of a sand spit at the mouth of a large river system: Sir Richard Peninsular and the MurrayMouth, South Australia. *Z. Geomorphol. Supp.* **81**, 63–83 (1991).
47. Bloss, C., Montazeri, M. & Eckert, G. Flood mapping of the River Murray floodplain in South Australia, Department of Environment, Water and Natural Resources (DEWNR) Technical Report 2015/57 (DEWNR 2015).
48. Gippel, C. J. & Blackham, D. Review of environmental impacts of flow regulation and other water resource developments in the River Murray and Lower Darling River system, Final Report by Fluvial Systems Pty Ltd, Stockton, to Murray-Darling Basin Commission (MDBC), Canberra, ACT (MDBC 2002).
49. Sloss, C. R., Murray-Wallace, C. V. & Jones, B. G. Holocene sea-level change on the southeast coast of Australia: a review. *The Holocene* **17**, 999–1014 (2007).
50. Bowman, G. & Harvey, N. Geomorphic Evolution of a Holocene Beach-Ridge Complex, LeFevre Peninsula, South Australia. *J. Coast. Res.* **2**, 345–362 (1986).
51. Tooley, M. J. Sea-level Changes: Northwest England during the Flandrian stage (Clarendon Press 1978).

Author Contributions

A.M.H., H.E.P. and T.C.T.H. designed the study. A.M.H. and H.E.P. developed and ran the models, and analysed and interpreted the results. A.M.H. wrote the manuscript with substantial contributions from all co-authors.

Additional Information

Supplementary information accompanies this paper at https://doi.org/10.1038/s41598-019-39516-4.

Competing Interests: The authors declare no competing interests.

Publisher's note: Springer Nature remains neutral with regard to jurisdictional claims in published maps and institutional affiliations.

SUPPLEMENTARY MATERIALS

Modelling Holocene analogues of coastal plain estuaries reveals the magnitude of sea-level threat

Authors: Anna M Helfensdorfer[1,2]*, Hannah E Power[2], Tom Hubble[1]

Affiliations:

1. School of Geosciences, The University of Sydney, Sydney, NSW 2006, Australia

2. School of Environmental and Life Sciences, The University of Newcastle, Callaghan, NSW 2308, Australia

*Correspondence should be addressed to A.M.H. (email: anna.helfensdorfer@sydney.edu.au)

Supplementary methods: Model calibration

Following a significant period of prolonged drought, BMT WBM were commissioned by the Murray-Darling Basin Authority (MDBA) to perform a feasibility study assessing the adoption of a virtual weir at Wellington (rkm 78) to provide an adequate fresh water supply for the region. This involved the establishment, calibration and validation of a hydrological model encompassing the LMR and Lower Lakes region downstream of Blanchetown (rkm 282, Lock 1). A validation dataset was collected, and the model calibrated for hydrodynamics - including water level, wind and river fluxes – and salinity. Model calibration adequately resolved short term (i.e. a single extreme saline intrusion event) and long term (i.e. entire 17 month dataset) trends.

Owing to the long-term temporal scale of modelling estuarine response to sea level change over the course of the mid- to late-Holocene, simplifications need to be applied based on best estimate assumptions to guide parameters for sensitivity testing. The model set up adopted in this study seeks to apply 'appropriate complexity' balancing a reductionist approach to input data based on geological correlation, to produce outputs which are computationally efficient yet meaningful (*52, 53*). Model manipulation and model scenarios involved a deviation from present day morphology, flow and flow obstructions, sea level and ocean outlet, resulting in models which inherently could not be calibrated against the present day. Instead, results were compared to the Holocene stratigraphic record. Water heights were compared to documented evidence of notches and wave-cut cliffs along the former shoreline of Lake Alexandrina (*37*), and inundation extents correlated with the Malcolm soil combination and sediments of the Cooke Plains Embayment (*31, 36*).

Wave data was excluded from our model as the primary influence of waves within a wave-dominated estuary is as a driver of morphological change through the formation of a barrier complex at the estuary mouth and this model does not incorporate a sediment transport or morphology component (*30*). Furthermore, although this estuary is wave-dominated at its entrance, owing to the immense scale of this system, areas subject to significant wave energy present a negligible component of the overall model domain (Fig. S5).

A Manning's coefficient of 0.025 was adopted across the model domain for this study. Applying a varying Manning's coefficient was not actually implementable without a robust understanding of surficial sediments at the Holocene highstand over the entire 282 rkm of the model domain. Given this impracticality, applying a global Manning's coefficient was deemed sensible and, although not an accurate representation of reality, this method nonetheless provides the means for direct comparison between results. The value of 0.025 was selected as it lies within the bounds of appropriate Manning's coefficients given the likely Holocene palaeo-environmental conditions (*45*). Further, this value was deemed appropriate as sensitivity testing conducted during calibration of the base model provided by BMT WBM revealed that results did not vary significantly given changes in the Manning's coefficient, but the model was best resolved when adopting values between 0.015 and 0.02538 (*42*). Reference 42 is a government funded study. For access, please contact the Murray Darling Basin Authority (MDBA) through: engagement@mdba.gov.au.

Supplementary methods: Morphology

To best assess the influence of morphology on the hydrodynamics of the system at the Holocene highstand, three surfaces were created. A pre-regulation surface (S_{up}) provided a modern-day end member, the depth to the Monoman – Coonambidgal Formation transition provided a Late Pleistocene –

Early Holocene end member (S_{low}), with the third surface a best estimate of highstand bathymetry and topography (S_{mid}). The S_{low} surface is certainly deeper than at Highstand, with the average depth of the body of Lake Alexandrina (between Point Sturt/Point McLeay and Pomanda Embayment) approximately -43 m AHD (Australian Height Datum; approximately mean sea level). By comparison the S_{up} surface has an average of approximately -3 m AHD over the same area, with the S_{mid} best estimate highstand surface at approximately -8 m AHD. Within the LMR, the average of three surfaces is more closely constrained, varying from approximately -15 m to -8 m.

To resolve the S_{up} pre-regulation surface, the lock, barrages (and associated sediment sills), man-made levies and modern flood tide delta were removed from modern day DEMs (Fig. S6a). To resolve the S_{low} Pleistocene – Holocene surface, depths were interpreted from over 100 sediment cores, as well as interpretation of data and maps by Barnett (*23*) and Von der Borch and Altmann (*35*) (Fig. S6b; Table S3). The location and depth of the palaeo-channel within Lake Alexandrina was based on an interpretation of the work of Barnett (*23*) and geological maps (Fig. S6b). The S_{mid} best-estimate highstand surface has the greatest uncertainty as it was resolved by subtracting regional sedimentation rates from the pre-regulation surface (*23, 54*) and dated sediment cores (n = 18; Fig. S6c). Within the LMR and thalweg seaward, a sedimentation rate of 0.69 mm/y was adopted (*23, 54*). All other elements were adjusted with a sedimentation rate of 0.16 mm/y (*23, 54*).

The spatial interval of the three bathymetric surfaces created is identical to that of the modern-day input dataset as values were adjusted at each individual cell. The cell/element size varies considerably across the model domain with an average of approximately 50 m in cell side length within the LMR, modern flood tide delta (seaward of Point Sturt/Point McLeay, rkm 40) and Lower Lake fringes, and palaeo-Murray thalweg, with a considerably larger cell/element size within the main body of the Lower Lakes.

The chain-of-islands evolution of Sir Richard and Younghusband Peninsulas (*13, 31, 37, 46*) was the guiding premise for the series of barrier morphologies presented in this study. Bourman and Murray-Wallace (*46*) and de Mooy (*31*) give detailed descriptions and maps of hypothesised former outlets of the LMR to the ocean. These maps were georeferenced and digitised and assessed relative to the modern-day topography of the barrier system. Furthermore, the presence or absence of Aboriginal middens within the Holocene barrier (*18, 37, 55, 56*) were also mapped and assessed relative to their radiocarbon ages. These data were combined and analysed to produce a series of best estimates of the morphology of the mouth of the LMR as it evolved throughout the Holocene. As this study imposes a static barrier configuration for each scenario, an assessment of the dynamic response of the barrier to events on short temporal scales, such as tides or storms, was beyond the scope of the study.

Supplementary methods: Comparison of 2D and 3D simulations

Estuarine stratification can cause a salt wedge at depth which cannot be resolved by a 2D simulation. The presence of a salt wedge has the potential to alter inferences drawn from estuarine zonation and the likelihood of deposition of a laminated sequence whereby flocculation may be assisted by salinity. The scale of the study area, with the model domain spanning some 282 river kilometres, precluded the use of a 3D model setup without justification as the computational power to run such a simulation is ten times that of its 2D counterpart. Therefore, a representative subset of models were run in 3D to assess the suitability of adopting 2D models for this study. This representative subset of models allowed for a comparative assessment of 2D and 3D results for all bathymetric surfaces ($S_{low}WL_2D_{av}B_{mod}$, $S_{mid}WL_2D_{av}B_{mod}$ and $S_{up}WL_2D_{av}B_{mod}$), both sea level scenarios ($S_{mid}WL_2D_{av}B_{mod}$ and $S_{mid}WL_0D_{av}B_{mod}$), all discharge scenarios

($S_{mid}WL_2D_-B_{mod}$, $S_{mid}WL_2D_{av}B_{mod}$ and $S_{mid}WL_2D_+B_{mod}$) and all barrier morphologies ($S_{mid}WL_2D_{av}B_0$, $S_{mid}WL_2D_{av}B_+$, $S_{mid}WL_2D_{av}B_{++}$ and $S_{mid}WL_2D_{av}B_{mod}$).

3D simulations retained the same model setup with the inclusion of a parametric vertical mixing model with a second order vertical solution and density coupled salinity. A comparative analysis of results suggests that 2D simulations are sufficiently representative of 3D simulations (Fig. S7). Minor differences in maximum salinity reached across the region does not alter the designation of the palaeo-environment with 2D simulations providing a conservative approximation of 3D results (Fig. S7 a-b). Crucially, the brackish limit (i.e. 1 psu) differed by a maximum of 1 rkm between 2D and 3D depth averaged results, with the exception of the pre-regulation (S_{up}) surface where the 3D simulation captured a salt wedge that penetrated 6 rkm further upstream ($S_{up}WL_2D_{av}B_{mod}$ scenario). A negligible change in the total area conducive to the deposition of a laminated sequence was also observed, with 2D simulations overestimating this area by an average of 4%, demonstrating that 2D approximations of 3D velocity magnitudes are appropriate (Fig. S7 c-d).
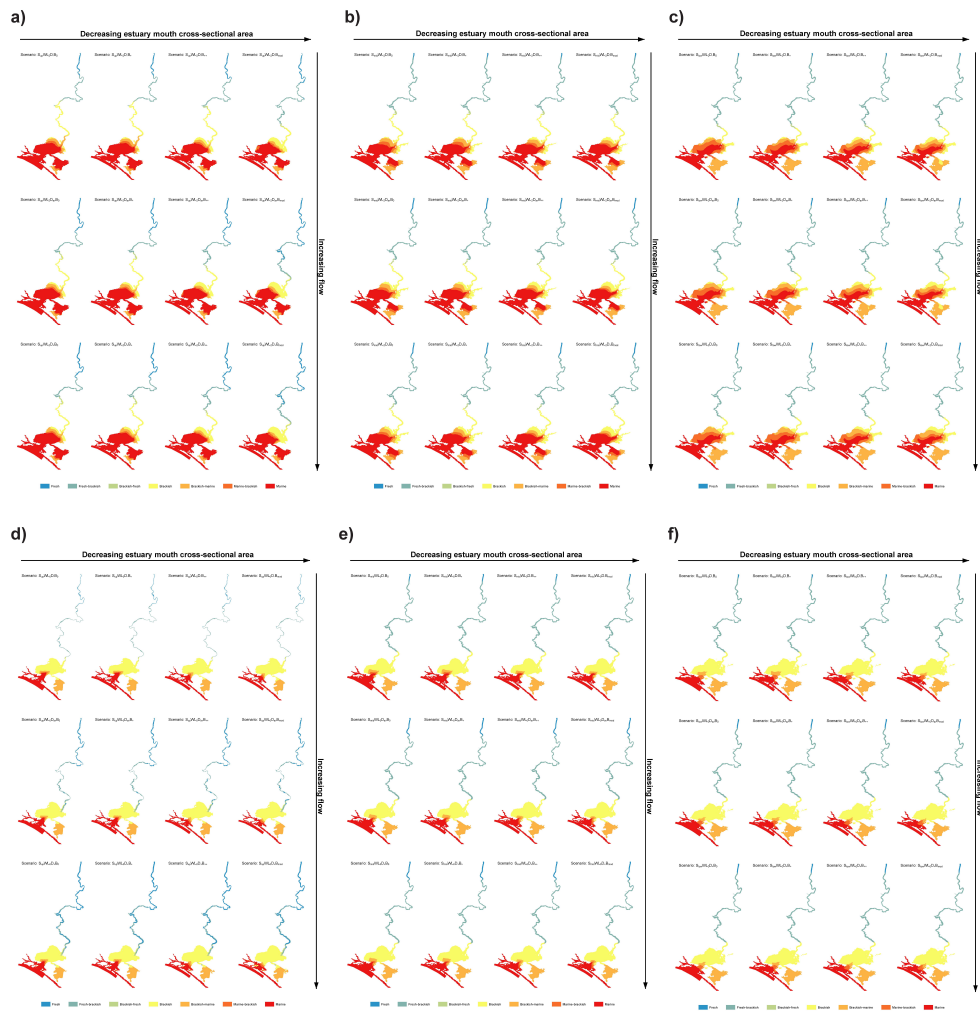
Figure S1: Maps of maximum salinity reached for each scenario. Maximum salinity is shown for each (**a**) $S_{up}WL_2$, (**b**) $S_{mid}WL_2$, (**c**) $S_{low}WL_2$, (**d**) $S_{up}WL_0$, (**e**) $S_{mid}WL_0$, (**f**) $S_{low}WL_0$ scenario. Salinity is measured based on the classification scheme of Tooley (*51*). Refer to Table S1 for scenario descriptions.
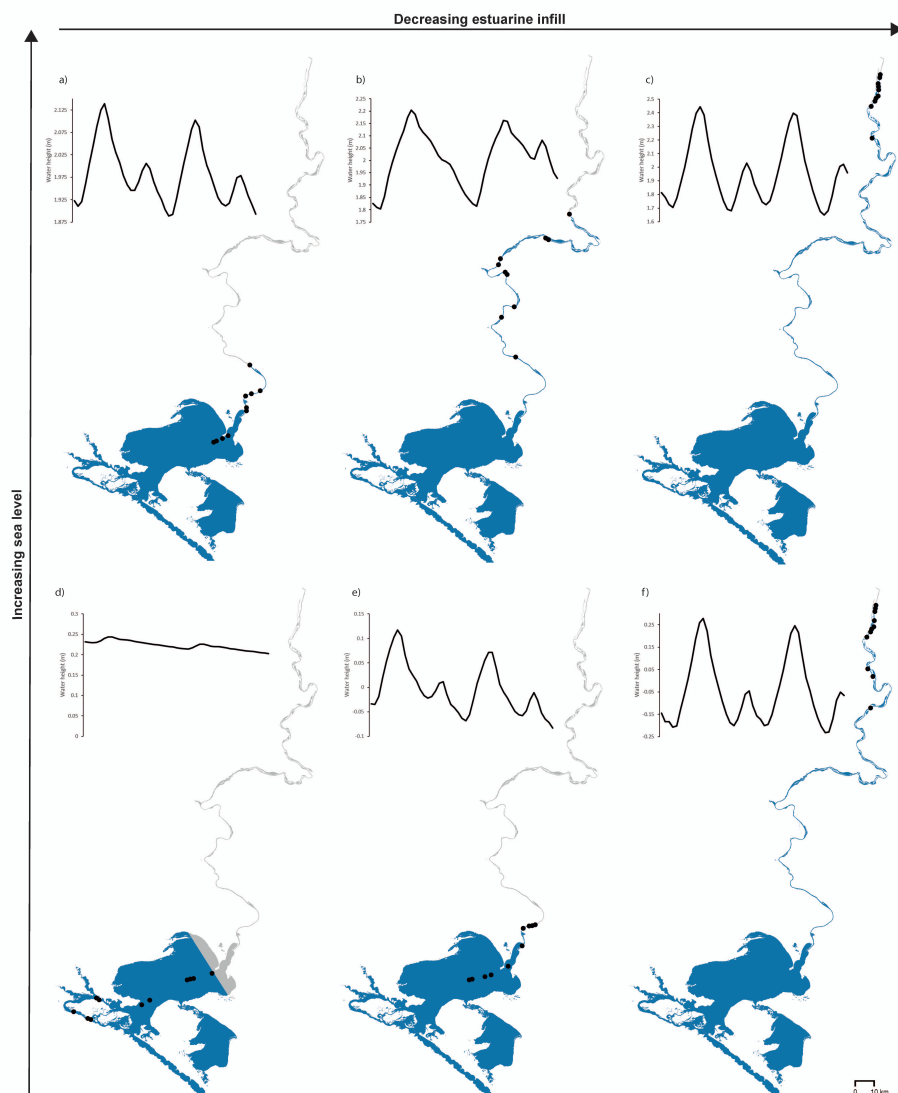
Figure S2: Characterisation of backwater zone and key representative tidal signatures. Maps show maximum upstream extent of velocity vector convergence for each scenario (black dots) in scenario category (**a**) $S_{up}WL_2$, (**b**) $S_{mid}WL_2$, (**c**) $S_{low}WL_2$, (**d**) $S_{up}WL_0$, (**e**) $S_{mid}WL_0$ and (**f**) $S_{low}WL_0$. Velocity vector convergence is taken as the point of convergence of upstream and downstream velocity vectors within the channel thalweg. Tidal signatures are given for the final 48 hours at the maximum upstream extent of upstream velocity vectors, in each scenario. Adopting Zaitlin's (*38*) nomenclature, the areas shaded in blue are characterised as the middle incised valley. At the Holocene highstand, an enlarged low-energy backwater setting was emplaced up to Walker Flat (**b**; rkm 206).

6

Figure S3: Maps of maximum velocity magnitude reached for each scenario. Maximum velocity magnitude is shown for each (**a**) $S_{up}WL_2$, (**b**) $S_{mid}WL_2$, (**c**) $S_{low}WL_2$, (**d**) $S_{up}WL_0$, (**e**) $S_{mid}WL_0$, (**f**) $S_{low}WL_0$ scenario. Areas are shaded red where maximum velocity > 0.3 m/s and therefore is not conducive to the deposition of a laminated silt-clay sequence (*25, 26, 27*). Refer to Table S1 for scenario descriptions.
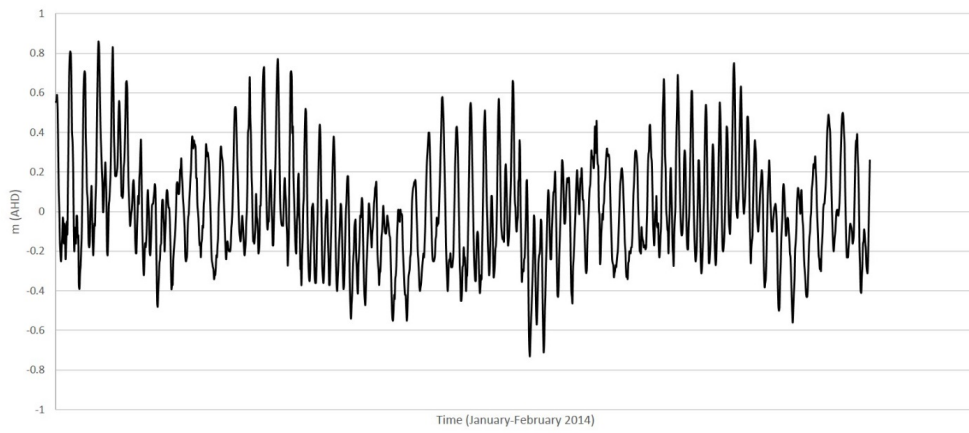
Figure S4: Tidal dataset adopted in this study. Data obtained from the Victor Harbour tidal gauge 01/01/2014 – 28/02/2014.

Figure S5: Overview map with site photos demonstrates the immense scale of the Murray estuary and lower Murray River. (**a**) The lower Murray River at Walker Flat (rkm 206) is entrenched in the Murray Gorge. Photo taken from the right bank looking east, main channel width approximately 170 m. (**b**) The lower Murray River exits the Murray Gorge at Wellington (rkm 78). Photo taken from the right bank looking east with the Wellington car ferry shown for scale, main channel width approximately 270 m. (**c**) The main body of Lake Alexandrina is so vast that the opposite shoreline cannot be seen by the naked eye. Photo taken looking east, distance to opposite shoreline approximately 37 km. (**d**) The final segment of the lower Murray River flows through the Goolwa channel (rkm 11) before reaching the Murray Mouth. Photo taken from the right bank looking east, approximate channel width 570 m. (**e**) Sir Richard Peninsula at Goolwa seen from a lookout point facing south east (rkm 12), where the lower Murray River meets the Southern Ocean. (**f**) Goolwa Beach on the Sir Richard Peninsula seen from the lookout point of (**e**) facing north west (rkm 12).

Figure S6: Overview of data used in the creation of three bathymetric surfaces. (**a**) Creation of the S_{up} surface involved manipulation of present day DEMs to remove man-made features including artificial levees (blue), Lock 1 at Blanchetown (rkm 282), Goolwa, Mundoo, Boundary Creek, Ewe Island and Tauwitchere barrages (purple), as well as Bird Island (grey), a modern flood tide deltaic island (*57*). (**b**) Creation of the S_{low} surface involved analysis of depth to the Coonambidgal-Monoman Formation transition, which is considered to mark the Pleistocene-Holocene boundary. Cores and CPTs analysed for creation of this surface (red) are given in Table S3. The location of the palaeo-Murray thalweg (blue) was inferred from data presented in Barnett (*23*). (**c**) Creation of the S_{mid} surface was resolved by subtracting regional sedimentation rates from the pre-regulation surface (*23, 54*) and dated sediment cores (red). Within the LMR and palaeo-Murray thalweg seaward (blue), a sedimentation rate of 0.69 mm/y was adopted (*23, 54*). All other elements were adjusted with a sedimentation rate of 0.16 mm/y (*23, 54*).
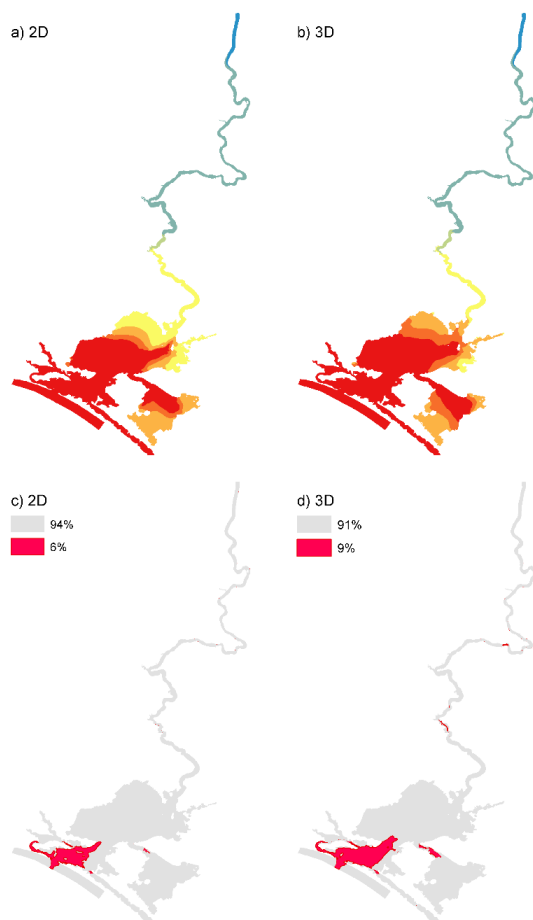
Figure S7: Comparison of $S_{mid}WL_2D_{av}B_{mod}$ 2D and 3D key outputs of maximum salinity and velocity magnitude. Maximum salinity reached in a best estimate Holocene highstand (**a**) 2D simulation is comparable to that of a (**b**) 3D simulation such that the classification of estuarine zonation remains consistent. 2D simulations provide a conservative approximation of 3D results. Salinity is measured based on the classification scheme of Tooley (*51*). Maximum velocity magnitude in a best estimate Holocene highstand (**c**) 2D simulation and a (**d**) 3D simulation. Areas are shaded red where maximum velocity > 0.3 m/s and therefore is not conducive to the deposition of a laminated silt-clay sequence (*25, 26, 27*). A 3% change in total area demonstrates the negligible difference in velocity magnitude between 2D and 3D simulations.

Table S1: The scenarios adopted in this study. Codes identify bathymetric surface (S_{up} = pre-modification condition, S_{mid} = highstand best estimate condition, S_{low} = Pleistocene-Holocene boundary condition), discharge (D_- = drought, D_{av} = pre-regulation average, D_+ = pre-regulation average with a flood event), and barrier morphology (B_0 = no barrier, B_+ and B_{++} = phases of chain-of-islands evolution (*13, 31, 37, 46*), and B_{mod} = present day). A code and category has been assigned to each scenario to facilitate interpretation. Scenario categories are grouped based on sea-level and bathymetric surface.

Initial sea level at 2 m (with respect to 2014 sea level)					Initial sea level at 0 m (with respect to 2014 sea level)				
Bathymetric Surface	Discharge	Barrier Morphology	Scenario Code	Scenario Category	Bathymetric Surface	Discharge	Barrier Morphology	Scenario Code	Scenario Category
S_{up}	D_-	B_0	$S_{up}WL_2D_-B_0$	$\mathbf{S_{up}WL_2}$	S_{up}	D_-	B_0	$S_{up}WL_0D_-B_0$	$\mathbf{S_{up}WL_0}$
		B_+	$S_{up}WL_2D_-B_+$				B_+	$S_{up}WL_0D_-B_+$	
		B_{++}	$S_{up}WL_2D_-B_{++}$				B_{++}	$S_{up}WL_0D_-B_{++}$	
		B_{mod}	$S_{up}WL_2D_-B_{mod}$				B_{mod}	$S_{up}WL_0D_-B_{mod}$	
	D_{av}	B_0	$S_{up}WL_2D_{av}B_0$			D_{av}	B_0	$S_{up}WL_0D_{av}B_0$	
		B_+	$S_{up}WL_2D_{av}B_+$				B_+	$S_{up}WL_0D_{av}B_+$	
		B_{++}	$S_{up}WL_2D_{av}B_{++}$				B_{++}	$S_{up}WL_0D_{av}B_{++}$	
		B_{mod}	$S_{up}WL_2D_{av}B_{mod}$				B_{mod}	$S_{up}WL_0D_{av}B_{mod}$	
	D_+	B_0	$S_{up}WL_2D_+B_0$			D_+	B_0	$S_{up}WL_0D_+B_0$	
		B_+	$S_{up}WL_2D_+B_+$				B_+	$S_{up}WL_0D_+B_+$	
		B_{++}	$S_{up}WL_2D_+B_{++}$				B_{++}	$S_{up}WL_0D_+B_{++}$	
		B_{mod}	$S_{up}WL_2D_+B_{mod}$				B_{mod}	$S_{up}WL_0D_+B_{mod}$	
S_{mid}	D_-	B_0	$S_{mid}WL_2D_-B_0$	$\mathbf{S_{mid}WL_2}$	S_{mid}	D_-	B_0	$S_{mid}WL_0D_-B_0$	$\mathbf{S_{mid}WL_0}$
		B_+	$S_{mid}WL_2D_-B_+$				B_+	$S_{mid}WL_0D_-B_+$	
		B_{++}	$S_{mid}WL_2D_-B_{++}$				B_{++}	$S_{mid}WL_0D_-B_{++}$	
		B_{mod}	$S_{mid}WL_2D_-B_{mod}$				B_{mod}	$S_{mid}WL_0D_-B_{mod}$	
	D_{av}	B_0	$S_{mid}WL_2D_{av}B_0$			D_{av}	B_0	$S_{mid}WL_0D_{av}B_0$	
		B_+	$S_{mid}WL_2D_{av}B_+$				B_+	$S_{mid}WL_0D_{av}B_+$	
		B_{++}	$S_{mid}WL_2D_{av}B_{++}$				B_{++}	$S_{mid}WL_0D_{av}B_{++}$	
		B_{mod}	$S_{mid}WL_2D_{av}B_{mod}$				B_{mod}	$S_{mid}WL_0D_{av}B_{mod}$	
	D_+	B_0	$S_{mid}WL_2D_+B_0$			D_+	B_0	$S_{mid}WL_0D_+B_0$	
		B_+	$S_{mid}WL_2D_+B_+$				B_+	$S_{mid}WL_0D_+B_+$	
		B_{++}	$S_{mid}WL_2D_+B_{++}$				B_{++}	$S_{mid}WL_0D_+B_{++}$	
		B_{mod}	$S_{mid}WL_2D_+B_{mod}$				B_{mod}	$S_{mid}WL_0D_+B_{mod}$	
S_{low}	D_-	B_0	$S_{low}WL_2D_-B_0$	$\mathbf{S_{low}WL_2}$	S_{low}	D_-	B_0	$S_{low}WL_0D_-B_0$	$\mathbf{S_{low}WL_0}$
		B_+	$S_{low}WL_2D_-B_+$				B_+	$S_{low}WL_0D_-B_+$	
		B_{++}	$S_{low}WL_2D_-B_{++}$				B_{++}	$S_{low}WL_0D_-B_{++}$	
		B_{mod}	$S_{low}WL_2D_-B_{mod}$				B_{mod}	$S_{low}WL_0D_-B_{mod}$	
	D_{av}	B_0	$S_{low}WL_2D_{av}B_0$			D_{av}	B_0	$S_{low}WL_0D_{av}B_0$	
		B_+	$S_{low}WL_2D_{av}B_+$				B_+	$S_{low}WL_0D_{av}B_+$	
		B_{++}	$S_{low}WL_2D_{av}B_{++}$				B_{++}	$S_{low}WL_0D_{av}B_{++}$	
		B_{mod}	$S_{low}WL_2D_{av}B_{mod}$				B_{mod}	$S_{low}WL_0D_{av}B_{mod}$	
	D_+	B_0	$S_{low}WL_2D_+B_0$			D_+	B_0	$S_{low}WL_0D_+B_0$	
		B_+	$S_{low}WL_2D_+B_+$				B_+	$S_{low}WL_0D_+B_+$	
		B_{++}	$S_{low}WL_2D_+B_{++}$				B_{++}	$S_{low}WL_0D_+B_{++}$	
		B_{mod}	$S_{low}WL_2D_+B_{mod}$				B_{mod}	$S_{low}WL_0D_+B_{mod}$	

Table S2: Description of stratigraphic formations and soil combinations within the study area.

Formation Name	Description
Coonambidgal	Holocene alluvial clays and silts comprising the upper valley fill within the LMR
Monoman	Holocene to late-Pleistocene alluvial sands comprising the lower valley fill within the LMR
Saint Kilda	Holcene coastal marine sediment
Bridgewater	Middle-Pleistocene sands
Padthaway	Holocene to early-Pleistocene lacustrine sands, silts and clays
Molineaux Sand	Holocene to late-Pleistocene aeolian sands

Soil Combination Name	Description
Malcolm	Holocene estuarine, alluvial and lacustrine clays demarcating the greatest Holocene inundation extent of Lake Alexandrina

Table S3: Sedimentological data used to inform the creation of the S$_{low}$ surface. Core logs (*23, 58, 59*) and cone penetrometer tests (*41*) were analysed for the transition from the Monoman to Coonambidgal formation, which is interpreted to represent the approximate Pleistocene to Holocene boundary (S$_{low}$). Depths were adjusted relative to present day bathymetry and topography to give elevation in meters AHD.

rkm	X	Y	S$_{low}$ Z (m AHD)	ID	Reference
3	305704	6064588	> 3.6	35	Barnett, 1993
10	300043	6067607	> 3.0	33	Barnett, 1993
18	305738	6069952	> 3.8	32	Barnett, 1993
25	317628	6080376	0.5	19	Barnett, 1993
30	315888	6069243	2.8	25	Barnett, 1993
30	315643	6066463	2.7	26	Barnett, 1993
32	317049	6064273	> 1.9	27	Barnett, 1993
35	321456	6063067	1.7	24	Barnett, 1993
36	325255	6062032	> 2.3	23	Barnett, 1993
39	323598	6069398	> 4.9	22	Barnett, 1993
40	321175	6077118	0.1	11	Barnett, 1993
40	320792	6081178	0.7	18	Barnett, 1993
40	321201	6075823	1.7	20	Barnett, 1993
43	328598	6068940	> 2.1	21	Barnett, 1993
46	335469.7	6068475	> -19.8	Narrung Ferry 3, #70435	SARIG
47	328808	6073753	> 4.8	15	Barnett, 1993
48	326907	6078155	1.3	16	Barnett, 1993
48	324273	6081247	0.4	17	Barnett, 1993
50	335386	6069807	> 0.8	14	Barnett, 1993
52	333115	6078087	1.5	13	Barnett, 1993
53	332968	6086037	1.1	9	Barnett, 1993
54	336659	6074639	> 4.8	12	Barnett, 1993
55	336077	6081656	1.4	10	Barnett, 1993
57	337929	6088161	> 1.3	8	Barnett, 1993
61	344830	6074599	> 2.0	6	Barnett, 1993
61	341063	6082300	0.2	7	Barnett, 1993
64	348312	6074474	> 0.3	5	Barnett, 1993
65	347387	6079188	-41.8	BH 2, #234134	SARIG
65	347477	6079083	> 2.0	3	Barnett, 1993
67	352233	6075279	> 1.5	4	Barnett, 1993
67	347256	6081111	> -20.6	BH 4, #234136	SARIG
69	349244	6082072	> 4.0	2	Barnett, 1993
76	352640	6087305	> 2.7	1	Barnett, 1993
78	353178	6089048	-14.8	Wellington	Hubble & De Carli, 2015
79	353311.8	6089252	-47.4	DEPT H & L G, #71577	SARIG
79	353169.8	6089073	-25.4	DEPT H & L G, #71668	SARIG
79	353346.8	6089207	-11.2	DEPT H & L G, #71581	SARIG
79	353112.8	6088951	-6.0	DEPT H & L G, #71669	SARIG
79	353306.8	6089250	> -35.0	DEPT H & L G, #71578	SARIG
79	353318.8	6089239	> -37.4	DEPT H & L G, #71580	SARIG
79	353318.8	6089239	> -30.7	DEPT H & L G, #71579	SARIG
79	353312	6089252	-48.5	6727-1105	Barnett, 1989
79	353170	6089073	> -22.4	6727-1196	Barnett, 1989
79	353233	6089803	> -2.7	Wellington East Marina	Hubble & De Carli, 2015
85	357350	6093006	> -0.4	Murray view Estates	Hubble & De Carli, 2015
85	357368	6093010	-21.7	Murray view Estates	Hubble & De Carli, 2015
88	358637.8	6093934	-0.6	Tailem Bend Pump 1, #71594	SARIG
92	359155.8	6097151	> -27.2	DEPT H & L G, #71665	SARIG

rkm	X	Y	S_{low} Z (m AHD)	ID	Reference
91.5	359156	6097151	> -27.4	6727-1193	Barnett, 1989
97	354771	6101444	-6.3	Westbrook	Hubble & De Carli, 2015
104	348576	6104196	-14.9	Riverglen Marina	Hubble & De Carli, 2015
104	348214	6104380	-27.2	Riverglen Marina	Hubble & De Carli, 2015
108	346634	6106805	-15.9	Bells Reserve Monteith	Hubble & De Carli, 2015
109	346395.8	6106955	-26.9	Monteith 1, #71337	SARIG
109	346396	6106955	-26.2	6727-865	Barnett, 1989
111	346364.8	6108814	-9.9	Swanport 6, #71336	SARIG
111.5	346365	6108814	-30.0	6727-864	Barnett, 1989
112	345553.8	6109505	-30.0	Swanport 4, #71334	SARIG
112	345554	6109505	> -29.2	6727-862	Barnett, 1989
113	345564	6110662	-3.9	Long Island Marina	Hubble & De Carli, 2015
113	345364	6110811	> -2.7	Long Island Marina	Hubble & De Carli, 2015
114	344665	6111528	-20.3	Long Island	Hubble & De Carli, 2015
114	344634	6111322	-12.7	Long Island Reserve	Hubble & De Carli, 2015
115	343532	6112394	> -1.9	Sturt Reserve, Murray Bridge	Hubble & De Carli, 2015
117	342847	6113083	-12.5	MB PUMP 1, #71347	SARIG
117	342824	6113068	-12.1	MB PUMP 2, #71348	SARIG
117	342807	6113023	-9.7	MB PUMP 3, #71349	SARIG
117	342732	6112903	-0.3	MD PUMP 7, #71354	SARIG
117	342847	6113083	> -20.2	6727-875	Barnett, 1989
117	342807	6113023	> -25.0	6727-877	Barnett, 1989
117	343129	6113921	-10.3	Thiele Reserve	Hubble & De Carli, 2015
119	344090.8	6114680	-21.9	CH2, #70979	SARIG
119	344067.8	6114650	-19.4	CH1, #70978	SARIG
119	344046.8	6114660	-9.7	PTH1, #70980	SARIG
119	344068	6114650	-18.9	6727-498	Barnett, 1989
119	344091	6114680	-21.3	6727-499	Barnett, 1989
119	344047	6114660	-9.4	6727-500	Barnett, 1989
120	345676	6115810	-13.1	Avoca Dell	Hubble & De Carli, 2015
133	350609	6123221	-9.6	6727-2201	Barnett, 1989
133	349935	6123145	-11.9	6727-2205	Barnett, 1989
133	349305	6123011	-19.5	6727-2214	Barnett, 1989
136	348350	6125995	-6.9	Woodlane Reserve	Hubble & De Carli, 2015
142	346193	6130131	-14.2	Wall Flat	Hubble & De Carli, 2015
147	341939	6129444	> -0.3	Neeta Irrigation Area	Hubble & De Carli, 2015
159	349749	6137775	-15.8	East Front Rd	Hubble & De Carli, 2015
160	349204.8	6137915	-11.8	LOWER MURRAY DAM 5 1, #73409	SARIG
161	350989.8	6138882	-4.0	LOWER MURRAY DAM 4 1, #73297	SARIG
172	360167	6140549	-9.2	Younghusband	Hubble & De Carli, 2015
175	363437	6139565	-11.9	Younghusband	Hubble & De Carli, 2015
179	366522	6139908	-10.3	6828-427	Barnett, 1989
180	367076.9	6139963	-12.9	TEAL FLAT PD11, #85363	SARIG
180	367141.8	6139778	-13.5	TEAL FLAT PD28, #85308	SARIG
180	367117	6139848	> -7.8	6828-431	Barnett, 1989
180	367227	6139833	-6.0	6828-434	Barnett, 1989
187	372520	6137668	-7.4	BowHill	Hubble & De Carli, 2015
194	375342	6140438	-15.6	Purnong	Hubble & De Carli, 2015

15

rkm	X	Y	S$_{low}$ Z (m AHD)	ID	Reference
208	367778	6149959	-4.4	Scrubby Flat	Hubble & De Carli, 2015
213	368198	6153555	-10.5	Walkers Flat	Hubble & De Carli, 2015
221	369210	6158135	-9.8	Wongulla	Hubble & De Carli, 2015
250	371056	6172095	1.1	6828-578	Barnett, 1989
250	370985	6172001	-11.7	6828-579	Barnett, 1989
250	371143	6172150	-7.9	6828-580	Barnett, 1989
250	371381	6172318	-5.6	6828-581	Barnett, 1989
250	371232	6172245	-8.2	6828-582	Barnett, 1989
251	370984.9	6172001	-15.8	Swan Reach 2, #85459	SARIG
251	371142.9	6172150	-11.0	Swan Reach 3, #85458	SARIG
251	370896.9	6171774	-10.4	PH5, #85384	SARIG
251	371055.9	6172095	-8.1	Swan Reach 1, #85458	SARIG
251	371497.9	6172390	-6.1	Swan Reach 10, #85463	SARIG
251	371380.9	6172318	-5.8	Swan Reach 7, #85461	SARIG
251	370896.9	6171774	-3.5	PH6, #85385	SARIG
280	373624	6195800	-3.1	6829-833	Barnett, 1989
280	372657	6195846	7.3	6829-829	Barnett, 1989
284	372922	6198708	-2.5	Blanchetown Bridge 5, #85879	SARIG
284	372612	6198638	0.0	Blanchetown Bridge 12, #85835	SARIG
284	372637	6198648	0.1	Blanchetown Bridge 13, #85836	SARIG
284	372577.1	6198633	0.3	Blanchetown Bridge 1, #85833	SARIG
284	372882	6198698	1.1	Blanchetown Bridge 10, #85878	SARIG
284	372577	6198628	1.2	Blanchetown Bridge 1A, #85834	SARIG
284	372677.1	6198653	2.2	Blanchetown Bridge 2, #85837	SARIG
284	373142	6198758	3.2	Blanchetown Bridge 11, #85881	SARIG
284	372982	6198723	5.1	Blanchetown Bridge 6, #85880	SARIG
284	372562	6198628	9.2	Blanchetown Bridge 9, #85832	SARIG
284	372547	6198623	18.9	Blanchetown Bridge 7, #85831	SARIG
283.5	372577	6198628	3.5	6829-170	Barnett, 1989
283.5	372677	6198653	2.8	6829-173	Barnett, 1989
283.5	372772	6198673	0.2	6829-212	Barnett, 1989
283.5	372922	6198708	6.7	6829-215	Barnett, 1989
284	373148	6199263	> -3.9	6829-1380	Barnett, 1989

16

Appendix B

Atypical responses of a large catchment river to the Holocene sea-level highstand: The Murray River, Australia

Authors: Anna M. Helfensdorfer[1,2]*, Hannah E. Power[2], Thomas C.T. Hubble[1]

Affiliations:

1. School of Geosciences, The University of Sydney, Sydney, NSW 2006, Australia

2. School of Environmental and Life Sciences, The University of Newcastle, Callaghan, NSW 2308, Australia

*Correspondence should be addressed to A.M.H. (email: anna.helfensdorfer@sydney.edu.au)

Abstract

Three-dimensional numerical modelling of the marine and fluvial dynamics of the lower Murray River demonstrate that the mid-Holocene sea-level highstand generated an extensive central basin environment extending at least 140 kilometres upstream from the river mouth and occupying the entire one to three kilometre width of the Murray Gorge. This unusually extensive, extremely low-gradient backwater environment generated by the two metre sea-level highstand captured most, if not all, the fine-grained sediment discharged from the 1.06 million square kilometre Murray-Darling catchment and sequestered this material within a >60 kilometre long, >10 metre thick valley-wide deposit of finely laminated mud. This previously unrecognised sediment trap persisted from 8,518 to 5,067 cal yr BP preventing sediment delivery to the marine environment. Its identification requires that mid-Holocene climate reconstructions for southeastern Australia based on fluctuations in the delivery of fine-grained sediment to the ocean offshore the lower Murray River's mouth should be re-evaluated.

Introduction

Effective natural resource management benefits from a thorough understanding of how a system functioned prior to anthropogenic modification. Palaeo-climatic data is often used to inform natural resource management, with sequences of Holocene sediments providing a record that constrains a system's predicted response to a changing climate and sea level (*1*). The political, economic and environmental ramifications of natural resource allocation decisions will become increasingly contentious in coming decades as the consequences of a changing climate become more apparent (*1, 2*). Managers will become increasingly reliant on high quality palaeo-climatic data to inform their policies (*1, 2*). This is particularly the case for intensively managed river systems, such as Australia's Murray-Darling Basin (MDB), that support large-scale agriculture whilst also being important ecological refuges (Fig. 1). The MDB comprises the Murray and Darling sub-catchments which drain over 1 million km² and is Australia's most economically important agricultural region. At the terminus of the MDB, the gorge-confined lower Murray River (LMR) debouches into Lake Alexandrina and then flows through the Murray Mouth to the Southern Ocean (Fig. 1). The Murray's barrier estuary developed in response to a rapidly rising sea level during the Holocene with the formation of Sir Richard and Younghusband peninsulas and the development of the central basin lakes Alexandrina and Albert (*3, 4*) (Fig. 1).

The MDB has been increasingly managed since 1900 to accommodate the competing needs of irrigation and drinking water supply for development while maintaining environmental flows in a hydroclimate that is prone to long-term droughts (*1*). Given the challenges of a warming and drying climate (*5*) the successful management of this system and its water allocation policy will be informed by an improved understanding of southeastern Australia's Holocene climate.

The Holocene climate of southeastern Australia is typically characterised by wetter than present-day conditions during the early- to mid-Holocene, before a shift to increased climatic variability and an overall trend to aridity in the late-Holocene (*6-8*). Within the MDB, approximately 90% of flow is derived from the Murray River and its tributaries (*9*), with the annual snow melt on the southeast Australian highstands producing significant seasonal flow variability within this sub-catchment. Murray sub-catchment annual rainfall and flow variability is currently dominated by the El Niño-Southern Oscillation (ENSO), which generates inter-annual variability, and the Pacific Decadal Oscillation (PDO) driving decadal to centurial variability (*2, 8, 10*). The semi-arid Darling sub-catchment receives its most significant flows from the Inter-Tropical Convergence Zone (ITCZ) summer monsoon (*2, 8, 10*). Analyses of a record of uninterrupted sediment deposition preserved in marine cores MD03-2611 and MD03-2607, taken offshore from the Murray's Mouth on the Lacepede Shelf, has been used to generate

the only available and commonly cited palaeo-climatic reconstruction derived from sediment captured from the entire MDB (*2, 6, 11*). Analyses of the terrigenous sediment flux within these cores led Gingele *et al.* (*6, 11*) to conclude that, except for a brief dry period from 9,000 – 8,000 yr BP, humid conditions prevailed throughout the early- to mid-Holocene. This was followed by a shift to increasingly arid conditions reaching conditions akin to the present-day by 5,500 yr BP (*6, 11*).

As sea level rose rapidly in the early-Holocene, river valleys were drowned and formed the precursor of the modern-day estuary and the river valleys of southeastern Australia's stable craton (*12, 13*). Increased availability of marine sediment saw the development of the Murray estuary's barrier complex from approximately 8,000 yr BP, prior to the +2 m Holocene highstand at 7,000 – 6,000 yr BP (*3, 12, 14-16*). Worldwide, landward migration of fluvial, estuarine, and marine environments caused a continuing decrease in the depositional gradient of coastal plain rivers which typically resulted in the deposition of an upward fining sequence within fluvial deposits in coastal incised valleys (*17*). This commonly presents as a transition from high-energy fluvial sands to low-energy mud-dominated sediments (*17*). This is also evident in the LMR where the valley-fill transitions from the braid plain sands of the Monoman Formation to the low-energy clays and silts of the Coonambidgal Formation (*18*). With their ample accommodation space, young estuaries were very efficient sediment traps, which sequestered terrigenous and marine sediment as they infilled (*12, 19, 20*). The estuarine fill in the main body of Lake Alexandrina is characterised by a laminated silt-clay central basin deposit, known as the St Kilda Formation, which began accumulating by at least 8,000 yr BP and was well-established and regionally extensive by 5,500 yr BP (*21, 22*).

A previous assessment of the extent of the palaeo-Murray estuary demonstrated that the +2 m higher-than-present sea level of the mid-Holocene highstand generated an estuarine environment throughout the Lower Lakes and well upstream into the LMR (*23*). The rapid rise in sea level inundated the entire width of the several kilometre-wide Murray Gorge and extended upstream at least to Blanchetown (river kilometre (rkm) 282), creating a single, continuous, body of water quite unlike the present-day channel and fringing swamps (*23*). At highstand, the flooded Murray Gorge presented an extensive backwater zone with an enlarged central basin environment that occupied Lake Alexandrina and the lower reaches of the LMR at least as far upstream as Monteith (rkm 104) and possibly upstream to Walker Flat (rkm 206) (*23*).

Here, we evaluate the findings of 3D hydrodynamic modelling of the Murray estuary during the Holocene highstand (*23*) against a well dated core and sediment data to understand the Holocene geomorphic evolution of the LMR and Murray estuary. Specifically, we:

a) Establish the lateral extent of the water body that occupied the Murray Gorge at the Holocene highstand by correlating thirteen closely spaced cone penetrometer soundings, taken along a transect perpendicular to the modern-day channel, with an undisturbed 30 m sediment core (Monteith-A) taken at Monteith, 104 rkm upstream of the Murray Mouth;

b) Conduct a sedimentary analysis on core Monteith-A, with analyses for grainsize, moisture content, bulk density, total organic carbon, and radiocarbon dating (to establish a chronology and sedimentation rates), to determine sedimentary units and assign facies designation constraining the timing and nature of geomorphic evolution;

c) Further confirm Helfensdorfer *et al.*'s (*23*) best-estimate Holocene highstand and pre-anthropogenic 2D hydrodynamic model in 3D to resolve the potential influence of estuarine stratification; and

d) Assess to what extent the Murray estuary propagated upstream into the confines of the Murray Gorge at the Holocene highstand and independently verify, through the combination of 3D modelling and sedimentology, the conclusion of Helfensdorfer *et al.* (*23*) that the palaeo-

Murray's central basin, characterised by a laminated silt-clay sequence as described by Barnett (*21, 22*), extended from Lake Alexandrina at least as far upstream as Monteith (rkm 104).

Results

Hydrodynamic modelling

A best-estimate 3D Holocene highstand scenario (model scenario code: $S_{mid}WL_2D_{av}B_{mod}$, see methodology) supports and extends the 2D model results of Helfensdorfer *et al.* (*23*), which showed that the +2 m sea level of the Holocene highstand generated an estuarine palaeo-environment throughout the Lower Lakes and upstream into the lower reaches of the LMR (Fig. 2a). This high-resolution 3D model suggests that the lower Murray Gorge flooded completely, with the depth-averaged marine-brackish (10 psu) limit penetrating upstream as far as Tailem Bend (rkm 91; Fig. 2a). The tidal limit extended beyond the model extent (minimum Blanchetown, rkm 282; Fig. 2a). A central basin environment occupied the region upstream of Point Sturt and Point McLeay (rkm 40) up into the Murray Gorge to Wall Flat (rkm 140; Fig. 2a), correlating well with the median extent given by the suite of 2D models in Helfensdorfer *et al.* (*23*) (median Mannum, rkm 147). At highstand, maximum flow velocities were < 0.3 m/s for 95% of the model domain, consistent with generating an environment conducive to the deposition of a laminated silt-clay sequence (*24-26*). Significant areas subject to velocities exceeding 0.3 m/s were only extant seaward of Point Sturt/Point McLeay (rkm 40, within the flood-tide delta; Fig. 2a).

Estuarine infill and a decline in sea level to present-day levels, representative of modern pre-modification conditions (model scenario code: $S_{up}WL_0D_{av}B_{mod}$, see methodology), significantly reduced saline incursion to the Lower Lakes and limited marine influence to the flood-tide delta region, with the brackish limit propagating only as far upstream as Wellington (rkm 85; Fig. 2b). Under these conditions, the central basin is inferred to be restricted to the Lower Lakes with the upstream limit remaining within the upper reaches of Lake Alexandrina at the Pomanda Embayment (rkm 72; Fig. 2b). The 2 m fall in sea level and the additional estuarine infill decrease maximum flow velocities and enable conditions suitable for the deposition of a laminated silt-clay sequence throughout almost the entire model domain (99%; Fig. 2b).

Analyses of core Monteith-A

Chronology

The chronology for core Monteith-A was determined with five ^{14}C radiocarbon dates with ages that span the early- to mid-Holocene from 10,249 – 10,506 cal yr BP to 6,509 – 6,636 cal yr BP (Table 1). These dates present an increasing age with depth, with two ages 2.18 m apart (at 7.36 m and 9.54 m) returning near identical calibrated ages of 7,966 – 8,169 and 7,927 – 8,162 cal yr BP respectively (Table 1). Assuming the surface is modern, the top 2.10 m (above the youngest date) has a markedly different sediment accumulation rate of 0.03 cm/yr (Fig. 3). Given the potential for disturbance of the near surface by agricultural activities, this top-most 2.1 m section of the core was excluded from further chronological analysis. For the period spanning the five radiocarbon ages (20.65 m), the age-depth model is very well constrained with a linear regression of $R^2 = 0.997$, such that depth in the core is considered to be a valid approximation of age (Fig. 3). The model returns a mean sediment accumulation rate of 0.60 cm/yr (Fig. 3), with minor variations from the mean rate that correspond to the rise of sea level during the period of deposition. The period 8,516 - 7,750 cal yr BP marks the most rapid sediment accumulation in the core, with an average of 0.77 cm/yr, and is likely a consequence of the rapid rise in sea level caused by the melting of the Laurentide ice sheet at approx. 8,200 yr BP (Fig. 4) (*13, 27*). The worldwide initiation of

Holocene estuaries has been attributed to this event and our chronology demonstrates that the response of the LMR is consistent with the world's other major river systems (*13, 27*). Sediment accumulation rates are slowest at highstand with an average of 0.48 cm/yr between 7,750 - 6,543 cal yr BP (Fig. 4).

Sediment grainsize and characteristics

High resolution optical imagery and radiographs of the Holocene sediments of core Monteith-A (up to 24.12 m) are presented in Figure S1. The weathered claystone basal unit (Unit 1; 30.12 – 29.52 m) underlies the Monoman Formation, which, in this core, presents as two distinct units: unit 2 and unit 3. Unit 2 (29.52 – 20.99 m) is comprised of fine and medium sands with an average mean grainsize of 186.6 µm and a clay:silt:sand (C:S:S) ratio of 3:18:79 (Fig. 4). The boundary between Units 2 and 3 (20.99 m; 10,112 cal yr BP) is marked by an abrupt change from unsorted grey (7.5Y 5/1) sands to banded finer greenish grey (5G 5/1) to coarser grey (7.5Y 5/1) sands (Fig. S1) and a sharp increase in moisture content and TOC (Fig. 4). Unit 3 (20.99 – 16.34 m) presents a decrease in average mean grainsize to 136.6 µm and a C:S:S of 14:23:63 (Fig. 4). The two sand units also differ in their physical properties with an increase in average moisture content and TOC and decrease in average dry bulk density from 20 to 36%, 1.21 to 4.36% and 1,775 to 1,448 kg/m^3 between Units 2 and 3 respectively (Fig. 4). A 3.73 m thick transitional sequence (16.34 – 12.61 m) comprising mottled fine and medium silts (Unit 4) separates the Monoman Formation sands and the Coonambidgal Formation muds with its basal boundary (9,200 cal yr BP) marked by a distinct colour and textural change (Fig. S1). This unit has an average mean grainsize of 19.1 µm and a C:S:S of 30:59:11 (Fig. 4). The transition out of this mottled grey (7.5Y 5/1), greenish grey (5G 5/1) and dark greenish grey (5G 3/1) sequence is gradational in colour and texture but presents a small incremental increase in TOC and moisture content and decrease in dry bulk density at 12.61 m (8,518 cal yr BP; Fig. 4). Units 4 and 5 differ in average moisture content, TOC and dry bulk density by 90 to 110%, 11.33 to 10.00% and 838 to 738 kg/m^3 respectively. Unit 5 presents alternating 0.5 to 2 mm thick dark-coloured grey (7.5Y 4/1) laminations comprising fine to medium silts (average grainsize of 8.6 µm and C:S:S of 31:61:8) and light-coloured greenish grey (5G 6/1) laminations comprised of clay to very fine silt (average grainsize of 1.8 µm and C:S:S of 65:33:2). Moisture content, dry bulk density and TOC averages of 104%, 766 kg/m^3 and 10% respectively, with the significant increase in TOC in the near surface material (0 – 0.7 m) due to the presence of roots (Fig. 4).

Cone penetrometer soundings profile

Interpretation of CPT results using Robertson's (*28*) soil behaviour type (SBT) identifies a clear distinction between two sedimentary sequences in all CPTs beyond the valley margins (i.e. with the exception of B61-06, CPT09 and CPT10): an upper sequence comprising clays and sensitive fine-grained sediments (Fig. S2 clusters C1-C2), and an underlying sequence comprising silts and sands (Fig. S2 clusters M1-M4). This cross-valley uniformity demonstrates a valley-wide transition from the coarse-grained Monoman Formation to the fine-grained Coonambidgal Formation which is consistent with previous accounts of the Murray Gorge's valley fill (*18, 29*). At the study site, this near horizontal transition from lower to upper valley fill occurs at a depth of approximately 14-19 m across the 1,200 m width of the drowned river valley, which is reflected in the mean grainsize of Units 2 and 3 when compared with Units 4 and 5 within core Monteith-A (Fig. 4).

This simple division between the Monoman and Coonambidgal Formations has been confirmed and further extrapolated to identify the sedimentary units across the valley through a correlation with core Monteith-A. A k-medoids clustering analysis (*30*) of Robertson's (*28*) SBT data obtained from the CPT collected adjacent to the sediment core (CPT08) identifies six clusters (see methodology) which, when plotted relative to depth, allows clusters to be linked to the facies identified in core Monteith-A (Fig. 5). Unit 2 presents in CPT08 as silt mixtures to sands (clusters M1 and M2) with the sequence boundary to

Unit 3 correctly placed (Fig. 5). The distinction between the lowstand and transgressive sand facies (Unit 2 to 3) is marked by a reduction in consolidation (Fig. 5); however, the clustering analysis suggests Unit 3 is better represented as two distinct units (clusters M3 and M4), with a sequence boundary at -19.5 m (9,844 cal yr BP). We interpret this division, which was not identified through analysis of core Monteith-A, as illustrating the highly transitional nature of the transgressive system during this period. The boundary between Units 3 and 4 is also correctly placed at -16.34 m (clusters M4 and C1; Fig. 5), however, a limitation is that the SBT analysis cannot distinguish between Units 3 and 2, but rather identifies both these units as typically comprising clays and sensitive fine-grained sediments (Fig. 5). The clustering analysis suggests a division at -6.3 m, which is not reflected through the analysis of core Monteith-A. Rather, we suggest that this is an artefact of drying during the Millennium drought (1997-2011) when the significant lowering of the water table caused clays of the reclaimed swamps, such as those at the study site, to crack to depths in excess of 3.5 m (*31*). This is consistent with the maximum depth of the sub-cluster (circled in Fig. 5a) of 4.35 m. Overall, the correlation of CPT08 with core Monteith-A confirms that the division of units assigned based on the visual log (Fig. S1) and sedimentary data (Fig. 4) can also be identified by the geotechnical properties of the sediment (Fig. 5). This calibration validates the use of CPT soundings to extrapolate the sedimentary units identified in core Monteith-A across the width of the valley.

A cross-valley profile generated from the thirteen cone penetrometer soundings demonstrates the presence of a uniform valley-fill sequence consisting of a 14-19 m thick layer of muds (clays and sensitive fine-grained sediments) that overlies an interlayered sequence of sand mixtures and clays before reaching consolidated silts and sands (Fig. 6b). Aside from the valley-fringes (B61-06, CPT09 & 10), each sounding presents an almost identical vertical trace with consistent and very low cone resistance within the upper mud layer (Units 4 and 5; 0.13 – 0.80 Mpa), a notable increase within Unit 3 (0.59 – 4.60 Mpa) and high, variable oscillating cone resistance typical of coarse to fine sands and coarse silts within Unit 2 (2.35 – 31.36 Mpa; Figs 6b, S2 & S3). Soundings within Unit 5 are punctuated by brief, sharp increases in qt at -9.5 m, most prominently within CPTs 01, 04, 05, 07 and B61-06, which is interpreted to represent a slightly coarse-grained lens of sandy silt. This corresponds to a sharp increase in grainsize and dry bulk density and a decrease in moisture content and TOC at the same depth in core Monteith-A (7,998 cal yr BP) further validating the cross-valley uniformity. Each of the ten CPTs away from the valley margins reach a much stronger, denser, underlying coarse-grained sand (Unit 2) which prevented further safe operational penetration of the cone and rods. The significant increase in material resistance due to the stiffness of the compacted sands present in the lower portions of Unit 2 prevented penetration to rock basement in most CPTs; this is a typical depth limiter of the CPT method when assessing Pleistocene-Holocene sequences (*32, 33*). The upper surface of this underlying consolidated sand layer varies between approximately -25 m and -19 m across the entire valley extent (Figs 6b & S3). Limestone and underlying weathered bedrock are abruptly encountered at the margins of the valley at a depth of approximately -10 m within B61-06 and -8 m within CPTs 09 and 10 (Figs 6b & S3).

Depositional history - system tract identification
The basal sequence boundary presented in core Monteith-A is marked by a transition from weathered claystone to fluvial sands (Unit 1 to 2). Deposition of this unit is inferred to have commenced at approximately 20,000 -18,000 yr BP contemporaneous with the last glacial maximum (*3, 34*). Unit 2 is interpreted to be a component of the lowstand systems tract (*17*) and likely represent aggradation of braided fluvial channels, comprising medium to fine sands, in response to a rising base level in the early stages of sea-level rise (Fig. 4 & Fig. S1). This lower sand deposit is 8.5 m thick and presents its upper surface at 20.99 m depth in core Monteith-A which marks the fluvial transgressive surface and a probable shift from braided to single-thread morphology at 10,112 cal yr BP (Fig. S1) (*18*). This event presents as a

transition from unsorted medium sands to alternating bands of silts and silty fine sands in core Monteith-A (Unit 3; Fig. 4 & Fig. S1). This is contrasted by the identified braided to meandering morphological transition exhibited upstream within the Riverine Plain (Fig. 1) (*18*), which is evidenced by an upward fining sequence, crevasse splay and point bar deposits (*29*). Similar sedimentary structures are absent in core Monteith-A (Fig. S1) suggesting that the rapidly declining energy gradient within the lower Murray Gorge during the transgressive phase of the early-Holocene prevented the development of a meandering channel at our study site.

The presence of cross-lamination, shell lenses and a sharp increase in TOC marks a transitional phase with deposition of a transitional facies from 16.34 m (9,200 cal yr BP; Unit 4) in response to continued base level rise (Fig. 4 & Fig. S1). We suggest that the unique characteristics of this coastal plain system - the incredibly low gradient, discharge and sediment yield - caused a significant reduction in energy at the study site which accounts for the similarity in appearance (sediment colour, composition and texture) between Units 4 and 3, with the reduction in TOC a consequence of increased depth and salinity due to backfilling from marine flooding (Fig. 4 & Fig. S1). A transition to a laminated silt-clay sequence at 12.61 m (8,518 cal yr BP; Unit 5) marks the establishment of the mid-Holocene palaeo-Murray estuary and widespread deposition of a central basin facies (Fig. 4 & Fig. S1). The timing of transition between depositional styles correlates with numerous accounts globally of back stepping events and estuary initiation as a response to the melting of the Laurentian ice sheet (e.g. *13, 27, 35, 36*). The laminated silt-clay sequence is 11 m thick and indicates continuous uninterrupted mud laminae deposition between 8,518 – 5,067 cal yr BP. Finally, the radiographs suggest that the top 1.65 m of core Monteith-A may be anthropogenically disturbed which hampers interpretation in this core (Fig. S1). Consequently, the transition from highstand central basin to stillstand deposits beyond 5,067 cal yr BP cannot be confidently identified.

Discussion

The sedimentary facies identified in core Monteith-A record a sequence of deposition from lowstand, through transgression, to highstand. These facies demonstrate an example of the response of a stable cratonic river system to the progressive flooding of an incised valley by a rising sea level (Figs 4 and 7) (*17, 20, 37*). This particular presentation of Zaitlin *et al.*'s (*17*) middle incised valley facies association located 104 rkm upstream of the present-day river mouth is an atypical response to sea-level rise during the Holocene. We attribute this remarkable example of inland estuarine deposition to the incredibly low relief, the fine-grained sediment load comprised almost exclusively of silt and clay, and to the large size of this semi-arid catchment. The unusually low energy of this system, indicated by modelled current velocities of < 0.3 m/s (Fig. 2), enabled the formation of a condensed sedimentary section where the full transition from braided fluvial to central basin deposition occurred in approximately 1,600 years (10,112 – 8,518 cal yr BP). This transition is presented in core Monteith-A by an upward fining section of sands and muds (Units 3 and 4; Fig. 4 & Fig. S1). The energy available within this system was too low to produce the range of depositional conditions normally expected within the middle incised valley facies association such that a continuous condensed section is instead apparent. This has allowed for the depositional response to a full sea level cycle within the 30 m of sediment captured in core Monteith-A. These results have been summarised to produce a revised geomorphic history of the LMR, shown in Figure 7.

Our 3D hydrodynamic models confirm the conclusions drawn from 2D scenarios (*23*) which demonstrate that, at the Holocene highstand, the Murray estuary's central basin extended 140 rkm upstream from the

present-day river mouth, well into the confines of the Murray Gorge (Fig. 2a). The 11 m thick central basin deposit presented within core Monteith-A (Fig. 4) confirms that a central basin facies was deposited at least as far upstream as Monteith (rkm 104) during the mid-Holocene (8,518 – 5,067 cal yr BP). The transect of CPT profiles indicate that this central basin was deposited across the entire width of the Murray Gorge at this location (Fig. 6b). Temporally and spatially, this sequence is contiguous with Lake Alexandrina's central basin deposit and presents comparable mean grainsize, moisture content and TOC content to cores within the main body and palaeo-thalweg of Lake Alexandrina (*21, 22*). This single, continuous depositional environment in the LMR and Lake Alexandrina confirms Helfensdorfer *et al.*'s (*23*) suggestion that the LMR's Coonambidgal Formation and Lake Alexandrina's St Kilda Formation should be considered equivalent units. The existence of this elongate estuary that was extant throughout the mid-Holocene should be considered when applying our understanding of Holocene palaeo-environments to assist in the development of management policies for the region.

In the intensively managed MDB, water use, policy and planning decisions are guided by the accuracy and quality of our knowledge of pre-anthropogenic conditions. A recent debate about the long-term variation in salinity of the Lower Lakes has been dominated by the need to maintain a freshwater supply for irrigation and environmental flows (*38-41*). The Lower Lakes are held fresh by closing a series of barrages within the flood tide delta, even during periods of extreme drought (Fig. 1). The impetus to maintain these lakes as bodies of fresh water is strengthened by the Ramsar listing of the Coorong and Lakes Alexandrina and Albert wetland, which declared the waters landward of the Goolwa barrage (Fig. 1) to be fresh, and imposes an international obligation to maintain them in this condition (*42*). There are numerous, and serious, consequences of this policy, which were demonstrated during the Millennium drought (1997-2011) when water levels within the Lower Lakes dropped to a record -1.05 m Australian Height Datum (AHD; i.e. below mean sea level) exposing acid sulphate soils to a major sub-areal oxidation event as well as causing extensive property and infrastructure damage due to riverbank collapse (*43, 44*). Opening the barrages would have probably prevented the oxidisation event and bank failure but at the cost of salinising the water in the Lower Lakes and downstream reaches of the LMR. The combination of our modelling results and the sedimentary sequences identified in core Monteith-A support the body of literature which suggests that the Lower Lakes were estuarine central basins subject to significant marine incursion at the Holocene highstand. A shift to a fresher water distribution within the Lower Lakes required a fall in sea level to present-day levels (Fig. 2b).

Applying the highly accurate chronology (R^2 = 0.997) to the facies designation of core Monteith-A allows Belperio *et al.*'s (*15*) sea level envelope to be constrained at the terminus of Australia's largest river. Initially, the older limit of the envelope is supported, with marine influence first reaching Monteith (rkm 104) at 8,518 yr BP (Fig. 6a). Core Monteith-A's sediment accumulation rate then supports a trend to the younger limit of Belperio *et al.*'s (*15*) envelope over the following 2,000 years (Fig. 6a). The location and age of shells, middens, and diatom assemblages in the Murray estuary's flood tide delta constrains the timing of sea-level stabilisation to the present-day level and the coincident shift to fresher water distribution to approximately 3,500 yr BP (*4, 45-47*).

Laminations that are planar in orientation, such as those deposited within the central basin of the Murray estuary, traditionally indicate that the suspended sediment settled in water that was still or almost stationary (*48*). However, recent studies on the deposition of mud flocs have demonstrated that the deposition and preservation of a distinctly laminated sequence can occur at current velocities up to 0.3 m/s (*24-26*). Our models demonstrate that this condition was extant over a minimum of 95% of the LMR and Murray estuary at the Holocene highstand (Fig. 2). Indeed, rhythmites or banded grainsize couplets are not uncommon in the transitional environment of the central basin of low energy estuaries and

commonly record seasonal (winter/summer) variation in fluvial suspended sediment load (*49-51*). We hypothesise that the Murray estuary's central basin deposit comprises such couplets as the present-day flow (which is dominantly derived from the Murray sub-catchment) is distinctly seasonal due to the annual spring/summer melting of the winter snow pack that develops on the Australian Alps. Evidence for such a pronounced seasonality within the LMR during the mid- to late-Holocene has previously been described through fluctuating palaeo-salinities identified in fish otoliths located immediately upstream from our study site (rkm 125 – 110) (*52*). This hypothesis forms the basis of a follow-up study which, if confirmed, may enable the extraction of a record of mid- to late-Holocene annual climatic variability for southeastern Australia from core Monteith-A.

The Holocene provides a useful analogue of potential future change to assist in the adaptation of natural resource management policies to the changing climate and rising sea level. Variation in the Holocene palaeo-climate of the MDB has been inferred from sedimentary analyses of two marine sediment cores collected from the Lacepede Shelf offshore from the Murray Mouth (MD03-2611 and MD03-2607) (*6, 11*). Several previous studies have used these high resolution, continuous sedimentary records, located at the terminus of the MDB, to constrain climatic conditions for the MDB during the Holocene (*2*). Climatic interpretation of cores MD03-2611 and MD03-2607 rely on the clay/silt-ratio, as a proxy for fluvial/aeolian terrigenous input, and illite concentration, as a proxy for sediments derived from the Murray sub-catchment (Fig. 4) (*6, 11*). However, our study demonstrates that a large natural sediment trap was extant in the lower Murray Gorge and Lake Alexandrina for much of the Holocene where the extensive central basin intercepted and likely prevented the delivery of terrigenous sediment derived from the MDB to the Southern Ocean and Lacepede Shelf. Other studies have demonstrated that the significant accommodation space provided by coastal plain estuaries, particularly during initial stages of estuarine development in the early- to mid-Holocene, can result in up to 95% of fluvial sediment being prevented from reaching the continental shelf (*53, 54*). The LMR is an extreme example of this phenomenon as this coastal plain river presents a particularly low gradient which significantly limits stream power (*55*). It follows therefore that there should have been significant terrigenous sediment sequestration within the Holocene sedimentary record of the young estuary – which our results demonstrate – and a consequential reduction in the delivery of terrigenous sediment and deposition in the sedimentary record immediately offshore.

Given the results we have presented here, we suggest an alternate and more plausible interpretation to the palaeo-climate signal presented in Gingele *et al.* (*6, 11*). We suggest that the transitional point marked by a sudden decrease in the clay/silt-ratio and a trend to decreasing illite concentrations from 8,500 – 8,300 yr BP (Fig. 4) (*6, 11*) is better explained by the inception and widespread development of the Murray estuary. This development of the central basin and estuary within the lower Murray Gorge is another example of the response of a large incised-valley river system to the melting of the Laurentian ice sheet and associated sudden increase in sea level between 8,500 – 8,200 yr BP that initiated estuaries globally (*13, 27, 35*). This elongate central basin afforded ample accommodation space for the sequestration of terrigenous sediments within the LMR and Lower Lakes. The timing of reduced clay/silt-ratios in MD03-2607 corresponds exactly with the transition from fluvial to estuarine deposits in core Monteith-A and is also contemporaneous with the commencement of deposition of the central basin laminated silt-clay sequence at 8,518 cal yr BP (Figs 4 and 6a). Gingele *et al.*'s (*6, 11*) continued trend of apparent increasing aridity cumulating in the commencement of arid conditions from 5,500 yr BP corresponds to the rapid deposition of an 11 m uninterrupted laminated sequence spanning from 8,518 – 5,067 cal yr BP in core Monteith-A (Fig. 4). Similarly, the sharp decrease in clay/silt-ratio and illite concentration that marks a transitional point in the sedimentary record within marine cores MD03-2607 and MD03-2611 (*6, 11*) corresponds to the Holocene sea-level highstand of +2 m between 7,000 – 6,000 yr BP (*15, 16*). At

this time, the incursion of central basin conditions into the lower Murray Gorge was at its maximum and likely presented over a 100 rkm section of Lake Alexandrina and the lower Murray Gorge to trap sediment (Fig. 4).

This study demonstrates the response of an extreme end-member (low discharge, low sediment load, low gradient, and large catchment) coastal plain system to a rising sea level during the Holocene, revealing valley-wide sequences from lowland, through transgression to highstand (Fig. 6). We adopt a novel approach to assessing palaeo-environmental change by independently verifying best-estimate Holocene highstand and late-Holocene 3D hydrodynamic models with sedimentary analyses, an approach which, to date, has not been conducted. Our results confirm and extend the conclusions of Helfensdorfer *et al.* (*23*) and show that the Holocene sea-level highstand induced an extensive estuarine environment in the LMR, driving the tidal and brackish limits well upstream into the Murray Gorge (Fig. 2). These results support the contention that the Lower Lakes developed as part of the Murray estuary and therefore could not have been freshwater bodies for the duration of the Holocene. We demonstrate that the mid-Holocene sea-level highstand created a single, vast central basin environment throughout the Lower Lakes and upstream to Wall Flat (rkm 140, Fig. 2), that was characterised by a finely laminated silt-clay sequence, as previously described within Lake Alexandrina by Barnett (*21, 22*). A 30 m sediment core (Monteith-A) and transect of CPT soundings independently verify the modelling in demonstrating that this deposit is valley-wide throughout the lower reaches of the LMR. This is consistent with previous accounts of the upper valley-fill as comprising the Coonambidgal Formation muds without evidence of coarse-grained channel sediments (*18*). The presence of an uninterrupted, valley-wide 11 m central basin deposit (8,518 - 5,067 cal yr BP) suggests that the rising sea level would have strongly supressed deposition of terrigenous sediment on the Lacepede Shelf and may have prevented the offshore delivery of terrestrial sediment entirely. Instead, this sediment was trapped within the young estuary and deposited in discrete laminations within the Lake Alexandrina and the lower reaches of the Murray Gorge. This finding suggests that palaeo-climatic inferences drawn from the terrigenous flux signal within marine cores MD03-2611 and MD03-2607 presented elsewhere may not be valid and that Holocene palaeo-climatic reconstructions which rely on conclusions drawn from the Lacepede Shelf cores should be re-evaluated and reconsidered. Further investigation of the record of sedimentation preserved in core Monteith-A has the potential to provide a detailed, reliable, high-resolution palaeo-climate signal for the MDB during the mid-Holocene.

Methodology

Hydrodynamic model

Best-estimate Holocene highstand and late-Holocene models from Helfensdorfer *et al.* (*23*) were replicated in 3D using TUFLOW FV, a finite volume numerical model. From the conclusions of Helfensdorfer *et al.* (*23*) the most appropriate scenarios that adequately captured the transition in palaeo-environmental character from the Holocene highstand to the pre-anthropogenic condition required a change in bathymetric surface and sea level only. The best-estimate Holocene highstand scenario adopts an inferred mid-Holocene bathymetry (S_{mid}) with modern-day barrier morphology (B_{mod}) (*23*). The average discharge prior to anthropogenic modification of the flow regime (D_{av}) is applied at Blanchetown (rkm 282), while +2 m is superimposed on a modern-day tidal dataset to represent sea level at the Holocene highstand (WL_2) (*15, 16, 23*). Together, this set of variables corresponds to Helfensdorfer *et al.*'s (*23*) scenario $S_{mid}WL_2D_{av}B_{mod}$. The corresponding late-Holocene scenario, depicting the natural system prior to anthropogenic alteration to the flow regime, differs only by the adoption of pre-regulation bathymetry (S_{up}) and a modern-day tidal dataset at present-day sea level (WL_0), corresponding to Helfensdorfer *et al*,'s (*23*) scenario $S_{up}WL_0D_{av}B_{mod}$.

The 3D models presented here used hybrid z-sigma coordinates with a total of 8 vertical layers – 6 z-layers and 2 surface sigma layers – and a second order vertical solution, parametric vertical mixing model, and density coupled salinity. All other aspects of the model set up were held constant to those of Helfensdorfer *et al.* (*23*). Details on the numerical model set up, morphology and sensitivity testing are given in Helfensdorfer *et al.* (*23*).

Under present day conditions, with artificially low lake levels and supressed marine influence, wind-waves are the primary driver of sediment resuspension within the Lower Lakes (*56*). The temporally and spatially extensive deposition of a laminated sequence throughout the main body of Lake Alexandrina during the mid- to late-Holocene (*21, 22*) suggests that salinity-assisted flocculation sufficiently counteracted the influence of wind-waves. Our results support this contention suggesting that the Lower Lakes were subject to significant marine influence at the Holocene highstand. The presence of a salt wedge at depth would have assisted floc formation and settling of fine suspended sediment (*57*). Previous studies into the influence of wind-generated waves on saline incursion have demonstrated that the dominant south-westerly wind direction results in wind-waves driving backflow events into the LMR (*58*). With wind-waves absent from our model, modelled saline incursion results reflect calm conditions and could therefore be considered conservative estimates when compared to likely conditions under the dominant wind regime.

Fieldwork
Monteith was chosen as the most suitable fieldwork site along the LMR as sensitivity testing of hydrodynamic models by Helfensdorfer *et al.* (*23*) indicated that this location marks the minimum upstream extent of the Murray estuary's central basin at the Holocene highstand. The study site, located at rkm 104, is situated within the Monteith Irrigation Management Zone and, as such, has been subject to artificial levee construction, land reclamation and laser levelling allowing access to naturally inundated land. For this study, ten CPTs were collected in a transect perpendicular to the channel at 100 m spacing, commencing 100 m from the left bank, using a 22 t 6x6 specialist CPT truck. To provide a whole-of-valley analysis, results of three CPTs taken on the opposite side of the channel at 100 m spacing, and employing the same specialist CPT truck, were acquired for analysis. For each of the thirteen CPTs, cone resistance (q_c), sleeve friction (f_s), dynamic pore pressure (u_2), inclination (I), friction ratio (R_f) and corrected cone resistance (q_t) were collected at 1 cm resolution in real time. The 30 m sediment core, Monteith-A, was taken at the location of CPT08 (Fig. 1) using a Commachio MC900 Multi-Sonic drilling rig, split at the time of extrusion into 1 m sections and placed immediately into cold storage.

Chronology
Five samples of > 63 µm charcoal fragments and 4 samples of fibrous organic fragment were submitted for AMS ^{14}C radiocarbon dating (lab ID: UBA) and calibrated using Calib 7.0.4 applying the SHCal13 calibration curve (*59*). An age-depth model was developed in R using Bacon 2.3.3 (*60*). Assuming the surface to be modern, there is a significantly different sediment accumulation rate above the youngest age, which is unrealistic particularly given the potential of disturbance of the near surface due to agricultural activities. To account for this, a hiatus was input into the model directly above the shallowest ^{14}C date at 2.10 m.

Sedimentary analyses
Core Monteith-A was subsampled at 10 cm resolution for sedimentary analyses. Grainsize samples were subject to 35% H_2O_2 to oxidise the organic material, then disaggregated by adding hexametaphosphate 50 g/L and rotating samples for 12 hours prior to analysis. Grainsize analyses were conducted using a Malvern Mastersizer 2000 and statistical analyses conducted using GRADISTAT 8.0 (*61*) adopting the classification scheme of Folk and Ward (*62*). Moisture content, unit weight and bulk density were

assessed by subsampling sediment into rings of a known weight and volume and oven drying overnight at 60°C. Subsequently, these dried samples were crushed and placed into a furnace at 550°C to ascertain a crude measure of the organic content of the sediment through loss on ignition (LOI).

Interpretation of cone penetrometer soundings

The high resolution, fast testing rate and low cost makes the CPT a novel and desirable method of interpreting sequence stratigraphy at a site (*32, 33*). The use of CPT data to infer sequence stratigraphy is particularly robust when calibrated against a sediment core taken at the same or adjacent location. CPT08 was calibrated against the particle size distribution of core Monteith-A to assess the suitability of extrapolating results to infer sedimentary units from the thirteen CPTs obtained across the valley. The two key parameters are: the cone tip resistance (q_c), which is considered indicative of the density and consistency of the sediment; and, the friction ratio (R_f), which is considered indicative of sediment grainsize and texture (*28, 32, 33*). Together these parameters are plotted using Robertson's (*28*) q_c/R_f classification chart to determine the soil behaviour type (SBT).

Previous studies which have used CPT soundings to determine estuarine stratigraphy typically attribute the bounds and average q_c/R_f values of each sediment facies in the calibrated CPT to the soundings across the valley to develop a whole-of-valley analysis (e.g. *32, 33, 63, 64*). Here, we enhance this methodology by adopting a k-medoids clustering analysis (*30*) in Matlab on the calibrated CPT soundings (CPT08). The 1 cm resolution soundings were averaged in 10 cm intervals so as to be directly comparable to the grainsize sampling resolution of core Monteith-A. Due to the incredibly low strength of the Coonambidgal Formation muds, negative friction values were recorded within CPTs B61-02, B61-04 and CPT05; these were excluded from the analysis. A k-medoids clustering analysis adopting a squared Euclidean distance metric was performed on $\log_{10}$ transformed q_c/R_f data for CPT08 (and cross referenced relative to depth, to assess whether the facies divisions identified in core Monteith-A were correctly captured through the SBT analysis). The elbow and average silhouette methods were adopted to determine the optimal number of clusters. Both approaches suggested two clusters was optimal, which differentiated the Monoman Formation sands and the Coonambidgal Formation muds. This was, however, insufficient for the identification of sequence stratigraphy. Both methods returned six clusters as the second most optimal number of clusters. Each of the remaining twelve CPT soundings were then assessed in turn by attributing each individual soundings to the nearest medoid of each of the six clusters identified in CPT08 also using a squared Euclidean distance measure. The results of this clustering analysis were then plotted relative to depth and distance across the valley to infer sequence stratigraphy (refer to supplementary materials).

Author contributions

A.M.H., H.E.P. and T.C.T.H. designed the study. A.M.H. and H.E.P. developed and ran the hydrodynamic models and CPT clustering analyses, and analysed and interpreted the results. A.M.H. conducted sedimentary analyses and, together with T.C.T.H., analysed and interpreted the results. A.M.H. wrote the manuscript with substantial contributions from all co-authors.

Competing interests: The authors declare no competing interests.

Data availability: The data sets generated and/or analysed during this study are available from the corresponding author on reasonable request.

References

1.   K. Mills *et al.*, Paleoclimate studies and natural-resource management in the Murray-Darling Basin I: past, present and future climates. *Aust. J. Earth Sci.* **60**, 547-560 (2013a).

2.   P. Gell *et al.*, "Palaeoclimate studies relevant to natural resource management in the Murray-Darling Basin," (Murray-Darling Basin Authority Report, 2009).

3.   P. J. Hill, P. De Deckker†, C. von der Borch, C. V. Murray-Wallace, Ancestral Murray River on the Lacepede Shelf, southern Australia: Late Quaternary migrations of a major river outlet and strandline development. *Aust. J. Earth Sci.* **56**, 135-157 (2009).

4.   R. P. Bourman, C. V. Murray-Wallace, A. P. Belperio, N. Harvey, Rapid coastal geomorphic change in the River Murray Estuary of Australia. *Mar. Geol.* **170**, 141-168 (2000).

5.   A. Reisinger *et al.*, in *Climate Change 2014: Impacts, Adaptation, and Vulnerability. Part B: Regional Aspects. Contribution of Working Group II to the Fifth Assessment Report of the Intergovernmental Panel on Climate Change* V. R. Barros *et al.*, Eds. (Cambridge University Press, Cambridge, United Kingdom and New York, NY, USA, 2014), pp. 1371-1438.

6.   F. Gingele, P. De Deckker, M. Norman, Late Pleistocene and Holocene climate of SE Australia reconstructed from dust and river loads deposited offshore the River Murray Mouth. *Earth Planet. Sci. Lett.* **255**, 257-272 (2007).

7.   J. Kemp, L. C. Radke, J. Olley, S. Juggins, P. De Deckker, Holocene lake salinity changes in the Wimmera, southeastern Australia, provide evidence for millennial-scale climate variability. *Quat. Res.* **77**, 65-76 (2012).

8.   C. Gouramanis, P. De Deckker, A. D. Switzer, D. Wilkins, Cross-continent comparison of high-resolution Holocene climate records from southern Australia — Deciphering the impacts of far-field teleconnections. *Earth-Science Reviews* **121**, 55-72 (2013).

9.   K. Walker. (2006), pp. 248-279.

10.   H. McGowan, S. Marx, J. Denholm, J. Soderholm, B. Kamber, Reconstructing annual inflows to the headwater catchments of the Murray River, Australia, using the Pacific Decadal Oscillation. *Geophys. Res. Lett.* **36**, (2009).

11.   F. X. Gingele, P. De Deckker, C.-D. Hillenbrand, Late Quaternary terrigenous sediments from the Murray Canyons area, offshore South Australia and their implications for sea level change, palaeoclimate and palaeodrainage of the Murray–Darling Basin. *Mar. Geol.* **212**, 183-197 (2004).

12.   P. S. Roy, B. G. Thom, L. D. Wright, Holocene sequences on an embayed high-energy coast: an evolutionary model. *Sediment. Geol.* **26**, 1-19 (1980).

13.   A. B. Rodriguez, A. R. Simms, J. B. Anderson, Bay-head deltas across the northern Gulf of Mexico back step in response to the 8.2 ka cooling event. *Quat. Sci. Rev.* **29**, 3983-3993 (2010).

14.   G. Bowman, N. Harvey, Geomorphic Evolution of a Holocene Beach-Ridge Complex, LeFevre Peninsula, South Australia. *J. Coast. Res.* **2**, 345-362 (1986).

15.   A. P. Belperio, N. Harvey, R. P. Bourman, Spatial and temporal variability in the Holocene sea-level record of the South Australian coastline. *Sediment. Geol.* **150**, 153-169 (2002).

16.   S. E. Lewis, C. R. Sloss, C. V. Murray-Wallace, C. D. Woodroffe, S. G. Smithers, Post-glacial sea-level changes around the Australian margin: a review. *Quat. Sci. Rev.* **74**, 115-138 (2013).

17.   B. A. Zaitlin, R. W. Dalrymple, R. Boyd, in *Incised-Valley Systems: Origin and Sedimentary Sequences* R. W. Dalrymple, R. Boyd, B. A. Zaitlin, Eds. (SEPM (Society for Sedimentary Geology), Tulsa, Oklahoma, U.S.A., 1994), vol. Special Publication No. 51, pp. 45-60.

18.   J. B. Firman, Stratigraphy of the Chowilla Area in the Murray Basin. *Quarterly Geological Notes* **20**, (1966).

19.   B. G. Thom, P. S. Roy, Relative sea-levels and coastal sedimentation in southeast Australia in the Holocene. *J. Sediment. Petrol.* **55**, 257-264 (1985).

20. R. W. Dalrymple, B. A. Zaitlin, R. Boyd, Estuarine facies models; conceptual basis and stratigraphic implications. *J. Sediment. Res.* **62**, 1130-1146 (1992).

21. E. J. Barnett, The Flinders University of South Australia, (1993).

22. E. J. Barnett, A Holocene paleoenvironmental history of Lake Alexandrina, South Australia. *J Paleolimnol* **12**, 259-268 (1994).

23. A. M. Helfensdorfer, H. E. Power, T. C. T. Hubble, Modelling Holocene analogues of coastal plain estuaries reveals the magnitude of sea-level threat. *Scientific Reports* **9**, 2667 (2019).

24. J. Schieber, Z. Yawar, A new twist on mud deposition - mud ripples in experiment and rock record. *The Sedimentary Record* **7**, 4-8 (2009).

25. J. Schieber, J. Southard, K. Thaisen, Accretion of Mudstone Beds from Migrating Floccule Ripples. *Science* **318**, 1760-1763 (2007).

26. J. H. Baas, J. L. Best, J. Peakall, Predicting bedforms and primary current stratification in cohesive mixtures of mud and sand. *J. Geol. Soc.* **173**, 12-45 (2016).

27. M. P. Hijma, K. M. Cohen, Timing and magnitude of the sea-level jump preluding the 8200 yr event. *Geology* **38**, 275-278 (2010).

28. P. K. Robertson, "Soil behaviour type from the CPT: an update," (Gregg Drilling & Testing, Signal Hill, CA, 2010).

29. Bureau of Mineral Resources, Geology and Geophysics, *Geology of the Murray Basin, Southeastern Australia* (1991).

30. L. Kaufman, P. J. Rousseeuw, *Finding Groups in Data: An introduction to cluster analysis*. (John Wiley & Sons, Inc., Hoboken, New Jersey, 2009).

31. R. W. Fitzpatrick, L. M. Mosley, F. J. Cook, *Understanding and managing irrigated acid sulfate and salt-affected soils: A handbook for the Lower Murray Reclaimed Irrigation Area*. Acid Sulfate Soils Centre Report: ASSC_086 (University of Adelaide Press, Adelaide, 2017), pp. 139.

32. M. Styllas, A simple approach to define Holocene sequence stratigraphy using borehole and cone penetration test data. *Sedimentology* **61**, 444-460 (2014).

33. S. Lafuerza, M. Canals, J. L. Casamor, J. M. Devincenzi, Characterization of deltaic sediment bodies based on in situ CPT/CPTU profiles: A case study on the Llobregat delta plain, Barcelona, Spain. *Mar. Geol.* **222-223**, 497-510 (2005).

34. A. P. Belperio, C. V. Murray-Wallace, J. H. Cann, The last interglacial shoreline in southern Australia: Morphostratigraphic variations in a temperate carbonate setting. *Quat. Int.* **26**, 7-19 (1995).

35. K. M. Cohen, M. P. Hijma, in *STRATI 2013: First International Congress on Stratigraphy At the Cutting Edge of Stratigraphy,* R. Rocha, J. Pais, J. C. Kullberg, S. Finney, Eds. (Springer International Publishing, Cham, 2014), pp. 925-929.

36. K. Hori, Y. Saito, An early Holocene sea-level jump and delta initiation. *Geophys. Res. Lett.* **34**, n/a-n/a (2007).

37. S. L. Nichol, R. Boyd, S. Penland, in *Incised-Valley Systems: Origin and Sedimentary Sequences,* R. W. Dalrymple, R. Boyd, B. A. Zaitlin, Eds. (SEPM Society for Sedimentary Geology, 1994).

38. J. Fluin, P. Gell, D. Haynes, J. Tibby, G. Hancock, Palaeolimnological evidence for the independent evolution of neighbouring terminal lakes, the Murray Darling Basin, Australia. *Hydrobiologia* **591**, 117-134 (2007).

39. J. Fluin, D. Haynes, J. Tibby, "An Environmental History of the Lower Lakes and the Coorong," (2009).

40. A. Gell Peter, Watching the tide roll away – advocacy and the obfuscation of evidence. *Pacific Conservation Biology (Retraction published 2019, Pacific Conservation Biology 25(1) p 111)*, (2018).

41.   P. A. Gell, Retraction notice to 'Watching the tide roll away - advocacy and the obfuscation of evidence.'; [Pacific Conservation Biology (2018) doi:10.1071/PC17048]. *Pacific Conservation Biology* **9999**, (9999).

42.   J. Pittock, C. M. Finlayson, A. Gardner, C. McKay, Changing character: the Ramsar Convention on wetlands and climate change in the Murray-Darling Basin, Australia. *Environmental and Planning Law Journal* **27**, 401-425 (2010).

43.   T. C. T. Hubble, E. De Carli, "Mechanisms and Processes of the Millennium Drought River Bank Failures: Lower Murray River, South Australia," *Goyder Institute for Water Research Technical Report* (Adelaide, South Australia, 2015).

44.   T. Job, D. Penny, Q. Hua, Metal enrichment in estuarine sediments proximal to acid sulfate soils as a novel palaeodrought proxy. *Sci. Tot. Environ.* **612**, 247-256 (2018).

45.   J. H. Cann, R. P. Bourman, E. J. Barnett, Holocene Foraminifera as Indicators of Relative Estuarine-Lagoonal and Oceanic Influences in Estuarine Sediments of the River Murray, South Australia. *Quat. Res.* **53**, 378-391 (2000).

46.   R. A. Luebbers, "The Coorong Report: An archaeological survey of the Northern Coorong," (Prepared for the South Australian Department for Environment and Planning, 1982).

47.   J. Fluin, Monash University, (2002).

48.   M. J. Zaleha, Fluvial and lacustrine palaeoenvironments of the Miocene Siwalik Group, Khaur area, northern Pakistan. *Sedimentology* **44**, 349-368 (1997b).

49.   J. R. L. Allen, Annual textural banding in Holocene estuarine silts, Severn Estuary Levels (SW Britain): patterns, cause and implications. *The Holocene* **14**, 536-552 (2004).

50.   W. P. Lanier, H. R. Feldman, A. W. Archer, Tidal sedimentation from a fluvial to estuarine transition, Douglas Group, Missourian-Virgilian, Kansas. *J. Sediment. Res.* **63**, 860-873 (1993).

51.   H.-E. Reineck, I. B. Singh, *Depositional sedimentary environments: with reference to terrigenous clastics*. (Springer-Verlag, Berlin, ed. Second, 1980).

52.   M. Disspain, L. A. Wallis, B. M. Gillanders, Developing baseline data to understand environmental change: a geochemical study of archaeological otoliths from the Coorong, South Australia. *J. Archaeol. Sci.* **38**, 1842-1857 (2011).

53.   J. D. Phillips, M. C. Slattery, Sediment storage, sea level, and sediment delivery to the ocean by coastal plain rivers. *Prog. Phys. Geog.* **30**, 513-530 (2006).

54.   R. H. Meade, Sources, Sinks, and Storage of River Sediment in the Atlantic Drainage of the United States. *The Journal of Geology* **90**, 235-252 (1982).

55.   E. D. Gill, in *Proceedings of Royal Society of Victoria,* J. W. Warren, Ed. (Melbourne, Australia, 1978), vol. 1, pp. 1-4.

56.   K. T. Aldridge, B. M. Deegan, S. Lamontagne, A. Bissett, J. D. Brookes, "Spatial and temporal changes in water quality and sediment character in Lake Alexandrina and Lake Albert during a period of rapid water level drawdown," (2009).

57.   B. Sutherland, K. Barrett, M. Gingras, Clay settling in fresh and salt water. *Environ. Fluid Mech.* **15**, 147-160 (2015).

58.   L. Ellicott, R. Hudson, "Modelling investigations into the Wellington 'Virtual Weir' concept: Phase 3 water level, wind data and wind setup analyses (including TUFLOW-FV wind design simulations)," (Prepared by BMT WBM for the Murray-Darling Basin Authority, 2010).

59.   M. Stuiver, P. J. Reimer, Extended 14C data base and revised CALIB 3.0 14C age calibration program. *Radiocarbon* **35**, 215-230 (1993).

60.   M. Blaauw, J. A. Christen, Flexible Paleoclimate Age-Depth Models Using an Autoregressive Gamma Process. *Bayesian Analysis* **6**, 457-474 (2011).

61.   S. J. Blott, K. Pye, GRADISTAT: a grain size distribution and statistics package for the analysis of unconsolidated sediments. *Earth Surf. Processes Landforms* **26**, 1237-1248 (2001).

62.   R. L. Folk, W. C. Ward, Brazos River bar: a study in the significance of grain size parameters. *J. Sediment. Petrol.* **27**, 3-26 (1957).

63.   C. Kyungsik, K. Ju Hyong, Identifying late Quaternary coastal deposits in Kyonggi Bay, Korea, by their geotechnical properties. *Geo-Mar. Lett.* **26**, 77-89 (2006).

64.   A. Amorosi, N. Marchi, High-resolution sequence stratigraphy from piezocone tests: an example from the Late Quaternary deposits of the southeastern Po Plain. *Sediment. Geol.* **128**, 67-81 (1999).

65.   M. J. Tooley, *Sea-level Changes: Northwest England during the Flandrian stage*. (Oxford: Clarendon Press, 1978).

66.   M. B. Jaksa, T. C. T. Hubble, Y. L. Kuo, E. De Carli, C. Liang, "Goyder Institute Research Project E.1.8 Riverbank Collapse in the Lower River Murray - Literature Reivew and Knowledge Gap Analysis," *Goyder Institute for Water Research Technical Report Series No. 13/15* (Adelaide, South Australia, 2013).

Figures
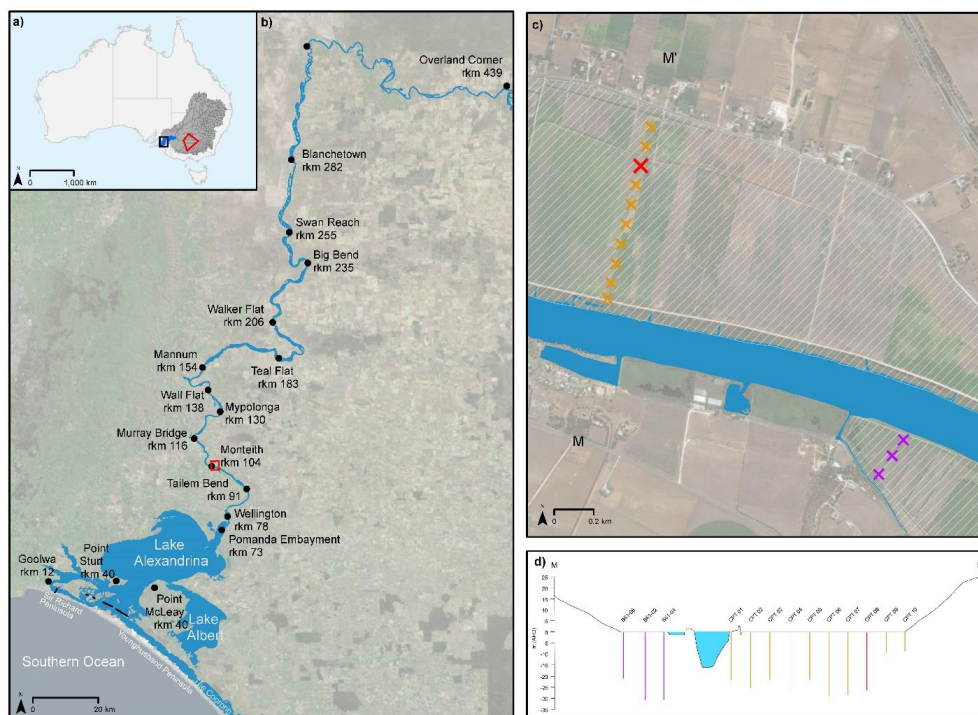
Figure 1: Overview of study sites (**a**) The Murray-Darling Basin (grey) drains the twin Murray and Darling catchments, whose major watercourses are shown in dark grey. The confluence of the Murray and Darling Rivers marks the upstream extent of the lower Murray River (blue) which flows to the Southern Ocean in South Australia. The extent of the Riverine Plain is given in red (see Discussion for context). (**b**) The lower Murray River enters the Murray Gorge at Overland Corner (rkm 439) and remains confined until debouching into Lake Alexandrina at Wellington (rkm 78). The modern-day estuary comprises the Lower Lakes, Alexandrina and Albert, together with the Coorong lagoon. The lower Murray River flows through the Murray Mouth into the Southern Ocean between Younghusband and Sir Richard Peninsulas. A series of five barrages (black) regulate saline incursion into the estuary. (**c**) Fieldwork was conducted at Monteith (rkm 104) on grazing land comprising a reclaimed backswamp (white hatch) situated behind an artificial levee on the left bank of the river. Ten CPTs were taken at 100 m spacing commencing 100 m from the channel (orange crosses), with core Monteith-A extruded at the same site as CPT08 (red crosses). Three CPTs collected as part of an alternate study completes the transect on the right bank of the river (purple crosses). (**d**) Elevation profile of transect M-M' showing the position of each CPT relative to the width of the Murray Gorge. CPTs were pushed until refusal with penetration depths reaching beyond 20 m in all but two at the valley margins. Satellite imagery source: Esri.
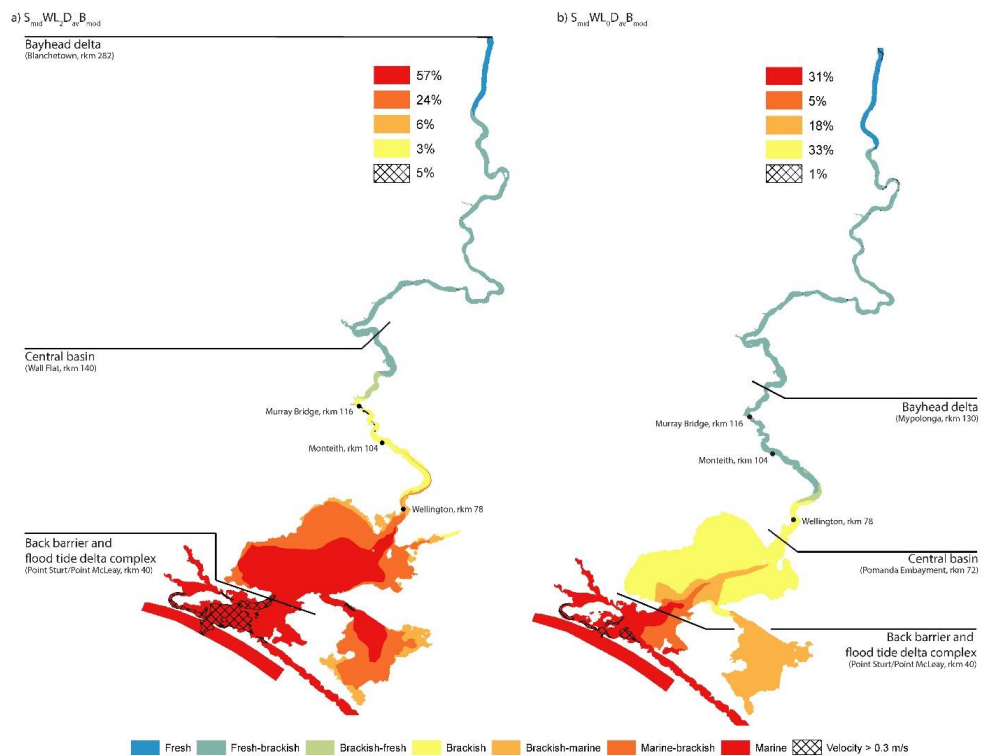
Figure 2: Modelled maximum salinity and velocity magnitude and inferred resulting morphological zonation. (**a**) 3D depth-averaged maximum salinity reached from a best-estimate Holocene highstand scenario ($S_{mid}WL_2D_{av}B_{mod}$) demonstrates that the Lower Lakes were subject to significant marine incursion driving the brackish limit beyond Murray Bridge (rkm 118). The flood-tide delta is the only region where maximum velocity magnitudes exceed the limit for deposition of a laminated sequence over significant areas (*24-26*). (**b**) The reduction of sea level in the late Holocene (modelled as scenario $S_{mid}WL_0D_{av}B_{mod}$) causes a significant change in the palaeo-environmental character of the region restricting the brackish limit to Wellington (rkm 85) and supressing marine incursion to the flood tide delta. Salinity categorisation is based on the classification scheme of Tooley (*65*).

Lab ID	Depth (m)	^{14}C date (yr BP ± 1 σ)	Material	Calibrated age (2 σ) (cal. yr BP)	Probability (%)	Median calibrated age (2 σ) (cal. yr BP)
UB-38709	2.11	5,761 ± 43	> 63 µm charcoal fragments	6,409 - 6,636	100	6,513
UBA-38326	5.06	6,413 ± 45	> 63 µm charcoal fragments	7,241 - 7,421	93.9	7,308
				7,178 - 7,214	6.1	
UBA-38765	7.36	7,282 ± 49	> 63 µm charcoal fragments	7,966 - 8,169	100	8,062
UBA-38710	9.54	7,221 ± 58	fibrous organic fragment	7,927 - 8,162	96.0	7,998
				7,871 - 7,895	4.0	
UBA-38325	12.60	7,748 ± 44	> 63 µm charcoal fragments	8,411 - 8,583	100	8,490
UBA-36739	15.17	8,006 ± 37	charred fibrous organic fragment	8,691 - 8,992	93.6	8,839
				8,649 - 8,678	5.4	
				8,683 - 8,689	1.0	
UBA-38766	18.33	8,757 ± 44	> 63 µm charcoal fragments	9,548 - 9,824	94.1	9,671
				9,843 - 9,869	3.4	
				9,872 - 9,887	2.0	
				9,827 - 9,831	0.5	
UBA-38186	19.91	8,884 ± 54	charred fibrous organic fragment	9,701 - 10,165	100	9,929
UBA-38187	22.76	9,256 ± 44	charred fibrous organic fragment	10,249 - 10,506	100	10,374

Table 1: Conventional and calibrated ages for core Monteith-A ^{14}C samples. Nine charcoal or fibrous organic samples were taken from the top 23 m of core and analysed at lab UBA. Calibrated ages with the greatest probability are referred herein.
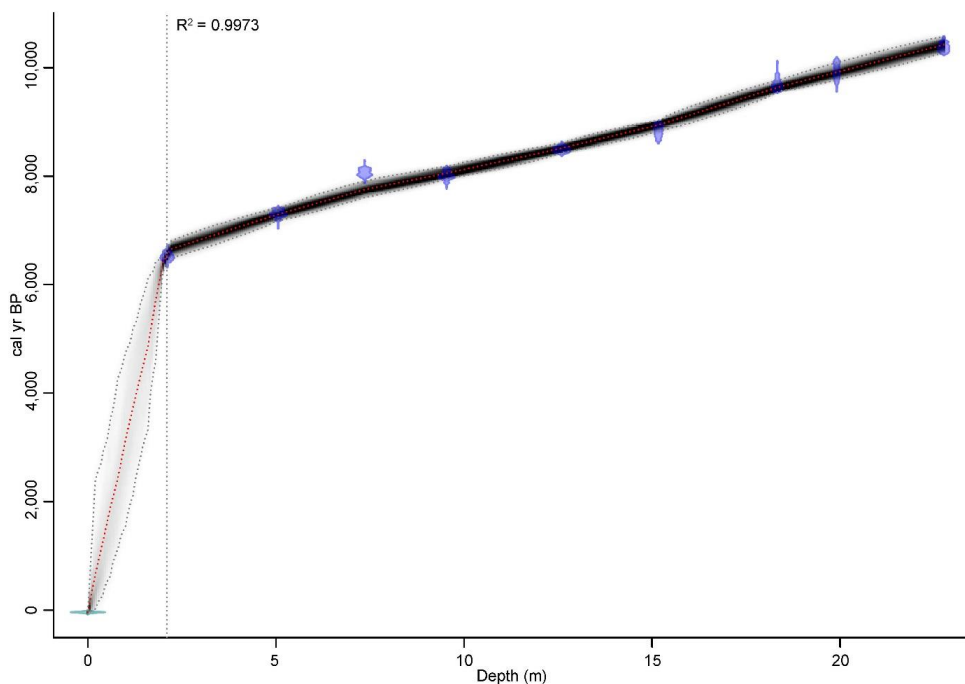
Figure 3: Bacon age-depth model produced from core Monteith-A dates. The model is very well constrained for the period between the youngest and oldest dates (6,513 – 10,374 yr BP; $R^2 = 0.997$), giving an average sediment accumulation rate of 0.14 cm/yr for this 20.65 m range. Assuming the surface of the core is modern, the model gives an average sediment accumulation rate of 0.03 cm/yr for the top 2.10 m. The model returns all calibrated ^{14}C dates (purple), the 'best' model based on the mean age for each depth (red dashed line) and the 95% confidence interval (grey dashed lines), with the degree of shading between the 95% confidence intervals representing the likelihood of the calendar age.

Figure 4: Sedimentary analysis of core Monteith-A relative to sea level and key proxies from offshore marine cores MD03-2611 and MD03-2607. Calibrated ages together with the grainsize distribution, moisture content, dry bulk density, TOC and sediment accumulation rate led to the interpretation of five units from basal weathered clay (Unit 1) to lowstand braided fluvial faces (Unit 2), and transgressive single-thread fluvial (Unit 3), transitional fluvial bayhead delta (Unit 4) and central basin facies (Unit 5). The top 1.65 m is potentially disturbed due to agricultural activities at the site. Fluctuations in the clay/silt ratio and illite percentage are given for offshore marine cores MD03-2607 and MD03-2611 respectively (*6, 11*). The timing of the Holocene sea-level highstand (7,000 – 6,000 yr BP) is demarcated by blue shading (*15, 16*), and the 8,500 – 8,200 yr BP worldwide estuarine initiation event by green shading (*13, 27, 35, 36*).
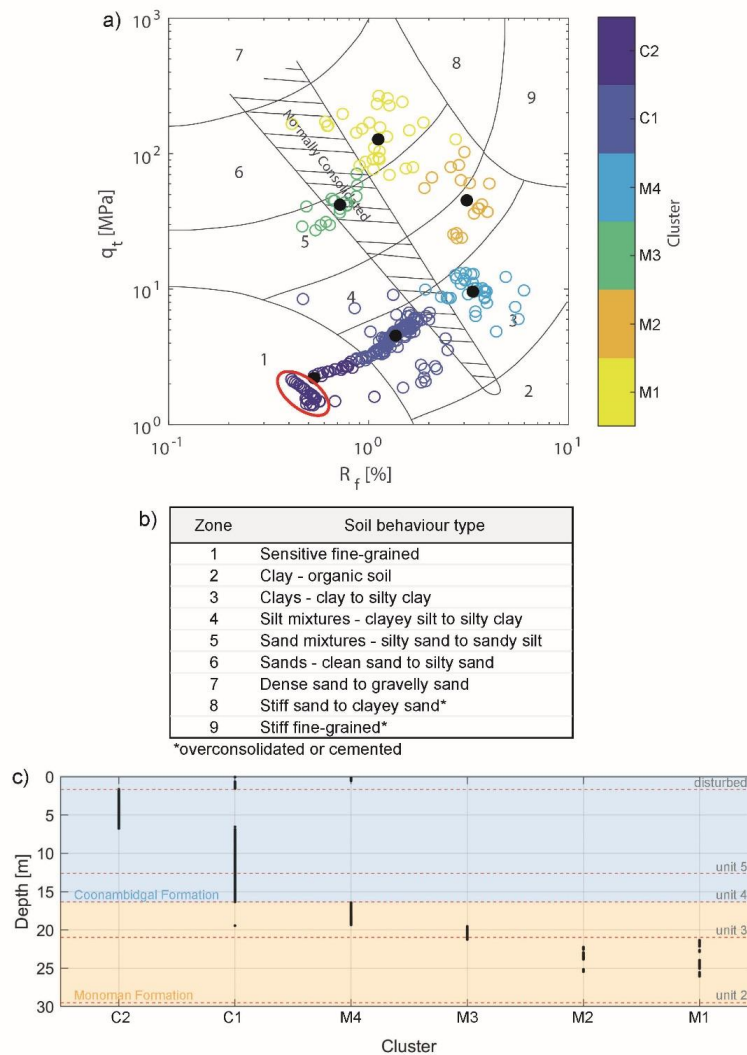
Figure 5: Correlation of facies identified in core Monteith-A to results of CPT08 applying Robertson's (*28*) SBT. (**a**) Plotting CPT08 on Robertson's (*28*) q_c/R_f plot and performing a k-medoids clustering analysis reveals six distinct clusters. A sub-cluster within cluster 1 (circled in red) comprises drought-affected surficial and shallow sediment. (**b**) Robertson's (*28*) SBT provides a description of sediment based on nine zones distinguished through CPT results q_c and R_f. (**c**) Plotting clusters relative to depth facilitates comparison with sedimentary units identified within core Monteith-A (red dashed lines). Sedimentary unit boundaries within core Monteith-A correlate well with the clustering analysis of q_c/R_f for CPT08.
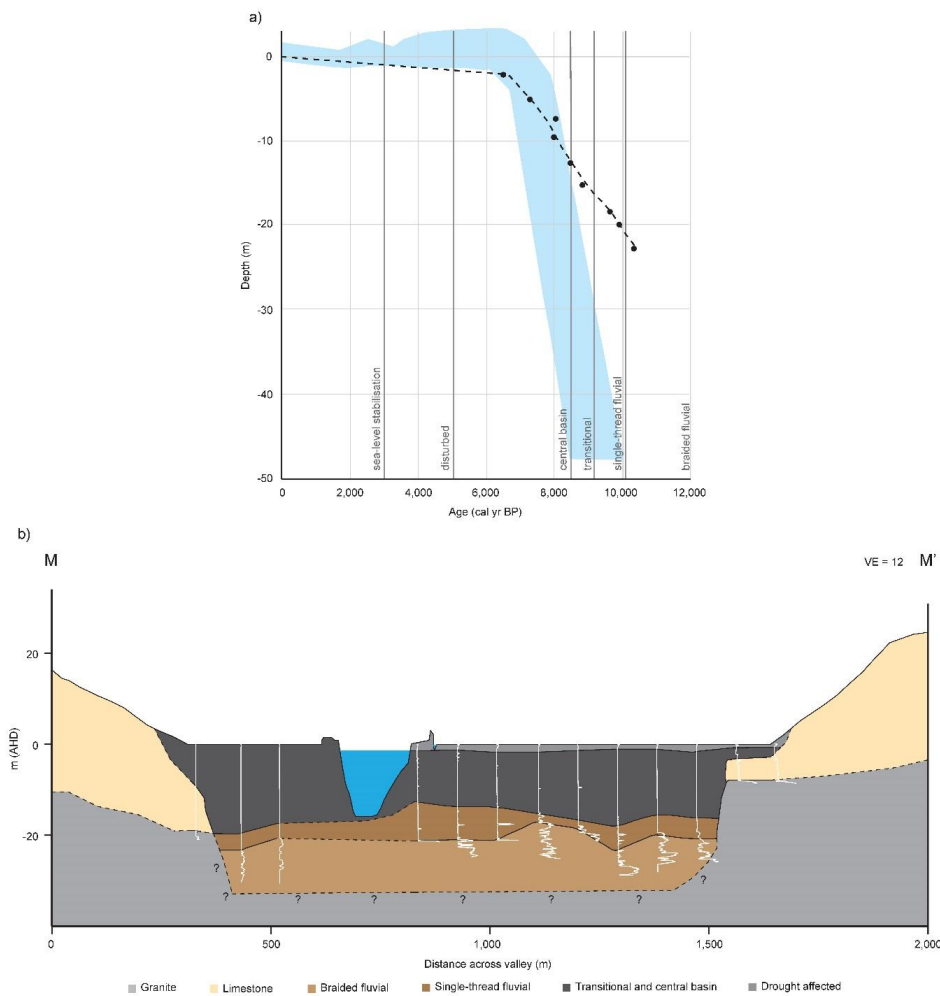
Figure 6: Core Monteith-A sedimentary facies relative to sea level and valley-wide cross section extrapolated from CPTs collected in transect. (**a**) The Bacon age-depth plot for core Monteith-A is plotted, relative to facies designation, against the Holocene sea-level envelope for the Southern Australian coast (*15*). The inception of the Murray estuary, and commencement of deposition of the central basin sequence, is synchronous with the onset of marine flooding at this location. Calibrated ^{14}C ages are denoted by black points, with the approximate timing of sea-level stabilisation to the present-day level shown as 3,500 yr BP (*4, 45-47*). (**b**) A valley-wide cross section at Monteith (rkm 104; transect M-M' given in Fig. 1c-d) developed from SBT analysis of thirteen CPTs reveals that the central basin (Unit 5) is uninterrupted across the whole width of the valley. The underlying single-thread fluvial (Unit 3) and braided fluvial (Unit 2) facies are interrupted only by limestone and bedrock outcrops at the extent of the valley. Dashed lines indicate uncertainty with question marks denoting uncertainty at depth.
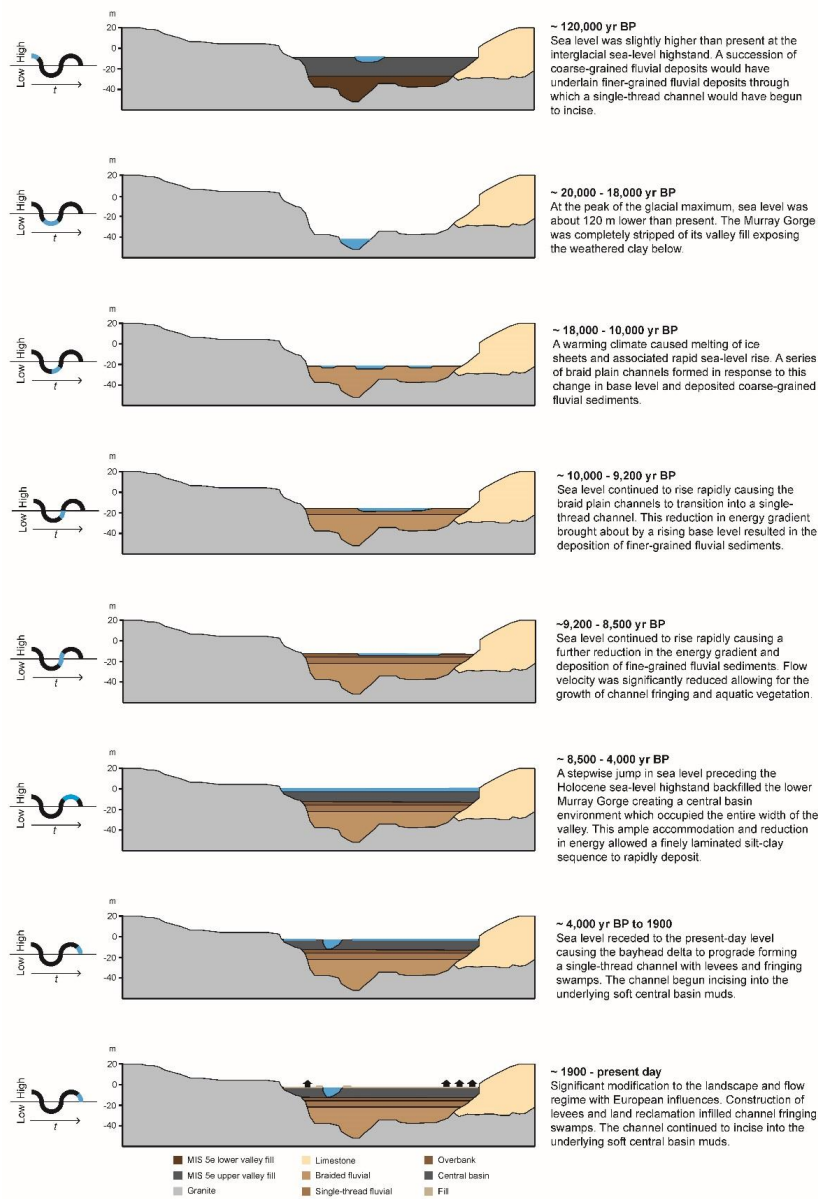
Figure 7: Revised geomorphic history of the LMR. The combination of results derived from hydrodynamic models and sedimentologic data allows for the development of a revised model of sedimentary infilling of the lower Murray Gorge. These results validate and modify some aspects of Jaksa *et al.*'s (*66*) model, while invalidating others, and serve as a complementary upstream counterpart to the Holocene geomorphic history of Lake Alexandrina presented by Barnett (*22*).

SUPPLEMENTARY MATERIALS

Atypical responses of a large catchment river to the Holocene sea-level highstand: The Murray River, Australia

Authors: Anna M. Helfensdorfer[1,2]*, Hannah E. Power[2], Thomas C.T. Hubble[1]

Affiliations:

1. School of Geosciences, The University of Sydney, Sydney, NSW 2006, Australia

2. School of Environmental and Life Sciences, The University of Newcastle, Callaghan, NSW 2308, Australia

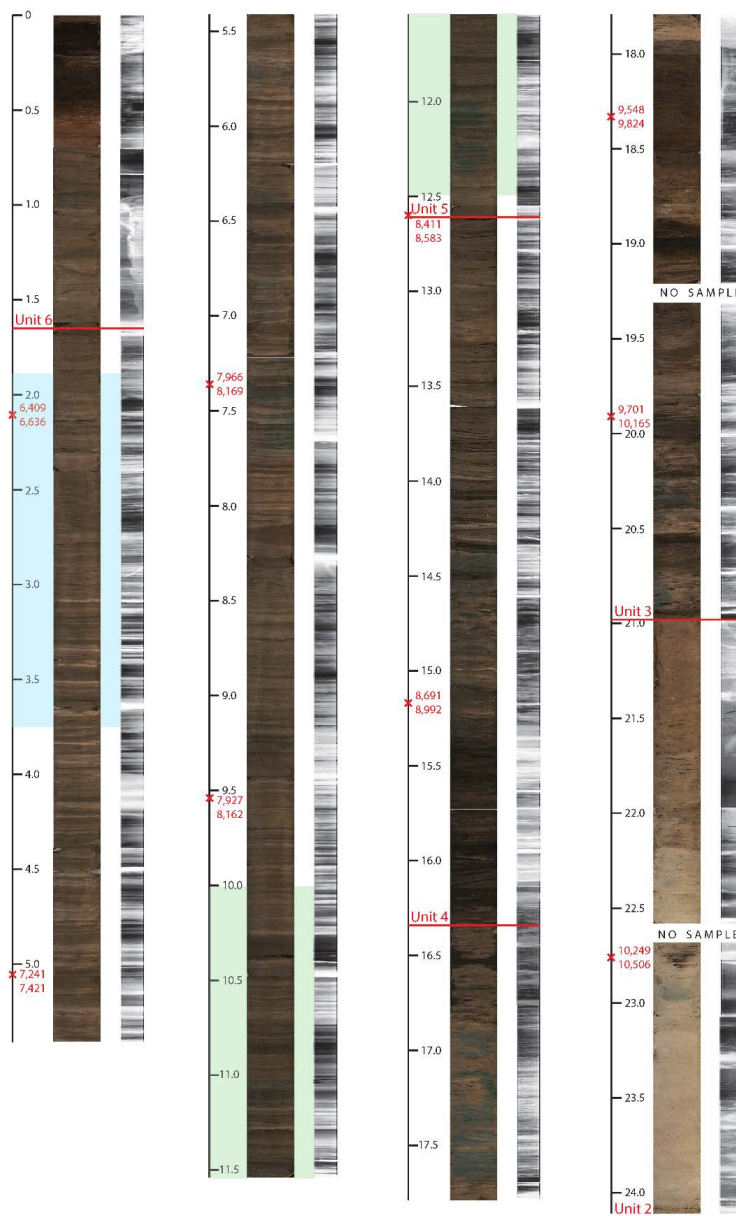*Correspondence should be addressed to A.M.H. (email: anna.helfensdorfer@sydney.edu.au)

Figure S1: Core Monteith-A imagery. Optical imagery and radiographs of 24.12 m of core Monteith-A showing locations of ^{14}C dates and calibrated ages (in cal yr BP). Unit boundaries (red), worldwide estuary initiation event (green) and sea-level highstand (blue) are given as per Figure 4. Scale is depth in meters.
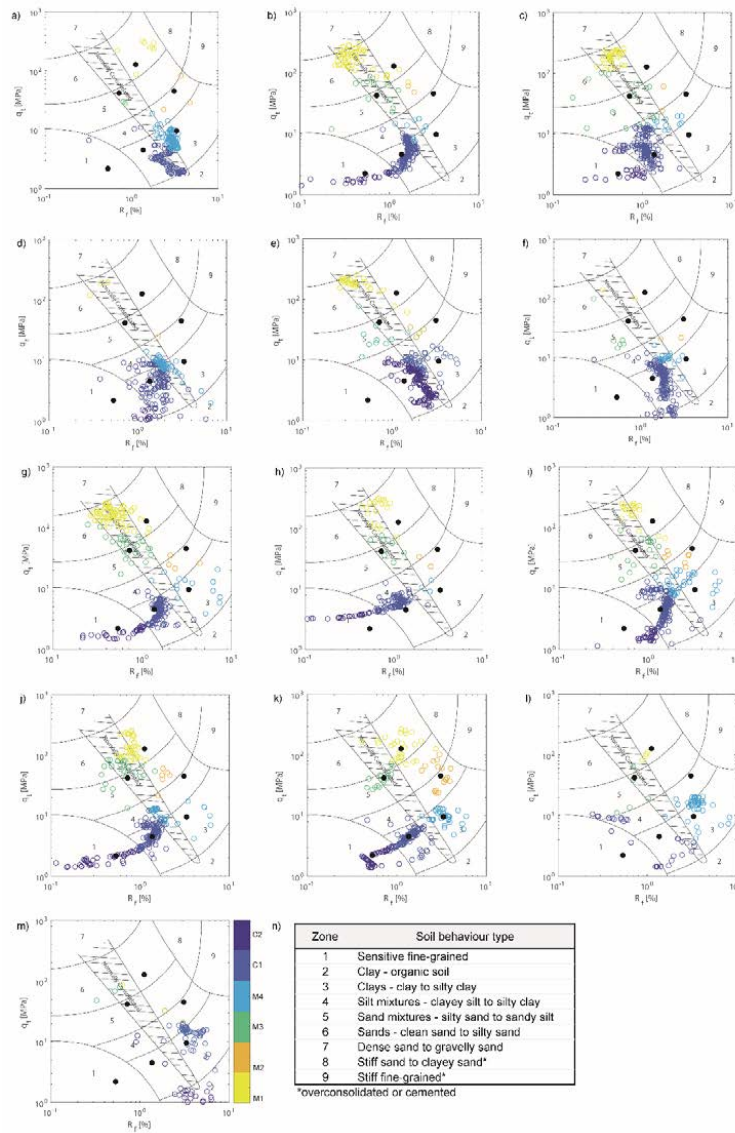
Figure S2: q_c/R_f plots for each CPT giving Robertson's (*28*) SBT coloured by cluster relative to the six clusters identified within CPT08. (**a**) B61-06; (**b**) B61-02; (**c**) B61-04; (**d**) CPT01; (**e**) CPT02; (**f**) CPT03; (**g**) CPT04; (**h**) CPT05; (**i**) CPT06; (**j**) CPT07; (**k**) CPT08; (**l**) CPT09; (**m**) CPT10; (**n**) description of soil behaviour type given by each of Robertson's (*28*) nine zones. Black points denote the medoid of each cluster identified for CPT08, with the cluster legend given in panel (**m**). Clusters M1-M4 comprise sediments of the Monoman Formation, while clusters C1-C2 comprise sediments of the Coonambidgal Formation.
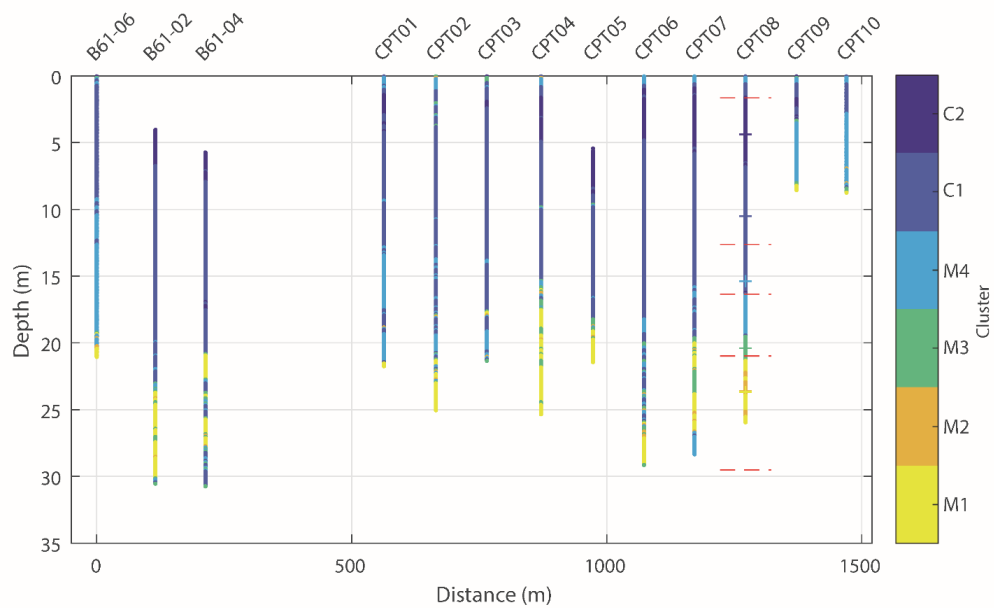
Figure S3: CPT cluster analysis by depth. Plotting the results of individual clustering analyses (Fig. S1) by depth and relative position across the valley reveals vertical and lateral trends in sediment geotechnical properties. The median depth of each cluster in CPT08 is denoted by a cross, with the red hatched line indicating the depth of each sedimentary unit identified within core Monteith-A. Negative sleeve friction values prevented q_c/R_f analysis for the top few meters of sediment within B61-02, B61-04 and CPT05. Data displayed here was used to inform the creation of the cross section in Figure 6b.